

Carbohydrates on Surfaces: Lectin Binding and Biosensing Applications

**A Thesis
Submitted in partial fulfilment of the requirements
of the degree of
Doctor of Philosophy**

**By
Madhuri Gade
ID: 20123186**



Indian Institute of Science Education and Research, Pune

**Research Supervisor
Dr. Raghavendra Kikkeri
Associate Professor
Indian Institute of Science Education and Research, Pune**

Dedicated to

My Family and Teachers

CERTIFICATE

This is to certify that the work incorporated in this thesis entitled “**Carbohydrates on Surfaces: Lectin Binding and Biosensing Applications** ” submitted by **Madhuri Gade** carried out by candidate at Indian Institute of Science Education and Research (IISER), Pune, under my supervision. The work presented here or any part of it has not been included in any other thesis submitted previously for the award of any degree or diploma from any other University or institution.

July 31th, 2017



Dr. Raghavendra V. Kikkeri

(Associate Professor)

IISER, Pune

Pune-411008, India

DECLARATION

I hereby declare that the thesis entitled “**Carbohydrates on Surfaces: Lectin Binding and Biosensing Applications**” submitted for Doctor of Philosophy in Chemistry at Indian Institute of Science Education and Research (IISER), Pune, has not been submitted by me to any other University or Institution. This work presented here was carried out at the, Indian Institute of Science Education and Research, Pune, India under the supervision of Dr. Raghavendra V. Kikkeri.

Madhuri Gade
ID- 20123186
(Senior Research Fellow)
Department of Chemistry, IISER
Pune- 411008, India

July 31th, 2017

Acknowledgments

This is the time to express my deepest gratitude and honest thanks to all the people who have guided, supported and helped me in various ways during the past four years. First of all I would like to express sincere appreciation to my thesis supervisor Dr. Raghavendra Kikkeri, for accepting me as a Ph.D. student and giving me opportunity to work in his lab. Without his backing I could have not able to finish my Ph.D. Thanks to him for his all support, guidance, opportunities, advice and patience.

I thank our Director, Prof. K. N. Ganesh for giving excellent research platform, financial support and facilities that I have been fortunate with during my research here Indian Institute of Science Education and Research, Pune. I would like to acknowledge my RAC member Dr. Sayam Sen Gupta, Dr. Pankaj Poddar, Prof. Srinivas Hotha for their valuable inputs during my RAC meetings. I would like to thank UGC India for financial support during my Ph. D. I am thankful to all the chemistry faculties in IISER-Pune for their support. I also thank to all administrative staff of our department. Heartfelt thank our collaborator Dr. Pankaj Poddar, Dr. H. V. Tulsiram, Dr. Dhanasekaran Shanmugam, NCL, Pune for giving me an opportunity to work in their lab. Thank to Dr. Rina Arad -Yellin, Semorex Selective Molecular Recognition, Israel, Dr. Bernd Lepenies, University of Veterinary Medicine, Hannover, Germany, Dr. Vered Karavani, Tel Aviv University, Israel.

In my daily work, I have been extremely fortunate and blessed with many cheerful and friendly colleagues, Dr. R. Murthy, Dr. Preeti, Dr. Rohan, Dr. Harikrishna, Dr. Sivakoti, Chethan, Bala, Suraj, Prashant, Phani, Catherine, Akhil, Sandhya, Amol, Keertana without them working would have become difficult. Here I also like to thanks my other friends Trimbak, Priya, Prabhaker, Dr. Madhuri, Dinesh, Shobha, Dershana for their encouragement. I also would like to acknowledge my teachers Dr. Sujata Kale, Dr. Arun Natu, Dr. Chikate for their support and encouragement.

My family especially my father, my husband, my gratitude becomes speechless when I think of you. Thank you, thank you and thank you! Finally, I would like to thank God who made all things possible in my life.

Thank you all

MadhuriGade

Contents

Index	i-v
Abbreviations	vi-xii
Abstract of Thesis	xiii-xiv
Publications	xv

Chapter 1

Multivalent Carbohydrates-Protein interactions

1.1. Introduction	2
1.2. Carbohydrate Binding Proteins	2
1.2.1. Plant Lectins	2
1.2.2. Bacterial lectins	3
1.2.3. Animal Lectins	4
1.2.4. Lectins on Pathogen	5
1.3. Multivalent carbohydrate-protein interactions	5
1.3.1. Glycopolymers	6
1.3.2. Glycodendrimers	7
1.3.3. Glyco-peptides	8
1.3.4. Glycoliposomes	9
1.3.5. Glyco-goldnanoparticles	10
1.4. Cyclodextrins as multivalent probe	11
1.5. Heterogeneity	13
1.6. Chirality	15
1.7. Why Surfaces?	16
1.8. Derivatization of surfaces with carbohydrates	17
1.8.1. Functionalization of surfaces with carbohydrate	17
1.9. Label free technique	21
1.9.1. Surface Plasmon Resonance	21
1.9.2. Plasmon Waveguide Resonance	24

1.9.3. FTIR-attenuated Total Reflection	26
1.9.4. Quartz Crystal Microbalance	26
1.9.5. Cantilever	28
1.9.6. Atomic Force Microscopy	30
1.9.7. Field-effect Transistor (FET)	30
1.9.8. Cyclic Voltammetry	32
1.9.9. Electrochemical Impedance Spectroscopy	33
1.10. References	34

Chapter 2

Part I

Immobilization of Multivalent Glycoprobes on Gold Surfaces For Sensing Proteins and Macrophages

2.1. Introduction	42
2.1.1. Results and Discussion	44
2.1.1.1. Synthesis of adamantyl linker	44
2.1.1.2. Synthesis of heptamannose β -CD and monomannose (M-2)	44
2.1.1.3. Functionalization of glass slide with adamantane linker	45
2.1.1.4. Characterization of slide	45
2.1.1.5. Characterization of slide by XPS	47
2.1.1.6. Evaluating carbohydrate protein interactions on slide	48
2.1.1.7 Assessing carbohydrate-protein interactions by Surface Plasmon Resonance (SPR)	48
2.1.1.8. Macrophage binding assay	51
2.1.2 Conclusion	53
2.1.3 Experimental part	53
2.1.3.1. General Information	53
2.1.3.2. Experimental Details	54
2.1.3.3. Surface Functionalization	57
2.1.3.4. Contact angle measurements	58
2.1.3.5. Spectroscopic ellipsometry	58
2.1.3.6. Estimation of concentration of sugar on slide	59

2.1.3.7. X-ray photoelectron spectroscopy	59
2.1.3.8. Atomic force microscopy	60
2.1.3.9. Surface Plasmon Resonance study	60
2.1.3.10. THP-1 differentiated Macrophage Binding Assay	61
2.1.4 References	61
2.1.5. NMR and HRMS of compounds	64

Part II

Supramolecular Scaffolds on Glass Slides as Sugar Based Rewritable Sensor for Bacteria

2.2 Introduction	78
2.2.1.1 Bacterial strains used	78
2.2.1.2 Synthesis of ferrocene and cyclodextrin derivatives	79
2.2.1.3 Functionalization of slide	79
2.2.1.4 Characterization of slides by SIMS-TOF and XPS	80
2.2.1.5 Bacterial Binding Assay	82
2.2.1.6 Sensitivity Study	83
2.2.1.7 Quantification by relative fluorescence unit	84
2.2.1.8 Regeneration of Slides	84
2.2.2 Conclusion	86
2.2.3 Experimental part	87
2.2.3.1 Experimental details	87
2.2.3.2 Surface Functionalization	88
2.2.3.2.1 Immobilization of ferrocene derivatives	88
2.2.3.2.2 Immobilization of cyclodextrin derivatives	
2.2.3.3 Time-of-Flight Secondary Ion Mass Spectrometer (SIMS-TOF) Characterization	88
2.2.3.4 Bacterial Strains growth	88
2.2.3.5 Bacterial detection	88
2.2.3.7 Rewriting the sugar substrate for continuous bacterial sensor	89
2.2.4 References	89

Chapter 3

Multivalent Homo and Hetero Glycodendrimers Allow Sequence Defined Carbohydrate-Protein Interactions

3.1. Introduction	99
3.2. Results and Discussion	100
3.2.1. Synthesis of tripod-active ester	100
3.2.2. One-pot glycosylation for synthesis of Mono, Di and Tri- mannose derivatives with Azido Linker	100
3.2.3. Synthesis of symmetric tripodal dendrimers of corresponding mannose derivatives	102
3.2.4. Synthesis of Hetero Glycodendrimers of Mannose and Galactose	103
3.3. Mannose glycodendrons microarray fabrication and binding experiments	103
3.4. Plant lectins binding affinity	105
3.5. Conclusions	106
3.6. Experimental Details	106
3.6.1. Glycan microarray details	132
3.6.1.1. Microarray fabrication	132
3.6.1.2. Microarray binding assay	132
3.7. References	133
3.8. NMR and HRMS of compounds	135

Chapter 4

Enantiomeric Effect of Sugar on Cellular and Bacterial Binding and Infections

4.1 Introduction	154
4.2 Result and Discussion	155
4.2.1 Synthesis of sugars	155
4.2.2 Immobilization of sugars on slides	156
4.2.3 XPS Analysis	156

4.2.4 Cell adhesion experiment1	58
4.2.5 Bacterial adhesion experiment	159
4.2.6 Bio-orthogonal reaction	160
4.2.7 Inhibition of bacterial infection	161
4.3 Conclusion	162
4.4 Experimental Section	162
4.4.1 Immobilization of sugar derivatives (1-4)	164
4.4.2. Cell-adhesion assay	169
4.4.3 Bacterial Strains growth	169
4.4.4 Bacterial detection	169
4.4.5 Parasite culture and purification of parasites	170
4.4.6 Generation of transgenic <i>T. gondii</i> expressing the reporter protein	170
4.4.7 Testing the binding of <i>T. gondii</i>	170
4.4.8 Biorthogonal reaction on HeLa cell surfaces	171
4.4.9 Inhibition assay	171
4.5. References	171

Abbreviations

abs = Absorption

ABTS = 2, 2'-azidobis(3-ethyl-benzo-thiazoline-6-sulfonic acid) diammonium salt

Ac = acetyl

AcOH = Acetic acid

AcSH = Thioacetic acid

AFM = Atomic force microscopy

AIBN = Azobisisobutyronitrile

Ar = Argon

BF₃.ET₂O = Boron trifluoride diethyl etherate

Boc = tert-Butyloxycarbonyl

Br = Bromine

bs = broad singlet

BSA = Bovine serum albumine

byp = bipyridine

CaCl₂ = Calcium chloride

Calc'd = Calculated

CD = Circular dichroism

CD₃OD = Deuterated methanol

CDCl₃ = Deuterated chloroform

CH₃ = methyl

CH₃CN = Acetonitrile

CHCl₃ = Chloroform

CHO = Chinese hamster ovary

CHOP = Nuclear transcription factor C/EBP homologous protein

CLR= C-type lectin receptor

cm = Centimeter

ConA = Concanavalin A

CrO₃ = Chromium trioxide

Cs₂CO₃ = Caesium carbonate

D₂O = Deuterium oxide

CH₂CL₂ = Dichloromethane

DC-SIGN = Dendritic cells Specific Intercellular adhesion molecule-3-Grabbing Non-integrin

deg = Degree

DFT = Density functional theory

DIC = N,N'-Diisopropylcarbodiimide

DIPEA = Diisopropylethylamine

DMAP = N,N-dimethylaminopyridine

DMEM = Dulbecco's modified eagle's medium

DMF = N,N'-Dimethylformamide

DMSO = Dimethyl sulfoxide

DNA = Deoxyribonucleic acid

EDC = 1-Ethyl-3-(3-Dimethylaminopropyl) carbodiimide

ELISA = Enzyme linked immunosorbent assay

em = Emission

eq. = equivalents

ER = Endoplasmic reticulum

ESI = Electrospray ionisation

ET = Electron transfer

et al. = and others (*et alii*)

Et₃N = Triethylamine

EtOAc = Ethylacetate

EtOH = Ethanol

FBS = Fetal bovine serum

FRET = Fluorescence resonance energy transfer

Gal = Galactose

Gg3 = Gangliosylceramide

GlcNAc = *N*-acetylglucosamine

Gly = Glycine

GM1 = Monosialotetrahexoseganglioside

GM3 = Monosialodihexosylganglioside

GNA = Galantus nivalis agglutinin

H = Hydrogen

H₂O₂ = Hydrogen peroxide

H₂SO₄ = Sulfuric acid

HEPES = (4-(2-hydroxyethyl)-1-piperazineethanesulfonic acid)

HNO₃ = Nitric acid

HOBT = Hydroxybenzotriazole

HPLC = high-performance liquid chromatography

HRMS = High resolution mass spectroscopy

HRP = Horseradish peroxidase

Hyp = Hydroxyproline

IC₅₀ = Inhibitory concentration

ICD = Induced circular dichroism

ICP-MS = Induced couple plasmon mass spectrometry

ITC = Isothermal titration calorimetry

J = Coupling constant

K = Formation constant

KSCN = Potassium isocyanate

LC = Ligand centered

m/z = Mass to charge ratio

MALDI = Matrix-assisted laser desorption ionization

Man = Mannose

MeOH = Methanol

MgSO₄ = Magnesium sulfate

MHz = Mega hertz

mL = Mille liter

MLCT = Metal to ligand charge transfer

mM = Millimolar

MS = Mass spectroscopy

MT = Mitochondria tracker

MTT = 3-(4, 5-dimethylthiazol-2-yl)-2, 5-diphenyltetrazolium bromide

Mw = Molecular weight

Na = Sodium

NaCl = Sodium chloride

NaIO₄ = Sodium periodate

NaN₃ = Sodium azide

NaOH = Sodium hydroxide

NaOMe = Sodium methoxide

ng = Nano gram

nm = Nano meter

NMR = Nuclear magnetic resonance

NOESY = Nuclear overhauser effect spectroscopy

PBS = Phosphate buffered saline

Phe = Phenylalanine

Phen = phenanthroline

PNA = Peanut agglutinin

ppm = parts per million

Pro = Proline

Py = Pyridine

q = Quadrate

QCM = Quartz crystal microbalance

QD = Quantum dots

rt = room temperature

R_f = Retardation factor

RNA = Ribonucleic acid

$RuCl_3$ = Ruthenium trichloride

s = Singlet

SD = Standard deviation

SDS = Sodium dodecyl sulfate

SEM = Scanning electron microscope

$SOCl_2$ = Thionyl chloride

SPR = Surface Plasmon resonance

STD = Saturation transfer difference

t = triplet

TEM = Transmission electron microscopy

TFA = Trifluoroacetic acid

THF = Tetrahydrofuran

TLC = Thin layer chromatography

TOF = Time of flight

TOPO = Trioctylphosphine oxide

Zn = Zinc

β -CD = Beta cyclodextrin

δ = chemical shift

μ M = Micromolar

Φ = Quantum yield

Abstract

Carbohydrates are recognized as information-rich biomolecules that play a major role in the human body. The surface of all mammalian cells is covered with carbohydrates that are attached to proteins and lipids embedded on cell membrane. The interaction with the extracellular world is achieved through interaction between these carbohydrates and carbohydrate-binding proteins (lectins) which are present on the surfaces of other mammalian cells, viruses, bacteria and bacterial toxins. To enhance the strength of cell surface binding, nature often assembles multiple protein-carbohydrate complexes to provide the necessary avidity. The effect of multivalency concerning sugars present on the surfaces compared to monovalency has been described by several investigators and was found to be of critical importance in the field of protein-carbohydrate interactions. Therefore, it is important to design a multivalent scaffold which is facile and presents non-covalent interactions. Inspired by a large number of the supramolecular assembly of adamantyl or ferrocene/ β -cyclodextrin associated complexes, I have investigated the role of host-guest interaction on interfaces and its potential biosensor applications.

Chapter 1 describes different multivalent scaffolds and surface techniques adopted to study carbohydrate-protein interactions. We highlighted the current efforts made in the synthesis of multivalent glycoprobes and the role of spatial arrangements, chirality and symmetry of these multivalent probes in carbohydrate-protein interactions. Finally, we also highlighted the recent label free techniques adopted to characterize carbohydrate-protein interactions.

Chapter 2 summarizes non-covalent host-guest strategy to immobilize heptavalent glyco- β -cyclodextrin on gold-coated glass slides to study multivalent carbohydrate-protein interactions. We have found that the localization of sugar entities on surfaces using β -cyclodextrin (**β -CD**) chemistry increased the avidity of carbohydrate-protein and carbohydrate-macrophage interactions compared to monovalent- **β -CD** sugar coated surfaces. Furthermore, the sugar functionalized β -Cyclodextrin-ferrocene glass slides were used to develop fully reversible bacterial biosensors. The prototype D-mannose - *E. coli* ORN 178, L-fucose - *P. Aeruginosa*- D-galactose interactions serve as a model to illustrate the new approach.

Chapter 3 deals with the synthesis of homo and heteromultivalent mono and oligomannose glycodendrons and their binding to a series of plant and animal lectins to understand specific factors influencing CPIs. Multivalency, heterogeneity and oligosaccharide have been successfully

adopted to increase the avidity of CPIs. However, there is still a lot of unanswered questions about whether these factors, are optional or obligatory to design the glycoclusters. Our microarray results clearly showed that each lectin displayed its own set of binding preferences. In case of ConA and PNA lectins, oligosaccharides multivalency is more important than heterogeneity. While GNA and galactin lectins displayed heterogeneity of the glycodendrons as critical factor for better CPIs. Overall these results demonstrate that each lectin possess its own set of rules for CPIs and difficult to be rationalized.

Chapter 4 demonstrates the inherent chirality of the sugar as one of the promising factors to generate bacterial recognition. We have shown that while D/L-enantiomers of α -mannose and β -galactose reveal significant differences in the recognition of bacteria (*E. coli*) and pathogen (*Toxoplasma gondii*), cell-adhesion and cell-proliferation were barely influenced by the two configurations. Finally, we have used bioorthogonal conjugation techniques to bind D/L-mannose enantiomers on HeLa cell surfaces and exploited the difference in cellular and bacterial binding recognition of the two molecules to prevent bacterial-cell infection.

Publications

1. Suraj Toraskar, **Madhuri Gade**, Sivakoti Sangabathuni, Hirekodathakallu V. Thulasiram, Raghavendra Kikkeri, Exploring the Influence of Shapes and Heterogeneity of Glyco-Gold Nanoparticles on Bacterial-Binding for Preventing Infections, June 2017. *ChemMedChem*, 12, 1116, June 2017.
2. Harikrishna Bavireddi, Raghavendra Vasudeva Murthy, **Madhuri Gade**, Sivakoti Sangabathuni, Catherine Alex, Preeti Madhukar Chaudhary, Raghavendra Kikkeri, Deciphering Carbohydrate-Protein Interactions using Homologous Supramolecular Chiral Ru(II)-Glyconanoclusters, *Nanoscale*, 8, 19696, October, 2016.
3. Harikrishna Bavireddi, Raghavendra Vasudeva Murthy, **Madhuri Gade**, Raghavendra Kikkeri, Supramolecular Metallo-glycodendrimers Selectively Modulate Lectin Binding and Delivery of Ru(II) Complex into Mammalian Cells, *Org. Biomol.Chem.*, 14, 10819, September, 2016.
4. Raghavendra Vasudeva Murthy, Priya Bharate, **Madhuri Gade**, Sivakoti Sangabathuni, Raghavendra Kikkeri, Effect of Transition Metals on Polysialic Acid Structure and Functions, *ChemMedChem*, 11, 667, April, 2016.
5. Preeti Madhukar Chaudhari, **Madhuri Gade**, Rina Arad-Yellin, Sivakoti Sangabathuni, Raghavendra Kikkeri, Targeting label free carbohydrate-protein interactions for biosensor design, *Analytical Methods*, 8, 3410, March, 2016.
6. **Madhuri Gade**, Puneet Khandelwal, Sivakoti Sangabathuni, Harikrishna Bavireddi, Raghavendra Vasudeva Murthy, Pankaj Poddar, Raghavendra Kikkeri, Immobilization of Multivalent Glycoprobes on Gold Surfaces For Sensing Proteins and Macrophages, *Analyst*, 141, 2250, February, 2016.
7. **Madhuri Gade**, Ajay Paul, Catherine Alex, Devika Choudhury, Hirekodathakallu V. Thulasiram, Raghavendra Kikkeri, Supramolecular Scaffolds on Glass Slides as Sugar Based Rewritable Sensor for Bacteria, *Chem. Commun.* 51, 6346, March, 2015.
8. Raghavendra Vasudeva Murthy, Harikrishna Bavireddi, **Madhuri Gade**, Raghavendra Kikkeri, Exploiting the Lactose-GM3 Interaction for Drug Delivery, *ChemMedChem*, 10, 792, March, 2015.

Chapter 1

Carbohydrates-Protein Interactions

1.1. Introduction

The human glycomic system consists of nine sugar codes responsible for over million glycan sequences and generates vast types of glycoproteins that play vital roles in many physiological and pathological functions.¹⁻³ Oligosaccharides, present on cell surfaces, regulate the interactions of cells with other cells, with the extracellular matrix and with effector molecules. Glycoproteins control and modulate the activity of carbohydrate receptors, especially those of cytokines and growth factors. Understanding the variation in glycosylation functions and interactions is pivotal for unraveling many puzzles in life sciences.⁴⁻⁵ Due to the structural complexity of glycans and to technological limitations, understanding the functional importance of glycans significantly lags behind the knowledge of DNA and proteins in spite of the remarkable progress in the field of glycomics that took place during the past 10 years and the new innovative technologies for identification and measurement of carbohydrate-protein interactions (CPIs).^{6,7} This chapter gives an overview of lectins and the synthesis of various multivalent glycoclusters, followed by their recognition properties toward diverse carbohydrates-binding proteins through label-free techniques.

1.2. Carbohydrate Binding Proteins

Interaction between various cell surface receptors and glycans occur through specific proteins called lectins.⁹ Lectins were discovered hundred years ago. Initially it was found only in plants, but now it known that animals, virus, bacteria also biosynthesize and express them on the cell surfaces. Lectins are divided in to various types according to their origin, namely plant lectins, bacterial lectins, animal lectin, and viral lectins.¹⁰ Here I will be discussing lectins that binds to simple sugars such as mannose, galactose and glucose.

1.2.1. Plant Lectins

1.2.1.1. Concanavalin A (ConA)

James B. Sumner from Cornell University isolated Concanavalin A (ConA) from Jack beans (*Canavalia ensiformis*).¹¹ ConA is homotetrameric lectin, with each monomer composed of 237 amino acids. Each monomer has identical monosaccharide binding sites. ConA exists as a dimer at pH less than 6 whereas at pH 7 and above, it exists as a tetramer. Initially it was known that ConA agglutinates various cells like erythrocytes, lymphocytes, various somatic and germ line cells. Further, it was found that it binds specifically to D-glucopyranosides and D-mannopyranosides.¹² Metal ions Ca^{2+} and Mn^{2+} are necessary for folding of ConA in its native

structure. Previous studies showed that removal of metal ions loses its binding ability with sugars, even though these metal ions are not directly interacting with carbohydrates. Metal ions help in structural stability and saccharide binding ability of ConA.¹³

1.2.1.2. GNA (Galanthus Nivalis Agglutinin)

GNA is isolated from Galanthus Nivalis (snowdrop bulbs). It has four identical subunits with molecular weight 50 kDa. GNA doesn't have the ability to agglutinate human erythrocytes, but it agglutinates rabbit erythrocytes.¹⁴ Unlike ConA, GNA binds utterly with D-mannose.¹⁵

1.2.1.3. PNA (Peanut agglutinin)

PNA is a plant lectin isolated from *Arachis hypogaea*. It has 4 identical subunits having 273 amino acid with a molecular weight of 110 kDa¹⁶. It binds specifically to D-galactose.¹⁷

1.2.2. Bacterial lectins

1.2.2.1. FimH Lectin

Bacterial lectins are found on the surface of the bacteria that bind to matching carbohydrates structures on the surface of the host cell. Bacterial lectins are present on the elongated sub microscopic protein appendages, known as fimbriae or pili. The fimbriae are 1–2 μm long and 7 nm thick fibres.¹⁸ Various bacteria such as *Escherichia coli* (*E. coli* ORN 178) and *Klebsiella pneumoniae*, *Salmonella enterica serovar typhimurium* (*S. typhimurium*) express different types of fimbriae.¹⁹ Most *E. coli* highly express type 1 fimbriae all over the bacterial surface. (Fig.1) FimH is the bacterial lectin present at the tip of type 1 fimbriae. Molecular weight of FimH is 29-31 kDa, which is binding specifically to the D-mannose and N-linked high-mannose structures.²⁰ FimH has two domains: one is responsible for binding with mannose and another amino terminal which links adhesion to the pilus.²¹ Single monomer of mannose is accommodated a binding pocket of FimH by hydrophobic interactions and hydrogen bonding.²²

1.2.2.2. Pseudomonas aeruginosa (PA) PA II Lectin

Pseudomonas aeruginosa (PA) is an opportunistic gram-negative pathogen. PA has two lectins on their surface PA-IL and PA-IIL that bind selectively to galactose and fucose, respectively.²³

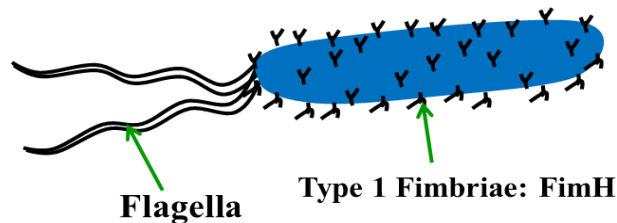


Figure 1 Common structure and position of bacterial fimbriae and flagella

Molecular weight of PA-IL is 51 kDa and is composed of four subunits of 121 amino acids. PA-IIL (47 kDa), composed of four subunits containing 114 amino acids.²⁴ PA-IIL lectin is tetramer with four independent subunits each of them containing two Ca^{2+} and fucose is sitting on two Ca^{2+} , these is unique among the carbohydrate protein interactions (CPIs).²⁵

1.2.3. Animal Lectins

1.2.3.1. C-type lectins

C-type lectins are the largest family of lectins found in animals.²⁶ C-type lectins are found solely on dendritic cells (DCs). These lectins bind to carbohydrates in a calcium dependant manner and hence the name. Ca^{2+} acts as a bridge between monosaccharides and carbohydrate recognition domain (CDR) (Fig.2). Amino acid residues of the CDR offer six-coordinate bonds for a Ca^{2+} ion and the carbohydrate donates two-coordinate bonds with its hydroxyls, so that the Ca^{2+} ion is octacoordinated²⁷. DC-SIGN, (Dendritic Cell-Specific Intercellular adhesion molecule-3-Grabbing Non-integrin) is a type II C-type lectin that functions as an adhesion molecule. They are very important lectins for normal functioning of immune system. C-type lectins were found to bind HIV envelope glycoprotein gp-120 protein.²⁸ It also enhances other pathogens like Ebola infection to T-cells.²⁹ Some of the C-type lectins dimerizes or oligomerize to increase the affinity.³⁰

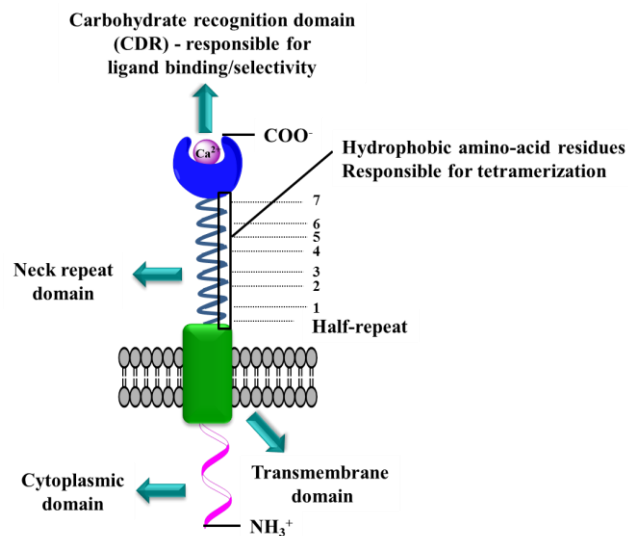


Figure 2 ³⁰DC-SIGN schematic structure

Depending on the molecular structure of C-type lectins, they are classified into 17 groups.¹⁰ Most of the group have single carbohydrate recognition domain which include Dectin-1, Dectin-2 and macrophage-inducible C-type lectin (Mincle), Dendritic cell-specific intercellular adhesion molecule-3-grabbing non-integrin (DC-SIGN), and DC-NK lectin group receptor-1 (DNKR-1)

and the macrophage mannose receptor (MMR) consists of several CDR domains. Dectin-1 binds specifically to β -glucans carbohydrates present in cell-wall of fungi³¹. Dectin-2 binds high mannose glycan and it induces cytokine production.³¹ Mincle is a member of Dectin-2 and recognizes α -mannose.³² DC-SIGN binds to various mannosylated envelope glycoproteins of various viruses like HIV-1, Ebola and dengue virus.

1.2.4. Lectins on Pathogen

1.2.4.1. TgMIC4

Toxoplasma gondii is an intracellular parasite of the phylum Apicomplexan, the causative agent of toxoplasmosis.³³ This parasite has *Toxoplasma gondii* microneme protein (TgMIC4) lectin on their surface, which has specificity for galactose terminating oligosaccharides.³⁴

1.3. Multivalent carbohydrate-protein interactions

Even though carbohydrate-protein interactions (CPIs) are essential in many biological processes, individual interactions between monomeric ligand and single binding site has weak binding affinities in the μM to mM range also exhibit low selectivity. Many biological systems choose multivalency as a key principle for strong binding interactions^{35,36} (Fig.3). Multiple carbohydrate ligand attached to the glycoprotein with proper orientation and spacing enhanced the overdoing interactions.⁹ Stable binding occurs carbohydrates on the cell surface and a receptor with multiple carbohydrate binding sites. Inspired by nature, over the past 20 years different groups developed many elegant probes for mimicking the multivalency using glycopolymer,³⁷ glycodendrimers,³⁸ glycopeptides,³⁶ glycoliposomes³⁹ and glyco-goldnanoparticles⁴⁰ (Fig. 4).

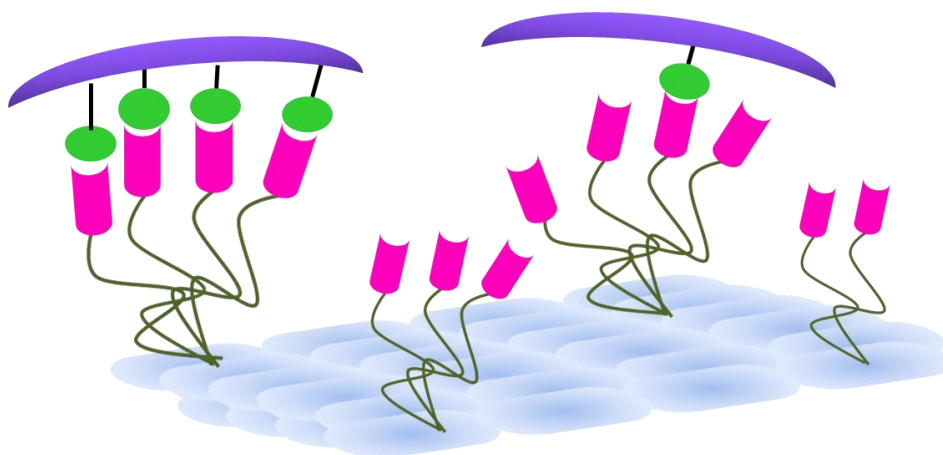


Figure 3 Schematic representation of monovalent vs multivalent carbohydrate protein interactions.

1.3.1. Glycopolymer

Glycopolymer are synthesized polymer with overhanging of carbohydrate ligand. Much development in polymerization process enables the mimicking of cell surface glycans. The properties of multivalent carbohydrate derivatives (their ability to exhibit high functional affinity and increased specificity) have stimulated the development of methods to synthesize defined multivalent carbohydrate derivatives, including polymers bearing pendant carbohydrates (glycopolymer). According to the need we can vary carbohydrate ligand density and spacing among the group.³⁷

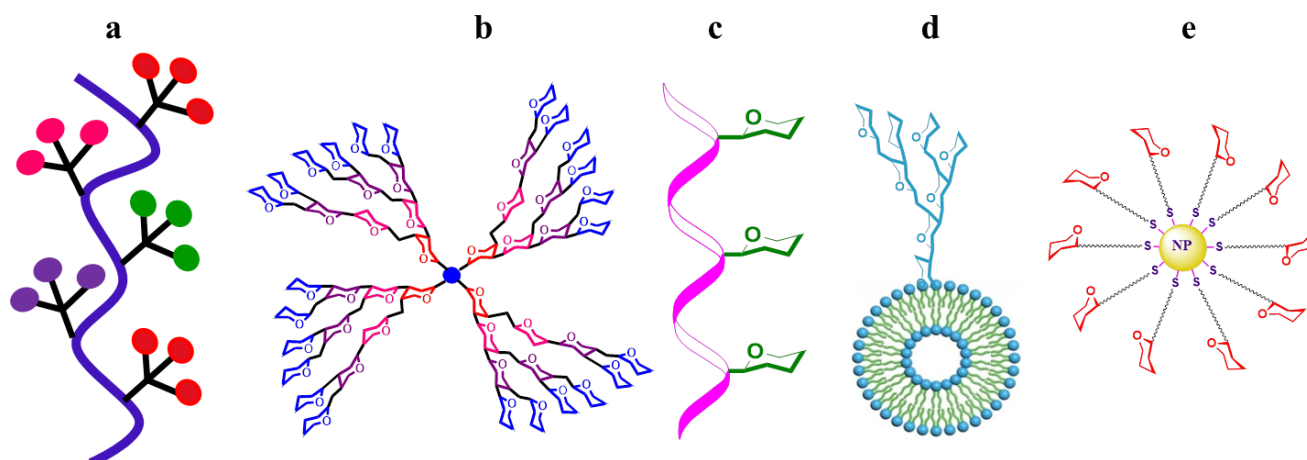


Figure 4 Carbohydrate based multivalent probes: (a) glyco-polymers; (b) glyco-dendrimers; (c) glyco-peptides; (d) glyco-liposomes; (e) glyco gold-nanoparticles.

Nicolas Winssinger and co-workers synthesized glycopolymer using peptide nucleic acids (PNAs) backbone and displayed high mannose oligosaccharides on it. Spacing of oligosaccharide varied on PNAs. Mannosylated PNA hybridizes with DNA strand. Since 2G12 antibody is known to neutralize HIV (gp120), they tested development of antibody against HIV. Author observed spacing is playing important role in antibody production.⁴¹ Shyam M. Rele et al synthesized 1st and 2nd generation dendrimers like PEO sulphated glycopolymer with β -lactose (Fig.5) which serves as L-selectin inhibitors.⁴² Author proved that synthesized heparinoid mimics show anti-inflammatory activity *in vivo*.

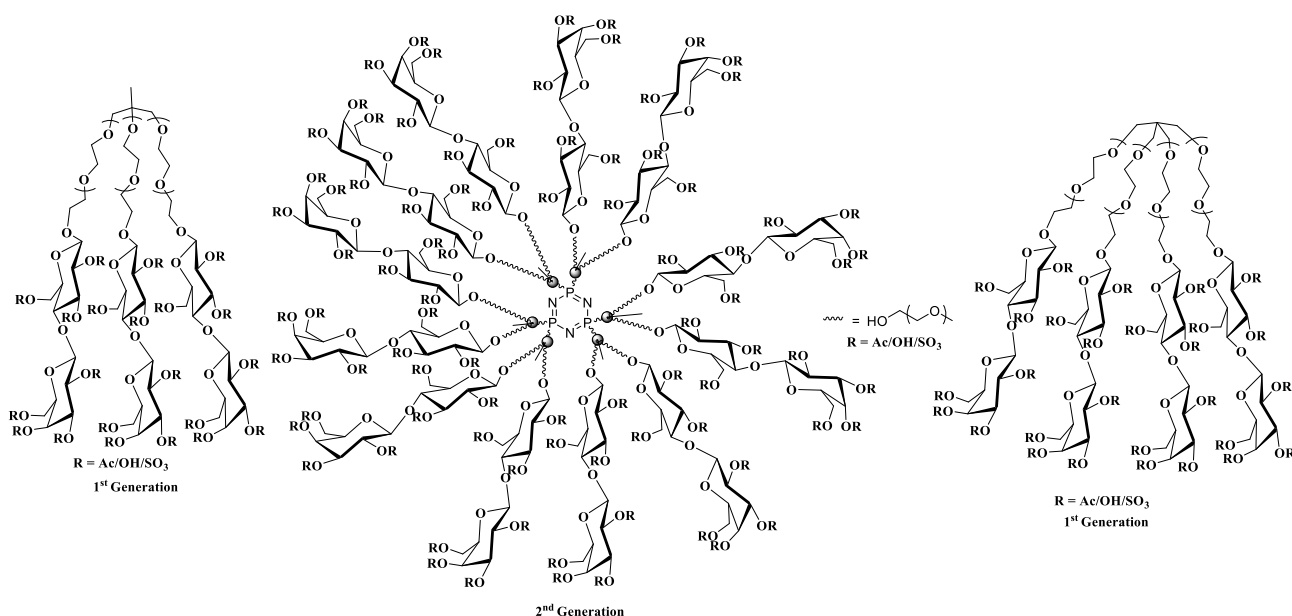


Figure 5 Structures of 1st and 2nd generation dendrimer like PEO sulphated glycopolymer with β lactose

1.3.2. Glycodendrimer

Dendrimers are highly branched structures and are also called globular molecule or cascade molecule. Exterior groups are saccharide in case of glycodendrimers. Glycodendrimers afford many budding application.^{35,38,43} Glycodendrimers are classified as carbohydrate-coated, carbohydrate-centred and carbohydrate-based and can be synthesized using two strategies, convergent and linear. J. Fraser Stoddart and co-workers synthesized dendrimer based poly(propylene imine) dendrimers (Fig.6).⁴⁴ D-galactose and lactose are attached to the primary amino group of DAB-dendr-(NH₂)_x by amide bond formation.

Galactose and lactose were protected with acetate to prevent unwanted reaction. Carbohydrate coated five generations of dendrimers has been synthesized. Synthesized glycodendrimers were characterized by NMR and mass spectroscopy. Author mentioned that these neoglycoconjugates with symmetrical structures offer ligands for carbohydrate protein interactions. Roy and co-workers synthesized glycodendrimers with T-antigen (Gal(β1-3)αGalNAc) using allyl glycosides which showing strong binding to monoclonal IgG antibodies and can be used in specific cancer cell targeting.

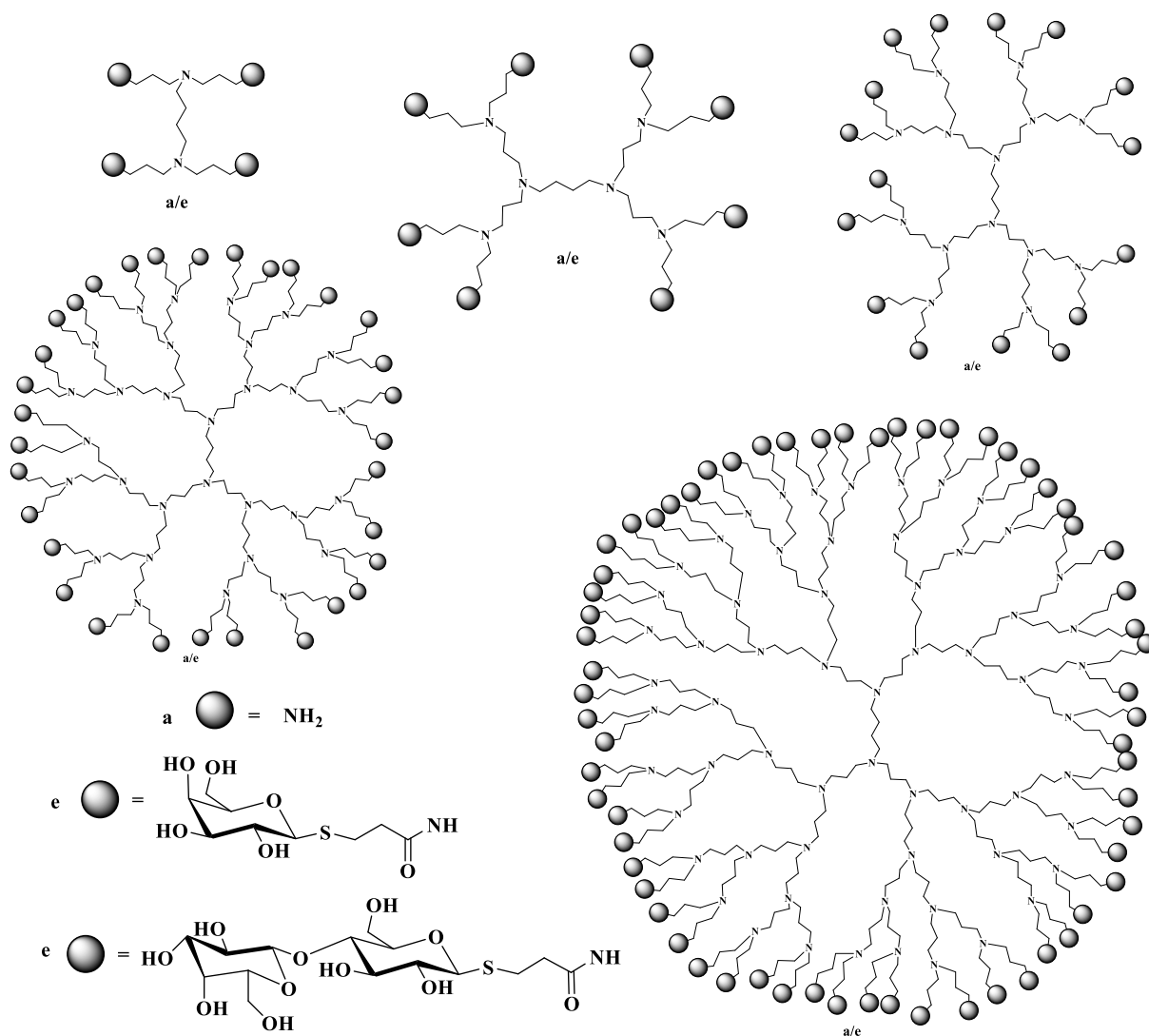


Figure 6 Schematic representations of Poly- (propylene imine) dendrimers with D-galactose and lactose.

1.3.3. Glyco-peptide

In glyco-peptides, saccharides are conjugated to the peptide backbone. Advancement in synthesis of peptide using both solid phase and solution phase make it easier to synthesize glycopeptides with varying backbone and spacing. We can mimic glycoproteins by *N*-linked, *O*-linked and *C*-linked glycopeptides.³⁶ Ulrich Sprengard et al synthesized the cyclic N-glycopeptides containing three asparagine-linked sialyl Lewis^x tetra saccharides.⁴⁵ The trivalent glycopeptide was synthesized using solid phase peptide synthesis strategy (Fig. 7). Author utilized synthesized cyclic glycopeptides for targeting E-selectin binding affinity. Trivalent cyclic glycopeptides showed strong inhibition of E-selectin mediated binding to HI-60 cells with IC₅₀ 0.35-0.6 mM, which is two to three times stronger than monomeric sialyl lewis^x.

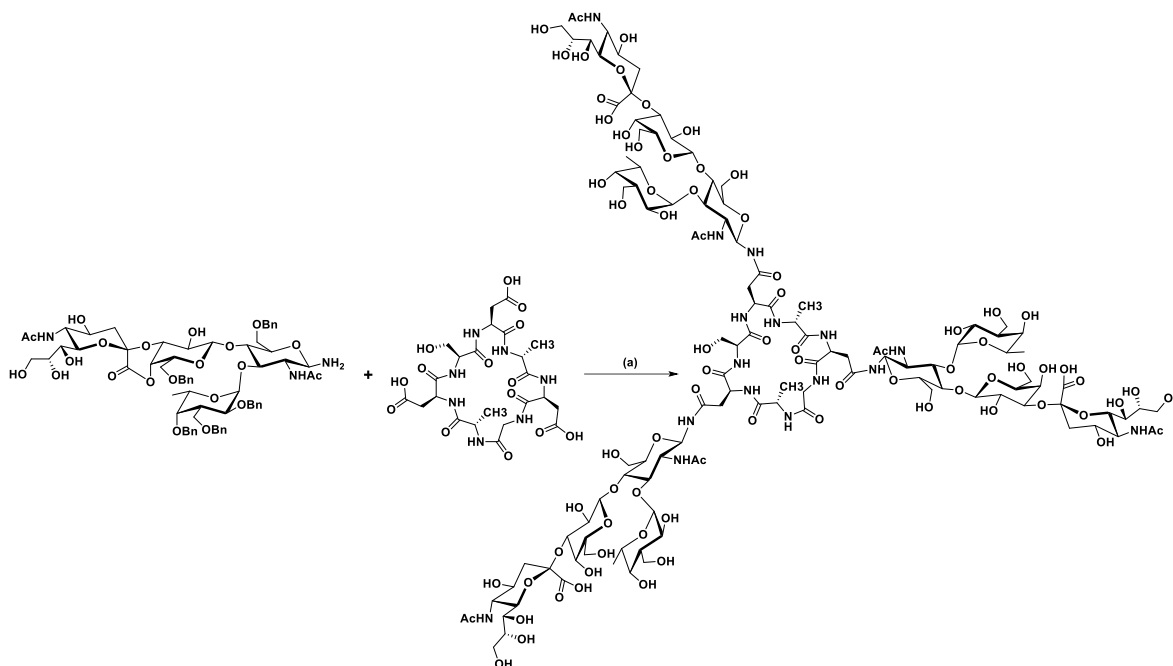


Figure 7 C₃-symmetry arrangement of sialyl lewis^x conjugated glycodendrimers

Kiick and co-worker synthesized glyco-polypeptide based glycopolymer with poly (L-glutamic acid) backbone where the author used galactose as a pendant carbohydrate and varied density and linker length.⁴⁶ These neoglycopeptides are used for inhibition of cholera toxin using competitive enzyme-linked immunosorbent assay and fluorescence titration experiments. Decrease in distance between two galactose moieties decreases inhibitory activity of Cholera toxin. Increasing in the length and hydrophobicity increases inhibitory activity.

1.3.4. Glycoliposomes

Glycoliposomes are having hydrophilic sugar segment and hydrophobic alkyl chain.

Size and shape of the liposomes vary with concentration of monomer and steric repulsion between sugar head. Exposed sugar density on surface can be tuned according to alkyl chain length.³⁹

Shawn A DeFrees and co-workers synthesized glycoliposomes with sialyl lewis^x-PEG-DSPE (PEG, poly(ethylene glycol)DSPE, distearoylphosphatidylethanolamine) derivative and formed liposomes were utilized for inhibition of E-selectin mediated cell adhesion using ELISA and it was found that liposomal oligosaccharide was 750 fold more potent compared to nonliposomal oligosaccharide and 5000 fold more compared to natural glycotope.⁴⁷ Yoichiro Harada et al prepared glycoliposomes from lactosyl- and N-acetyl-lactosaminyl-phospholipids as a mimic of naturally occurring lactosylceramide glycolipid (Fig. 8).⁴⁸ With formed liposomes lectin binding

assay was performed using fluorescently labelled Ricinus communis agglutinin; which showed binding in nanogram concentration.

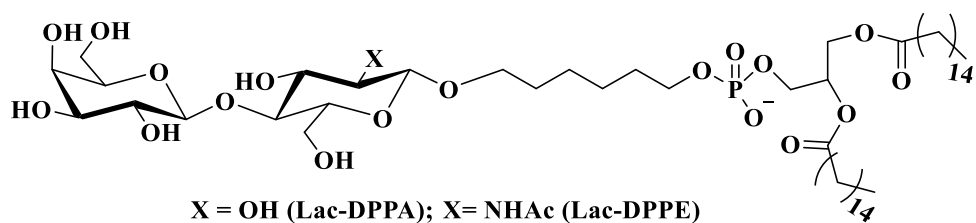


Figure 8 Structure of lactose and N-acetyl-lactosamine containing phospholipids.

Xue-long Sun et al synthesized glycoliposomes with sialic acid and used it for the inhibition of influenza virus proteins hemagglutinin and neuraminidase.⁴⁹ Distearoylphosphatidylethanolamine (DSPE) conjugated sialic acid showed stronger binding affinity with influenza compared to monomeric sialic acid.

1.3.5. Glyco-goldnanoparticle

Gold nanoparticles have unique physical properties. They shift their surface plasmon peak between the dispersed and aggregated state, which can be observed by the naked eye and can be used to develop calorimetric sensors. Nanoparticles can be prepared in various size and shape by controlling the conditions. Nanoparticles with various shapes like spheres, rods, star, cluster, cube, branched with size is in the range of 1-100 nm can be prepared. Characterization is easy using UV-visible and transmission electron microscopy.^{40,50,51} Glyconanoparticles have extensive applications in carbohydrate protein interactions (CPIs) and *in vivo* cell imaging and biolabeling. Soledad Penades in 2001, first functionalized goldnanoparticle with oligosaccharides and named it as glyconanoparticles.⁵² Penades and co-workers synthesized neoglycoconjugates with disaccharide lactose (Gal- β -(1 \rightarrow 4)-Glc- β -1-OR) and the trisaccharide LeX (Gal- β -(1 \rightarrow 4)-[Fuc- α -(1 \rightarrow 3)]-GlcNAc- β -1-OR) and functionalized it with gold nanoparticle by Au-sulphur covalent bond. Conjugated glycogoldnanoparticles were characterized by ¹H NMR, UV/Vis, FT-infrared (IR) spectroscopy, elemental analysis, and transmission electron microscopy (TEM).

Yen-Jun Chuang et al prepared gold glyconanoparticles using microwave irradiation energy in one step. Gold nanoparticles are modified with hydrazide and conjugated unmodified carbohydrates. Carbohydrate protein interactions were studied using calorimetric assay.⁵³

Recently in Kikkeri group synthesized a library of different shapes of glyco-gold nanoparticle (Fig. 9) and utilized it as a tool for cellular uptake. ELISA assay revealed that selectivity and sensitivity not only depends on sugars composition but also on shape of the gold nanoparticle. *In vitro* and *in vivo* experiments showed that rod shaped glyco-goldnanoparticles have high affinity as compared to the star and sphere. Mechanistic study showed that glyco-goldnanoparticles were internalized by clathrin mediated endocytosis pathway.⁴⁰

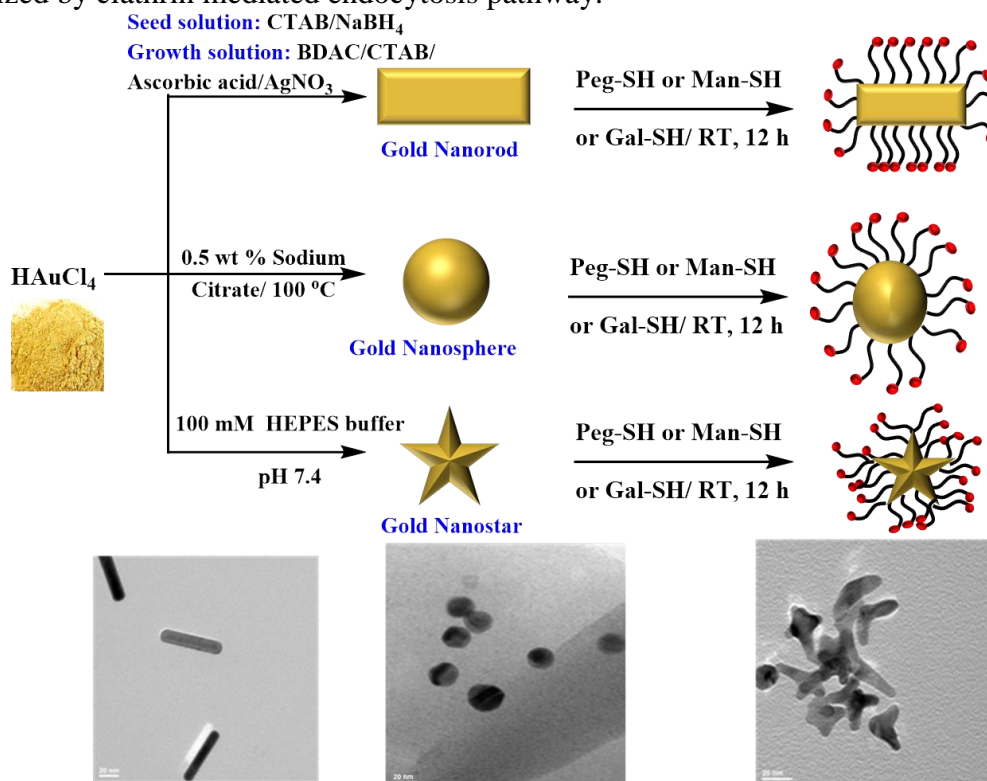


Figure 9 Synthesis of gold-nanoparticles and glyco-gold-goldnanoparticle (G-AuNPs)

1.4. Cyclodextrins as multivalent probe

As explained above the importance of multivalency in carbohydrate-protein interactions we choose cyclodextrin (CD) as a multivalent probe to study multivalent interactions. Cyclodextrins are naturally occurring oligosaccharides also known as cycloamyloses, cyclomaltoses or Schardinger dextrans made up of D-glucose connected by α -1-4 linkages.⁵⁴ Cyclodextrins were discovered by Villiers from France in 1891, he named it as Cellulosine because of its similar behaviour with cellulose. Whatever cyclodextrins (CDs) that was used by Villiers was impure. In 1903, after 10 years, Schardinger, an Austrian microbiologist was able to isolate two CDs. In

1911, Schardinger described that the bacterial strain *Bacillus macerans* could produce cyclodextrin, later many fractionation technique were developed to produce cyclodextrins. Most commonly observed subtypes of cyclodextrins are α -cyclodextrins (α -CD), β -cyclodextrins (β -CD) and γ -cyclodextrins (γ -CD) and they have 6, 7, 8 D-glucose units respectively (Fig. 10).⁵⁵ Three-dimensional structure of CDs is cone shaped. Primary hydroxyl groups are located at narrow side and secondary hydroxyl groups are at wider side of cone which is making hydrophobic cavity inside (Fig. 10).

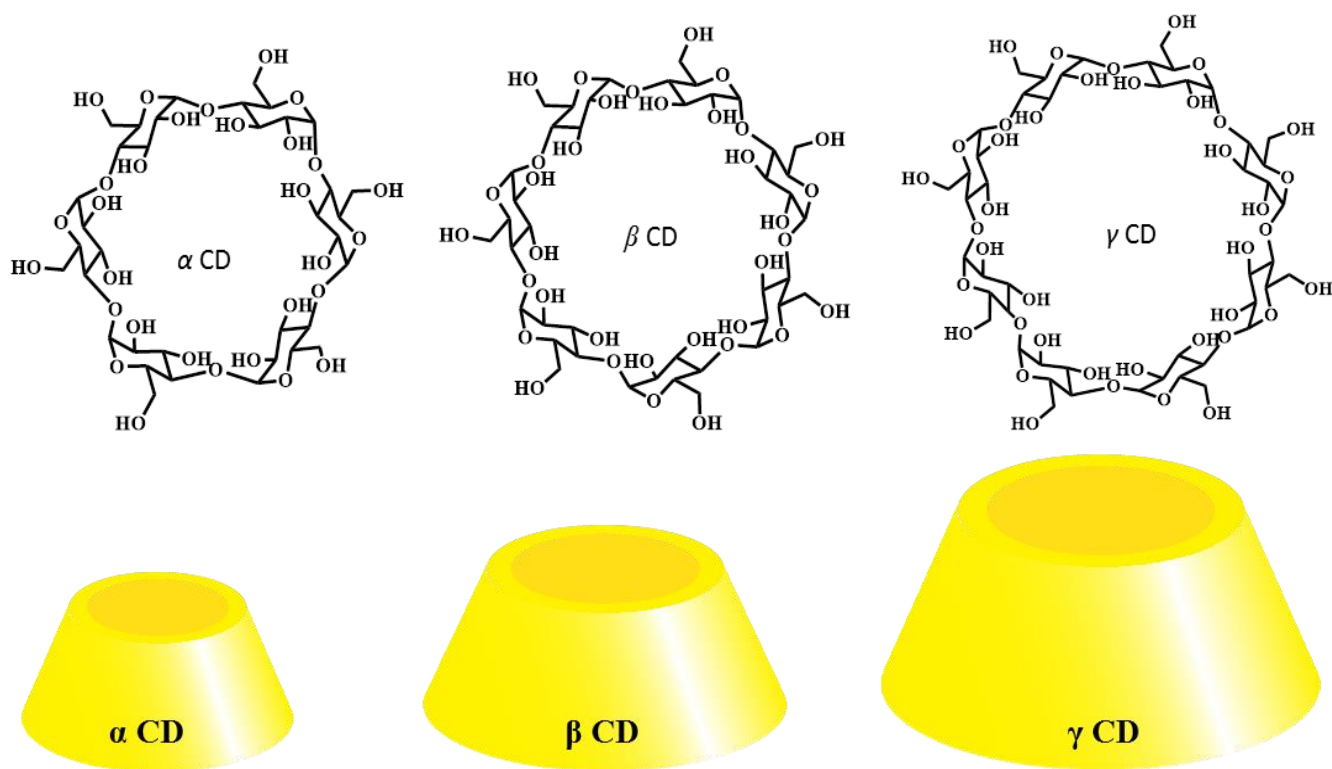


Figure 10 Structures of subtypes of cyclodextrins

Inner cavity of α -CD is 0.57 nm, β -CD is 0.78 nm and γ -CD is 0.95 nm. CDs can accommodate guests of suitable size even polymers inside its hydrophobic cavity (Fig. 11). Forces involved in formation of host guest inclusion complexes are Van der Waals, hydrophobic interactions and hydrogen bonding.⁵⁶

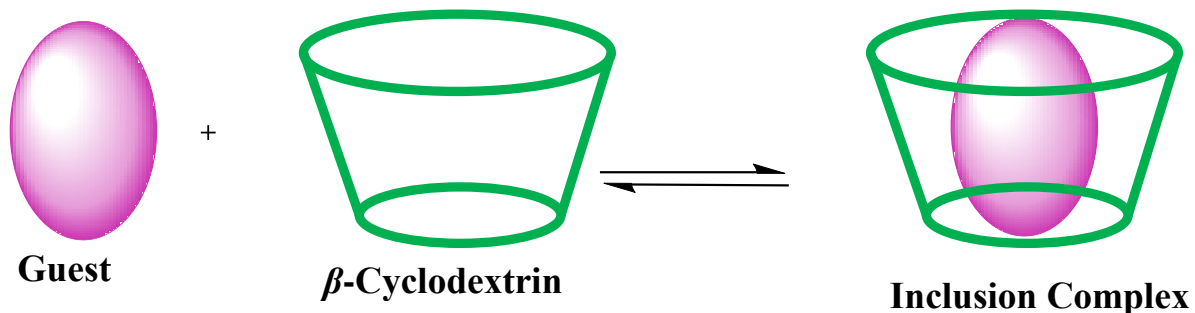


Figure 11 Schematic representation of inclusion complex (host –guest complex) formation (1:1) between CD and a guest molecule.

CD has two reactive domains; first is the various glycan structure displayed and second is property of inclusion complex formation and hence CDs are used in pharmaceutical science,⁵⁷ analytical science,⁵⁸ catalysis,⁵⁹ cosmetics,⁶⁰ textiles,⁶¹ packaging industries⁶² and also for gene delivery.⁶³ Among all three subtypes β CD is used most because of inner cavity size is appropriate for forming 1:1 complex with guest molecule.

Bart Jan Ravoo and co-worker synthesized amphiphilic β -cyclodextrin and adamantane conjugated to lactose and maltose. Amphiphilic β -cyclodextrin is forms vesicle and after mixing with sugar functionalized adamantane, it forms host-guest complexation. They observed that maltose decorated vesicles of β -cyclodextrin is aggregated in case of ConA whereas lactose-decorated vesicles aggregated in the presence of PNA. Lectin binding study was done using optical density measurement at 400 nm.⁶⁴ Kikkeri group was able to synthesized host guest complexes between β -CD and trioctylphosphine oxide (TOPO) on quantum dots; this assembly was characterized by FT-IR, ¹H-NOESY NMR spectroscopy and TEM and carbohydrate protein interactions (CPIs) were studied using colloidal aggregation with ConA, GNA and PNA lectins. *In vitro* studies indicated that β -CD modification of QDs enabled good cell viability of human hepatocellular carcinoma cell line (HepG2). Flow cytometry and confocal imaging studies revealed that β -CD galactose capped QDs undergo preferential binding with HepG2 cells. These results clearly demonstrated that β -CD capped QDs could be a promising candidate for further carbohydrate-based biomedical applications.⁶⁵

1.5. Heterogeneity

As explained in above section, multivalency is important in carbohydrate protein interactions (CPIs). But along with multivalency arrangement of carbohydrate do play important role in CPIs.

However, nature exhibit inherent heterogeneity in biological systems. To understand the role of heterogeneity in molecular recognition, various groups have synthesized homoglycans and heteroglycans displaying different saccharides.⁶⁶ The exposure of particular sugar on the surface is expected to be affected by amount and location of neighbouring sugars and this directly affects the binding with various receptors.⁶⁷ Jose´ M. Garcia Fernandez synthesized 21-antennary heteroglycoclusters using D-mannose, D-glucose and lactose on core β -cyclodextrin. Binding affinity was studied with ConA using enzyme linked lectin assay (ELLA). The mixed-type heteroglycoclusters showed more binding to ConA compared to homo-glycoclusters which have less number of binding sugars.⁶⁸ Laura Hartmann synthesized heteromultivalent and homomultivalent oligomers with D-mannose, D-glucose and D-galactose by sequential click reaction on solid support (Fig. 12). They varied number, spacing, position, and type of sugar ligands. All hetero-oligomers were found to have high affinities compared to homo-oligomers. Galactose is non-binding sugar but it promotes steric shielding of hetero-oligomers and results in increase in binding affinity.⁶⁹ Lindhorst in 2002 synthesized mixed glycoclusters or hetero glycoclusters where they derivatized D-galactopyranose with different sugar series like α -D-mannose, α -L-fucose and β -lactose. Different sugars were added by sequentially activating amine or carboxylic acid group resulting in the formation of amide or thiourea.⁷⁰

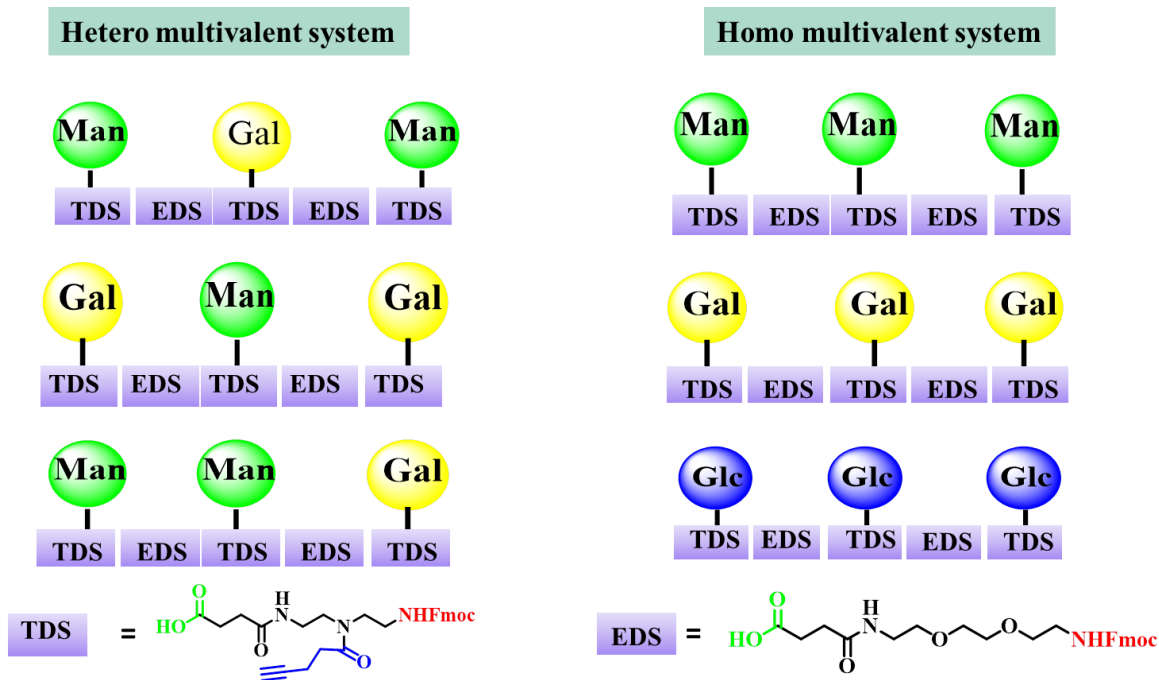


Figure 12 List of hetero-multivalent and homo-multivalent systems used for lectin binding assay

They explored anti-adhesive property of mixed glycoclusters with mannose specific bacterial lectin FimH. However, assay did not show significant inhibition as compared to methyl D-mannopyranosides.⁷¹

Blanco and co-workers synthesized high and low density homo- and hetero-glycoclusters and checked binding of glycoconjugates with ConA using enzyme-linked lectin assays (ELLA), isothermal titration micro calorimetry (ITC) and surface plasmon resonance (SPR). High density glycoclusters showed increase in binding with ConA compared to low-density glycoclusters. Effect of non-binding sugars was irrelevant.⁷²

1.6. Chirality

Along with multivalency and heterogeneity one more factor affecting CPIs is chirality. Chirality exists in biological system. During evolution, nature selected the L-amino acids as building blocks of life and D-sugars as components of DNA and RNA and on cell surfaces. Nermin Seda Kehr demonstrated use of enantiomerically functionalized periodic mesoporous organosilicon (PMO) and generated 3D nanocomposite hydrogels. Interaction between functionalized enantiomer on PMO and cells were described. HeLa and 3T3 cells were seeded on D- and L-mannose PMO for 1 day and then 4 days then cells were counted. The results showed quantity of cell adhesion was different on enantiomeric PMO.⁷³

Kikkeri group has synthesized distinct series of metalloglycodendrimers (MGDs).⁷⁴ They synthesized 1st ligand, where D- and L- alanine adamantyl group was linked to the 4,4'-bipyridine by amide bond. Racemic and D- and L- alanine adamantyl linked ligands were mixed with RuCl₃ in ethanol and refluxed to produce metal complexes, where it is forming two diastereomers of Ru complexes Δ -Ru(II) and Λ -Ru(II) which was confirmed by circular dichroism.

Chiral mannosylated β -CD derivatives were synthesized. Ru (II) complexes having adamantyl core were complexed with β -cyclodextrin (β -CD) derivatives by mixing stoichiometric amounts (1 : 6) thereby yielding a library of metalloglycodendrimers (M1-M12 fig. 13). Formation of metalloglycodendrimers were characterized by circular dichroism, NMR and host-guest complexation by ESI-MS (soft ionization). Binding activity of MGDs were checked with mannose specific C-type lectins (h-DC-SIGN-Fc, m-SIGNR3-Fc), Dectin-1-Fc and plant lectins (ConA and PNA). ConA and Dectin-1-Fc showed an approximately 1.5 fold binding difference between Δ & Λ -complexes and a nearly 10-fold difference compared to DC-SIGN-Fc and no

binding to PNA lectin. Finally, the optical properties of the Ru(II) complexes were exploited to track cell uptake (Fig. 13) *in vitro* and *in vivo*.

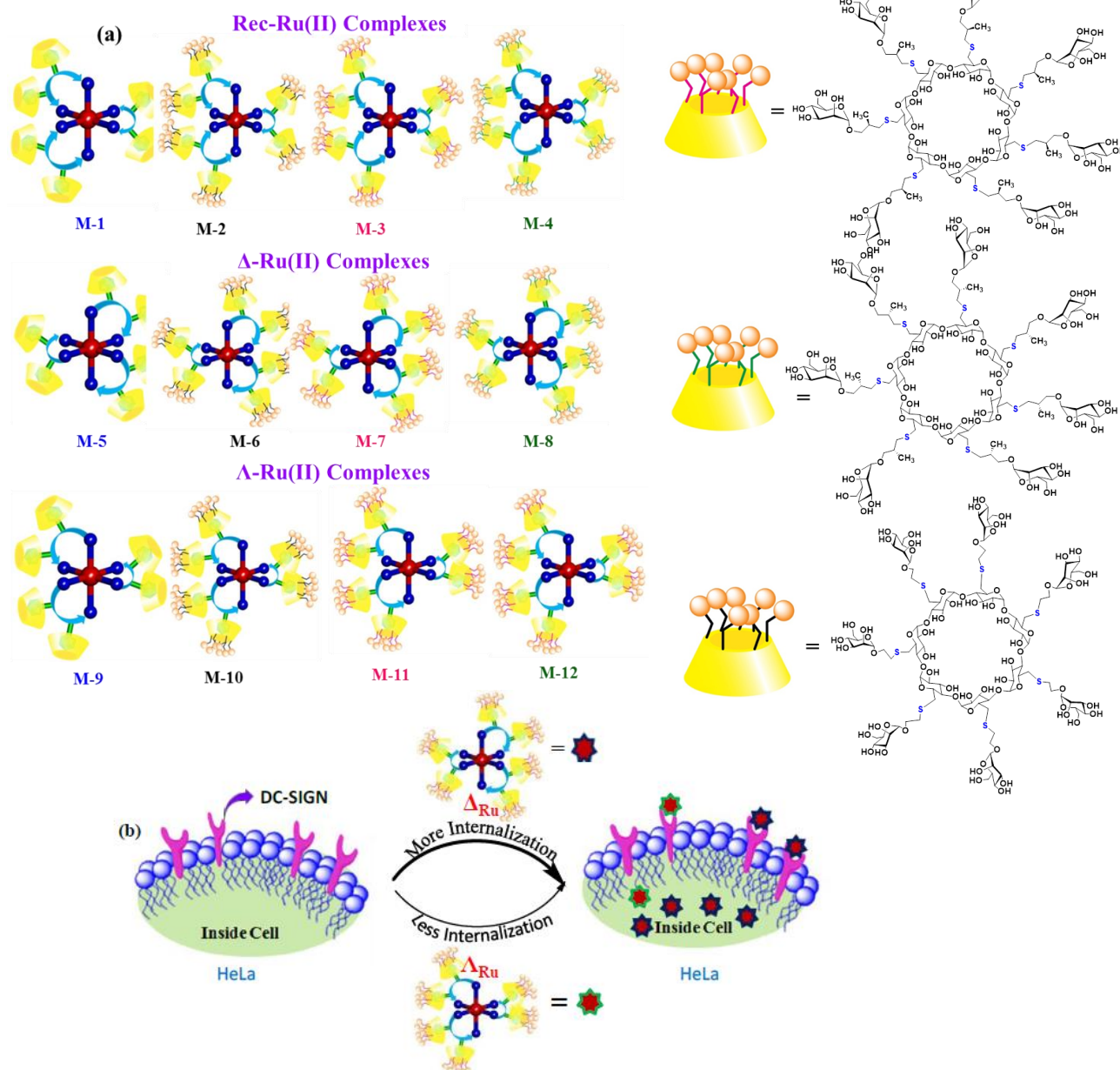


Figure 13 (a) Chiral metallo-glycodendrimers; (b) Internalization of Ru(II) complexes in HeLa cells

1.7. Why Surfaces?

Display of carbohydrates on surface mimics the presentation of carbohydrates on the cell surface (Fig.14) thus allowing for multivalent binding interactions which strengthens the weak carbohydrate protein interactions (CPIs) by cluster effect. Surface carbohydrate ligand density can be tuned accordingly as needed.

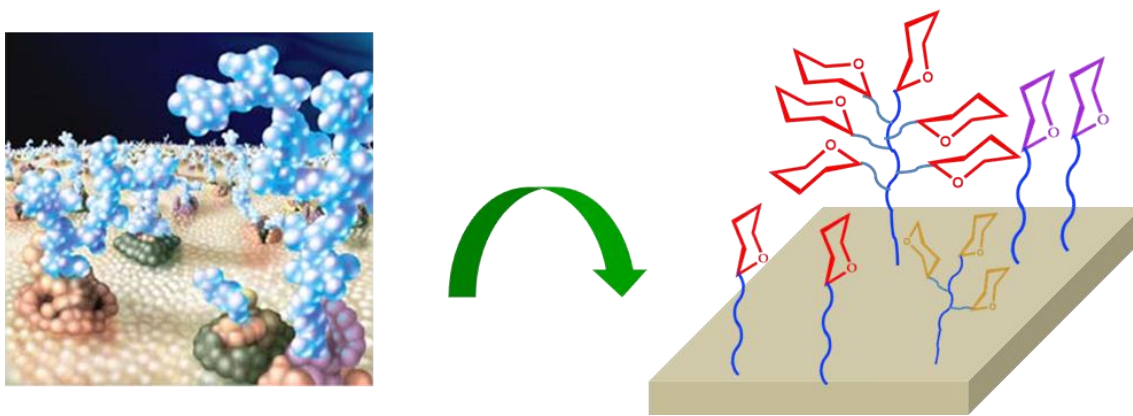


Figure 14 Carbohydrates on surface mimic the presentation of carbohydrates on the cell surface

1.8. Derivatization of surfaces with carbohydrates

Numerous research groups have developed various elegant approaches for immobilization of glycans on surfaces for detection of various binding events with lectins and pathogens. For construction of good glycan biosensors we have to take account of choice of surface, protocol for immobilization, detection platform and what we want to detect?^{75,76}

1.8.1. Functionalization of surfaces with carbohydrate: There are two means for immobilize carbohydrate on surfaces non-covalent immobilization and covalent immobilization.

1.8.1.1. Non-covalent immobilization

Non-covalent immobilization is not a technically demanding approach even though this is the straightforward way to immobilize carbohydrate on surfaces. Complex carbohydrates can be directly immobilized on surfaces without any active groups. Electrostatic interactions, π -effects, van der Waals forces, and hydrophobic effects are the forces involved in non-covalent immobilization between immobilized and analyte partner (Fig. 15). Various proteoglycans, glycolipids, and other glycoconjugates can be immobilized non-covalently. Crude cells or tissue extracts can also be immobilized.⁸

Denong Wang and co-workers immobilized microbial polysaccharides on nitrocellulose coated surface without chemical conjugation. (Fig.15a) They immobilized dextran of different molecular weight ranging from 20kD to 2000 kDa and studied anti-infection responses. They observed that immobilized carbohydrate molecules preserve their antigenic property on nitrocellulose coated glass slide. The system is sensitive allowing detection of broad range of antibody specificity. In their strategy, dextrans with high molecular weight retain strappingly on surface compare to low molecular weight.⁷⁷

The Wang et al approach was limited due to low molecular weight of oligosaccharide. Willats et al immobilized diverse glycans on polystyrene coated surface without prior functionalization (Fig. 15b). In Willats's methods, they conjugated low molecular weight saccharide to protein and then, these neoglycoproteins polysaccharides, proteoglycans and plant cell extracts attached to oxidised polystyrene surface and studied specific carbohydrate epitope binding with monoclonal antibody.⁷⁸ Kiessling and co-workers synthesized mannose-derivatized glycolipids noncovalently bound to gold coated surfaces through lipid bilayer formation (Fig. 15c). Interactions were studied by surface plasmon resonance (SPR). It was observed that there was low affinity for monovalent ligands and high-affinity for multivalent ConA ligands.⁷⁹ Another approach was which is fluorine based, in which glass slide was derivatized with fluorine. Binding of C₈F₁₇ tail to carbohydrate is sufficient and was used for biological screening (Fig. 15d). These non-covalent interactions are based on solvophobic effects.⁸⁰ This can be used for various glycosaminoglycan fragments. Uzawa et al synthesized novel polyanionic glycopolymer carrying globobioside (Gb(2)), beta-lactoside (β -Lac), or α -D-mannoside (α -Man) residues and developed a method of carbohydrate immobilization by electrostatic studied binding with Shiga toxin by surface plasmon resonance (SPR) (Fig. 15e).⁸¹

Shao et al presented a new method where they used biospecific streptavidin biotin coupling on polystyrene surface, glycans were biotinylated (Fig. 15f). Studied binding with lectins ConA, Wheat germ agglutinin, Phaseolus vulgaris erythro agglutinin, Lens culinaris agglutinin, Datura stramonium agglutinin and Sambucus nigra agglutinin conjugated to horseradish peroxidase were studied.⁸²

1.8.1.2. Covalent immobilization

Covalent immobilization is preferred over non-covalent immobilization. In covalent immobilization, we need both chemically modified surfaces as well as glycan structures with particular functional groups. It has higher stability compared to non-covalent interaction. In covalent immobilization method length of spacer is important because it provides proper presentation of carbohydrate on surface and avoids non-specific binding. People have developed several methods to immobilize carbohydrates (Fig. 16).⁸ Shin et al. developed a technique in which mono-, di- and polysaccharides were attached to hydrazide-coated glass slides by covalent immobilization (Fig. 16 a). These surfaces were applied for analysis of specific carbohydrate-proteins interactions and pathogen detection.⁸³

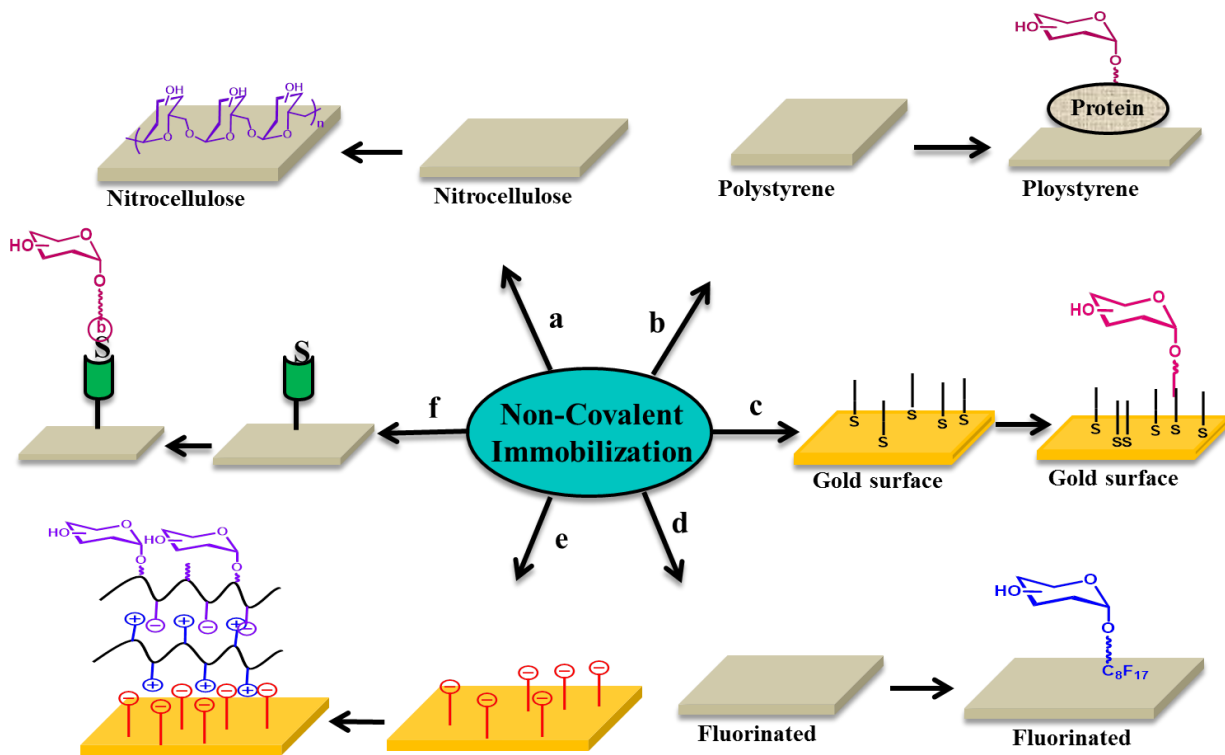


Figure 15 Noncovalent immobilization (a) Attachment of glycans to nitrocellulose, (b) Attachment of neoglycoproteins to polystyrene (c) Attachment of biotin-linked sugars to the streptavidin-coated surface (d) Immobilization of ionic glycoconjugates via layer-by-layer deposition. (e) Attachment of fluorinated sugars to the fluoro-alkylated surface, (f) Glycolipid self-assembled on the alkane thiol.

Gold coated slide is another approach which is frequently used for reviewing binding on communication on surfaces (Fig. 16 b). Thiol terminated glycosides are establish self-assembled monolayers. Ligand density can be controlled by diluting glycosides with alkane thiols for better binding. The anchoring sulphur atoms can form co-valent bond with gold which is very stable over the period.⁸⁴ Interactions were studied using SPR and Quartz crystal microbalance (QCM). Fritz et al used thiol terminated hexasaccharide deposited as self-assembled monolayers (SAMs) onto gold surfaces. Slides were characterized by X-ray photoelectron spectroscopy (XPS), ellipsometry, contact angle measurements, and imaging time-of-flight secondary ion mass spectroscopy (iToF-SIMS)⁸⁵ to determine homogeneity, chemical composition and thickness. Gruber et al. immobilized trimannose, nonamannose and galactose (as an internal control) on cantilevers via thiol–gold chemistry. The binding of Cyanovirin-N (CV-N) to nonamannose

produced 20% stronger deflection as compared to the trimannose and this protein could be detected down to a concentration of 91 pM.⁸⁶

Seeberger et al immobilized thiolated linear trimannoside, hexamannoside, and nonamannoside, on to maleimide-derivatized glass slides (Fig. 16 c) and studied binding with ConA and Cyanovirin-N (CVN).⁸⁷

People have used another method where they immobilized thiol moiety on gold surface and functionalized oligosaccharide with maleimide group. Chemo selective ligation of maleimide linked sugars to thiol-coated glass slides was applied by Shin et al. The carbohydrates were stably immobilized via thioether linkages to the glass substrates. It was mentioned that the fabricated microarrays are stable for several months, without degradation, when stored in a desiccator. While studying the influence of the tether length on interactions of the immobilized carbohydrates with lectins, authors found that a certain minimal length was needed to ensure stable and specific binding.⁸⁸

Another technique utilized by Shin et al was that they derivatized surfaces with epoxide and reacted with hydrazide functionalized small molecules (Fig. 16 d). The length of the tether governed protein binding. Slides with long tether exhibited stronger binding. This technique is suitable for covalently attaching various molecules such as saccharides, peptides and small molecules to glass surfaces.⁸⁹

Liang et al used N-hydroxysuccinimide (NHS) activated glass surfaces, to which glycans functionalized with amine were covalently attached (Fig. 16 e). Lectins ConA, Lens culinaris agglutinin (LCA), Pisum sativum agglutinin (PSA), and the human monoclonal antibody 2G12 were incubated with sugar arrays in different concentrations studied by using SPR.⁹⁰

Seeberger et al used aldehyde functionalised surfaces and then they incubated the aldehyde with Bovine Serum Albumin (BSA) amine will get coupled to the surface covalently (Fig. 16 f). This was followed by functionalization of BSA with maleimide group. Then synthetically modified thio oligosaccharides were added so that it will undergo hetero Michael addition.⁸⁷

Wong and co-workers derivatized surfaces with alkyne and clicked with azide functionalized oligosaccharides (Fig. 16 g).⁹¹

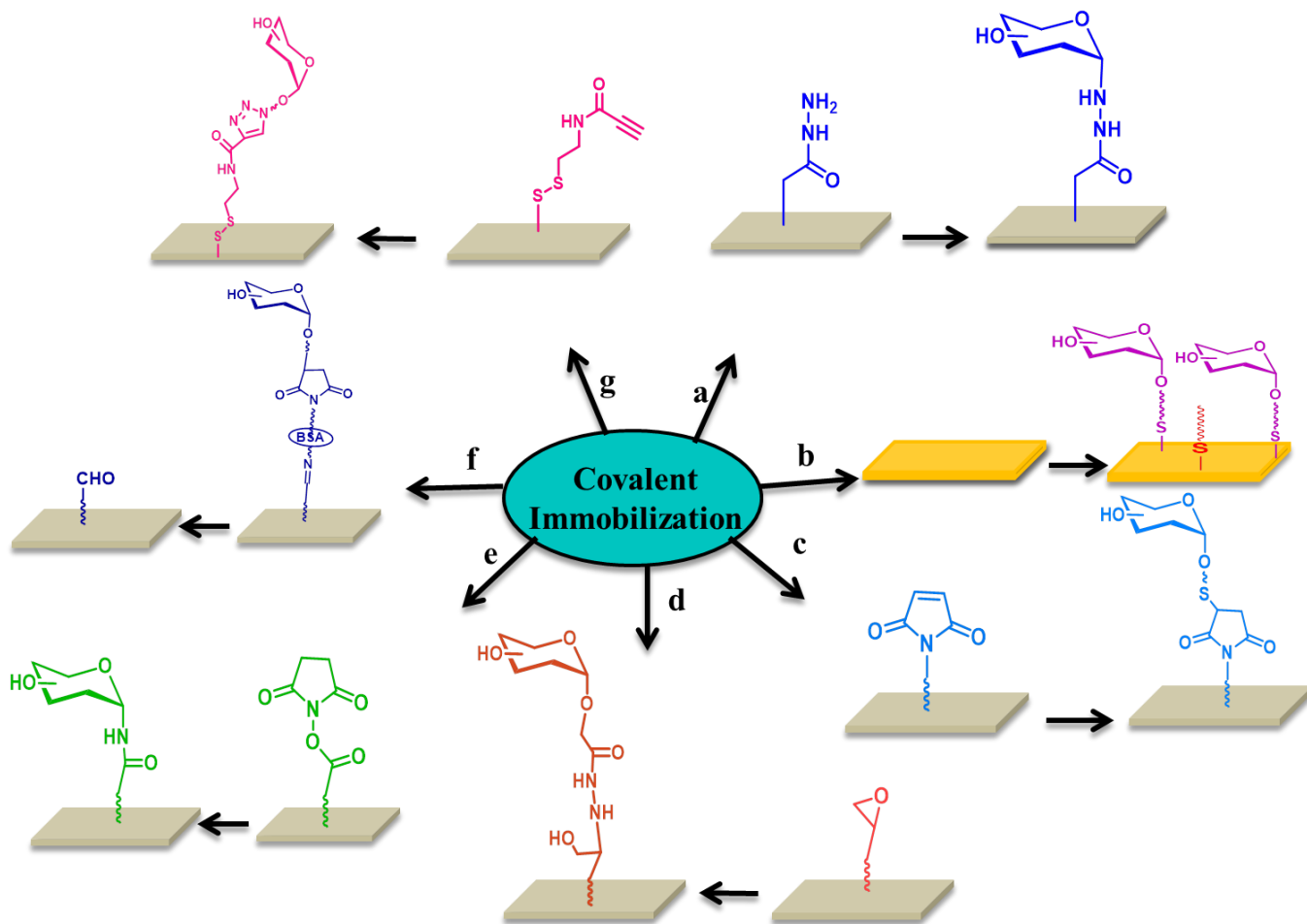


Figure 16 Covalent immobilization (a) Attachment glycans to hydrazide-coated glass slides, (b) Self-assembly of alkane thiols on gold surfaces, (c) Attachment of thiol-linked glycans to the maleimide-coated surfaces, (d) Attachment of hydrazide linked sugars to the epoxide-coated surfaces, (e) attachment of amine-linked sugars to the NHS ester-coated surfaces, (f) Covalent attachment of neoglycoproteins to aldehyde coated surfaces.

1.9. Label free technique

1.9.1. Surface Plasmon Resonance

Surface Plasmon Resonance (SPR) is a technique based on changes in the refractive index (RI) of the field created on gold-coated glass surfaces and is used to measure dynamic adsorption of biological molecules on the sensor chip surface in situ and in real-time (Fig. 17). The concentration of the adsorbed molecules is proportion to the resonance angle offset and is determined by it. There are myriad advantages to this method over other analytical methods, which include higher resolution, no need to tag the measured molecule and requirement for minimal amount of samples. The results are expressed as changes in resonance angle (RA) and are proportional to the density of the molecules on the sensor surface.⁹² SPR has been

extensively used in label-free, real-time analysis of different bio-recognition events (Fig. 17b).^{93, 94} Yu et al.

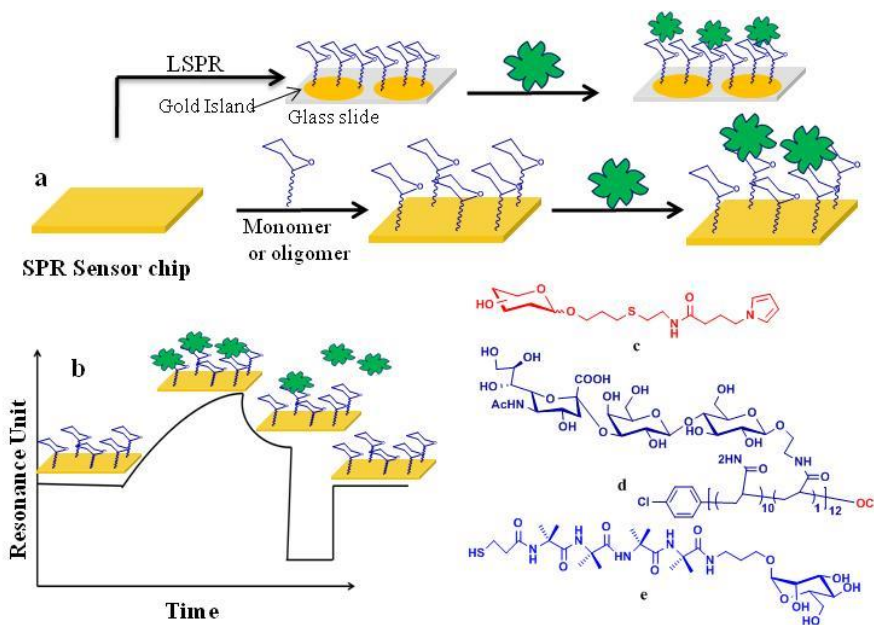


Figure 17 (a) Fabrication of the sensor surface for SPR and LSPR; (b) SPR signals at different stages; Structure of glycans used for surface functionalization: (c) Pyrrole-carbohydrate conjugates, (d) sialyllactose-containing cyanate group. (e) Mannose linked to PEG-SH.

used SPR to measure the binding affinity kinetics and to quantify the interactions between the lectin ConA and mannose, and to correlate it with the molecular and structural features of the sugars presented on the glycocalyx mimicking on surfaces.⁹⁵ The experiment was carried out by grafting polymer chains carrying carbohydrate residues on gold surfaces with tightly controlled grafting density, degree of polymerization, and carbohydrate density. The layers, composed of mono or multivalent mannose polymers, were utilized to study the interactions between lectins and mannose. A 1000-fold increase in the equilibrium binding constant was observed when the layer of polymers modified with mannose residues was replaced with chains containing multivalent carbohydrates, a result attributed to the spatial distribution of the carbohydrates within the surface-grafted polymer layer. Another method to form carbohydrate layers on gold surfaces, based on conformationally constrained peptides of α -aminoisobutyric acid (Aib), and functionalized with carbohydrates for SPR measurements, was described by Maran et al. (Fig. 17e).⁹⁶ The well-packed self-assembled monolayers (Aib-SAMS) were used for studying mannose – ConA interactions. In yet another experiment, carbohydrate-

modified dendritic polyesters with different densities of functional groups and sulfur functionalities (sulfide or disulfide) were used to form self-assembled dendriatic monolayers (SADMs) on gold surfaces,⁹⁷ and the cell scavenging ability of these sensor surfaces for *E. coli* MS7fim+ were studied using SPR techniques. Result showed 2.5-fold improvement in the scavenging capacity of mannosylated SADM compared to hydroxylated SADMs. SPR and surface-initiated atom transfer radical polymerization were used to study the correlation between the structure of glycopolymer brushes and the affinity of lectin adsorption⁹⁸ where sugar epitope density was controlled by graft copolymerization. Bulard et al. developed SPR-based carbohydrate microarray for detection of the foodborne pathogenic bacteria *E. Coli* O145, O157.⁹⁹ The array was able to distinguish between closely related bacteria and discriminate among sub serotypes based carbohydrate binding fingerprints. Different pyrrole carbohydrate conjugates were grafted on gold surface by pyrrole co-electropolymerization (Fig. 17c), which could be regenerated by careful washing with 2% SDS followed by 0.02 M sodium hydroxide, so that many measurements could be done using the same surface. This surface modification were shown to detect samples containing less than 10^2 CFU·mL⁻¹ of bacteria. Zagorodako et al. checked shear force dependent uropathogenic *E. coli* UTI89 adhesion on heptyl α -D-mannopyranoside-modified gold SPR substrates.¹⁰⁰ For this study microfluidic channel was used in combination with SPR to control flow rate from 10 to 30 μ l. mL⁻¹ (shear force 5 to 100 mPa). With increase in flow rate the binding of *E. coli* UTI89 found to increase to SPR surface and reach to maxima at highest flow rate. In another surface modification method, sialic acid glycans were attached to SPR chips by isourea and the binding of α 2, 3 and α 2, 6 sialylated glycans and influenza hemagglutinins (HA) lectin was studied (Fig. 17d).¹⁰¹ This type of measurements can be envisioned as a potential tool for virus diagnosis. Maalouli and co-workers compared two methods for ‘surface decorating’, namely photocoupling strategy (with perfluorophenyl azide functionalized surfaces) and the corresponding surface decorating process through the “click” approach catalyzed by Cu(I) ions.¹⁰² Both methods were used for covalent immobilization of mannose and lactose sugars onto perfluorophenyl azide-functionalized novel lamellar Ti/Au/silicon dioxide interfaces and azide-functionalized surfaces, respectively. Lectin recognition studies done on these surfaces using SPR showed that the difference in change in the SPR signal is somewhat larger in the case of the mannose interface formed through the photocoupling approach compared with that fabricated via the “click” strategy and that the

sugars maintain their expected binding affinity and specificity towards their partner lectins although this immobilization scheme might not necessarily give sugars linked exclusively via their anomeric positions. To achieve the high sensitivity in biological interactions modification in SPR technique is carried out namely localized surface plasmon resonance (LSPR). LSPR is based on the phenomenon of change in the refractive index near noble metal nanostructures that affect the surface plasmon extinction band. The common experimental scheme for LSPR sensing consists of immobilization of a receptor layer on the nanostructured metal surface of the transducer and monitoring variations in the optical response resulting from local changes in the refractive index occurring upon binding of the biological analyte (Fig. 17a). Bellapadrona and coworkers developed LSPR sensor surface based on gold island films that was prepared by evaporation on glass and annealing.¹⁰³ Mannose modified with PEG-thiol linkers were attached to the gold islands to form mannose coated transducers that showed excellent selectivities towards ConA even in the presence of large excess of BSA. Another LSPR sensor was developed by immobilization of carbohydrates on colloidal gold surface by using cyanuric chloride which links between amino residues of polyamidoamine (PAMAM) dendrimer-coated colloidal gold surface and amino residues of 12-aminododecyl glycoside.¹⁰⁴ The sensitivity of a LSPR based sensor was corroborated by study of the binding specificity of wheat germ agglutinin (WGA) and Ricinus communis agglutininI (RCA₁₂₀) lectins with colloidal surfaces modified with GlcNAc and lactose, respectively.

A novel sandwich SPR sensor for sensitive detection of ConA was developed using graphene oxide (GO) as a substrate for the immobilization of phenoxy derivatized dextran (Dex-P) and dextran modified gold nanoparticles (DexAuNPs) as amplification reagent.¹⁰⁵ The sensing interface GO/DexP was conveniently constructed by assembling DexP on GO-coated gold film through π - π stacking. The sandwich GO-DexP/ConA/Dex-AuNPs has provided enhancement in SPR signal, with high sensitivity, good selectivity and reproducibility of ConA detection.

1.9.2. Plasmon Waveguide Resonance

In recent years, another label free technology, Plasmon Waveguide (PWG) resonance, is widely used for large scale screening in addition to SPR. PWG sensors are composed of an arrangement of dielectric material, in which a low refractive index periodic surface structure made of plastic is coated with a high refractive index film of Nb₂O₅ or TiO₂. The reflected wavelength is changed

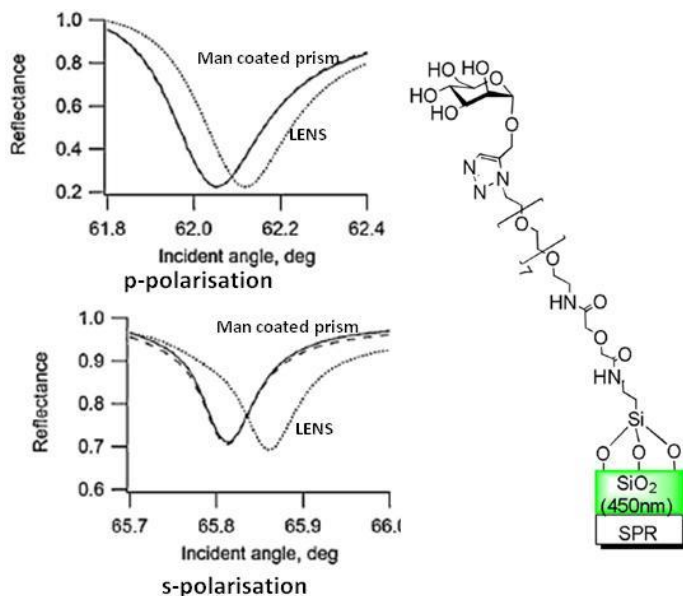


Figure 18 Mannose functionalized prism surface for detection of lectin interaction using PWG

by attaching biomolecules on the plate surface. A detection instrument illuminates the underside of the plate where the target material is loaded onto the bottom of the microplate well, and is capable of measuring all the sensors within one microplate in several seconds. Plasmon waveguide resonance is highly sensitive to changes in the refractive index under both polarizations, s and p polarization of light, and enables mass density measurements.¹⁰⁶PWR provides information about molecular order and conformation of oriented anisotropic materials.¹⁰⁷In SPR, self-assembled materials on gold surfaces are measured while in PWR, measurements with the analyte bound on a variety of substrates, including silica, hydrogel surfaces and more is possible. Alves and coworkers attached mannose to waveguides substrates and used the resulting interfaces to explore CPIs.¹⁰⁸The covalent binding to the silica-based waveguides was performed by a combination of silanization of the surface followed by amide formation and ended with a “click” reaction to alkynyl-derivatized mannose (Fig. 18). The specific interaction of lectins from *Lens culinaris* (LENS) vs *Arachis hypogaea* (PNA) with the mannose was studied with PWR. It was shown that the resonance signal obtained by PWR was much sharper than the signal recorded with classic SPR.

1.9.3. FTIR-attenuated Total Reflection Spectroscopy

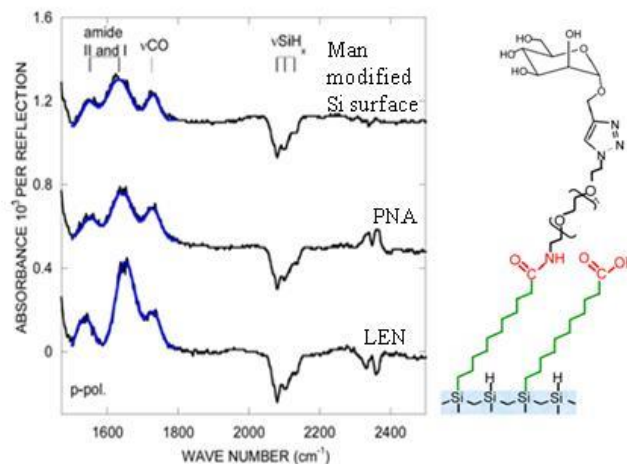


Figure 19 Mannose-terminated crystalline Si (111) surface and ATR-FTIR spectra in p-polarization

FTIR-attenuated total reflection spectroscopy (FTIR-ATR) technique is based on the absorption of an IR evanescent wave traveling through a high refractive index prismatic crystal in close contact with a sample thus eliminating the need of further preparation.¹⁰⁹ This technique was used by Yang and co-workers in studying the interactions of carbohydrates with lectins.¹¹⁰ Carboxydecyl-terminated crystalline silicon (111) surfaces functionalized with either mannosyl moieties or a mixture of mannose and spacer alcohol molecules to provide “diluted” surfaces. The quantification of binding interactions of lectins with these surfaces has shown that the right dilution of glycans on surfaces enhanced the binding yield to specific lectins. FTIR-ATR method provided for the first time the ratio of interacting glycans to bound lectin. A similar type of mannose modified silicon surfaces was used by Gouget-Laemmel et al. for studying the interaction with *Lens culinaris* lectin (Fig. 19),¹¹¹ where they proved the specificity of protein to glycans in the presence of other glycan binding proteins.

1.9.4. Quartz Crystal Microbalance

Quartz crystal microbalance (QCM) is a simple, cost-effective, high-resolution mass sensing device, based upon the piezoelectric effect. It provides qualitative and quantitative information about biomolecular interactions by translating changes in mass at the probe-immobilized surface of the crystal sensor into measurable changes in the resonant frequency of the quartz crystal. It is used for probing the solution-surface interface of a wide range of molecular systems,

biopolymers, in particular bio recognition processes.¹¹²The read signal reflects changes in the resonance frequency that stems from and is proportional to changes in the mass of the pre-

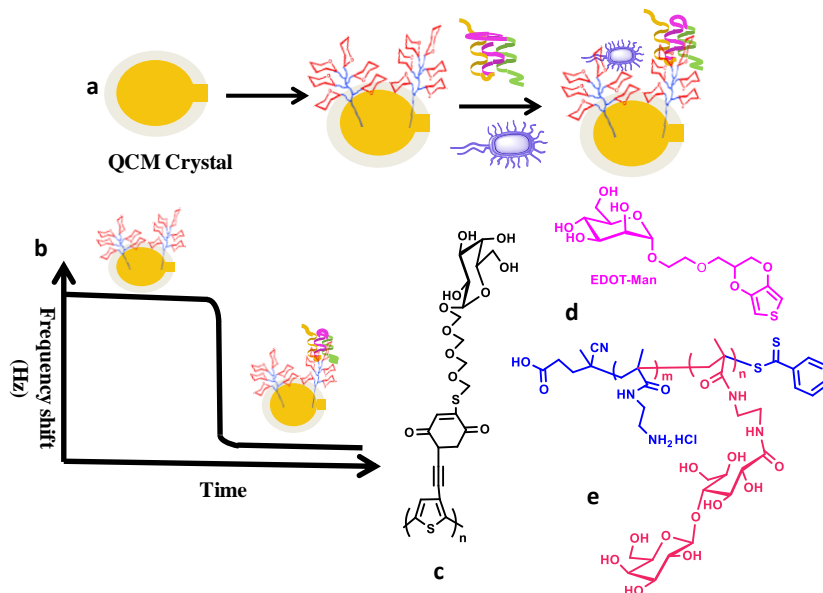


Figure 20 (a) Schematic illustration of the immobilization on QCM substrate; (b) Graphical representation of frequency change in QCM; (c) thiolated mannose (TM)/quinone functionalised polythiophene glycopolymer; (d) poly-(3,4-ethylenedioxy thiophene); (e) (poly (2-lacto bionamido ethylmethacrylamide) (PLAEMA)).

immobilized molecules on the quartz crystal surface (Fig. 20). Not like SPR, QCM can be affected by solvent molecules that interact with the immobilized molecules and by conformational changes of these molecules. QCM technique is widely used in studying interactions between a great variety of materials because of the assortment of substrate materials, i.e., plain quartz, gold, metals, polymeric materials and immobilization techniques that facilitate immobilization.¹¹²Electrically active platform with sugar-grafted conjugated polymers were obtained from the mannosylated monomer EDOT-Man (Fig. 20d), prepared from hydroxymethyl-functionalized 3,4-ethylenedioxythiophene and triethylene glycol (EDOT-EG3) by electro-copolymerization. The surface density of the mannose ligands on QCM surface was easily adjusted by controlling the composition of the mixture of monomers EDOT-EG3 before polymerization.¹¹³Binding of ConA to the sugars on the surface was monitored in real time by QCM. The possibility of recycling the substrate for use in multiple binding events is a significant advantage of using QCM in this study.

Another method for immobilization of sugar molecules on substrates was based on conductive polymers of thiophene with fused quinone moieties (TQ) and the well-established quinone based coupling chemistry for incorporating carbohydrate functionalities, fabricating innovative carbohydrate biointerfaces (Fig. 20c).¹¹⁰ The resulted sensor revealed high sensitivity and selectivity with the detection limit of 8×10^4 cells/mL of *E. Coli* by Pili-Mannose Binding. Better sensitivity was achieved for ConA and binding of *E. coli* with a lower detection limit of 50 cells/mL.¹¹⁴

Mahon et al.¹¹⁵ developed multilayered lectin and glyconanoparticles architectures on QCM substrates for enhanced detection of CPIs. In this case multilayered glyco-nanoparticle–lectin constitutional system was build up in a layer by layer fashion. This multilayered system has amplified the sensitivity of QCM via increase in the mass of the interaction protein.

Traditional QCM technique uses only change in mass for targeted biorecognition process. Recently QCM with dissipation (QCM-D) technique has come up, which provides detail insight about change in thickness of molecular layer on sensor surface along with their masses.

Ogiso et al. described the use of QCM-D (QCM with dissipation monitoring) for studying the interaction between glycolipids and antibodies or lectins.¹¹⁶ They used polyamidoamine (PAMAM)dendrimers for immobilizing lysoganglioside-GM1 (Fig. 20e) and 12-aminododecyl-N-acetyl glucosaminide (GlcNAc–C12–NH₂) and attached the amino groups of the dendrimers to the surface using the cross-linker cyanuric chloride. The binding was confirmed by the specific interaction with anti-ganglioside GM1 antibody or WGA.

This method enabled to construct carbohydrate clusters that mimic cell surfaces and the study of CPIs at the molecular level. Wang et al used QCM-D biomimetic surfaces modified with thermoresponsive polymers to detect *Pseudomonas auriginosa*.³⁷ The polymers, glyco-poly(N-isopropyl acrylamide) was synthesized using RAFT polymerization and was deposited on the QCM surfaces using dithioester terminated linkers adsorbed onto the gold surfaces. At temperatures above the thermally responsive polymers the QCM-D surfaces became hydrophobic, which promoted bacterial adhesion through CPIs.

1.9.5. Cantilever

Cantilever microarray is a technique for detecting CPIs based on mass change transduction.¹¹⁷ According to this method, a surface stress is generated upon biomolecular recognition of a ligand in solution, resulting in a bending of the microcantilever due to steric hindrance and electrostatic

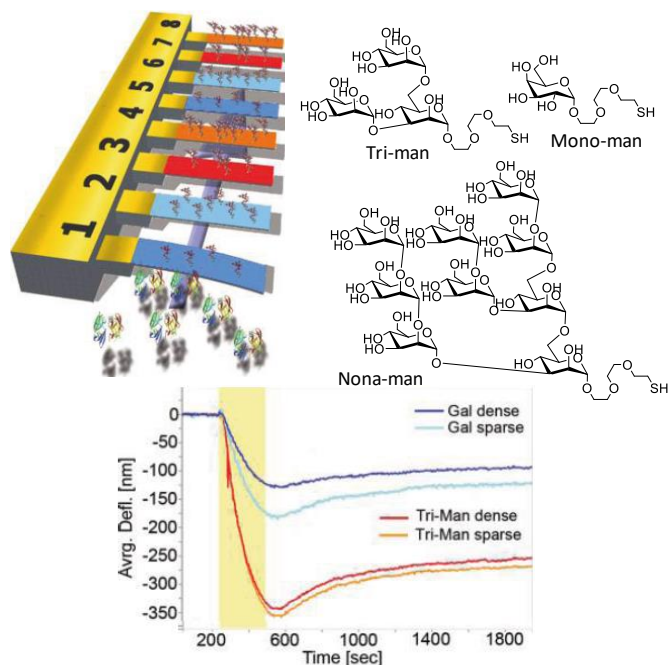


Figure 21 Schematic presentation of a cantilever array and structures of different mannoside effects. High sensitivity in the pM level is obtained by deflection of a laser beam (Fig. 21).¹¹⁸ In a typical experiment, one side of the cantilever surface is modified by attaching biorecognition elements while the other side is passivated to resist any binding. The recognition event is monitored by changes in the angle of the laser beam. Gruber et al.⁸⁶ studied binding interactions of mannosides and the protein cyanovirin-N using this method. The cantilever surface was functionalized with different densities of three sugars, namely, trimannose, nonamannose and galactose using thiol-gold chemistry. Nonamannose functionalized cantilevers exhibited 20% greater deflection compare to triamannose upon cyanovirin binding. A similar cantilever surface was used by Mader et al.¹¹⁹ for detection and discrimination of different *E. coli* Strains. On bacterial binding with nonamannose modified cantilever the signal was higher compared to mono and tri mannose coating, which is attributed to the increased potential for multisite and multivalent binding of the carbohydrate and the bacteria that translates into more binding events on these surfaces. Kesel and coworkers¹²⁰ studied the adhesion of the biofilm forming *B. subtilis* wild-type strain NCIB 3610 to mannose and galactose using coated gold cantilevers. *B. subtilis* showed strong binding to bare gold surfaces but a considerable reduction in bacterial adhesion was obtained when the gold cantilevers were coated with carbohydrates. The experiment demonstrated that even mono- and disaccharide coating of hydrophobic surfaces can lead to a

considerable reduction of bacterial adherence and proves that carbohydrates play important role in biofilm formation.

1.9.6. Atomic Force Microscopy.

Non-covalent associative forces control a number of biological recognition process that form the basis for biosensor development. Atomic force microscope (AFM) has the ability to manipulate and measure forces between individual molecules and has gained enormous importance in the study of non-covalent biological interactions.¹²¹ Bower and coworkers investigated the effect of applied contact force on the probability of observing a rupture event, the normalized number of blockable rupture events per pull, and rupture force and length distribution in force versus extension plots.¹²² Amino functionalized silicon nitride AFM tips were conjugated to a PEG maleimide, which was further covalently bound to thiopentyl lactoside, and thiopentyl mannoside (Fig. 22a). His6-galectin-3 and his6-KDPG aldolase were immobilized via N-terminal-his6-Ni²⁺ coordination to a covalently anchored nitrilotriacetate (NTA)-maleimide linker on mercaptosilanized silicon <111> (Fig. 22b). The effect of contact forces on unbinding profile of lactose-galectin 3 was investigated in the form of rupture force and length in the presence of control pairs lactose-KDPG aldolase, and mannose-galectin-3 with no known interactions in solution phase. It was found that with the increased contact force, the nonspecific rupture pattern shown by lactose-KDPG aldolase, and mannose-galectin-3 is indistinguishable from specific lactose-galectin 3 pattern. This suggests that careful experiment design with minimum contact force need to be applied to probe specific binding interactions.

1.9.7. Field-effect Transistor (FET)

A field-effect transistor (FET) is a type of transistor commonly used for weak-signal amplification. It provides a novel nanodevice platform for highly selective detection of biomolecular interactions.¹²⁴ In FET a biological receptor is anchored on the surface of the sensor (silicon nanowire, carbon nanotube, hydrogel etc.) and when binding to a target analytes occurs, the surface potential changes accompanied with modulation in the channel conductance, which are recorded and further processed by the electric measurement system (Fig. 23).¹²⁵ In the FET, current flows along a semiconductor path called the channel. At one end of the channel, there is an electrode called the source and at the other end of the channel, there is an electrode called the drain. The physical diameter of the channel is fixed, but its effective electrical diameter can be

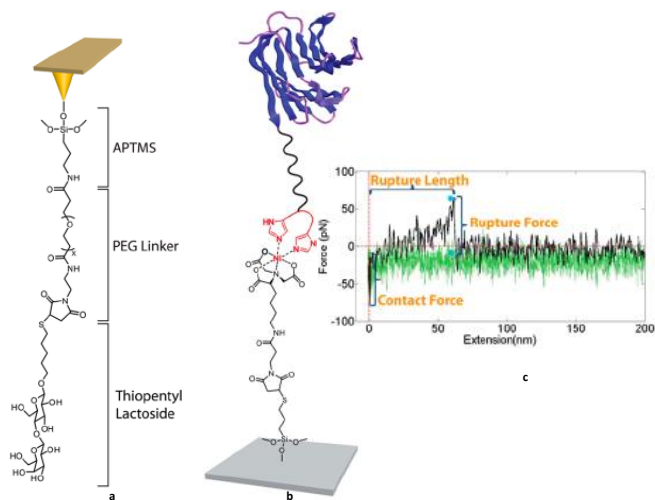


Figure 22 (a) AFM tip modification with lactoside; (b) Galectin functionalization on Silicon ¹²³ surface; (c) Force distance curve for lectin interaction.

varied by the application of a voltage to a control electrode called the gate. The conductivity of the FET depends, at any given instant in time, on the electrical diameter of the channel. A small change in gate voltage can cause a large variation in the current from the source to the drain. FET based glycan biosensors have detection limits in nM, fM or aM levels depending on the construction formats.

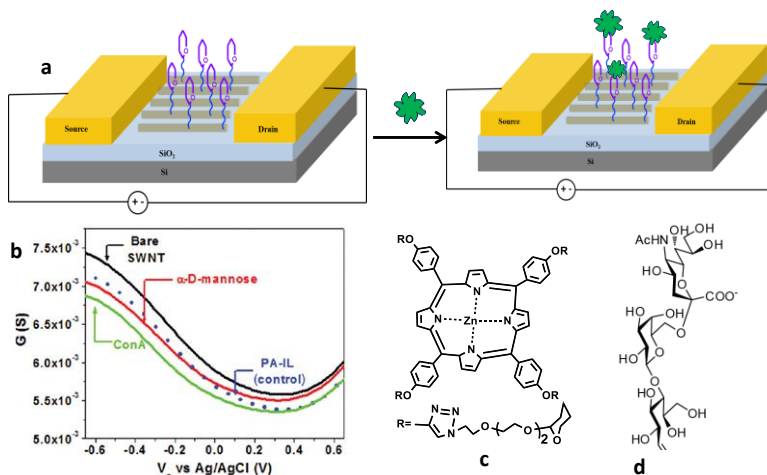


Figure 23 (a) Schematic diagrams of the SiNW biosensor for label-free detection of carbohydrate-protein interactions. (b) Signals [conductance (*G*) vs gate voltage (*V_g*)] recorded for measuring carbohydrate-lectin interactions; (c) porphyrin-based glycoconjugate; (d) Sialolactose glycan

Hideshima et al., modified the surface of FET device by immobilizing 3'-sialylactose and 6'-sialyllactose glycans on a self-assembled monolayer (SAM) of aminoxy terminated with silane coupling reagent¹²⁶ (Fig. 23d) and found that the FET device clearly distinguished between subtypes H1 (human) and subtypes H5 (avian) of hemagglutinin molecules at the attomolar level.

Silicon nanowire (SiNW)-based biosensor capable to detect label-free CPIs with high selectivity and sensitivity was developed by immobilization of unmodified carbohydrates on the sensor surface. Carbohydrates (mannose and galactose) were immobilized on the SiNW surface via oxime bonds¹²⁷ and the surfaces were used to study the interaction with ConA and *Erythrina cristagalli* (EC) lectin, respectively. Vedala et al., developed single-walled carbon nanotube field-effect transistor (NTFET) by non-covalent immobilization of porphyrin-based glycoconjugates of mannose, galactose and fucose¹²⁸ (Fig. 23c) and used it for studying specific binding interaction with PA-II and PA-III from *Pseudomonas aeruginosa* and the plant lectin conA. The single-walled carbon nanotube networks acted as conducting channels that transduce the binding between glycoconjugates and lectins into electrical signals. In yet another study, mannose gels were synthesized by radical co-polymerization in the shape of capillaries¹²⁹ and the detection of mannose and ConA interactions, converted into electrical signals for FET, was based on the direction and magnitude of gel swelling.

1.9.8. Cyclic Voltammetry.

Cyclic voltammetry (CV) is an electrochemical technique sensitive to changes in the thickness and the density of the biomolecules on the sensors surface¹³⁰ and to changes in the current detected from redox species (Fig. 24a). CV measures the current by variation of the potential on a working electrode in the presence of a redox probe at a defined scan rate.

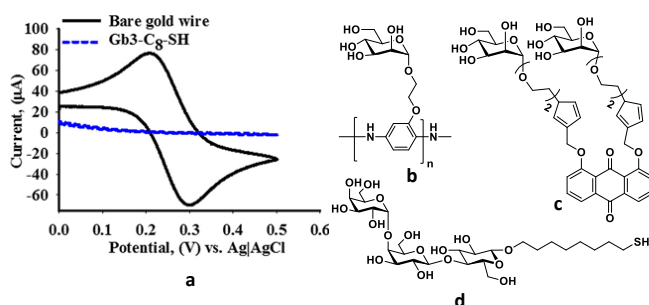


Figure 24 (a) Cyclic voltammogram; (b) mannose aniline polymer (c) anthraquinolin mannoside; (g) globotriose

Zhu co-workers developed an electrochemical sensor that is based on the modification of graphene electrode through noncovalent interactions of anthraquinolin mannoside (Fig. 24c).¹³¹ This fabricated sensor showed reproducible impedance response for recognition of ConA with high selectivity in the presence of other lectins. A similar type of graphene-based modified electrode with glycosyl anthraquinones was used for detection of transmembrane glycoprotein

receptors expressed on a hepatoma cell line. The biomimetic surface recognized successfully asialoglycoprotein receptors on live Hep-G2 cells when simple electrochemical techniques like CV were used. In another study, mannose aniline polymer was probed as an electrochemical platform for studying the interactions with ConA (Fig. 24b).¹³² The conductivity of the polymer changes on ConA binding due to the interconversion of amine to imine. Other studies were carried out with self-assembled monolayers (SAMs) of β -D-Gal-(1,4)- β -D-Gal-(1,4)- β -D-Glc-mercaptopentane (globotriose, Gb3-C8-SH) with soybean agglutinin (SBA, Fig. 24d).¹³³ Single and mixed component SAMs were prepared using Gb3-C8-SH and octane-thiol or 8-mercaptopentane-3,6-dioxaol on nanoporous gold and flat gold surfaces. CV measurement showed that nanoporous SAM shows a much larger charging current compared to that of the flat gold wire SAMs, because of the large surface area of nanoporous gold.

1.9.9. Electrochemical Impedance Spectroscopy

Electrochemical impedance spectroscopy (EIS) is the response of an electrochemical system (cell) to an applied potential. EIS can monitor sensitive changes in the conductivity/resistivity or the charging capacity of an electrochemical interface¹³⁴ and became, therefore a powerful tool in the study of biorecognition processes using electrodes modified with biological receptors on their surfaces (Fig. 25). If the measurement is accompanied by a redox charge transfer across the electrode interface, it is termed Faradaic- and when no redox charge transfer is taken place, it is called non-Faradaic EIS.¹³⁵ Hushegyi and coworker succeeded to develop an EIS based biosensor for detection of lectins and influenza hemagglutinins with sensitivity as low as attomolar concentrations (aM).¹³⁶

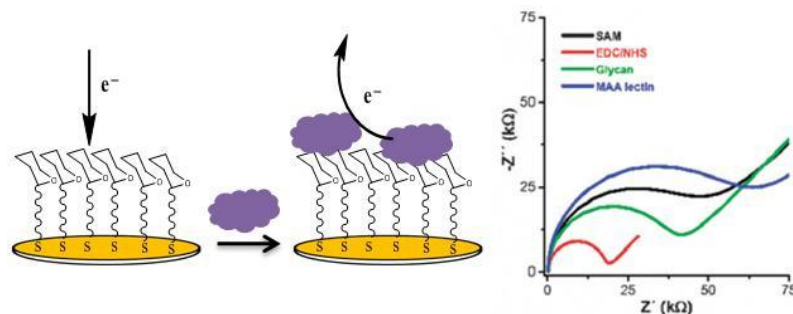


Figure 25 Schematic illustration of glycan immobilized electrode for highly sensitive and specific detection of lectins using EIS

Ultrasensitive analyses were achieved using an optimized immobilization process with controlled density of glycans on gold electrodes. It was achieved by patterning the gold surfaces by mixed

self-assembled monolayers (SAMs) prepared from 11-mercaptoundecanoic acid diluted to different extents by 6-mercaptohexanol. The varying densities of functional carboxylic groups were used for linking glycans via amide bonds. These modified electrodes were utilized for studying the interactions between the carbohydrates with *Maackia amurensis* agglutinin and with the two influenza hemagglutinins H5N1, H1N1, using EIS in the form of charge transfer resistance. This showed detection limit 7 order of magnitude lower than the best described glycan biosensor.

1.10. References

1. N. Sharon, *Sci. Am*, 1980, **243**, 90-116.
2. N. Sharon and H. Lis, *Sci. Am.*, 1993, **268**, 82-89.
3. H. Lis and N. Sharon, *Chem. Rev.*, 1998, **98**, 637-674.
4. S. Horiya, I. S. MacPherson and I. J. Krauss, *Nat. Chem. Biol.*, 2014, **10**, 990-999.
5. T. Buskas, P. Thompson and G. J. Boons, *Chem. Commun. (Camb)*, 2009, 5335-5349.
6. C. R. Bertozzi and L. L. Kiessling, *Science*, 2001, **291**, 2357-2364.
7. M. Cohen and A. Varki, *Int Rev Cell Mol. Biol.*, 2014, **308**, 75-125.
8. K. Larsen, M. B. Thygesen, F. Guillaumie, W. G. Willats and K. J. Jensen, *Carbohydr. Res.*, 2006, **341**, 1209-1234.
9. Y. C. Lee and R. T. Lee, *Acc.Chem. Res.*, 1995, **28**, 321-327.
10. E. O. G. A. Varki et al., 2nd Edition, 2009.
11. N. Sharon and H. Lis, *Glycobiology*, 2004, **14**, 53r-62r.
12. G. M. Edelman, B. A. Cunningham, G. N. Reeke, Jr., J. W. Becker, M. J. Waxdal and J. L. Wang, *Proc. Natl. Acad. Sci. U S A*, 1972, **69**, 2580-2584.
13. S. Kaushik, D. Mohanty and A. Surolia, *Biophys. J.*, 2009, **96**, 21-34.
14. N. Shibuya, I. J. Goldstein, E. J. M. Vandamme and W. J. Peumans, *J. Biol. Chem.*, 1988, **263**, 728-734.
15. C. S. Wright, H. Kaku and I. J. Goldstein, *J. Biol. Chem.*, 1990, **265**, 1676-1677.
16. R. Lotan, E. Skutelsky, D. Danon and N. Sharon, *J. Biol. Chem.*, 1975, **250**, 8518-8523.
17. N. M. Young, R. A. Johnston and D. C. Watson, *Eur. J. Biochem.*, 1991, **196**, 631-637.
18. N. Sharon, *Biochimic. Biophys. Acta*, 2006, **1760**, 527-537.
19. K. Kato and A. Ishiwa, *Trop. Med. Health*, 2015, **43**, 41-52.
20. K. A. Krogfelt, H. Bergmans and P. Klemm, *Infect. Immun.*, 1990, **58**, 1995-1998.
21. J. Bouckaert, J. Berglund, M. Schembri, E. De Genst, L. Cools, M. Wuhrer, C. S. Hung, J. Pinkner, R. Slattegard, A. Zavialov, D. Choudhury, S. Langermann, S. J. Hultgren, L. Wyns, P. Klemm, S. Oscarson, S. D. Knight and H. De Greve, *Mol. Microbiol.*, 2005, **55**, 441-455.
22. C. S. Hung, J. Bouckaert, D. Hung, J. Pinkner, C. Widberg, A. DeFusco, C. G. Auguste, R. Strouse, S. Langermann, G. Waksman and S. J. Hultgren, *Mol. Microbiol.*, 2002, **44**, 903-915.
23. E. M. V. Johansson, S. A. Crusz, E. Kolomiets, L. Buts, R. U. Kadam, M. Cacciarini, K.-M. Bartels, S. P. Diggle, M. Cámara, P. Williams, R. Loris, C. Nativi, F. Rosenau, K.-E. Jaeger, T. Darbre and J.-L. Reymond, *Chemistry & Biology*, 2008, **15**, 1249-1257.

24. A. Imberty, M. wimmerova, E. P. Mitchell and N. Gilboa-Garber, *Microbes Infect.*, 2004, **6**, 221-228.
25. E. Mitchell, C. Houles, D. Sudakevitz, M. Wimmerova, C. Gautier, S. Perez, A. M. Wu, N. Gilboa-Garber and A. Imberty, *Nat. Struct. Biol.*, 2002, **9**, 918-921.
26. D. C. Kilpatrick, *Biochim. Biophys. Acta*, 2002, **1572**, 187-197.
27. M. M. Harding, *Acta Crystallogr D Biol Crystallogr.*, 2006, **62**, 678-682.
28. B. M. Curtis, S. Scharnowske and A. J. Watson, *Proc. Natl. Acad Sci. U S A*, 1992, **89**, 8356-8360.
29. F. Lasala, E. Arce, J. R. Otero, J. Rojo and R. Delgado, *Antimicrob. Agents. Chemother.*, 2003, **47**, 3970-3972.
30. U. Svajger, M. Anderluh, M. Jeras and N. Obermajer, *Cell Signal.*, 2010, **22**, 1397-1405.
31. I. M. Dambuza and G. D. Brown, *Curr. Opin. Immunol.*, 2015, **32**, 21-27.
32. E. Ishikawa, T. Ishikawa, Y. S. Morita, K. Toyonaga, H. Yamada, O. Takeuchi, T. Kinoshita, S. Akira, Y. Yoshikai and S. Yamasaki, *J Exp Med*, 2009, **206**, 2879-2888.
33. C. A. Hunter and L. D. Sibley, *Nat. Rev. Micro.*, 2012, **10**, 766-778.
34. J. Marchant, B. Cowper, Y. Liu, L. Lai, C. Pinzan, J. B. Marq, N. Friedrich, K. Sawmynaden, L. Liew, W. Chai, R. A. Childs, S. Saouros, P. Simpson, M. C. Roque Barreira, T. Feizi, D. Soldati-Favre and S. Matthews, *J. Biol. Chem.*, 2012, **287**, 16720-16733.
35. W. B. Turnbull and J. F. Stoddart, *J. Biotechnol.*, 2002, **90**, 231-255.
36. C. Fasting, C. A. Schalley, M. Weber, O. Seitz, S. Hecht, B. Kokschi, J. Dervede, C. Graf, E. W. Knapp and R. Haag, *Angew. Chem. Int. Ed. Engl.*, 2012, **51**, 10472-10498.
37. L. L. Kiessling and J. C. Grim, *Chem. Soc. Rev.*, 2013, **42**, 4476-4491.
38. R. Roy and T. C. Shiao, *Chem. Soc. Rev.*, 2015, **44**, 3924-3941.
39. N. Jayaraman, K. Maiti and K. Naresh, *Chem. Soc. Rev.*, 2013, **42**, 4640-4656.
40. S. Sangabathuni, R. Vasudeva Murthy, P. M. Chaudhary, M. Surve, A. Banerjee and R. Kikkeri, *Nanoscale*, 2016, **8**, 12729-12735.
41. K. Gorska, K. T. Huang, O. Chaloin and N. Winssinger, *Angew. Chem. Int. Ed. Engl.*, 2009, **48**, 7695-7700.
42. S. M. Rele, W. Cui, L. Wang, S. Hou, G. Barr-Zarse, D. Tatton, Y. Gnanou, J. D. Esko and E. L. Chaikof, *J. Am. Chem. Soc.*, 2005, **127**, 10132-10133.
43. O. A. Matthews, A. N. Shipway and J. F. Stoddart, *Prog. Polym. Sci.*, 1998, **23**, 1-56.
44. S. E. B. Peter R. Ashton, Christopher L. Brown, Sergey A. Nepogodiev, and H. W. I. P. E. W. Meijer, and J. Fraser Stoddart, *Chem. Eur. J.*, 1997, **3**, 974-984.
45. U. S. M. S. Wolfgang and S. G. K. a. H. Kunz, *Angew. Chem. Int. Ed. Engl.*, 1996, **35**, 321-324.
46. B. D. Polizzotti and K. L. Kiick, *Biomacromolecules*, 2006, **7**, 483-490.
47. S. A. DeFrees, L. Phillips, L. Guo and S. Zalipsky, *Angew. Chem. Int. Ed. Engl.*, 1996, **118**, 6101-6104.
48. Y. Harada, T. Murata, K. Totani, T. Kajimoto, S. M. Masum, Y. Tamba, M. Yamazaki and T. Usui, *Biosci. Biotechnol. Biochem.*, 2005, **69**, 166-178.
49. X.-L. Sun, Y. Kanie, C.-T. Guo, O. Kanie, Y. Suzuki and C.-H. Wong, *Eur. J. Org. Chem.*, 2000, **2000**, 2643-2653.
50. M. Marradi, F. Chiodo, I. Garcia and S. Penades, *Chem. Soc. Rev.*, 2013, **42**, 4728-4745.
51. P. M. Chaudhary, S. Sangabathuni, R. V. Murthy, A. Paul, H. V. Thulasiram and R. Kikkeri, *Chem. Commun. (Camb)*, 2015, **51**, 15669-15672.

52. J. M. de la Fuente, A. G. Barrientos, T. C. Rojas, J. Rojo, J. Canada, A. Fernandez and S. Penades, *Angew. Chem. Int. Ed. Engl.*, 2001, **40**, 2258-+.
53. Y. J. Chuang, X. Zhou, Z. Pan and C. Turchi, *Biochem. Biophys. Res. Commun.*, 2009, **389**, 22-27.
54. F. van de Manakker, T. Vermonden, C. F. van Nostrum and W. E. Hennink, *Biomacromolecules*, 2009, **10**, 3157-3175.
55. E. M. M. Del Valle, *Process Biochem.*, 2004, **39**, 1033-1046.
56. A. Martinez, C. Ortiz Mellet and J. M. Garcia Fernandez, *Chem. Soc. Rev.*, 2013, **42**, 4746-4773.
57. T. Loftsson and D. Duchene, *Int. J. Pharm.*, 2007, **329**, 1-11.
58. S. Li and W. C. Purdy, *Chem. Rev.*, 1992, **92**, 1457-1470.
59. J. Hu, Z. Tao, S. J. Li and B. L. Liu, *J. Mater. Sci.*, 2005, **40**, 6057-6061.
60. H. J. S. Buschmann, *E. J. Cosmet. Sci.* 2002, **53**, 185-191.
61. H. J. K. Buschmann, D.; Schollmeyer, *E. J. Incl. Phenom. Macrocycl. Chem.* 2001, 169–172.
62. H. J. I. P. M. C. Hashimoto, *44*, 57–62.
63. C. O. Mellet, J. M. G. Fernandez and J. M. Benito, *Chem. Soc. Rev.*, 2011, **40**, 1586-1608.
64. R. V. Vico, J. Voskuhl and B. J. Ravoo, *Langmuir*, 2011, **27**, 1391-1397.
65. H. Bavireddi and R. Kikkeri, *Analyst*, 2012, **137**, 5123-5127.
66. J. L. Jimenez Blanco, C. Ortiz Mellet and J. M. Garcia Fernandez, *Chem. Soc. Rev.*, 2013, **42**, 4518-4531.
67. M. Gomez-Garcia, J. M. Benito, A. P. Butera, C. Ortiz Mellet, J. M. Garcia Fernandez and J. L. Jimenez Blanco, *J. Org. Chem.*, 2012, **77**, 1273-1288.
68. M. Gomez-Garcia, J. M. Benito, D. Rodriguez-Lucena, J. X. Yu, K. Chmurski, C. Ortiz Mellet, R. Gutierrez Gallego, A. Maestre, J. Defaye and J. M. Garcia Fernandez, *J. Am. Chem. Soc.*, 2005, **127**, 7970-7971.
69. D. Ponader, P. Maffre, J. Aretz, D. Pussak, N. M. Ninnemann, S. Schmidt, P. H. Seeberger, C. Rademacher, G. U. Nienhaus and L. Hartmann, *J. Am. Chem. Soc.*, 2014, **136**, 2008-2016.
70. A. Patel and Thisbe K. Lindhorst, *E. J. Org. Chem.*, 2002, **2002**, 79-86.
71. T. K. Lindhorst, K. Bruegge, A. Fuchs and O. Sperling, *Beilstein J. Org. Chem.*, 2010, **6**, 801-809.
72. M. Gomez-Garcia, J. M. Benito, R. Gutierrez-Gallego, A. Maestre, C. O. Mellet, J. M. G. Fernandez and J. L. J. Blanco, *Org. Bio. Chem.*, 2010, **8**, 1849-1860.
73. N. S. Kehr, *Biomacromolecules*, 2016, **17**, 1117-1122.
74. H. Bavireddi, R. Vasudeva Murthy, M. Gade, S. Sangabathuni, P. M. Chaudhary, C. Alex, B. Lepenies and R. Kikkeri, *Nanoscale*, 2016, **8**, 19696-19702.
75. P. M. Chaudhary, M. Gade, R. A. Yellin, S. Sangabathuni and R. Kikkeri, *Anal. Methods*, 2016, **8**, 3410-3418.
76. P. H. Seeberger and D. B. Werz, *Nature*, 2007, **446**, 1046-1051.
77. D. Wang, S. Liu, B. J. Trummer, C. Deng and A. Wang, *Nat. Biotechnol.*, 2002, **20**, 275-281.
78. W. G. Willats, S. E. Rasmussen, T. Kristensen, J. D. Mikkelsen and J. P. Knox, *Proteomics*, 2002, **2**, 1666-1671.

79. D. A. Mann, M. Kanai, D. J. Maly and L. L. Kiessling, *J. Am. Chem. Soc.*, 1998, **120**, 10575-10582.
80. K. S. Ko, F. A. Jaipuri and N. L. Pohl, *J. Am. Chem. Soc.*, 2005, **127**, 13162-13163.
81. H. Uzawa, H. Ito, P. Neri, H. Mori and Y. Nishida, *ChemBiochem*, 2007, **8**, 2117-2124.
82. M. C. Shao, *Anal. Biochem.*, 1992, **205**, 77-82.
83. M. R. Lee and I. Shin, *Org. Lett.*, 2005, **7**, 4269-4272.
84. J. C. Love, L. A. Estroff, J. K. Kriebel, R. G. Nuzzo and G. M. Whitesides, *Chem. Rev.*, 2005, **105**, 1103-1169.
85. M. C. Fritz, G. Hahner, N. D. Spencer, R. Burli and A. Vasella, *Langmuir*, 1996, **12**, 6074-6082.
86. K. Gruber, T. Horlacher, R. Castelli, A. Mader, P. H. Seeberger and B. A. Hermann, *ACS Nano*, 2011, **5**, 3670-3678.
87. D. M. Ratner, E. W. Adams, J. Su, B. R. O'Keefe, M. Mrksich and P. H. Seeberger, *ChemBiochem*, 2004, **5**, 379-382.
88. S. Park and I. Shin, *Angew. Chem. Int. Ed. Engl.*, 2002, **41**, 3180-3182.
89. M. R. Lee and I. Shin, *Angew. Chem. Int. Ed. Engl.*, 2005, **44**, 2881-2884.
90. P. H. Liang, S. K. Wang and C. H. Wong, *J. Am. Chem. Soc.*, 2007, **129**, 11177-11184.
91. M. C. Bryan, F. Fazio, H. K. Lee, C. Y. Huang, A. Chang, M. D. Best, D. A. Calarese, O. Blixt, J. C. Paulson, D. Burton, I. A. Wilson and C. H. Wong, *J. Am. Chem. Soc.*, 2004, **126**, 8640-8641.
92. I. Shin, S. Park and M. R. Lee, *Chemistry*, 2005, **11**, 2894-2901.
93. Y. Yanase, T. Hiragun, K. Ishii, T. Kawaguchi, T. Yanase, M. Kawai, K. Sakamoto and M. Hide, *Sensors (Basel)*, 2014, **14**, 4948-4959.
94. A. Szabo, L. Stolz and R. Granzow, *Curr. Opin. Struct. Biol.*, 1995, **5**, 699-705.
95. K. Yu, A. L. Creagh, C. A. Haynes and J. N. Kizhakkedathu, *Anal. Chem.*, 2013, **85**, 7786-7793.
96. J. M. Kaplan, J. Shang, P. Gobbo, S. Antonello, L. Armelao, V. Chatare, D. M. Ratner, R. B. Andrade and F. Maran, *Langmuir*, 2013, **29**, 8187-8192.
97. K. Oberg, J. Ropponen, J. Kelly, P. Lowenhielm, M. Berglin and M. Malkoch, *Langmuir*, 2013, **29**, 456-465.
98. X. L. Meng, Y. Fang, L. S. Wan, X. J. Huang and Z. K. Xu, *Langmuir*, 2012, **28**, 13616-13623.
99. E. Bulard, A. Bouchet-Spinelli, P. Chaud, A. Roget, R. Calemczuk, S. Fort and T. Livache, *Anal. Chem.*, 2015, **87**, 1804-1811.
100. O. Zagorodko, J. Bouckaert, T. Dumych, R. Bilyy, I. Larroulet, A. Yanguas Serrano, D. Alvarez Dorta, S. G. Guin, S. O. Dima, F. Oancea, R. Boukherroub and S. Szunerits, *Biosensors (Basel)*, 2015, **5**, 276-287.
101. S. N. Narla and X. L. Sun, *Biomacromolecules*, 2012, **13**, 1675-1682.
102. N. Maalouli, A. Barras, A. Siriwardena, M. Bouazaoui, R. Boukherroub and S. Szunerits, *Analyst*, 2013, **138**, 805-812.
103. G. Bellapadrona, A. B. Tesler, D. Grunstein, L. H. Hossain, R. Kikkeri, P. H. Seeberger, A. Vaskevich and I. Rubinstein, *Anal. Chem.*, 2012, **84**, 232-240.
104. M. Ogiso, J. Kobayashi, T. Imai, K. Matsuoka, M. Itoh, T. Imamura, T. Okada, H. Miura, T. Nishiyama, K. Hatanaka and N. Minoura, *Biosens. Bioelectron.*, 2013, **41**, 465-470.
105. C. F. Huang, G. H. Yao, R. P. Liang and J. D. Qiu, *Biosens. Bioelectron.*, 2013, **50**, 305-310.

106. G. T. Z. Salamon, *Spectroscopy*, 2001, **15**, 161-175.
107. E. Harte, N. Maalouli, A. Shalabney, E. Texier, K. Berthelot, S. Lecomte and I. D. Alves, *Chem. Commun. (Camb)*, 2014, **50**, 4168-4171.
108. I. Alves, I. Kurylo, Y. Coffinier, A. Siriwardena, V. Zaitsev, E. Harte, R. Boukherroub and S. Szunerits, *Anal. Chim. Acta*, 2015, **873**, 71-79.
109. S. G. Kazarian and K. L. Chan, *Appl. Spectrosc.*, 2010, **64**, 135A-152A.
110. J. Yang, J. N. Chazalviel, A. Siriwardena, R. Boukherroub, F. Ozanam, S. Szunerits and A. C. Gouget-Laemmel, *Anal. Chem.*, 2014, **86**, 10340-10349.
111. A. C. Gouget-Laemmel, J. Yang, M. A. Lodhi, A. Siriwardena, D. Aureau, R. Boukherroub, J. N. Chazalviel, F. Ozanam and S. Szunerits, *J. Phy. Chem. C*, 2013, **117**, 5513-5513.
112. C. I. Cheng, Y. P. Chang and Y. H. Chu, *Chem. Soc. Rev.*, 2012, **41**, 1947-1971.
113. S. C. Luo, E. A. Kantchev, B. Zhu, Y. W. Siang and H. H. Yu, *Chem. Commun. (Camb)*, 2012, **48**, 6942-6944.
114. F. Ma, A. Rehman, H. Liu, J. Zhang, S. Zhu and X. Zeng, *Anal. Chem.*, 2015, **87**, 1560-1568.
115. E. Mahon, Z. Mouline, M. Sillion, A. Gilles, M. Pinteala and M. Barboiu, *Chem. Commun. (Camb)*, 2013, **49**, 3004-3006.
116. M. Ogiso, K. Matsuoka, T. Okada, T. Imai, M. Itoh, T. Imamura, Y. Haga, K. Hatanaka and N. Minoura, *J. Colloid. Interface Sci.*, 2013, **393**, 257-263.
117. M. W. J. W. Ndieyira, A. D. Barrera, D. Zhou, M. V€ogtli, M. Batchelor, M. A. Cooper, T. Strunz, M. A. Horton, Ch. Abell, T. Rayment, G. Aeppli, R. A. McKendry, *Nat. Nanotechnol.*, 2008, **35**, 691-696.
118. M. K. G. T. Braun, N. Backmann, W. Grange, P. Boulanger, L. Letellier, H.-P. Lang, A. Bietsch, Ch. Gerber, M. Hegner, *Nat. Nanotechnol.*, 2008, **8**, 179-185.
119. A. Mader, K. Gruber, R. Castelli, B. A. Hermann, P. H. Seeberger, J. O. Radler and M. Leisner, *Nano Lett.*, 2012, **12**, 420-423.
120. S. Kesel, A. Mader, P. H. Seeberger, O. Lieleg and M. Opitz, *Appl. Environ. Microbiol.*, 2014, **80**, 5911-5917.
121. Y. F. Dufrene, D. Martinez-Martin, I. Medalsy, D. Alsteens and D. J. Muller, *Nat. Methods*, 2013, **10**, 847-854.
122. C. M. Bowers, D. A. Carlson, M. Rivera, R. L. Clark and E. J. Toone, *J. Phys. Chem. B*, 2013, **117**, 4755-4762.
123. A. Matsumoto and Y. Miyahara, *Nanoscale*, 2013, **5**, 10702-10718.
124. X. Luo and J. J. Davis, *Chem. Soc. Rev.*, 2013, **42**, 5944-5962.
125. M. O. Noor and U. J. Krull, *Anal. Chim. Acta*, 2014, **825**, 1-25.
126. S. Hideshima, H. Hinou, D. Ebihara, R. Sato, S. Kuroiwa, T. Nakanishi, S. Nishimura and T. Osaka, *Anal. Chem.*, 2013, **85**, 5641-5644.
127. G. J. Zhang, M. J. Huang, J. J. Ang, Q. Yao and Y. Ning, *Anal. Chem.*, 2013, **85**, 4392-4397.
128. H. Vedala, Y. Chen, S. Cecioni, A. Imberty, S. Vidal and A. Star, *Nano Lett.*, 2011, **11**, 170-175.
129. A. M. Y. Maeda, Y. Miura and Y. Miyahara, *Nanoscale Res. Lett.*, 2012, **7**, 108-115.
130. F. Harnisch and S. Freguia, *Chem. Asian J.*, 2012, **7**, 466-475.
131. L. C. B.W Zhu, X. P. He, G. R. Chen, Y. T. Long, 2014, **8**, 67-72.

132. Z. Wang, C. Sun, G. Vegesna, H. Liu, Y. Liu, J. Li and X. Zeng, *Biosens. Bioelectron.*, 2013, **46**, 183-189.
133. B. Pandey, Y. H. Tan, A. R. Parameswar, P. Pornsuriyasak, A. V. Demchenko and K. J. Stine, *Carbohydr. Res*, 2013, **373**, 9-17.
134. X. Y. Zhang, L. Y. Zhou, H. Q. Luo and N. B. Li, *Anal. Chim. Acta*, 2013, **776**, 11-16.
135. J. S. Daniels and N. Pourmand, *Electroanalysis*, 2007, **19**, 1239-1257.
136. A. Hushegyi, T. Bertok, P. Damborsky, J. Katrlík and J. Tkáč, *Chem. Commun. (Camb)*, 2015, **51**, 7474-7477.

CHAPTER 2

Part I

Immobilization of Multivalent Glycoprobes on Gold Surfaces For Sensing Proteins and Macrophages

Abstract

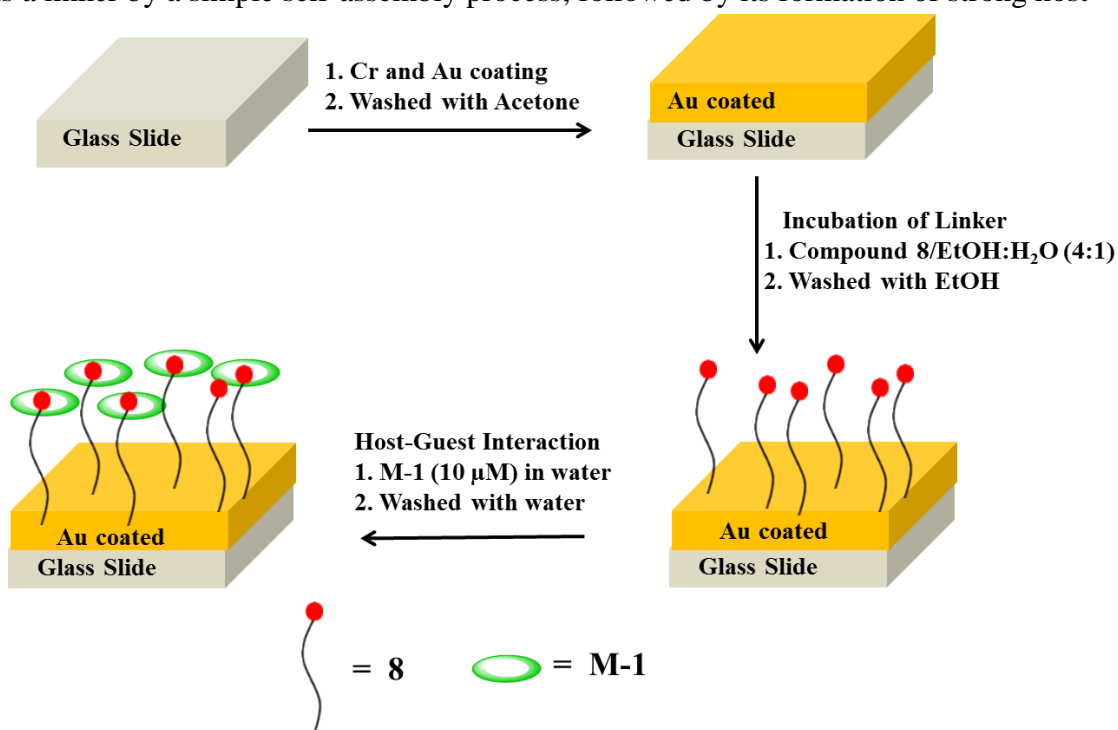
The multivalent display of carbohydrates on the cell surface provides cooperative binding to improve the specific biological events. In addition to multivalency, the spatial arrangement and orientation of sugars with respect to external stimuli also trigger carbohydrate–protein interactions. Herein, we report a noncovalent host–guest strategy to immobilize heptavalent glyco- β -cyclodextrin on gold-coated glass slides to study multivalent carbohydrate–protein interactions. We have found that the localization of sugar entities on surfaces using β -cyclodextrin (β -CD) chemistry increased the avidity of carbohydrate–protein and carbohydrate–macrophage interactions compared to monovalent- β -CD sugar coated surfaces. This platform is expected to be a promising tool to amplify the avidity of sugar-mediated interactions on surfaces and contribute to the development of next generation bio-medical products.

2.1. Introduction

Carbohydrates are recognized as information-rich biomolecules that play an important role in the human body. The surface of all mammalian cells is covered with carbohydrates that are attached to proteins and lipids embedded on the cell membrane. The interaction with the extracellular world is achieved through interaction between these carbohydrates and carbohydrate-binding proteins (lectins) which are present on surfaces of other mammalian cells, viruses, bacteria and bacterial toxins.¹ To enhance the strength of cell surface binding, nature often assembles multiple protein-carbohydrate complexes to provide the necessary avidity. The effect of multivalency concerning sugars present on surfaces as compared to monovalency has been described by several investigators²⁻³ and was found to be of critical importance in the field of protein-carbohydrate interactions. In addition to increase in avidity, multivalency enhances the selectivity of a particular interaction and amplifies small differences in the intrinsic binding avidity.⁴⁻⁵ Recently, the effort has been initiated to synthesize multivalent probes using peptides,⁶ polymers,⁷ dendrimers,⁸⁻⁹ nanoparticles and supramolecular complexes,¹⁰ for studying the carbohydrate-protein interactions in solution based techniques.¹¹⁻¹³ Alternatively, surface immobilization of monovalent sugars present multivalent arrays to facilitate the analysis of lectin binding and can be relevant to the cell surface carbohydrate presentation.¹⁴⁻¹⁹ To date, there are several methods reported to immobilize carbohydrates in an array format to study carbohydrate-lectin interactions. Carbodiimide coupling procedure is a well-studied technique that yield glycan arrays for evaluating high-throughput analysis.²⁰⁻²² Thiol-ene/-yne reactions were used to evaluate lectin-carbohydrate binding by quartz crystal microbalance (QCM) flow-through instrument.²³ Other techniques described in the literature include boronic acid-diol interaction, maleimido-thio interaction, click reactions, Staudinger reaction and epoxide-amine reaction.²⁴⁻²⁷ Although these methods can improve the immobilization of carbohydrates on the surfaces, it is still limited by the orientation, spatial arrangement and local concentration of sugars on the surfaces to increase the avidity of specific carbohydrate-protein interactions.²⁸ Recently, host-guest interactions such as those of β -CD systems have proven to be important for constructing patternized surfaces.²⁹⁻³² The advantage of host-guest method is that they can provide structural versatility and localized sugar concentration. More importantly, they have been used as a regeneration platform with high reproducibility for continuous modification of same sugar or

different sugar substrates to study the interaction with different glycoproteins and bacteria.³³⁻
³⁶This method can be used in the point of care devices.

With the goal of creating multivalent carbohydrate surfaces, we report here β -CD based host-guest scaffold which is synthetically facile and also displays localized multivalent carbohydrates. The technique that we report includes immobilization of PEGylated adamantyl molecule (AD) to serve as a linker by a simple self-assembly process, followed by its formation of strong host-



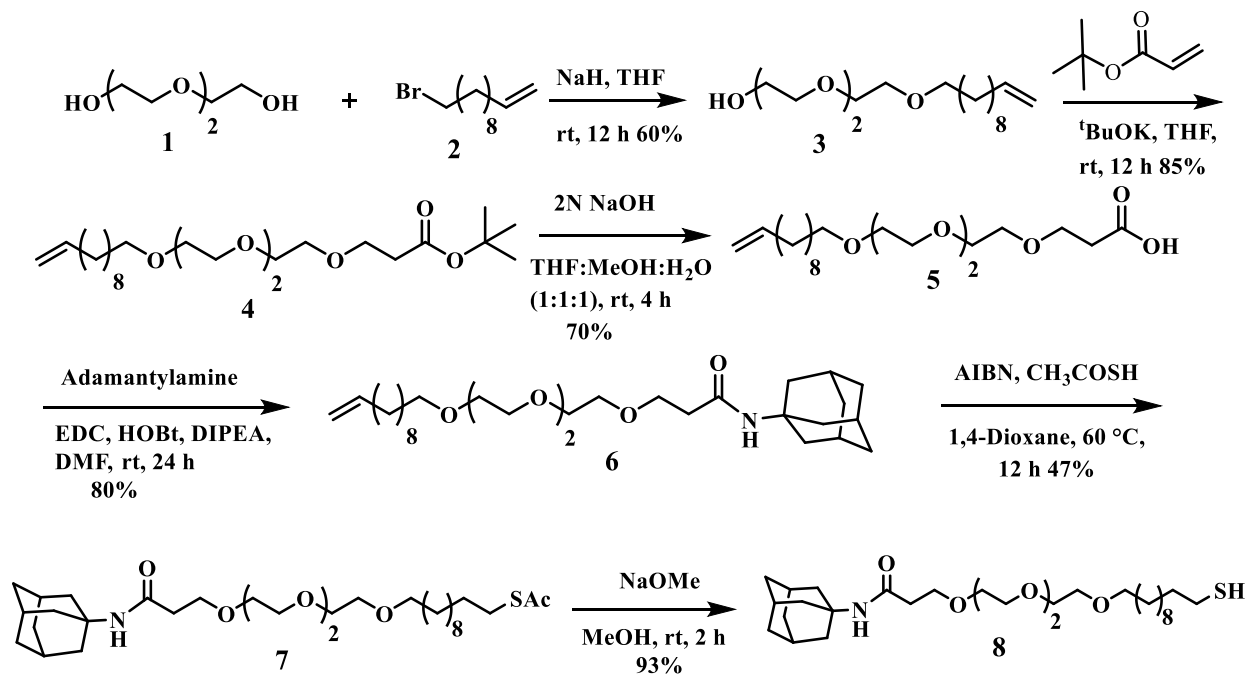
Scheme 1 Schematic of the different steps to immobilize supramolecular scaffold on gold coated glass slides

guest complexes with β -CD derivatives that were modified by attaching mannose residues (scheme 1). The existence of host-guest complexes on the gold substrates was characterized by surface analysis techniques. A combination of surface plasmon resonance (SPR) and THP-1 differentiated macrophage binding assay were employed to demonstrate the advantage of multivalent carbohydrate-protein interactions on the surfaces. The rationale for choosing **ConA** lectin is due to its selective binding with mannose or glucose sugars. The significant advantage of this approach is the simplicity of integrating a system with multivalent carbohydrate aggregates that interact with lectins and cells. Such a system is essential for tuning the selectivity and sensitivity of the specific carbohydrate-protein interactions.

2.1.1. Results and Discussion

2.1.1.1. Synthesis of adamantyl linker

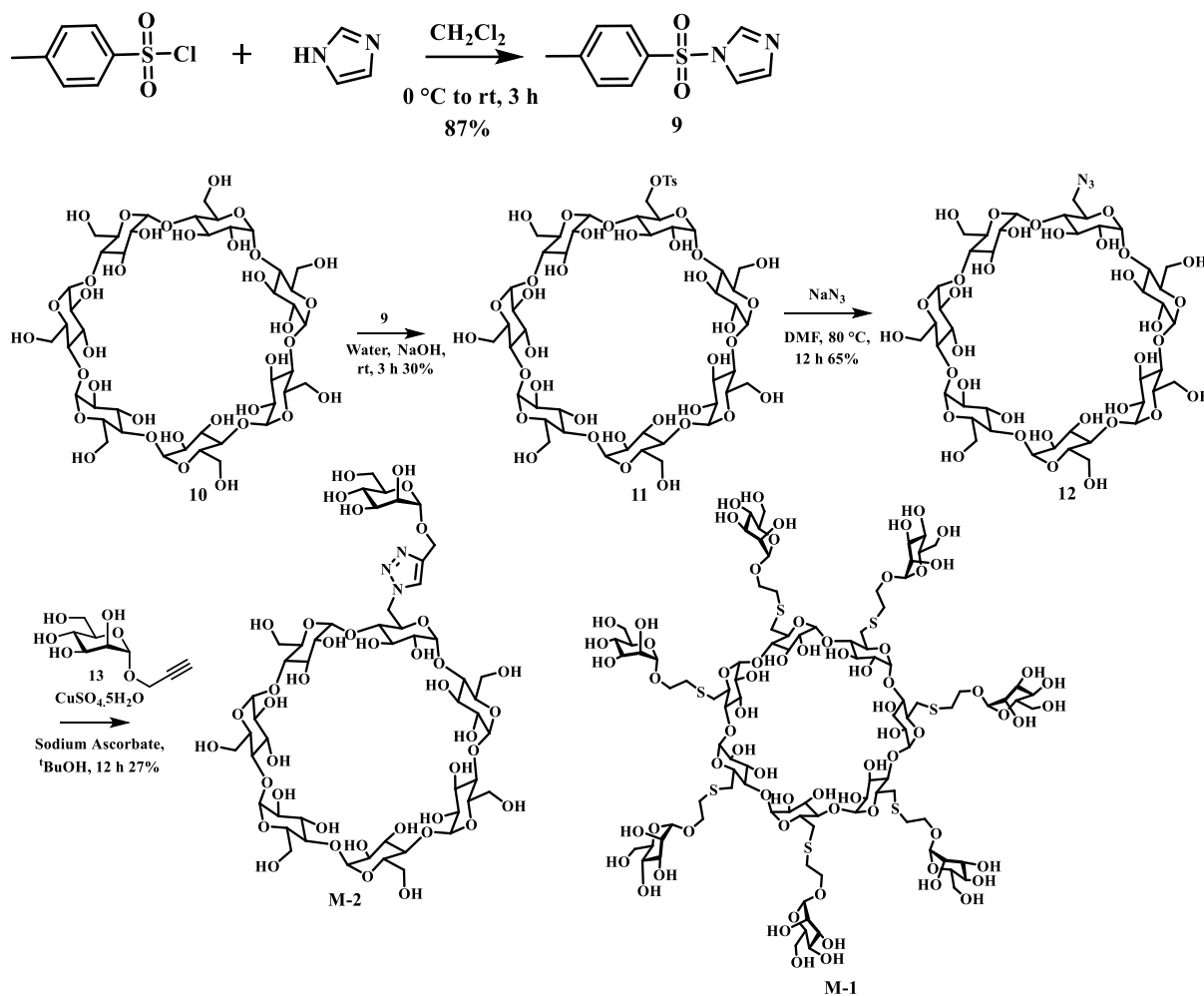
The chemical structures of the molecules used for the formation of the self-assembled glycoclusters (**M-1**, **M-2**, and **8**) are depicted in Scheme 2 and 3. The adamantyl derivative (**AD**) **8** was prepared in several steps, starting from conjugation of triethylene glycol **1** with 11-bromoundec-1-ene **2**, followed by its reaction with *t*-butyl acrylate to yield compound **4**. After hydrolysis with NaOH, the carboxylic acid **5** was obtained and coupling with 1-adamantylamine yielded adamantyl derivative **6**. The compound was treated with thioacetic acid and azoisobutyronitrile (AIBN), followed by deacetylation with NaOMe to yield compound **8** (scheme 2).



Scheme 2 Synthesis of adamantyl linker

2.1.1.2. Synthesis of heptamannose β -CD and monomannose (**M-2**)

Mannose modified β -CD derivatives (**M-1**) were synthesized as described by García-Barrientos.³⁷ For mono-mannose substituted β -CD (**M-2**) synthesis first we prepared imidazole complex **9** with tosyl chloride. Using complex **9** we did monotosylation of β -CD **11** further tosyl substituted with azide using sodium azide **12**. Further click reaction between β -CD-mono azide and propargyl mannosides to yield monomannose- β -CD (**M-2**).



Scheme 3 Synthesis of monomannose β -CD (M-2) and structure of heptamannose β -CD

2.1.1.3. Functionalization of glass slide with adamantane linker

Glass slides (approx. 1x1cm) were washed with EtOH, coated with chromium (10 nm) and gold (100 nm) by using gold evaporation chamber at a pressure of about 4×10^{-6} mbar. Samples were immersed in an ethanol solution of **8** (0.2, 0.02 and 0.005 M) for 48 h. The adamantyl coated glass slides were then rinsed with ethanol to remove physisorbed materials (Scheme 1) and were stored at controlled conditions.

2.1.1.4. Characterization of slide

Monolayers were characterized by a combination of methods, namely, aqueous contact angles, atomic force microscopy (AFM) (Fig. 1), ellipsometry and X-ray photoelectron spectroscopy (XPS) (Fig. 2). Contact angle measurements revealed a 60° angle for the freshly cleaned gold substrate which shifted to 64° , 78° and 85° for the adamantyl monolayer surface (in 0.005, 0.02 and 0.2 M ethanolic solution of **8** respectively), reflecting the hydrophobic character of the

surface. The thickness of **8** (0.02 M) monolayer, measured by ellipsometry, was $\sim 13.9 \text{ \AA}$ (Table 1, Entry 1) which is in good agreement with the values described for similar linker models in literature.³⁸ AFM images of the bare gold surfaces were relatively homogeneous with some nodules whereas gold-coated glass slides monolayer of **8** showed rough surface. The root-mean-square surface roughness (R) was found to be $\sim 1.4 \text{ nm}$ (Fig. 1b). The host-guest complex was prepared by the formation of complexes between $\beta\text{-CD}$ and the adamantyl residues found as monolayers on the gold substrates. Freshly prepared adamantyl monolayers (prepared from 0.2, 0.02 M and 0.005 M solutions) were immersed in a solution of **M-1** ($10 \text{ }\mu\text{M}$) for 24 hours at RT. The functionalized substrates were rinsed with deionized water to remove physisorbed materials and the contact angles were measured. The results indicated that the concentration and spatial arrangement of **8** dictates the number of complexes on the gold surface. As expected, 0.2 M of **8** resulted weak host-guest interaction due to the dense coating of hydrophobic adamantyl moiety, whereas 0.02 and 0.005 M of **8** resulted in a strong host-guest interaction, indicating that the host-guest interactions are better when the adamantyl units are distant from each other. This was further supported by phenol-sulfuric acid analysis of mannose concentration.

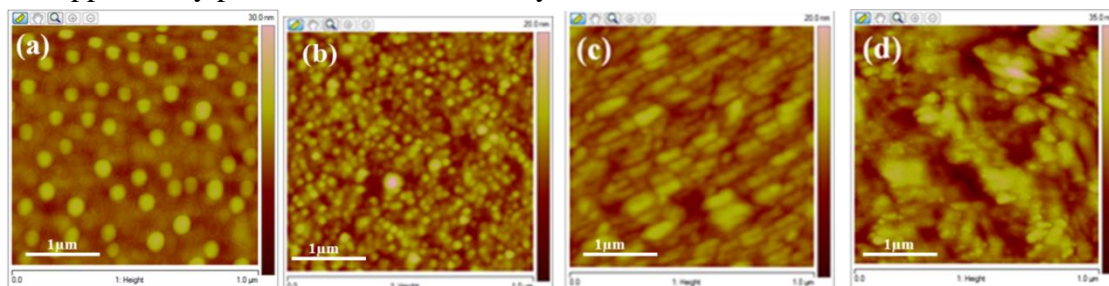


Figure 1 AFM images of the different surfaces: (a) bare Au, (b) Au substrate coated with **8** (0.02 M); (c) **8/M-1** (0.02 M/ $10 \text{ }\mu\text{M}$) coated Au substrate and (d) **8/M-1/ConA** (0.02 M/ $10 \text{ }\mu\text{M}$ / 1 mg/mL) coated Au substrate.

Table 1: Contact angle and length of monolayer measured in ellipsometry. Conc **M-1** = 10 μ M and Conc **ConA** = 1 mg/1 mL

Entry	Type of coverage on Slides	Contact angle ($^{\circ}$) (Conc 8)	Ellipsometry (\AA)	Conc of Mannose ($\mu\text{g}/\text{cm}^2$) (conc 8)
1	Au + 8	85 ± 2 (0.2 M)	13.9 ± 0.172 ³⁹	-
		78 ± 2 (0.02 M)		
		64 ± 2 (0.005 M)		
2	Au + 8 + M-1 (10 μ M)	71 ± 2 (0.2 M)	29.82 ± 0.129	0.2 ± 0.01 (0.2 M)
		33 ± 2 (0.02 M)		1.9 ± 0.01 (0.02 M)
		49 ± 2 (0.005 M)		1.3 ± 0.03 (0.005 M)
3	Au + 8 + M-1 + ConA	Not measured	92.93 ± 0.794	-

A similar observation was described by Park *et al.*³⁹ For our experiment; we selected 0.02 M solution of linker **8** to avoid non-specific interactions between vacant gold surface and proteins or cells. The thickness of the film, after formation of the complexes, as indicated by ellipsometric measurements, increased to 29.82 \AA (Table 1 Entry 2), which is 2-fold more than that of the layer before the formation of the host-guest complex and it reflects the thickness of the β -CD moiety. The presence of the complexes on the surfaces was further confirmed by AFM measurements, which also revealed the morphology of surfaces and the root-mean-square roughness had increased from ~ 1.4 nm to ~ 1.7 nm (Fig. 1c).

2.1.1.5. Characterization of slide by XPS

XPS analysis was performed to confirm the binding of **8** to the Au film (Fig. 2). A comparison between the XPS spectra of bare Au film and **8** coated Au film for the binding energy of C 1s core level electrons and Au 4f core level electrons has been done. The C 1s spectrum for bare Au film was fitted with the single peak centered at 284.6 eV. On the other hand, C 1s spectrum of **8** coated Au film was best fitted with two peaks centered at 284.6 and 286.7 eV. These peaks were assigned to hydrocarbons (C-C/C-H, 284.6 eV) and ether/alcohol carbon (C-O-X, 286.7 eV) of **8** molecules present onto the Au film. Figure 2c shows that Au 4f spectrum for the bare Au film was resolved in two peaks situated at 84.6 and 88.2 eV for Au 4f_{7/2} (Au⁰) and Au 4f_{5/2} (Au⁰). On the contrary, Au 4f spectrum for **8** coated Au film was deconvoluted in four peaks, centered at 83.3, 84.6, 86.9 and 88.2 eV, attributed to Au 4f_{7/2} (Au⁰), Au 4f_{7/2} (Au-S), Au 4f_{5/2} (Au⁰) and Au 4f_{5/2} (Au-S), respectively (Fig. 2d). The chemical shift of 1.3 eV towards the low binding energy in the Au 4f_{7/2} (Au⁰) and Au 4f_{5/2} (Au⁰) peaks, and appearance of Au 4f_{7/2} (Au-S) and Au 4f_{5/2} (Au-S) peaks after **8** deposition confirms the binding of **8** to the Au film.

2.1.1.6. Evaluating carbohydrate protein interactions on slide

After assessing the structure of the gold substrates, we used them for investigating multivalent carbohydrate–protein interactions. The lectin **ConA** served as model for these studies since it selectively binds to α -mannopyranosides. **ConA** molecules were immobilized on the substrates by immersing the **8/M-1** coated slides in **ConA** solution (1 mg/1 mL in HEPES) for 1 h, followed by washing with water. Ellipsometry measurements revealed a very strong increase in the thickness of the layers, $\sim 92.93 \text{ \AA}$ as compared to $\sim 29.82 \text{ \AA}$ (Table 1 Entry 3) and R value was found to be $\sim 4.2 \text{ nm}$ (Fig. 1d). The large increase in the height is indicative of the immobilization of the proteins on the gold substrates.⁴⁰

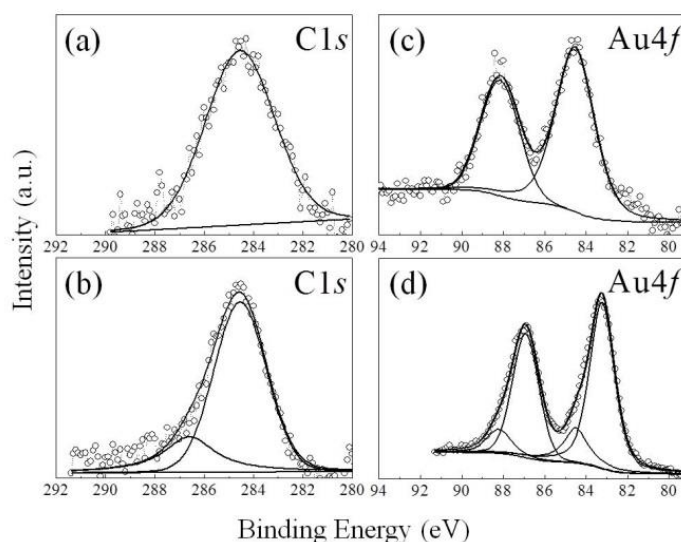


Figure 2 XPS spectra of (a) C 1s for bare Au film, (b) C 1s for **8** coated Au film, (c) Au 4f for bare Au film (d) Au 4f for **8** coated Au film

2.1.1.7 Assessing Carbohydrate-protein interactions by Surface Plasmon Resonance (SPR)

In order to assess the protein-carbohydrate interactions we studied their surface Plasmon resonance (SPR) measurements with **ConA** lectin. The cyclodextrin scaffolds (**M-1**, **M-2** and β -**CD**) on comp **8** were immobilized on the gold chip before the solutions of different concentrations of **ConA** (0 to $3.5 \mu\text{M}$) were flowed over the chip. Before conducting the carbohydrate-protein interactions, the host-guest properties of compound **8** and β -**CD** were confirmed. Two different concentrations of **8** was immobilized on the gold coated SPR sensor chips to generate low-density (**8-LD**, 0.01 mM) and high-density (**8-HD**, 0.1 mM) adamantane surfaces. SPR and kinetic analyses were based on a 1:1 interaction model. The SPR analyses of high and low density of adamantane showed marginal difference in binding affinity (Table 2, Fig.

3), indicating that the concentration of adamantane backbone is critical for host-guest interactions as reported by park et al.³⁹ Based on the above results, we constructed four host-guest complexes of **8** and **M-1** (**H-1**, **H-2**, **H-3**, and **H-4**) at an optimal concentration useful for **ConA** binding and then studied how multivalency and host-guest interactions were influencing the carbohydrate-protein interactions (Fig. 4). In case of **H-1** and **H-2**, the density of adamantyl linker **8** was maintained low (0.01 mM) and **M-1** concentration was increased to 5 and 50-folds with respect to

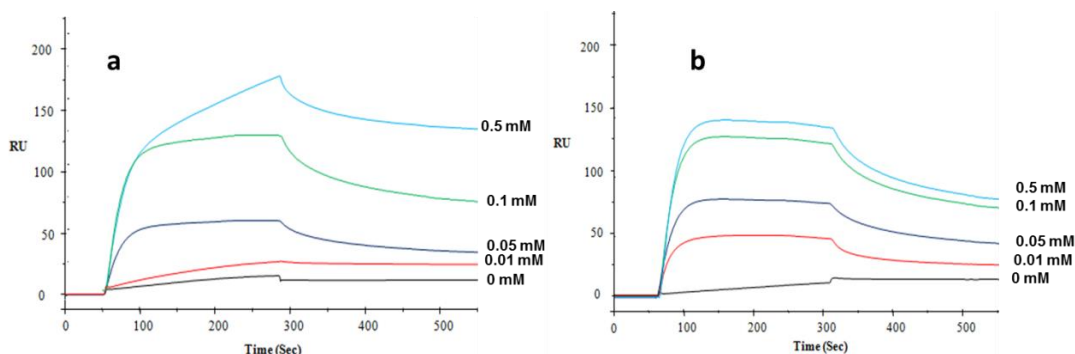


Figure 3 SPR sensograms for different concentrations of β -CD incubated with (a) **8** (0.01 mM), (b) **8** (0.1 mM)

8, resulting in optimum host-guest interaction. Whereas, in case of **H-3** and **H-4**, the density of **8** was high (0.1 mM) and close proximity of the group results weak host-guest complexes, result low sugar density on the surface. The SPR analyses of these four mannose surfaces with different concentration of **ConA** revealed that **H-2** binds 2-fold strongly as compared to **H-1**, a similar experiment with **H-3** and **H-4** displayed almost identical binding and displayed much weaker binding compared to **H-2**. Overall, these results are comparable with reported values.⁴¹⁻⁴² On the basis of these results, we hypothesized that at low density of **8**, adamantane groups are well separated to host substantial amount of **M-1** to increase the **ConA** binding. On the other hand, the large number of **M-1** also restricts **ConA** interaction to 2-fold increase. At high density of **8**, the close proximity of adamantane groups restricts hosting of **M-1** moieties to increase the binding affinity. To confirm the influence of hepta-valent sugar topology, we performed the SPR experiments with four different concentrations of **8** and **M-2** (**H-5**, **H-6**, **H-7** & **H-8**) complexes (Fig. 5). SPR analyses revealed weak association and dissociation constant as compared to **H-2**. The K_d value of **H-5** to **H-8** are comparable to monovalent mannose-**ConA** binding affinity.^{41,43} This outcome clearly showed that spatial arrangement of hepta-valent sugar on β -CD not only increases the sugar density, but also increases the binding interactions (Fig. 4, 5, Table 2). Finally,

to confirm the role of β -CD in carbohydrate-protein interactions, SPR analysis of $8/\beta$ -CD complex (**H-9 & H-10**) was carried out. As expected, β -CD complex showed a weak binding with **ConA** lectin (Fig. 6 and Table 2).

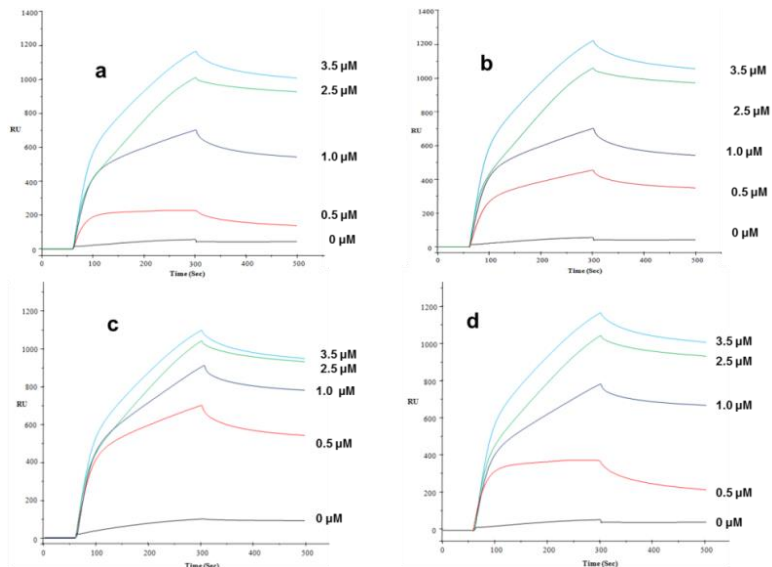


Figure 4 SPR sensograms for different concentrations of **ConA** incubated with (a) **H-1 : 8** (0.01mM) & **M-1** (0.05 mM); (b) **H-2:8** (0.01 mM) & **M-1** (0.5 mM); (c) **H-3:8** (0.1mM) & **M-1** (0.05 mM); (d) **H-4:8** (0.1 mM) & **M-1** (0.5mM)

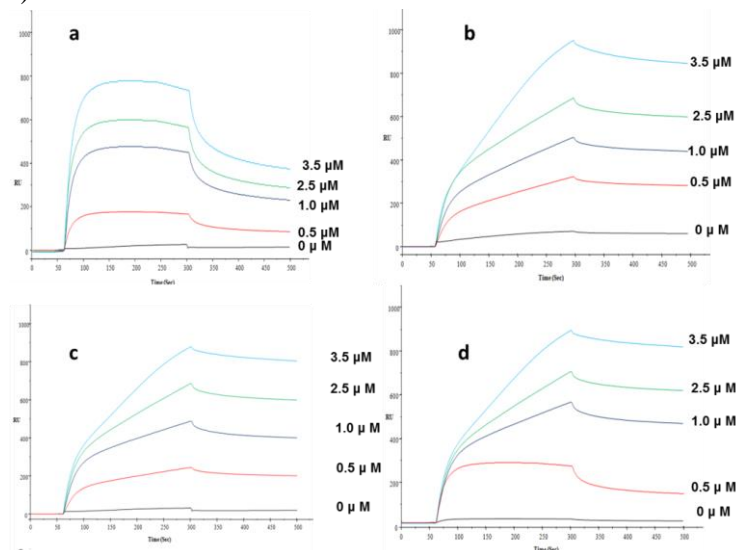


Figure 5 SPR sensograms for different concentrations of **ConA** incubated with (a) **H-5:8** (0.01mM) & **M-2** (0.05 mM); (b) **H-6:8** (0.01 mM) & **M-2** (0.5 mM); (c) **H-7:8** (0.1mM) & **M-2** (0.05 mM), (d) **H-8:8** (0.1 mM) & **M-2** (0.5 mM)

Together these results show that, in the context of a host-guest multivalent platform, the strength of the binding interactions between **ConA** and mannose directly correlates with spatial arrangement of mannose-capped- β -CD.⁴⁴ Similar experiments with **H-1** and **H-2** complex with PNA (galactose specific lectin) revealed no binding, proving the specificity (Fig. 7 and Table 2).

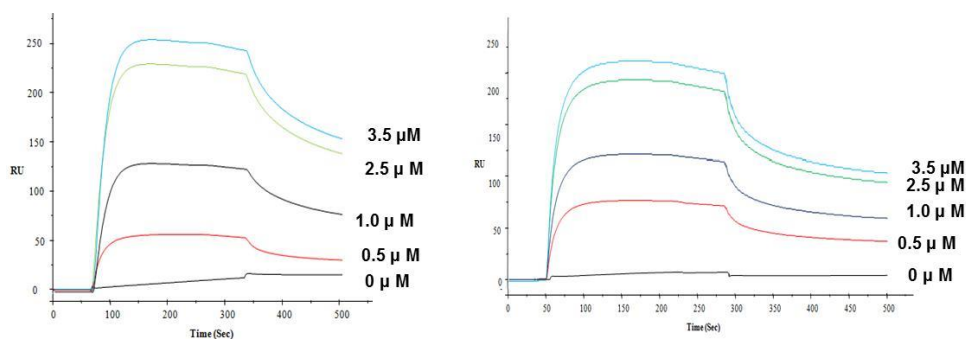


Figure 6 SPR sensograms for different concentrations of ConA incubated with (a) **8** (0.01mM) & β -CD (0.05 mM), (b) **8** (0.01 mM) & β -CD (0.5 mM)

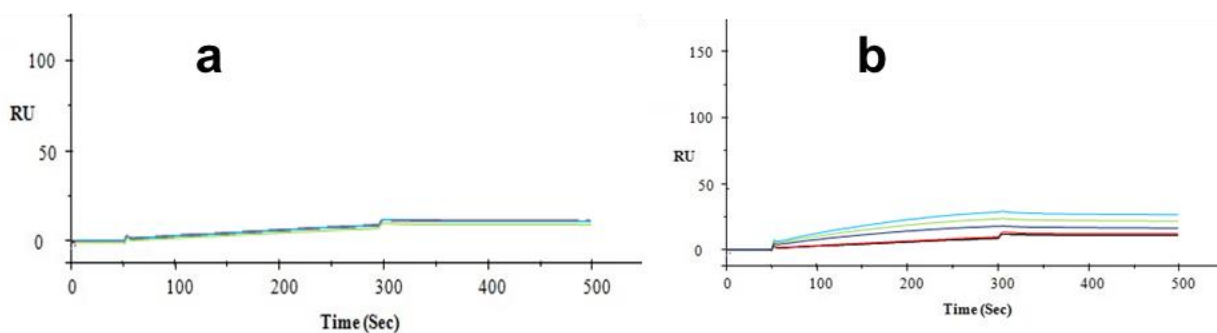


Figure 7:SPR sensograms for different concentrations of PNA incubated with (a) **6** (0.01mM) & **M-1** (0.05 mM), (b) **6** (0.01 mM) & **M-2** (0.5 mM); [--- (0 μ M), --- (0.5 μ M), --- (1.0 μ M), --- (2.5 μ M) and --- (3.5 μ M)].

2.1.1.8. Macrophage binding assay

A possible application of our system composed of mannose capped β -CD that interact strongly with lectin was illustrated by the adhesion of THP-1 differentiated macrophage cells on the gold coated glass surfaces. Macrophage cells are reported to have C-type lectin receptors that recognize high-mannose glycans.⁴⁵ Previously, multivalent mannosylated β -CD scaffolds have been well characterized towards binding macrophage mannose receptor.⁴⁶ Thus we hypothesized that **8/M-1** could bind macrophages more strongly than **8/M-2**. To study this, sugar coated gold slides were constructed using multivalent **8/M-1** and monovalent **8/M-2** respectively. The glyco-

surfaces were exposed to solutions containing a known number of macrophage cells and incubated for 24 h. After washing with PBS, the slides were exposed for bright microscopic imaging. Maximum numbers of cells were observed on **8/M-1**-coated slides

Table 2 Kinetic parameters for the interaction between **ConA** and mannose- based monovalent and multivalent derivatives

Composition (mM)		Entry	vs	$K_A (M^{-1} s^{-1})$	$K_D (s^{-1})$	$K_d(M^{-1})$
8 (0.01mM)			β -CD	1.21×10^2	6.15×10^{-2}	0.19×10^4
8 (0.1mM)			β -CD	1.12×10^2	4.90×10^{-2}	0.23×10^4
8 (0.01mM)	M-1 (0.05mM)	H-1	ConA	1.14×10^6	2.22×10^{-5}	0.55×10^{11}
	M-1 (0.5mM)	H-2	ConA	2.67×10^6	2.20×10^{-5}	1.21×10^{11}
8 (0.1mM)	M-1 (0.05mM)	H-3	ConA	3.55×10^5	1.69×10^{-5}	0.21×10^{11}
	M-1 (0.5mM)	H-4	ConA	5.35×10^5	1.49×10^{-5}	0.36×10^{11}
8 (0.01mM)	M-2 (0.05mM)	H-5	ConA	1.38×10^4	3.04×10^{-4}	0.45×10^8
	M-2 (0.5mM)	H-6	ConA	1.04×10^4	1.01×10^{-4}	1.04×10^8
8 (0.1mM)	M-2 (0.05mM)	H-7	ConA	0.228×10^4	1.75×10^{-4}	0.13×10^8
	M-2 (0.5mM)	H-8	ConA	0.56×10^4	2.81×10^{-4}	0.19×10^8
8 (0.01mM)	β -CD (0.05mM)	H-9	ConA	1.44×10^2	3.62×10^{-2}	0.439×10^4
	β -CD (0.5mM)	H-10	ConA	1.59×10^2	3.76×10^{-2}	0.42×10^4
8 (0.01mM)	M-1 (0.05mM)	H-1	PNA	-	-	-
	M-1 (0.5mM)	H-2	PNA	-	-	-

(Fig.8b). Whereas **8/M-2** (Fig. 8c) and **8/ β -CD** (Fig. 8a) coated surfaces appeared to have less number of bound cells with spherical morphology. Closer examination of **8/M-1** coated slides revealed that most cells have highly spread fashion. The statistical analysis of the complete slides indicated 3-4 fold difference between **8/M-1** vs **8/M-2** (Fig. 8d). These results indicate that multivalent sugars on β -CD increase the local concentration of sugars to influence the avidity of carbohydrate-protein interactions.

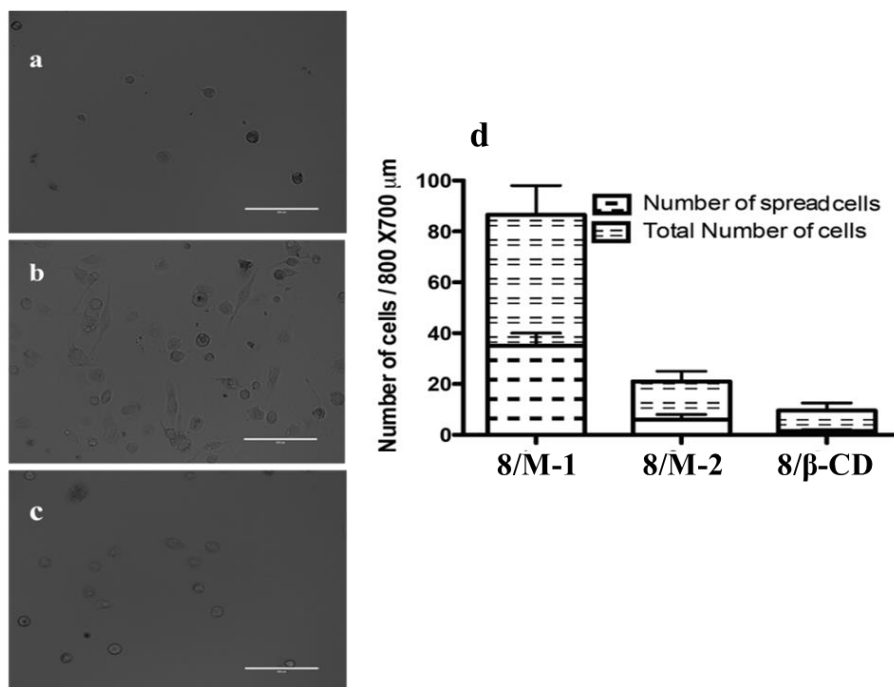


Figure 8 Representative images of macrophage adhesion to substrates covered with (a) **8/β-CD**, (b) **8/M-1** and (c) **8/M-2** after 24 h incubation. Scale bar length is 200 μm. (d) Quantitative analysis of macrophage adhesion after 24 h incubation

2.1.2 Conclusion

We have developed a technique for immobilizing multivalent carbohydrates on surfaces that is based on self-assembly-driven host-guest interactions between **β-CD** and adamantane molecules. This approach is simple, sensitive, and applicable for the study of carbohydrate-protein and carbohydrate-cell interactions using surface bound sugars. This strategy enables one to explore the significance of spatial arrangements of sugars on the surfaces for the interaction with lectins and to probe the role of monovalent sugar vs multivalent sugar immobilization. In addition, it can be used for high throughput, reversible and sensitive carbohydrate based biomedical devices.

2.1.3 Experimental part

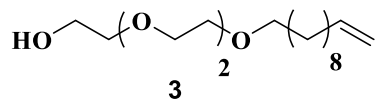
2.1.3.1. General Information

All chemicals were of reagent grade and unless otherwise noted were used as supplied. TLC was performed on Merck silica gel 60 F254 plates (0.25 mm) and visualized by UV or by dipping the plate in CAM/ninhydrin solution and heating. Column chromatography was carried on Fluka Kieselgel 60, mesh 100–200. ¹H and ¹³C NMR spectra were recorded on Jeol 400 MHz. Chemical shifts (δ) are reported in ppm, coupling constants (J) in Hz. Residual solvents, for

CDCl_3 $-\delta_{\text{H}}$, 7.26 and δ_{C} 77.3, for CD_3OD . δ_{H} 3.31, and δ_{C} 49.0, D_2O $-\delta_{\text{H}}$, 4.75, were used as internal references.

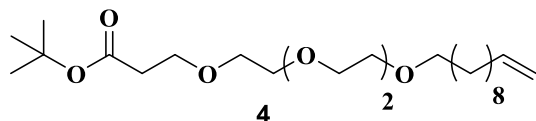
2.1.3.2. Experimental Details

2-(2-(2-(undec-10-en-1-yloxy)ethoxy)ethoxy)ethanol (**3**).



2,2'-(ethane-1,2-diylbis(oxy)bis(ethan-1-ol)) (5 mL, 29.90 mmol) and 11-bromoundec-1-ene (2.61 mL, 11.96 mmol) were dissolved in THF (10 mL) and the solution was cooled to 0 °C. Sodium hydride (0.29 g, 11.96 mmol) was added and the reaction mixture was warmed to 22 °C and allowed to stir for 12 h. Water (10 mL) was slowly added to quench the excess of base. The solution was extracted with EtOAc (25 mL) and the aqueous phase was washed 3 times with EtOAc (3×50 mL). The combined organic layer was dried over Na_2SO_4 and concentrated under reduced pressure. The residue was purified by flash column chromatography (pet ether/EtOAc 1:8). The solvent was removed using reduced pressure and the product was dried with high vacuum. The product 2-(2-(2-(undec-10-en-1-yloxy)ethoxy)ethoxy)ethanol (**3**) was obtained as oil (5.96g, 60% yield). ^1H NMR (400 MHz, CDCl_3): δ 5.87-5.77 (m, 1H), 5.02-4.92 (m, 2H), 3.75-3.58 (m, 12H), 3.46 (t, $J = 6.41$ Hz, 2H), 2.07-2.01 (m, 2H), 1.62-1.55 (m, 2H), 1.36-1.26 (m, 12H). ^{13}C NMR (100 MHz, CDCl_3): δ 139.13, 114.02, 72.47, 71.50, 70.51, 70.23, 69.91, 61.60, 33.72, 29.46, 29.44, 29.37, 29.34, 29.02, 28.83, 25.96. HRMS (ESI) m/z : calc'd for $\text{C}_{17}\text{H}_{34}\text{O}_4\text{Na}$, 325.2354; Found, 325.2357.

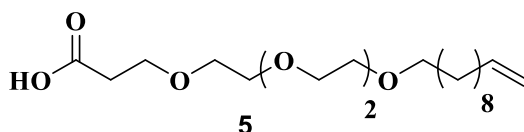
tert-butyl 4, 7, 10, 13-tetraoxatetracos-23-enoate (**4**)



Compound **3** (0.5 g, 1.65 mmol) was dissolved in THF (5 mL), a catalytic amount of potassium tert-butoxide (0.05 g, 0.45 mmol) was added followed by dropwise addition of tert-butyl acrylate (0.21 mL, 1.65 mmol). The reaction mixture was stirred at room temperature for 16 h and neutralized with 1M HCl. The solvent was removed and the oily residue was taken up in brine (30 mL) and extracted with EtOAc (3×15 mL). The combined organic layer was washed with brine (50 mL) and dried over Na_2SO_4 . The solvent was removed *in vacuo*, and the residue was purified by column chromatography (silica gel, pet ether/ EtOAc 1: 8). Tert-butyl 4, 7, 10, 13-

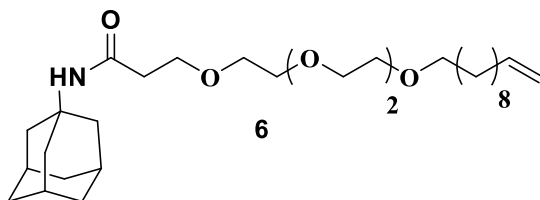
tetraoxatetracos-23-enoate (**4**) was obtained as oil (0.73g, 85% yield). $^1\text{H NMR}$ (400 MHz, CDCl_3): δ 5.84-5.75 (m, 1H), 5.01-4.90 (m, 2H), 3.71 (t, $J = 6.87$ Hz, 2H), 3.65-3.56 (m, 12H), 3.44 (t, $J = 6.87$ Hz, 2H), 2.50 (t, $J = 6.41$ Hz, 2H), 2.06-1.98 (m, 2H), 1.60-1.53 (m, 2H) 1.44(s, 9H), 1.36-1.27 (bm, 12H); $^{13}\text{C NMR}$ (100 MHz, CDCl_3): δ 170.88, 139.18, 114.07, 80.45, 71.50, 70.57, 70.47, 70.34, 70.01, 66.86, 36.22, 33.77, 29.58, 29.50, 29.43, 29.39, 29.08, 28.89, 28.05, 26.04. HRMS (ESI) m/z : calc'd for $\text{C}_{24}\text{H}_{46}\text{O}_6\text{Na}$, 453.3192; Found, 453.3190.

4, 7, 10, 13-tetraoxatetracos-23-enoic acid (**5**)



Compound **4** (0.4 g, 0.93 mmol) was dissolved in MeOH: THF (8 mL, 1:1). Aqueous 4M NaOH (3 mL, 12 mmol) was added and the solution was stirred at room temperature for 4 h. The solvent was removed under reduced pressure and the resulting suspension was acidified with aqueous 6M HCl (4 mL) while cooling at 0 °C. CH_2Cl_2 (50 mL) was added and the organic layer was separated and dried over Na_2SO_4 . Removal of the solvent and after drying yielded compound **5** as oil (0.24g, 70% yield). $^1\text{H NMR}$ (400 MHz, CDCl_3): δ 5.85-5.77 (m, 1H), 5.00-4.90 (m, 2H), 3.76 (t, $J = 5.95$ Hz, 2H), 3.65-3.58 (m, 12H), 3.45 (t, $J = 6.87$ Hz, 2H), 2.62 (t, $J = 5.95$ Hz, 2H), 2.04 (q, $J = 7.33$ Hz, 2H), 1.59-1.54 (m, 2H), 1.36-1.25 (bm, 12H); $^{13}\text{C NMR}$ (100 MHz, CDCl_3): δ 175.55, 139.17, 114.05, 71.51, 70.57, 70.50, 70.41, 70.20, 69.95, 66.39, 34.90, 33.75, 29.63, 29.47, 29.43, 29.38, 26.06, 28.86, 25.96. HRMS (ESI) m/z : calc'd for $\text{C}_{20}\text{H}_{39}\text{O}_6$, 375.2746; Found, 375.2742.

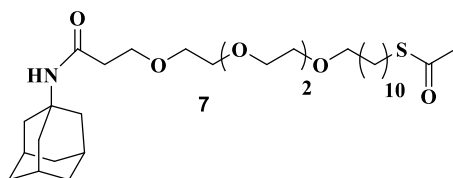
N-(adamantan-1-yl)-3-(2-(but-3-en-1-yloxy)ethoxy)propanamide (**6**).



Compound **5** (0.34 g, 0.90 mmol) and adamantan-1-amine (0.15 g, 0.90 mmol) were dissolved in DMF (10 mL) then HOBt (0.15 g, 1.09 mmol), EDC (0.20 g, 1.09 mmol) and DIPEA (0.39 mL, 2.25 mmol) were added. The reaction mixture was stirred for 24 h. DMF was evaporated under reduced pressure. The residue was taken up in 30 mL of brine and extracted 3 times with 15 mL

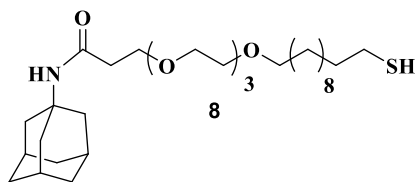
of EtOAc. The combined organic layer was washed with 50 mL brine and dried over Na₂SO₄. The solvent was removed *in vacuo*, and residue was purified column chromatography (silica gel, pet ether/ EtOAc 1:8) and dried under reduced pressure and high vacuum to give the corresponding **6** (0.36g, 80%) as oil. ¹H NMR (400 MHz, CDCl₃): δ 6.13(bs, 1H), 5.85-5.77 (m, 1H), 5.02-4.92 (m, 2H), 3.68 (t, *J* = 5.95 Hz, 2H), 3.66-3.58 (m, 12H), 3.45 (t, *J* = 6.87 Hz, 2H), 2.39 (t, *J* = 5.95 Hz, 2H), 2.04-2.03 (bm, 5H), 1.98 (bs, 6H), 1.67 (bs, 6H), 1.59-1.54 (m, 2H), 1.36-1.26 (m, 12H); ¹³C NMR (100 MHz, CDCl₃): δ 171.13, 139.22, 114.10, 71.57, 70.63, 70.55, 70.40, 70.33, 70.01, 67.52, 51.78, 41.50, 36.34, 33.79, 29.59, 29.53, 29.45, 29.39, 29.11, 28.91, 26.06. HRMS (ESI) *m/z*: calc'd for C₃₀H₅₃NaO₅N, 530.3821; Found, 530.3810.

S-(2-(2-(2-(3-(adamantan-1-ylamine)-3-oxopropoxy)ethoxy)ethoxy)ethyl) ethanethioate (7)



Compound **6** (0.25g, 0.49 mmol) and AIBN (0.49 g, 2.95 mmol) were dissolved in dioxane (7 mL). Thioacetic acid (0.90 mL, 12.81 mmol) was added and the solution was stirred for 12 h at 60 °C. The solvent was removed and the crude was purified by flash column chromatography (silica gel, pet ether/EtOAc 1:1 to 1:9) and dried to give the product **7** as yellowish oil (0.13 g, 47% yield). ¹H NMR (400 MHz, CDCl₃): δ 6.02(bs, 1H), 3.69 (t, *J* = 5.95 Hz, 2H), 3.65-3.56 (m, 12H), 3.44 (t, *J* = 6.87 Hz, 2H), 2.85 (t, *J* = 7.33 Hz, 2H), 2.37 (t, *J* = 5.95 Hz, 2H), 2.32 (s, 3H), 2.06-2.05 (bm, 3H), 1.99 (bm, 6H), 1.67 (bs, 6H), 1.58-1.53 (m, 4H), 1.28-1.25 (bm, 14H); ¹³C NMR (100 MHz, CDCl₃): δ 196.05, 170.67, 71.52, 70.60, 70.53, 70.39, 70.31, 69.99, 67.58, 51.59, 41.54, 38.10, 36.35, 30.60, 29.57, 29.45, 29.38, 29.10, 29.06, 28.76, 26.03. HRMS (ESI) *m/z*: calc'd for C₃₂H₅₈SO₆, 584.3985; Found, 584.3993.

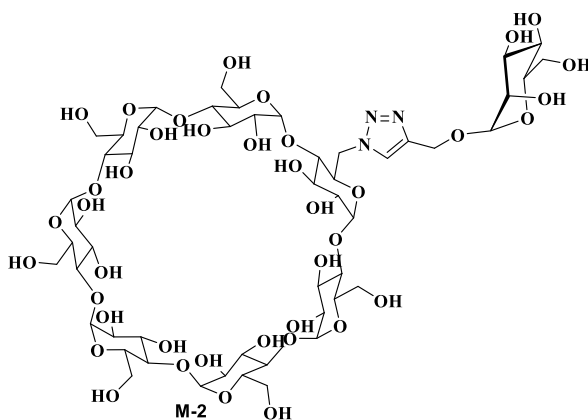
N-(adamantan-1-yl)-3-(2-(4-ercaptobutoxy)ethoxy)propanamide (8)



Compound **7** (0.15 g, 0.26 mmol) was dissolved in MeOH (7 mL). Sodium methoxide (0.066 g, 1.28 mmol) was added and the reaction was stirred at RT for 1 h. The solution was neutralized

with Resin Amberlite H⁺ IR 120. The polymer was filtered through filter paper and washed with MeOH (15 mL). The solvent was removed under reduced pressure and the residue was dried under high vacuum to give the **8** as yellowish oil (0.12 g, 93% yield). ¹H NMR (400 MHz, CDCl₃): δ 6.00(s, 1H), 3.6 (t, *J* = 5.95 Hz, 2H), 3.63-3.54 (m, 12H), 3.42 (t, *J* = 6.87 Hz, 2H), 2.67-2.63 (m, 1H), 2.52-2.46 (m, 1H), 2.35 (t, *J* = 5.95 Hz, 2H), 2.03(bs, 3H), 1.79 (bs, 6H), 1.64 (bs, 6H), 1.58-1.51 (m, 2H), 1.36-1.24 (bm, 16H); ¹³C NMR (100 MHz, CDCl₃): δ 170.62, 71.52, 70.57, 70.52, 70.37, 70.28, 69.96, 67.58, 51.56, 41.52, 38.11, 36.34, 29.56, 29.43, 29.37, 29.19, 28.47, 26.03. HRMS (ESI) *m/z*: calc'd for C₃₀H₅₆NSO₅, 542.3878; Found, 542.3875.

Mono-mannose substituted β-cyclodextrin (M-2).



Compound **12** (100 mg, 1.15 mmol), mannose alpha propargyl (10 mg, 1.73 mmol), sodium ascorbate (3mg, 14.7 μmol) and copper(II) sulfate pentahydrate (2 mg, 7.3 μmol) were suspended in 5 mL dimethylformamide in a round bottom flask and stirred at RT overnight. The solvent was evaporated and the product was purified by sephadex column using pure water as a solvent yielded (32 mg, 27%) of **M-2**. ¹H NMR (400 MHz, D₂O) δ 7.29 (bs, 1H), 4.94 (bs, 7H), 3.84-3.77 (m, 10H), 3.75-3.69 (m, 12H), 3.67-3.60 (m, 10H), 3.56-3.44 (m, 18H), ¹³C NMR (100 MHz, D₂O): 130.5, 129.4, 101.9 (anomeric-C), 99.6, 80.9, 73.2, 72.1, 71.3, 69.5, 63.3, 60.1, 59.7 MS (MALDI-TOF) *m/z* calc'd for C₅₁H₈₃NaN₃O₄₀, 1400.4451; Found 1400.8681.

2.1.3.3. Surface Functionalization

Preparation of adamantyl monolayer: Glass slides (approx. 1x1 cm) were washed with EtOH and coated with a gold substrate (100 nm) using gold evaporation chamber (Minilab deposition system type ST80A, UK) at a pressure of about 4x10⁻⁶ mbar. Samples were immersed in an ethanolic solution of **8** (0.2, 0.02 and 0.005 M) for 48 h. The adamantyl coated glass slides were rinsed with ethanol and stored at controlled conditions.

Immobilization of cyclodextrin derivatives: The gold substrate (modified with adamantyl SAM) was washed twice with ethanol and immersed in a solution of **M-1** (10 μ M solution in deionized water) for 24 h. The samples were rinsed with water, dried under a stream of nitrogen, and used as such for contact angle, ellipsometry and AFM measurements.

Lectin immobilization: The gold substrate (modified with **M-1**) was immersed in a solution of **ConA** lectin (1 mg/1mL in 10 mM HEPES, 150 mM NaCl, 2 mM CaCl₂, 2mM MnCl₂, pH 7.3) for 1 h and washed with water and dried under nitrogen. The substrates were used as such for ellipsometry, and AFM measurements.

2.1.3.4. Contact angle measurements

Contact angle analyses were performed using optical contact angle apparatus (Holmarc's HO-IAD-CAM-01) equipped with a CCD camera and high performance aberration corrected imaging with precise manual focus adjustment. Image J software was used for data acquisition. Rectangular gold coated substrates were fixed and kept constant throughout the analysis by means of sample holder. The contact angle of water in air was measured by the sessile drop method by gently placing a drop of 4 μ L of Milli-Q water onto the coated surface. The whole analysis was conducted at room temperature. A minimum of 20 droplets were examined for each surface. The resulting mean contact angle value was used for the following calculations.

2.1.3.5. Spectroscopic ellipsometry

The thicknesses of the **8** (0.02 M), **8/M-1** (0.02 M/10 μ M) and **8/M-1/ConA** (0.02 M/10 μ M/1 mg/mL) coated glass slides were measured by a commercial spectroscopic ellipsometer (M2000 from Woollam Inc., Lincoln, Nebraska) in the transmission mode in a spectral range from 250 to 800 nm with the compensator making 100 rev/s. Measurements were recorded at various angles of incidence between 60° to 70°. A four-layer model (Au coated BK7 glass substrate and three successive organic layers) was used in the fitting with WVASE software to obtain the thickness of the layers of **8**, **M-1** and **ConA** from the measured Ψ and Δ curve.

The Ψ and Δ values are related to the reflection coefficients as

$$\tan(\Psi) \cdot e^{i\Delta} = \frac{R_p}{R_s} = \rho(\lambda, d, N) \text{ ----- (1)}$$

Where R_p and R_s are the reflection coefficients of p- and s-polarized light, λ is the wavelength of the incident light, d is the thickness of the film and N is the complex refractive index. The

complex function ρ is ratio of amplitude Ψ and phase difference Δ between the p- and s-polarized light waves. Equation 1 was used for the fitting of ellipsometric data. The best fit to the experimental data was determined by minimizing the mean-square error (MSE)^[2] where K is the number of (Ψ , Δ) pairs, M is the number of the model parameters, and the mod and exp refer to model and experimental values, respectively.

$$MSE = \frac{1}{2K-M} + \sum_{j=1}^k [(\Psi_j^{mod} - \Psi_j^{exp})^2 + (\Delta_j^{mod} - \Delta_j^{exp})^2] \quad \text{-----}(2)$$

The Ψ and Δ curve measurements were performed in 4 sets: (a) **Au**, (b) **8/Au**, (c) **Au/8/M-1** and (d) **Au/8/M-1/ConA** coated glass slides. As Δ values are very sensitive to the film thickness, we have plotted Δ vs. λ curves for an angle of incidence of 60° for all the samples. These curves clearly indicate the decrease in the Δ values upon increase in the film thickness (i.e. from bare Au coated glass slide to **Au/8/M-1/ConA** coated glass slides). Since the Au film deposited on glass plate was opaque, the thickness of Au film was ignored and was taken as an infinitely absorbing material. Therefore, only the optical constants of Au were considered for fitting. The ellipsometry data for organic layers were fitted using a Cauchy model layer which is quite well acceptable for transparent films. For Cauchy layers, the data was fitted for thicknesses only. The thickness for **8**, **8/M-1** and **8/M-1/ConA** layers were measured to be 13.9 Å , 29.82 Å and 92.93 Å, respectively.

2.1.3.6. Estimation of concentration of sugar on slide

The concentration of mannose sugar on gold coated glass slides were determined by the phenol-sulfuric acid method. A sugar functionalized-glass slide was dipped in concentrated sulfuric acid (750 μ L, 100%) and aqueous phenol solution (5% w/v, 100 μ L) was added to the test tube and heated to 80 °C. After 5 min, the Au-slides were removed and cooled to room temperature. The absorbance coefficient at 490 nm was measured. The sugar concentration was estimated by comparing the absorption of the sample with a standard curve.

2.1.3.7. X-ray photoelectron spectroscopy

XPS experiments were performed on a VG Micro Tech ESCA 3000 instrument at a pressure of $< 1 \times 10^{-9}$ Torr. The overall resolution was limited to the bandwidth of X ray source (~ 1 eV). The spectra were recorded with monochromatic Al K α radiation at pass energy of 50 eV and an electron take off angle of 60° . C 1s energy binding peaks centered at 284.6 eV was used for

calibration. The deconvolution of the XPS peaks was done by a XPS peak fitting program (XPSPEAK 4.1). The XPS spectra were background corrected using the Shirley algorithm, and chemically distinct peaks were resolved using a nonlinear least-square fitting procedure.

2.1.3.8. Atomic force microscopy

Atomic force microscopy (AFM) measurements were performed with Au coated glass slides with **8**, with **8/M-1** and with **8/M-1/ConA** using a Multimode scanning probe microscope equipped with a Nanoscope IV controller from Veeco Instrument Inc., Santa Barbara, CA. All AFM measurements were done under ambient conditions using the tapping-mode AFM probes model Tap190Al purchased from Budget Sensors. The radii of tips were less than 10 nm, and their height was $\sim 17 \mu\text{m}$. The cantilever' resonant frequency was ca. 162 kHz and nominal spring constant of ca. 48 N/m, with a 30 nm thick aluminum reflex coating on the back side of the cantilever of the length 225 μm . For each sample, three locations with a surface area of $1 \times 1 \mu\text{m}^2$ and $500 \times 500 \text{ nm}^2$ each were imaged at a rate of 1 Hz and at a resolution of 512×512 .

2.1.3.9. Surface Plasmon Resonance study

Binding kinetics was determined by SPR using a BIACORE 300 biosensor instrument (GE Biosystems). Concanavalin A was purchased from Sigma-Aldrich. The gold sensor chip and different running buffers were obtained from GE Healthcare Life Science (India). All SPR experiments were performed using Biacore 3000. For the preparation of host-guest coated surfaces, gold sensor chip was activated with **8** (0.01 mM or 0.1 mM) injected at a flow rate $10 \mu\text{L} \cdot \text{min}^{-1}$ for 3 minutes which resulted in adamantyl coated surface for host-guest functionalization. Finally, cyclodextrin moiety was incorporated on adamantyl surface by injecting **M-1** or **M-2** or **β -CD** (0.05 mM or 0.5 mM) at a flow rate of $5 \mu\text{L} \cdot \text{min}^{-1}$ for 7 minutes. This was followed by injecting **ConA** (0.5, 1.0, 2.5, 3.5 μM in 10mM *HEPES*, 150mM NaCl, 2mM *CaCl*₂, 2mM *MnCl*₂, pH7.3) for 250 s at $10 \mu\text{L} \cdot \text{min}^{-1}$, followed by dissociation using buffer at $30 \mu\text{L} \cdot \text{min}^{-1}$ for 200 s. The equilibrium dissociation constant (K_D) was determined globally by fitting to the kinetic simultaneous K_a/K_d model, assuming Langmuir (1:1) binding, using BIA evaluation software (BIAcore). The surfaces were strictly regenerated with multiple pulses of α -D-methyl mannose followed by an extensive wash procedure using running buffer.

2.1.3.10. THP-1 differentiated Macrophage Binding Assay

Human THP-1 monocytic cell line (from NCCS, Pune) was grown at 37 °C and 5% CO₂ in RPMI-1640 (Invitrogen) medium with 10% heat inactivated FBS, 50 $\mu\text{g}/\text{mL}$ streptomycin and

100 µg/mL penicillin (pH 7.2). THP-1 cells were differentiated by stimulating with PMA (10 ng/mL = 16 nM; from Sigma Aldrich, St Louis, MO, USA) for 3-4 days. Cells were detached by treating with 0.05% trypsin/EDTA solution. THP-1 derived macrophage cells were seeded on **8/β-CD**, **8/M-1** and **8/M-2** coated plates at a density of 5000 cells/cm². After 24 h of incubation, slides were gently rinsed thrice with PBS to remove the unbound cells. The bound cells were imaged by using normal bright field microscopy.

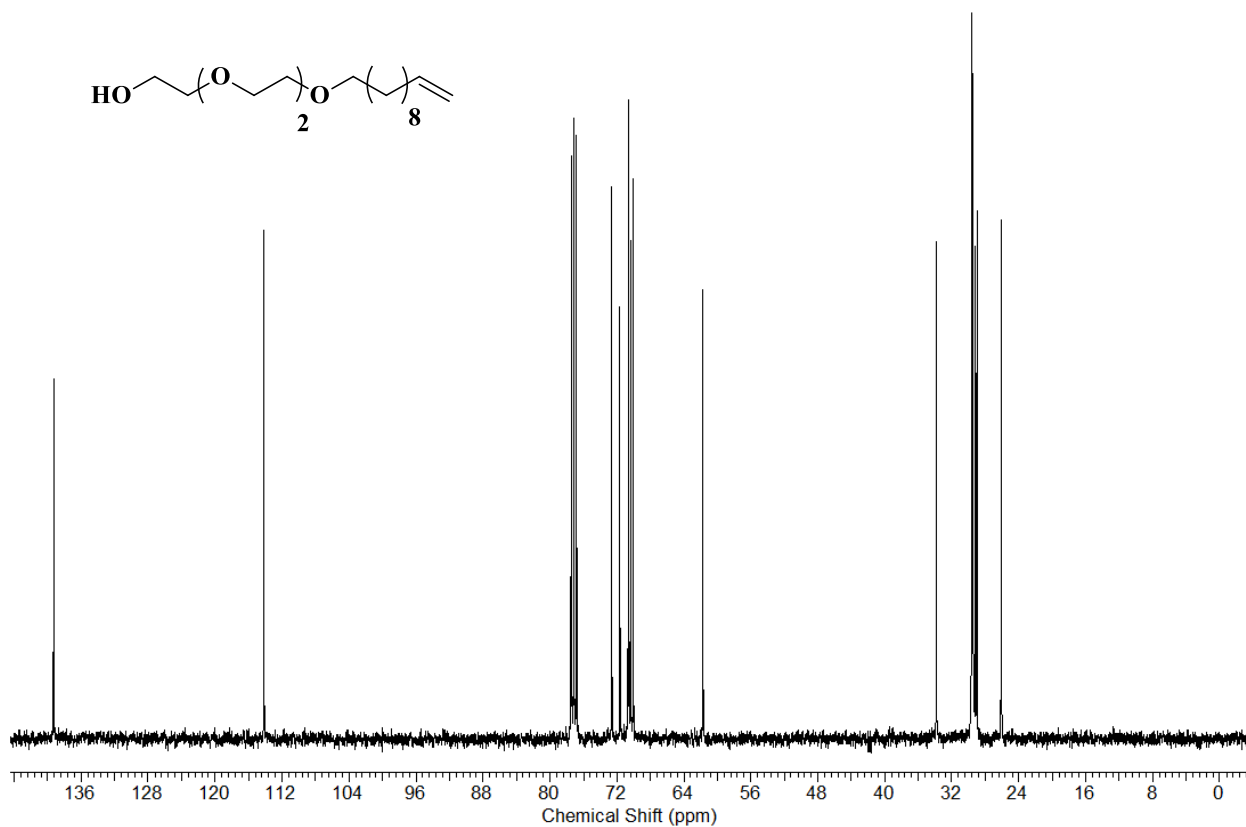
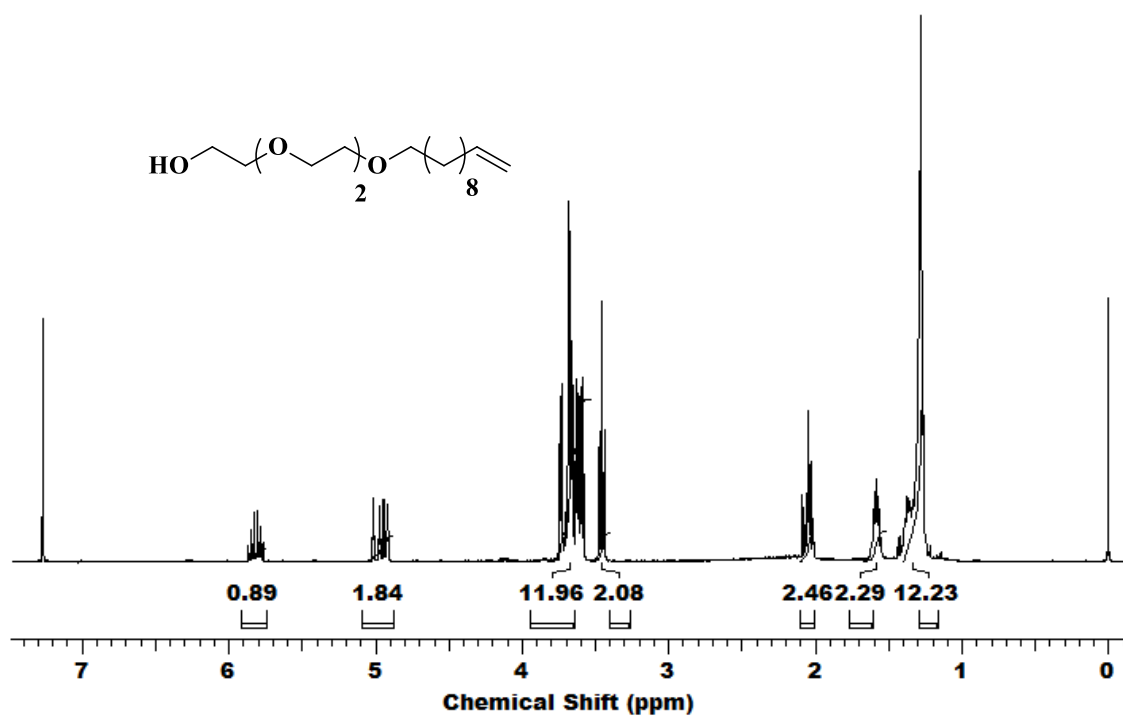
2.1.4 References

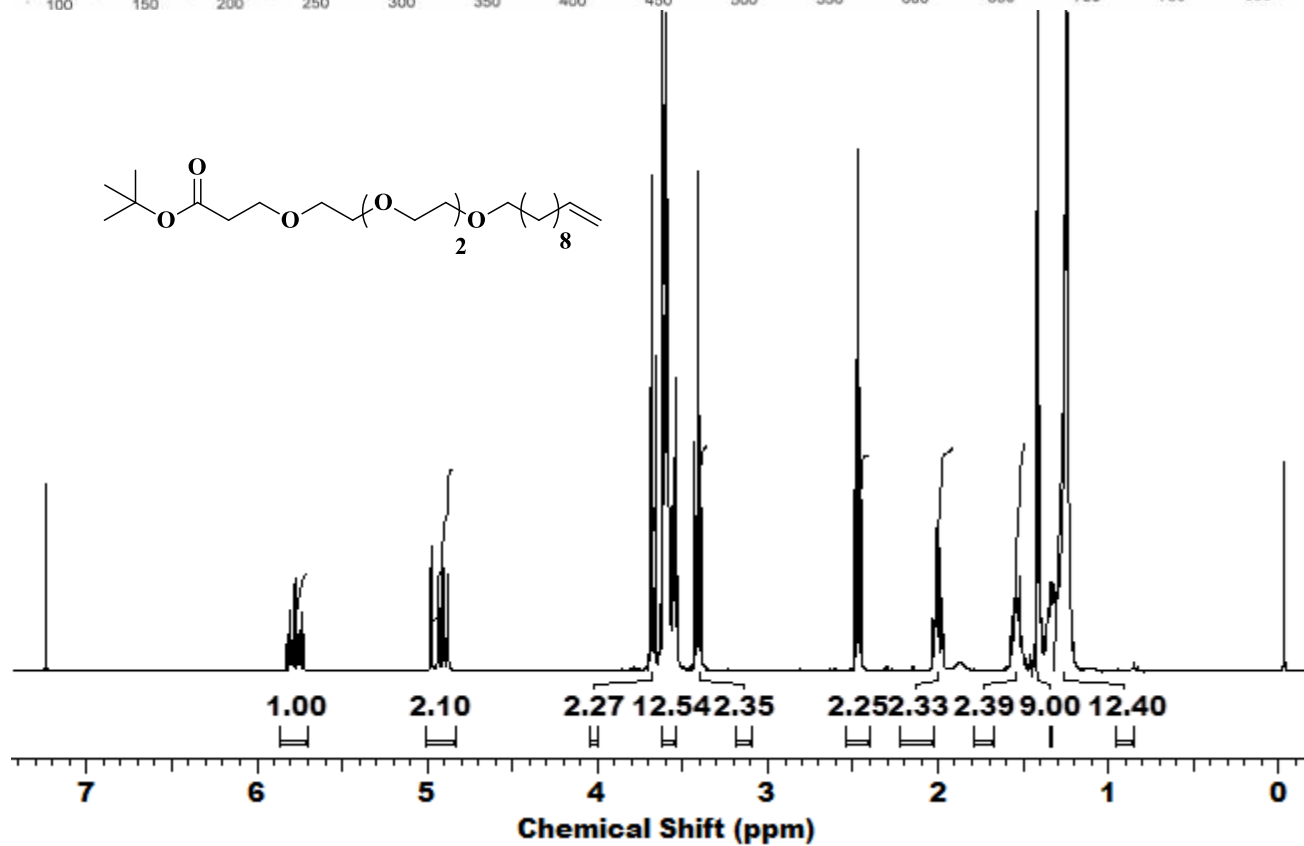
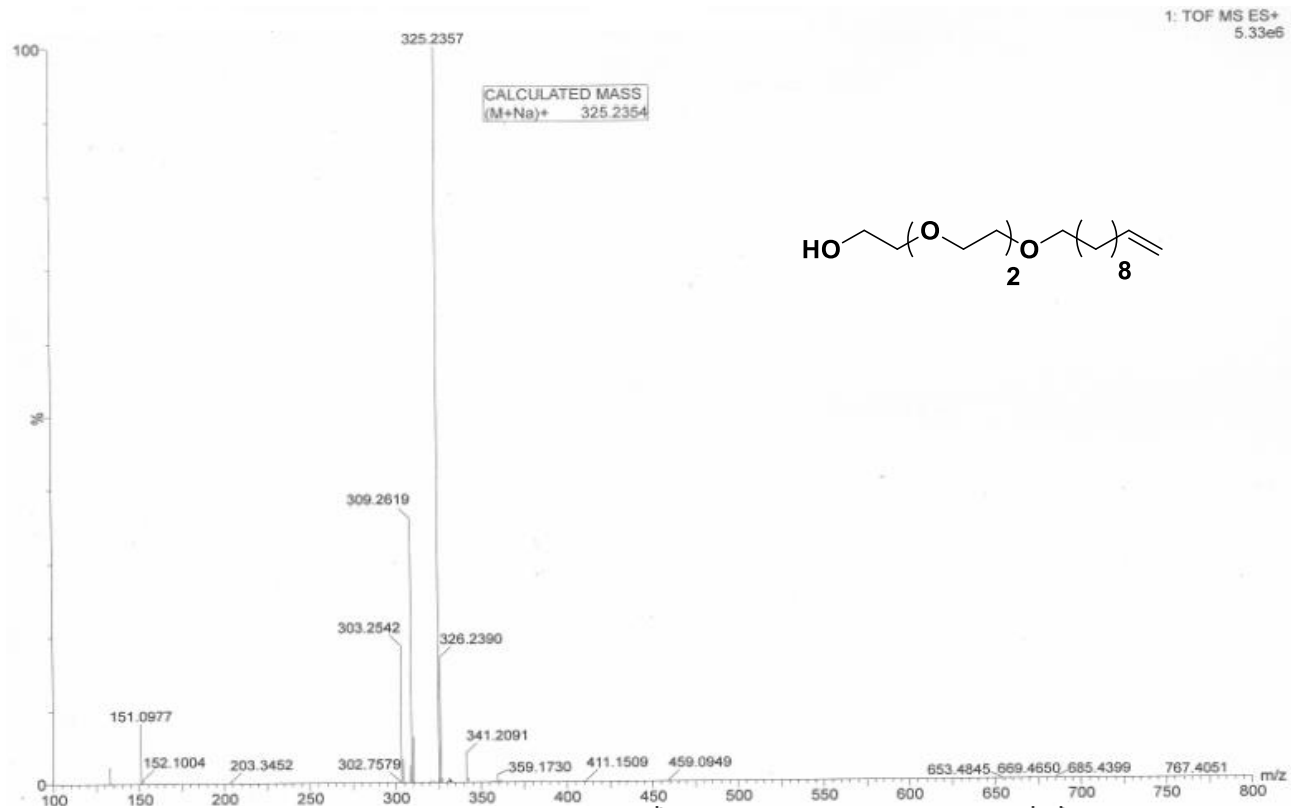
1. K. Drickamer and M. E. Taylor, *Annu. Rev. Cell. Biol.*, 1993, **9**, 237-264.
2. H. Lis and N. Sharon, *Chem. Rev.*, 1998, **98**, 637-674.
3. F. T. Liu, *Clin. Immunol.*, 2000, **97**, 79-88.
4. P. H. Seeberger and D. B. Werz, *Nat. Rev. Drug. Discov.*, 2005, **4**, 751-763.
5. M. Paolino, L. Mennuni, G. Giuliani, M. Anzini, M. Lanza, G. Caselli, C. Galimberti, M. C. Menziani, A. Donati and A. Cappelli, *Chem. Commun.*, 2014, **50**, 8582-8585.
6. C. Fasting, C. A. Schalley, M. Weber, O. Seitz, S. Hecht, B. Koksche, J. Dervede, C. Graf, E. W. Knapp and R. Haag, *Angew. Chem. Int. Ed.*, 2012, **51**, 10472-10498.
7. L. L. Kiessling, J. E. Gestwicki and L. E. Strong, *Angew. Chem. Int. Ed.*, 2006, **45**, 2348-2368.
8. S. M. Dimick, S. C. Powell, S. A. McMahon, D. N. Moothoo, J. H. Naismith and E. J. Toone, *J. Am. Chem. Soc.*, 1999, **121**, 10286-10296.
9. M. Paolino, H. Komber, L. Mennuni, G. Caselli, D. Appelhans, B. Voit and A. Cappelli, *Biomacromolecules*, 2014, **15**, 3985-3993.
10. S. Galeazzi, T. M. Hermans, M. Paolino, M. Anzini, L. Mennuni, A. Giordani, G. Caselli, F. Makovec, E. W. Meijer, S. Vomero and A. Cappelli, *Biomacromolecules*, 2010, **11**, 182-186.
11. A. Martinez, C. O. Mellet and J. M. G. Fernandez, *Chem. Soc. Rev.*, 2013, **7**, 4746-4773.
12. J. L. J. Blanco, C. O. Mellet and J. M. G. Fernandez, *Chem. Soc. Rev.*, 2013, **7**, 4518-4531.
13. K. Hatano, K. Matsuoka and D. Terunuma, *Chem. Soc. Rev.*, 2013, **7**, 4574-4598.
14. C. Fasting, C. A. Schalley, M. Weber, O. Seitz, S. Hecht, B. Koksche, J. Dervede, C. Graf, E. W. Knapp and R. Haag, *Angew. Chem. Int. Ed.*, 2012, **15**, 10472-10498.
15. S. Park, J. C. Gildersleeve, O. Blixt and I. Shin, *Chem. Soc. Rev.*, 2013, **42**, 4310-4326.
16. T. Horlacher and P. H. Seeberger, *Chem. Soc. Rev.*, 2008, **37**, 1414-1422.
17. D. Wang, S. Liu, B. J. Trummer, C. Deng and A. Wang, *Nat. Biotechnol.*, 2002, **20**, 275-281.
18. K. A. Barth, G. Coullerez, L. M. Nilsson, R. Castelli, P. H. Seeberger, V. Vogel and M. Textor, *Adv. Funct. Mat.*, 2008, **18**, 1459-1469.
19. S. N. Narla and X. L. Sun, *Biomacromolecules*, 2012, **13**, 1675-1682.
20. M. R. Lee and I. Shin, *Org. Lett.*, 2005, **7**, 4269-4272.
21. S. Park, M. R. Lee and I. Shin, *Bioconjug. Chem.*, 2009, **20**, 155-162.

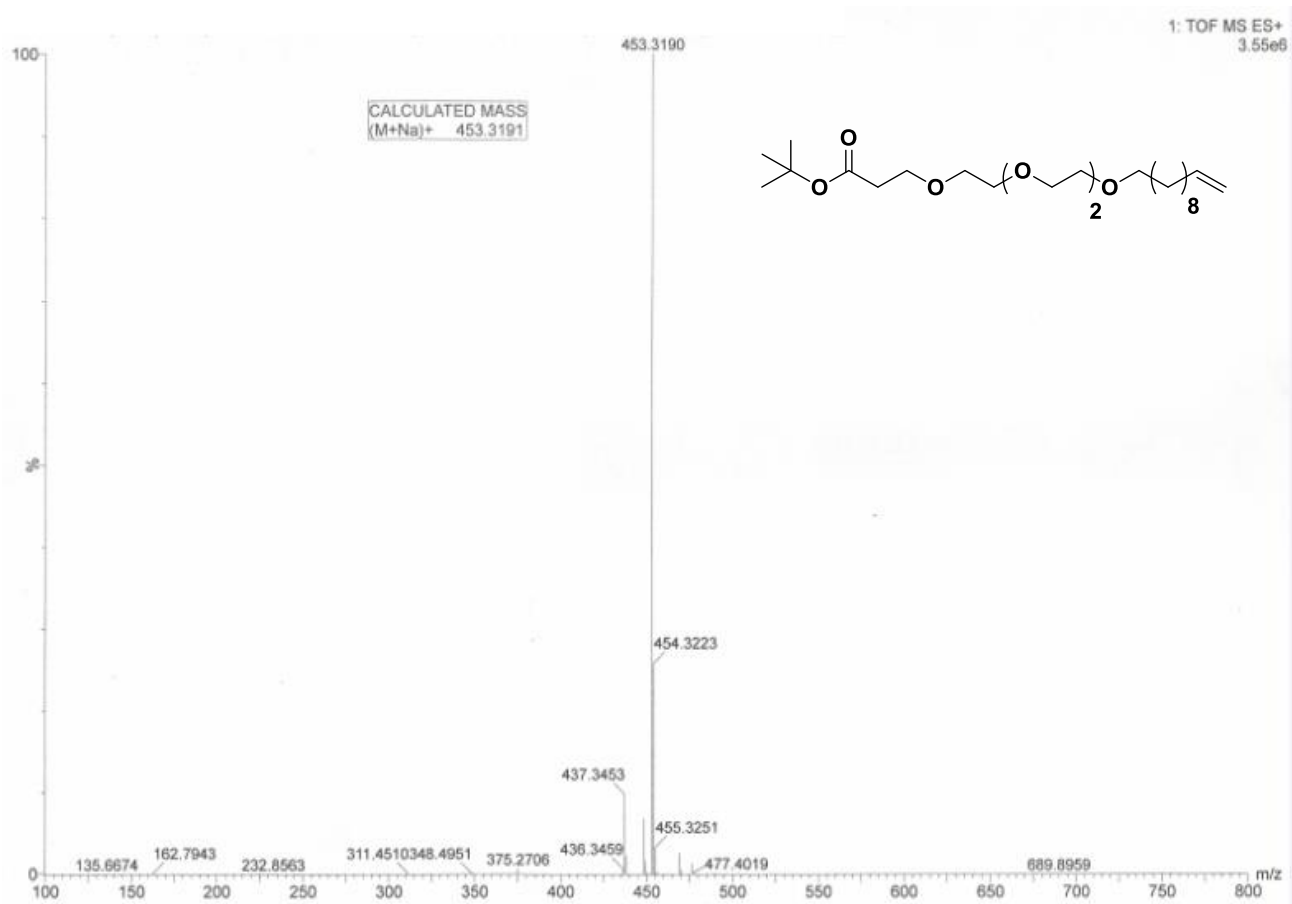
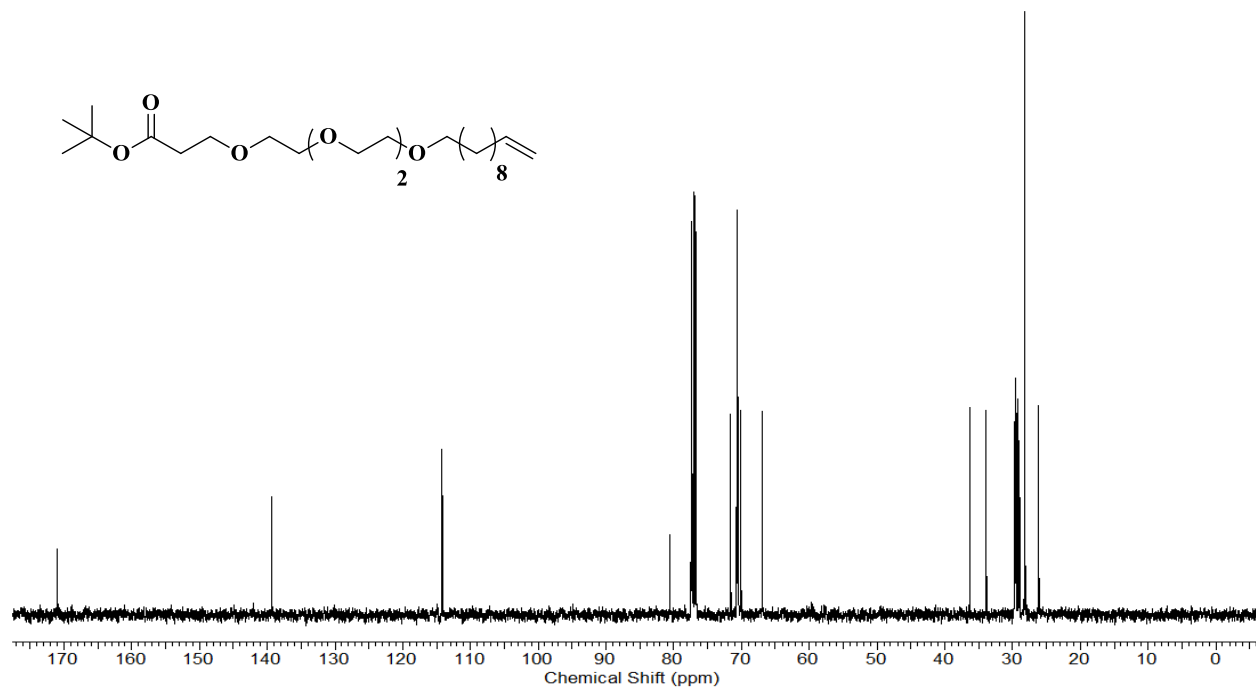
22. Z. Pei, H. Yu, M. Theurer, A. Walden, P. Nilsson, M. Yan and . Ramstrom, *ChemBioChem*, 2007, **8**, 166-168.
23. S. Park, M. R. Lee, S. J. Pyo and I. Shin, *J. Am. Chem. Soc.*, 2004, **126**, 4812-4819.
24. Y. Zhang, C. Campbell, Q. Li and J. C. Gildersleeve, *Mol. BioSyst.*, 2010, **6**, 1583-1591.
25. C. Y. Huang, D. A. Thayer, A. Y. Chang, M. D. Best, J. Hoffmann, S. Head and C. H. Wong, *Proc. Natl. Acad. Sci. USA.*, 2006, **103**, 15-20.
26. K. Godula, D. Rabuka, K. T. Nam and C. R. Bertozzi, *Angew. Chem. Int. Ed.*, 2009, **48**, 4973-4976.
27. M. Kohn, R. Wacker, C. Peters, H. Schroeder, L. Soulere, R. Breinbauer, C. M. Neimeyer and H. Waldmann, *Angew. Chem. Int. Ed.*, 2003, **42**, 5830-5834.
28. Y. Sato, K. Yoshioka, T. Murakami, S. Yoshimoto and O. Niwa, *Langmuir*, 2012, **28**, 1846-1851.
29. M. Paolino, F. Ennen, S. Lamponi, M. Cernescu, B. Voit, A. Cappelli, D. Appelhans and H. Komber, *Macromolecules*, 2013, **46**, 3215-3227.
30. L. Voskuhl, C. Wendeln, F. Versluis, E. C. Fritz, O. Roling, H. Zope, C. Schulz, S. Rinnen, H. F. Arlinghaus, B. J. Ravoo and A. Kros, *Angew. Chem. Int. Ed.*, 2012, **51**, 12616-12620.
31. D. Dorokhin, S. H. Hsu, N. Tomczak, C. Blum, V. Subramaniam, J. Husken, D. N. Reinhoudt, A. H. Velders and G. J. Vancso, *Small*, 2010, **6**, 2870-2876.
32. A. G. Campo, S. H. Hsu, L. Puig, J. Huskens, D. N. Reinhoudt and A. H. Velders. *J. Am. Chem. Soc.*, 2010, **132**, 11434-11436.
33. L. Yang, A. G. Casado, J. F. Young, H. D. Nguyen, J. C. Danes, J. Huskens, L. Brunsveld and P. Jonkheijm, *J. Am. Chem. Soc.*, 2012, **134**, 19199-19206.
34. C. A. Nijhuis, J. K. Sinha, G. Wittstock, J. Huskens, B. J. Ravoo and D. N. Reinhoudt, *Langmuir*, 2006, **22**, 9770-9775.
35. M. Gade, A. Paul, C. alex, D. Choudhury, H. V. Thulasiram and R. Kikkeri, *Chem. Commun.*, 2015, **51**, 9185-9187.
36. Q. Zhenhui, P. Bharate, H. L. Chian, Z. Benjamin, B. Christoph, S. Andrea, B. Fabian, H. Benjamin, M. Rolf, P. H. Seeberger and H. Rainer, *Nano Lett.*, 2015, **15**, 6051-6057.
37. A. G. Barrientos, J. J. G. Lopez, J. I. Garcia, F. O. Caballero, U. Uriel, A. V. Berenguel and F. S. Gonzalez, *Synthesis*, 2001, 1057-1064.
38. F. Vitale, I. Fratoddi, B. Battocchio, E. Piscopiello, L. Tapfer, M. V. Russo, G. Polzonetti and C. Giannini, *NanoScale Res. Lett.*, 2011, **6**, 103-111.
39. J. H. Park, S. Hwang and J. Kwak, *ACS Nano*, 2010, **4**, 3949-3958.
40. P. N. Kanellopoulos, K. Pavlou, A. Perrakis, B. Agianian, C. E. Vorgias, C. Mavrommatis, M. Soufi, P. A. Tucker and S. J. Hamodrakas, *J. Struct. Biol.*, 1996, **116**, 345-355.
41. W. Vornholt, M. Hartmann and M. Keusgen, *Biosensor Bioelectron.*, 2007, **22**, 2983-2988.
42. T. Mori, M. Toyoda, T. Ohtsuka and Y. Okahata, *Anal. Biochem.* 2009, **395**, 211-216.
43. G. Bellapadrona, A. b. Tesler, D. Grunstein, L. H. Hossain, R. Kikkeri, P. H. Seeberger, A. Vaskevich and I. Rubinstein, *Anal. Chem.*, 2012, **84**, 232-240.

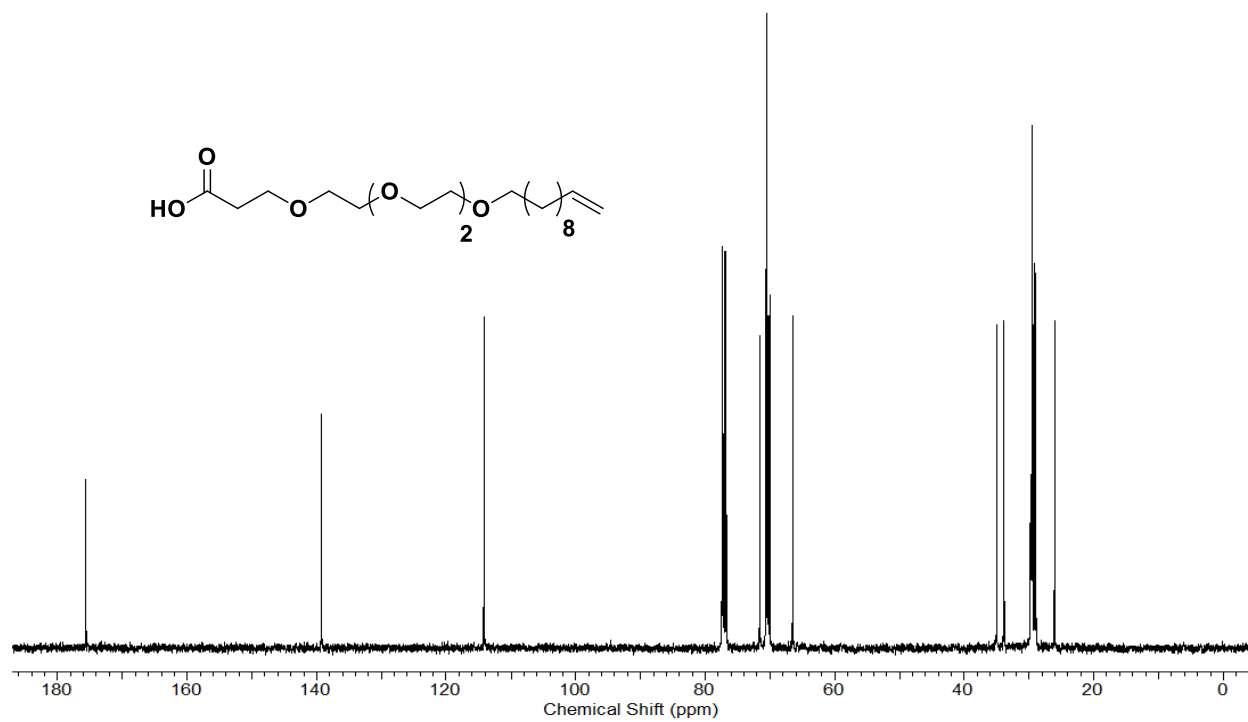
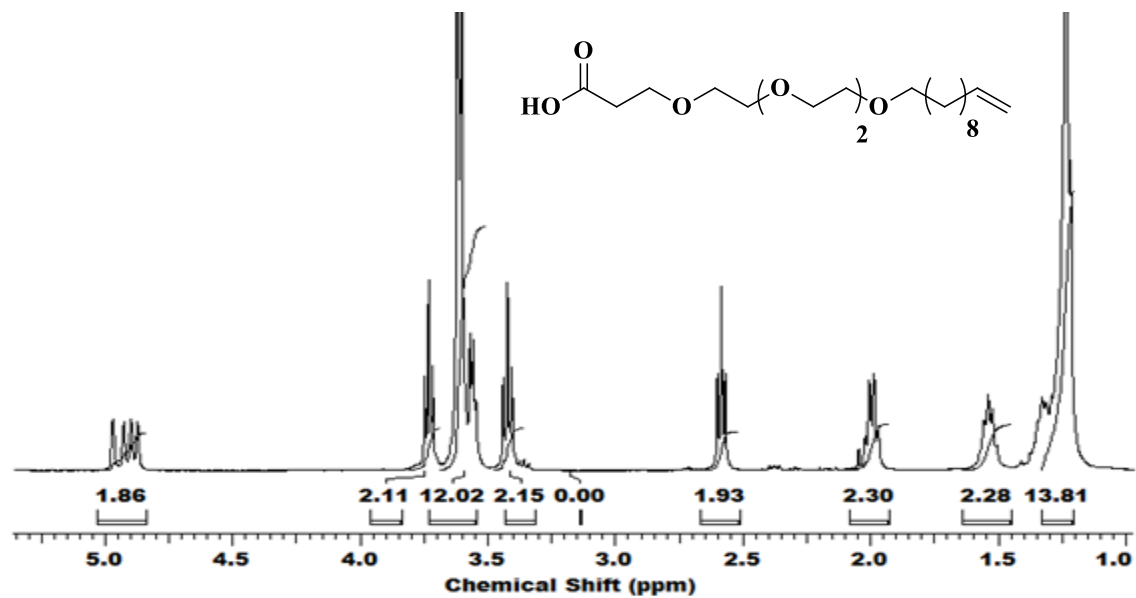
44. D. Grunstein, M. Maglinao, R. Kikkeri, M. Collot, K. Barylyuk, B. Lepenies, F. Kamena, R. Zenobi and P. H. Seeberger, *J. Am. Chem. Soc.*, 2011, **133**, 13957-13966.
45. T. E. Wileman, M. R. Lennartz and P. D. Stahl, *Proc. Natl. Acad. Sci. USA.*, 1986, **83**, 2501-2505.
46. J. M. Benito, M. G. García. C. O. Mellet, I. Baussanne, J. Defaye and J. M. G. Fernandez, *J. Am. Chem. Soc.*, 2004, **126**, 10355-10363.

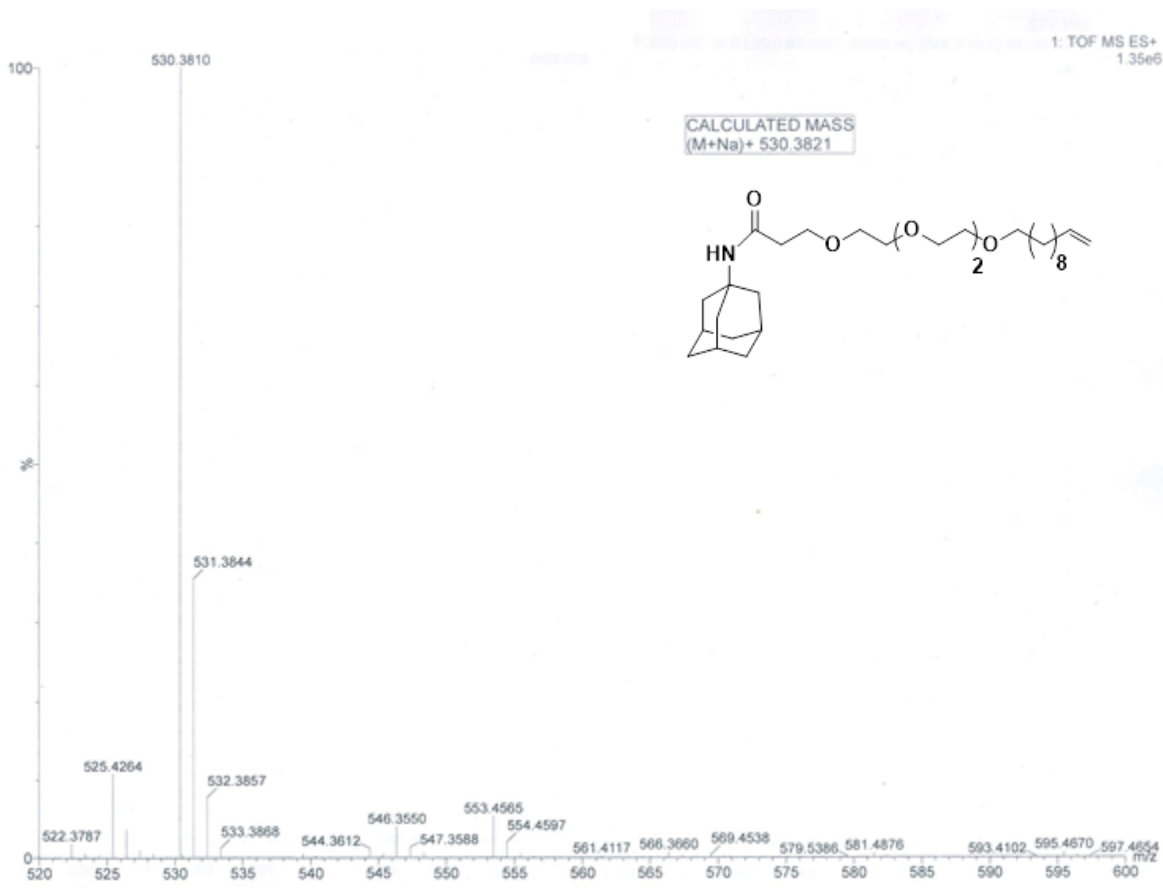
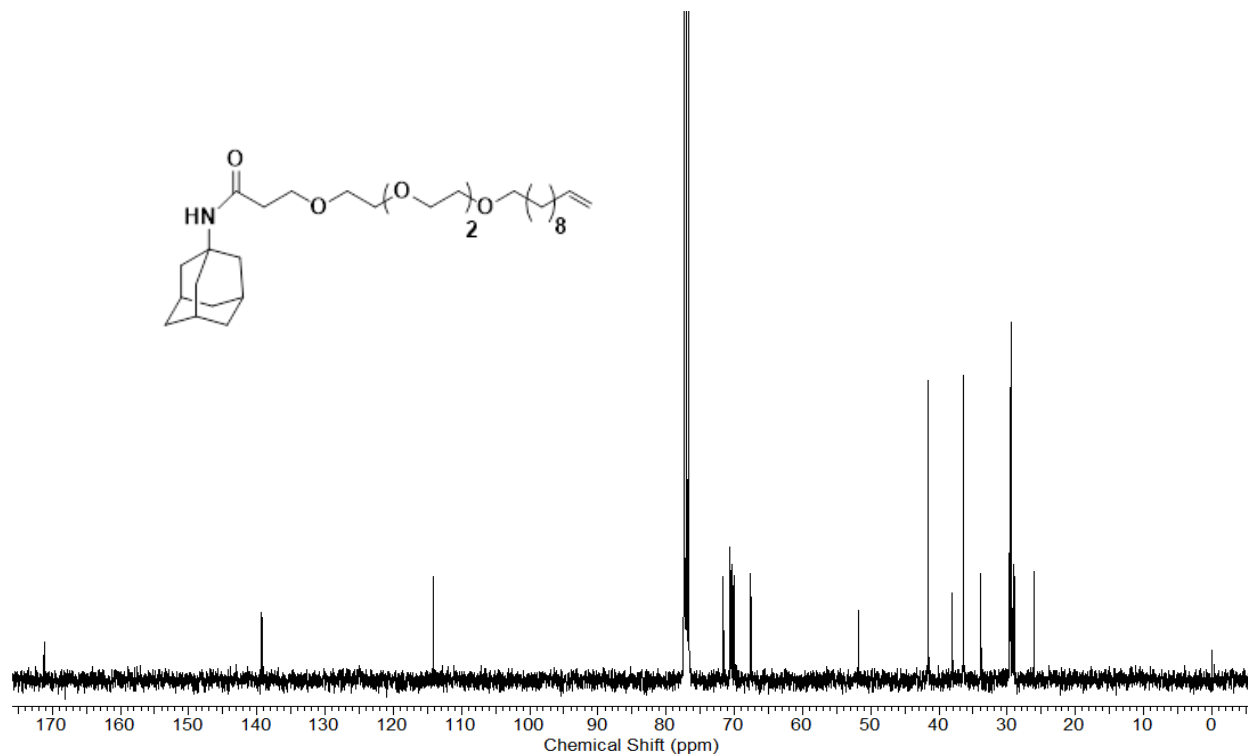
2.1.5. NMR and HRMS of compounds

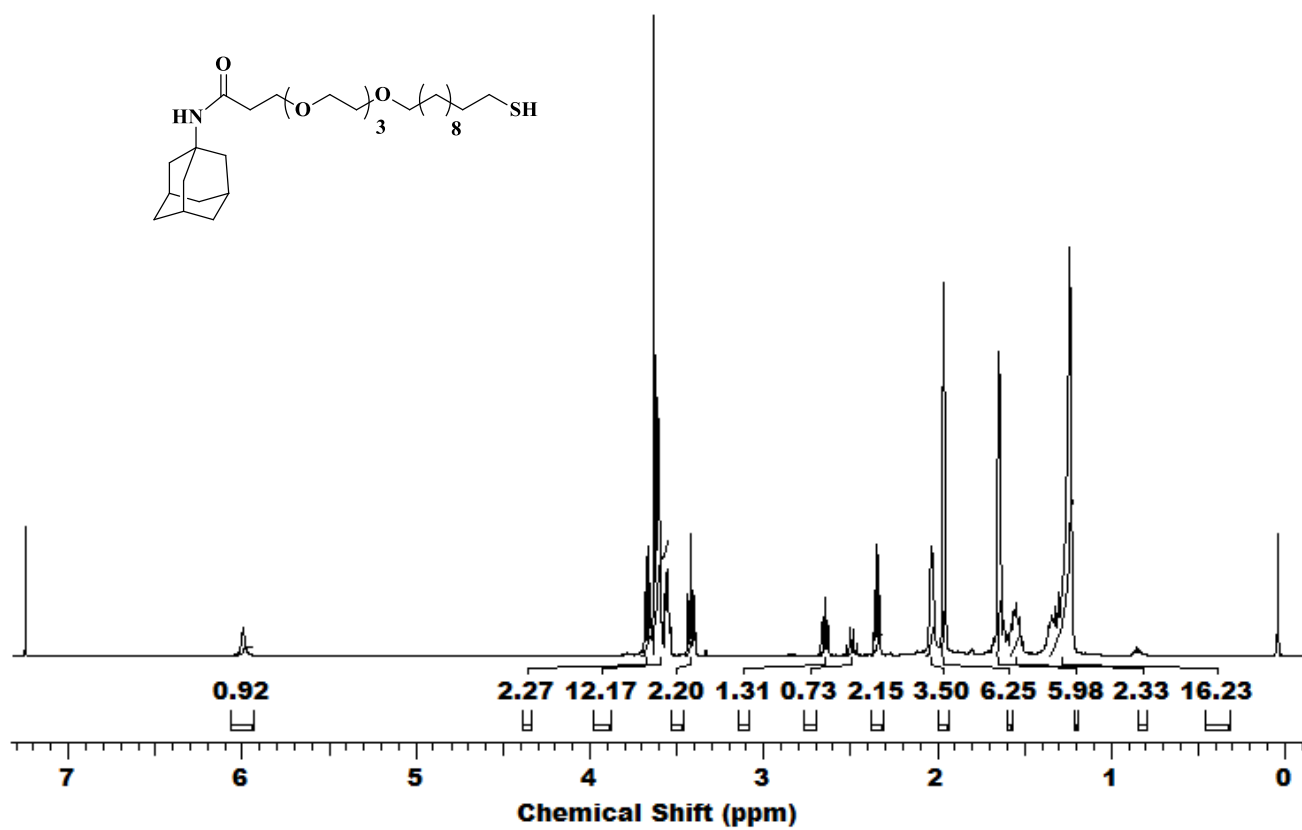
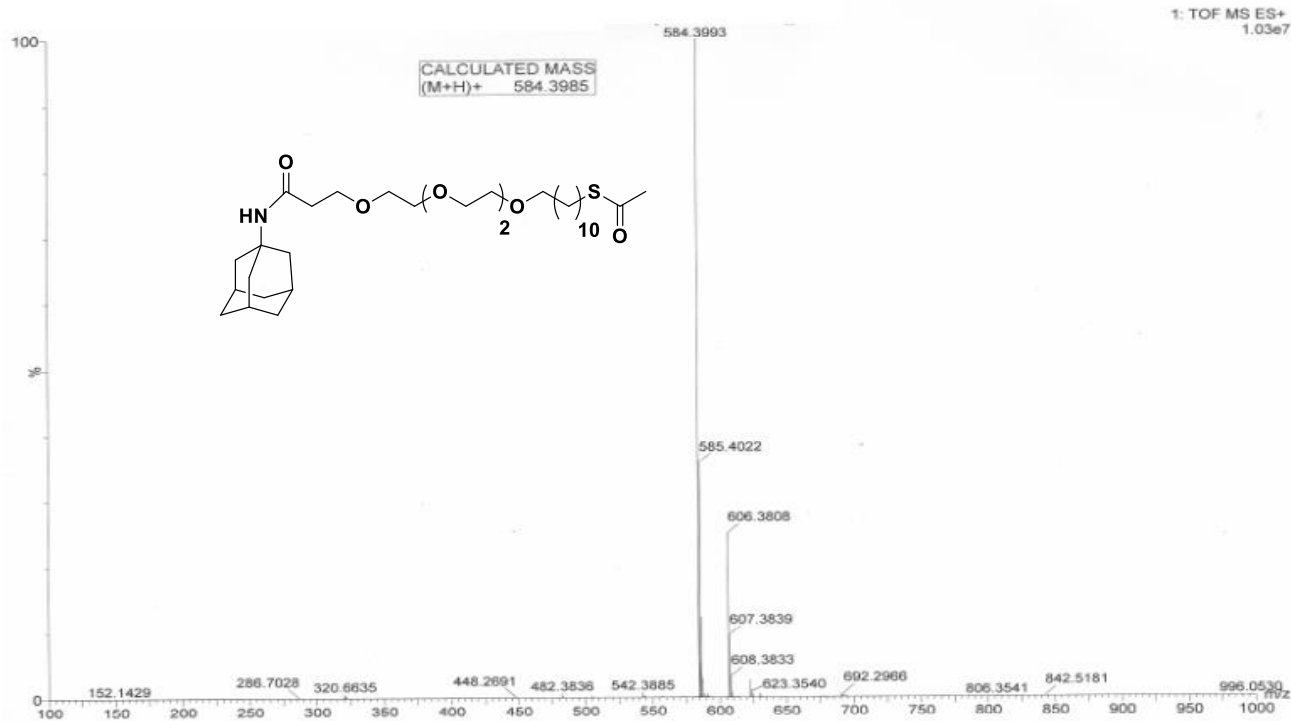


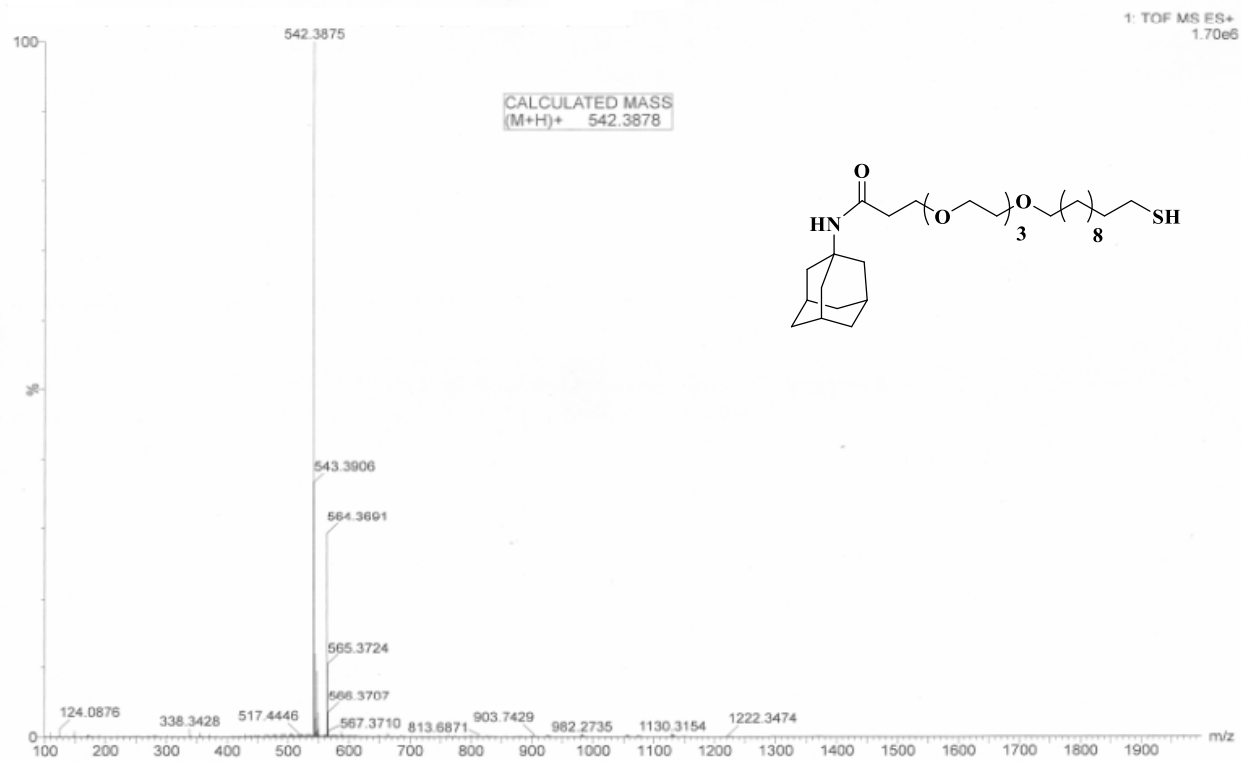
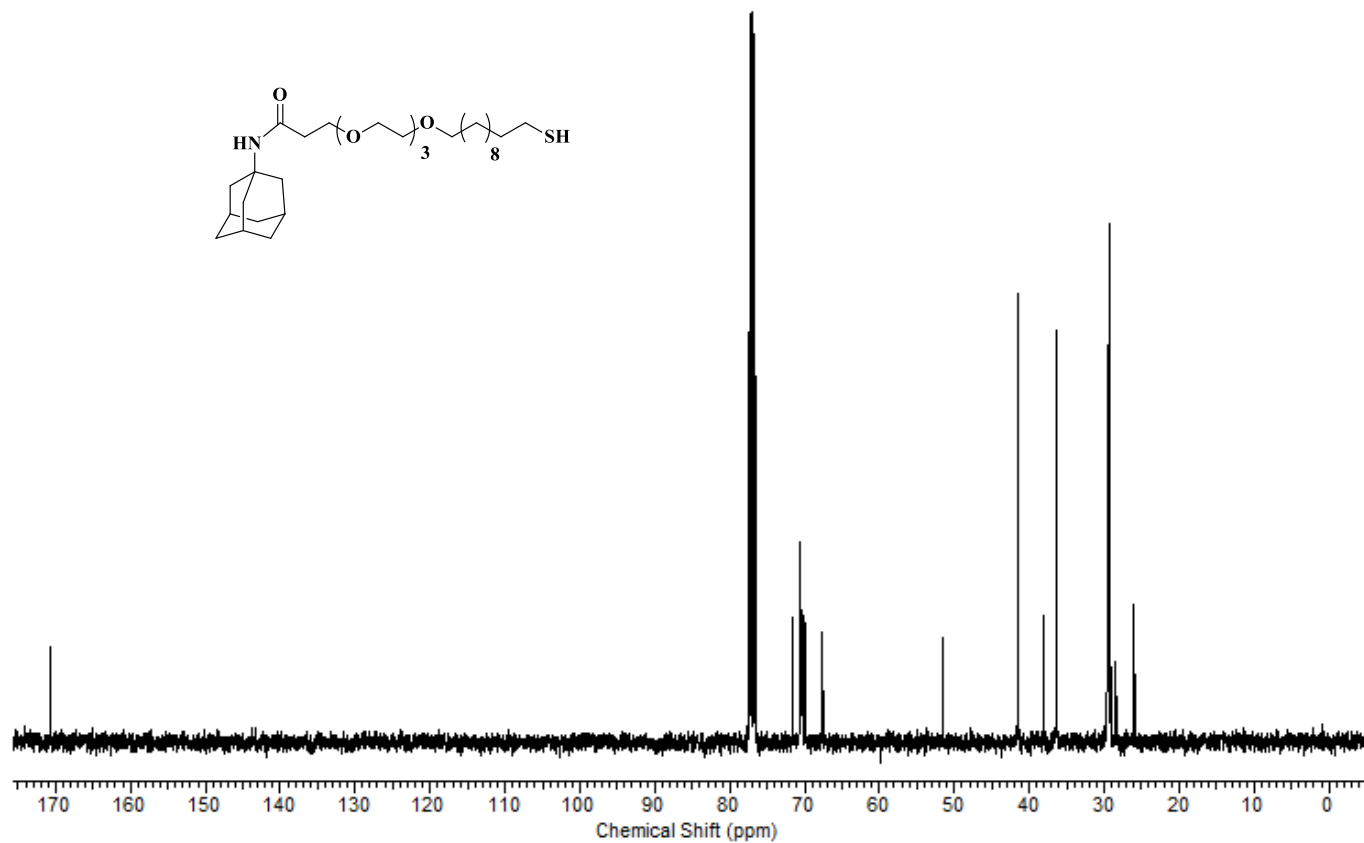


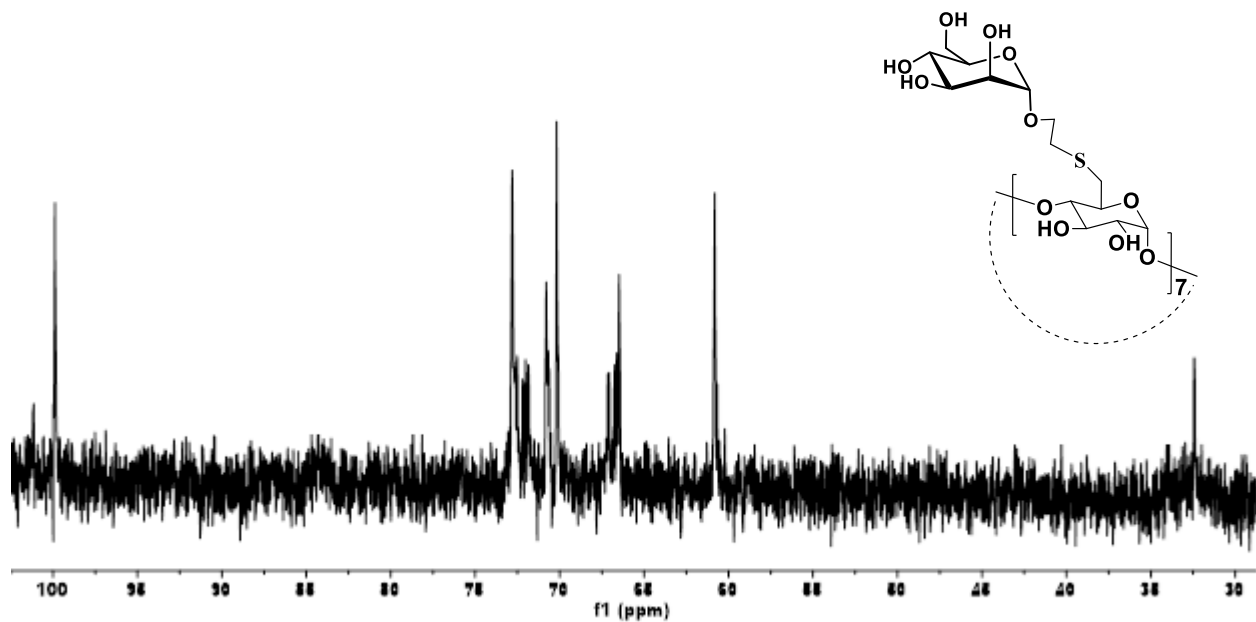
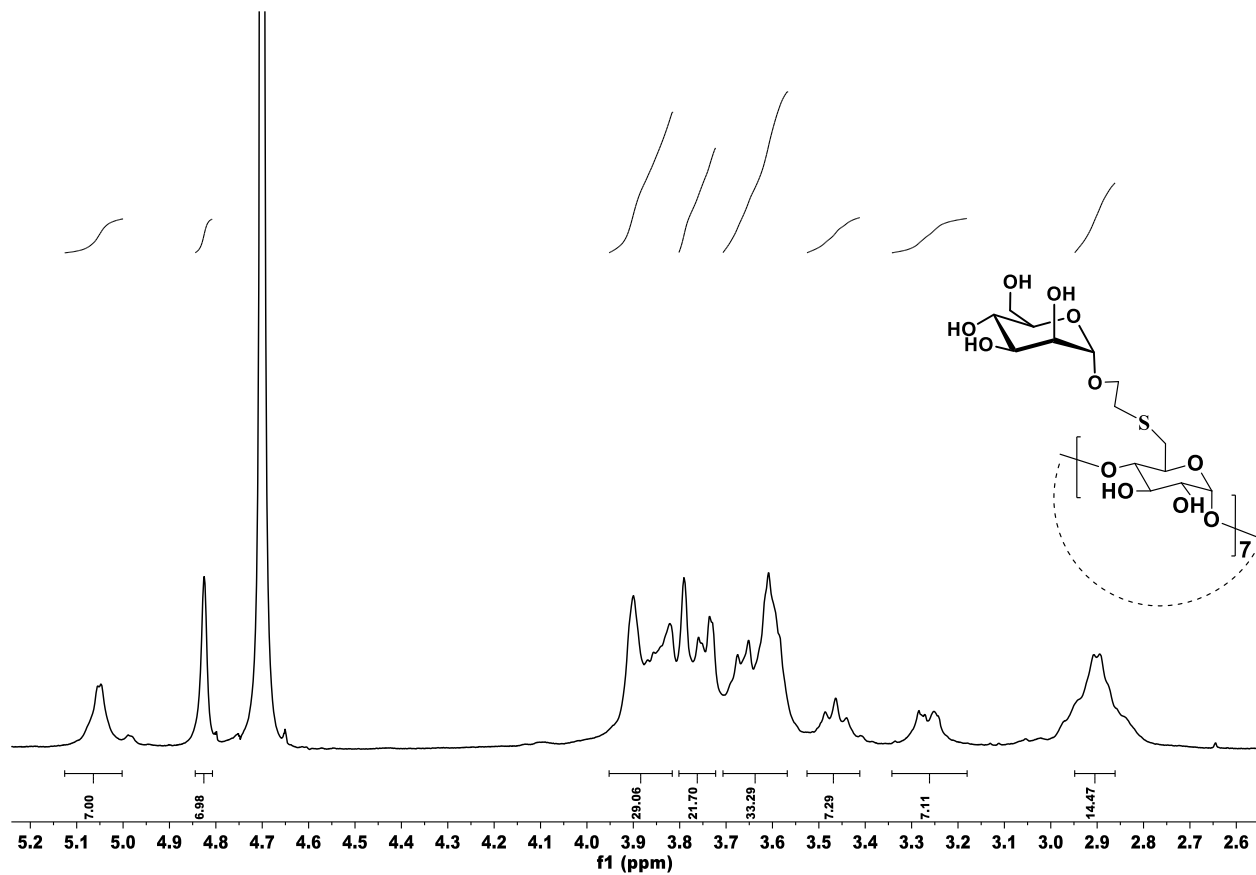


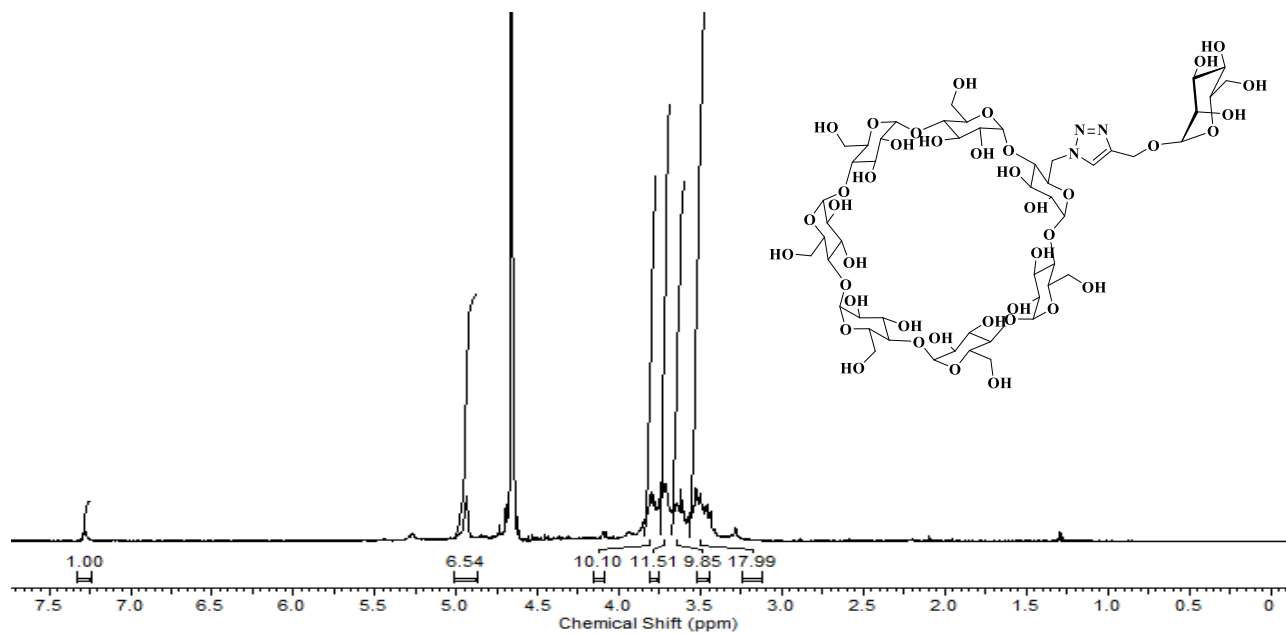
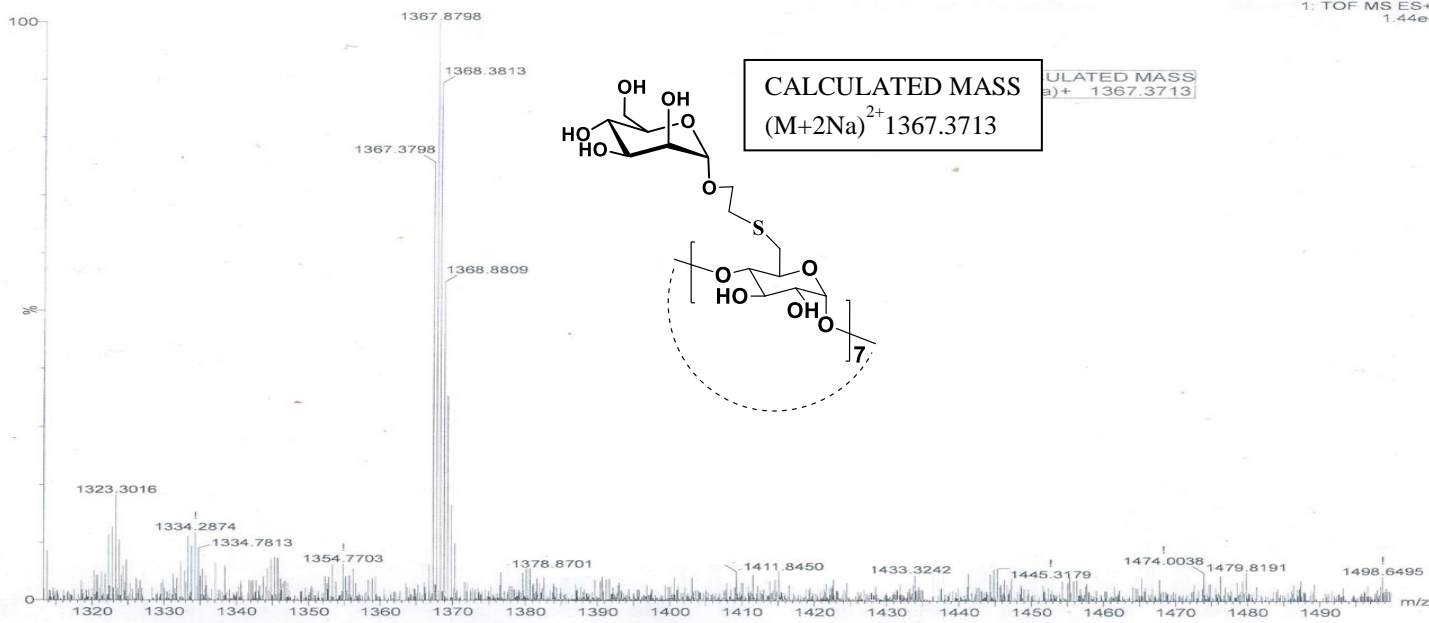


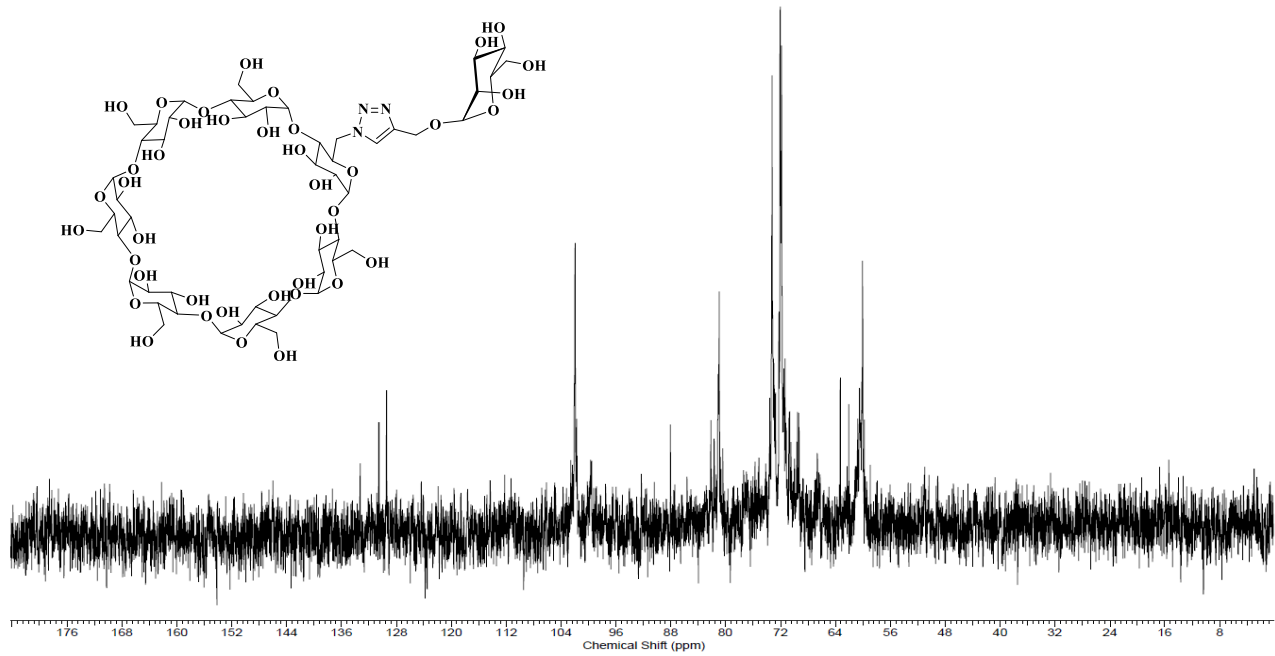




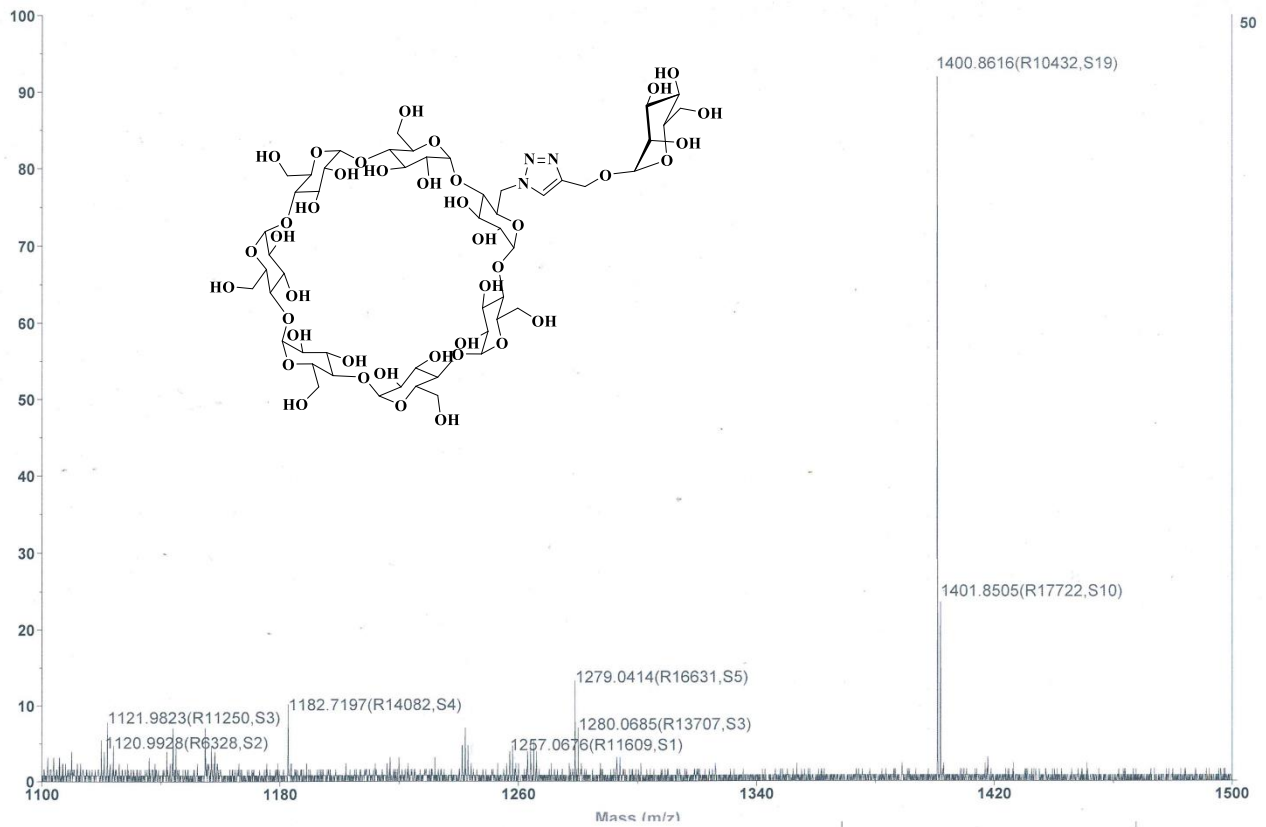








Final - Shots 1000 - IISER-4; Run #290; Label P1



Chapter 2

Part II

Supramolecular Scaffolds on Glass Slides as Sugar Based Rewritable Sensor for Bacteria

Abstract

We describe here the sugar functionalized β -cyclodextrin–ferrocene glass slides as fully reversible bacterial biosensors under the influence of external adamantane carboxylic acid. The prototype D-mannose- *E. coli* ORN 178 and L-fucose – *P. aeruginosa* interactions serve as a model to illustrate the new approach.

2.2 Introduction

Food- and water-borne diseases cause over 3 million deaths every year, of which, according to WHO publication, about 90% are children younger than 5 years from poor families and communities in developing countries.^{1,2} Major reasons for rapid increase in global pathogen infections are strain mutations and emergence of antibiotic resistance.³⁻⁵ However, appropriate medical treatment based on early diagnosis can decrease fatalities. Currently, detection of pathogenesis using DNA based PCR assay and protein-based ELISA⁶⁻¹³ techniques but these methods require trained personnel and are also influenced by the environment. A different approach for detection is based on carbohydrates that are used as biomarkers for pathogens and is based on the highly selective recognition of bacterial lectins through specific oligosaccharide epitopes.¹⁴⁻¹⁸ Carbohydrate-protein interactions are weak but multivalent interactions amplify recognition.¹⁹⁻²⁶ We and others have harnessed these interactions as templates for recognition of bacteria.²⁷⁻⁴⁰

In this part we describe a technique to prepare a glass substrate covered with sugar dendrimers which can be used as a platform for detection of bacteria. Our approach utilizes the special high tendency of β -cyclodextrin (β -CD) to form host-guest complexes with small molecules, especially with adamantane and ferrocene molecules⁴¹⁻⁴⁵ and the ability to attach a multitude of sugar molecules in close proximity by attaching them to its skeleton. We have synthesized a heptavalent sugar β -CD scaffold which contains seven sugar molecules with increased carbohydrate mediated interactions. This new sugar-modified β -CD derivative was used for developing a sensor on glass substrates. The attachment of this compound to the glass surface was achieved by formation of host-guest β -CD-ferrocene complexes. The specific advantage of ferrocene over adamantane linker is the difference in the strength of the host-guest complexation⁴¹⁻⁴⁵, which yield facile method to regenerate the surface to develop a protocol for removal of the bacteria and sugar after binding so that the same slide can be used continuously for similar or different pathogen-carbohydrate interactions.

2.2.1 Results and Discussion

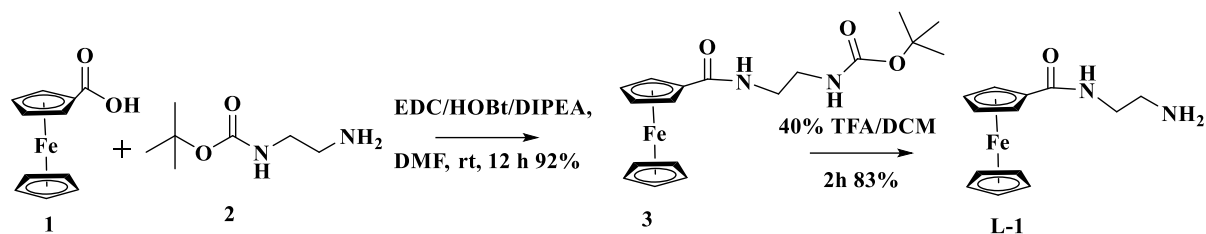
2.2.1.1 Bacterial strains used

We used mannose- and fucose as sugars and the specific bacterial strains mannose-FimH of *E. coli* ORN 178 and fucose-PIM-2 of *P. aeruginosa* to establish the selectivity, sensitivity and reversibility of the detection platform.⁴⁶⁻⁵³

2.2.1.2 Synthesis of ferrocene and cyclodextrin derivatives

Mannose-modified β -cyclodextrin (**M-1**) and Fucose modified β -cyclodextrin (**M-4**) was synthesized as described previously (Fig. 1).⁵⁴

Ferrocene derivative **L-1** was prepared by coupling mono-boc protected ethylene diamine and ferrocene monocarboxylic acid, followed by deprotection using TFA in CH₂Cl₂ (Scheme. 1).



Scheme 1 Synthesis of compound **L-1**

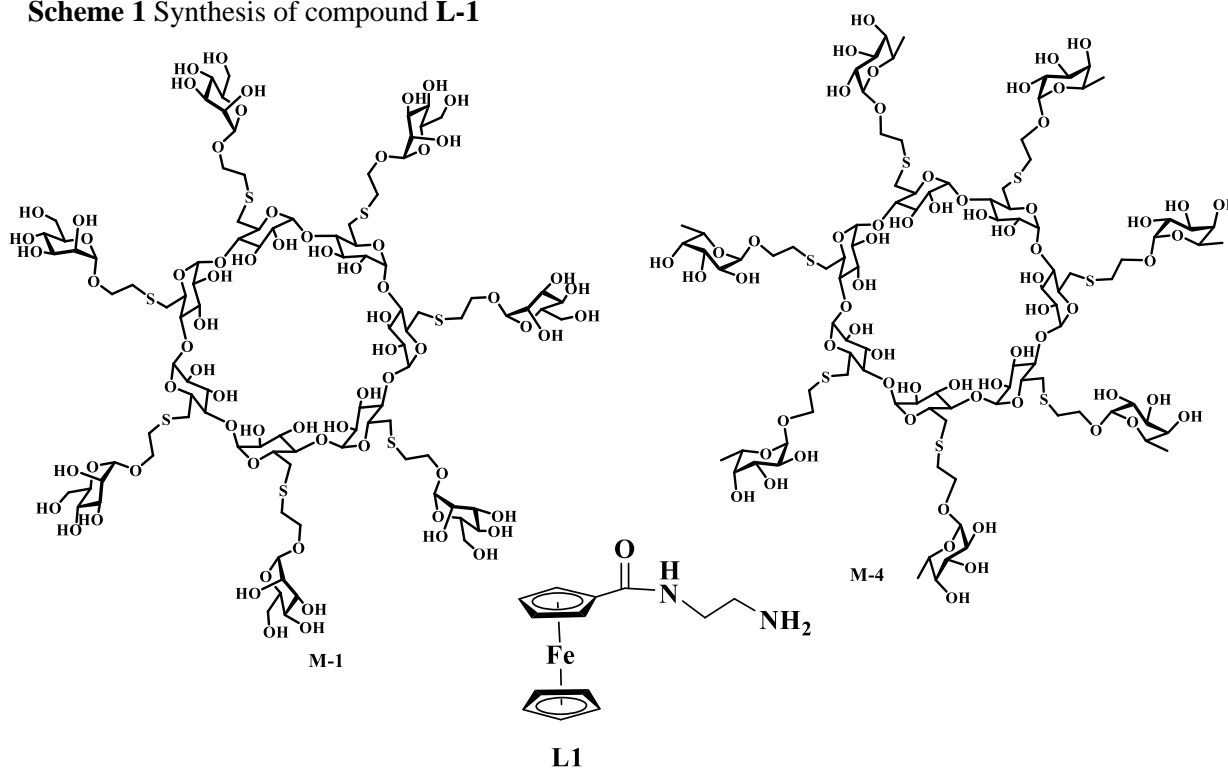
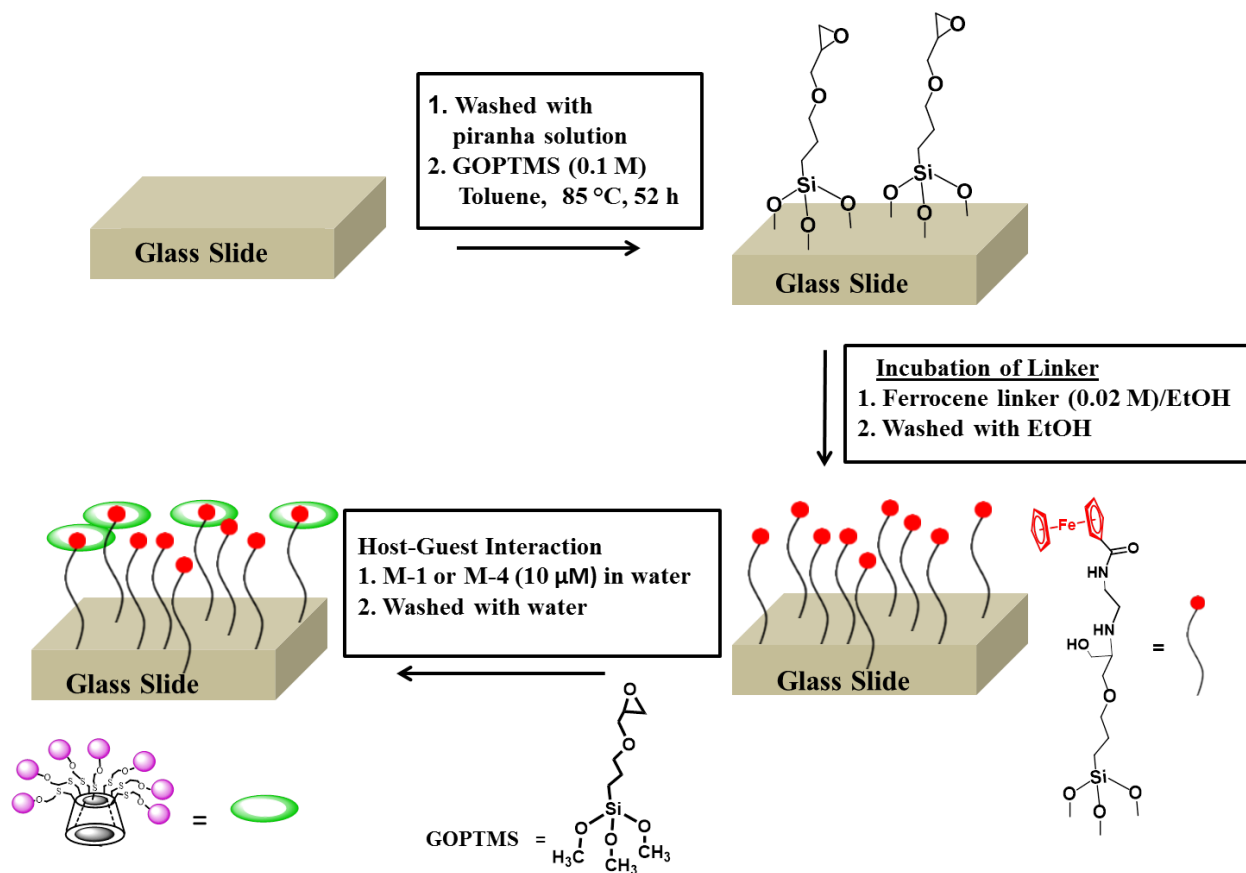


Figure 1 Molecular structures used for developing a sensor on glass substrates

2.2.1.3 Functionalization of slide

Robust ferrocene-based monolayers were formed by assembling ferrocene derivative L-1 on silyl epoxide-coated glass or silicon slides. This was done by washing glass slides (approx. 1x1 cm in size) with piranha solution followed by dipping them immediately into a solution of 3-glycidyloxypropyltrimethoxysilane (GOPTMS) in toluene. The substrates were heated at 85 °C for 52 h a pressure tube, rinsed with toluene to remove excess GOPTMS and were dipped in a solution of L-1 (0.02 mM) in ethanol for 24 h. Finally the substrates were rinsed with ethanol to remove excess ferrocene derivative and to remove residual epoxide groups (scheme 2).



Scheme 2 Schematic representation of different steps to immobilize sugar-modified β -CD supramolecular scaffolds onto glass slides

2.2.1.4 Characterization of slides by SIMS-TOF and XPS

The process yielded glass slides covered with monolayers of the ferrocene derivative L-1 which were analyzed by SIMS-TOF and XPS.⁵⁵⁻⁵⁷ Presence of L-1 on the glass slides was confirmed by the relative abundance of carbon, oxygen and iron atoms on the chips (Fig. 2 & 3). In the final step, the freshly prepared ferrocene monolayers were immersed in solutions of the β -CD

derivatives, **M-1** or **M-4** (10 μ M), for 30 mins at RT, and sugar coated surfaces were formed by complexation of the ferrocene skeleton in the cyclodextrin cavity. The substrates were rinsed with deionized water to remove the uncomplexed compound and the slides were checked again by SIMS-TOF and XPS to reveal the presence of sulphur atoms in addition to those that were found on the slide before complexation, confirming the presence of **M-1** or **M-4** on the surfaces (Fig 2 & 4)

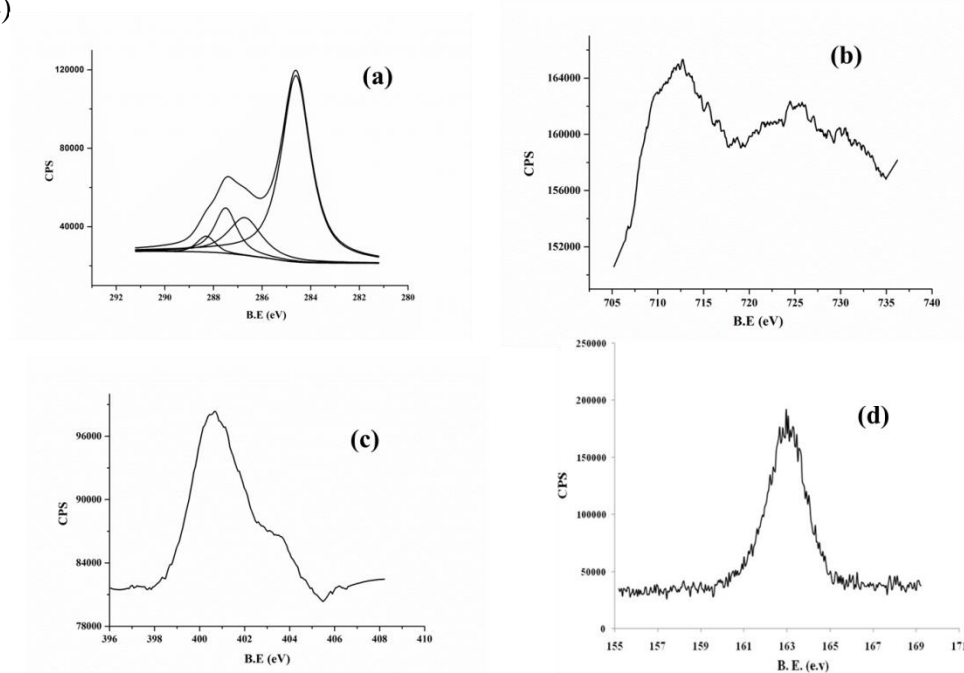


Figure 2 XPS spectra of (a) C 1S; (b) Fe 2P; (c) N 1S of **L-1** coated glass slide and (D) S 2P of **M-1/L-1** glass slide

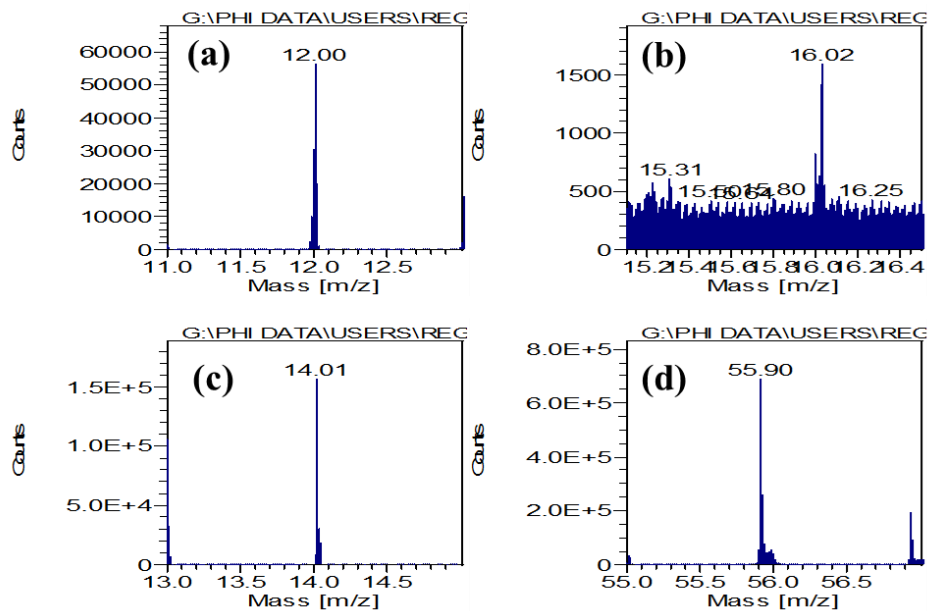


Figure 3 TOF-SIMS mass spectra of individual elements on **L-1** coated surface: (a) carbon, (b) oxygen (c) nitrogen, (d) iron

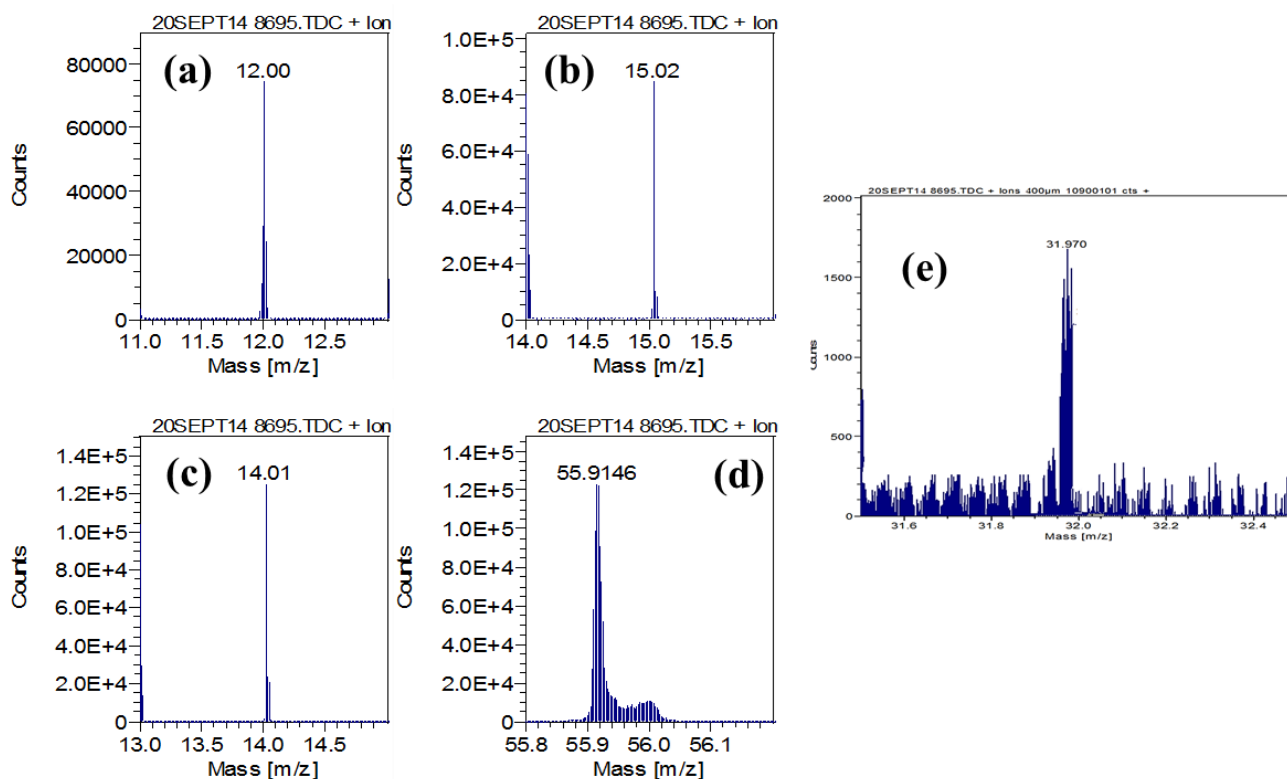


Figure 4 TOF-SIMS mass spectra of individual elements on **L-1/M-4** coated surface: (a) carbon, (b) oxygen (c) nitrogen, (d) iron, (e) sulphur

2.2.1.5 Bacterial Binding Assay

Glass slides thus modified were used for binding different bacterial strains *via* interaction with the sugar molecules found on the slides. Three bacterial strains, differing in their sugar recognition properties, were used to assess whether the sugar functionalized glass slides could recognize specific bacterial strain. We used *E. coli* ORN 178 having mannose receptor (FimH), its mutant strain *E. coli* ORN 208 and *P. aeruginosa* having fucose binding PIM-2 receptor. First, bacteria were grown at 37 °C and a standard growth curve was recorded at OD₆₀₀. Glass slides coated with **L-1**, **β-CD/L-1**, **M-1/L-1** and **M-4/L-1** were dipped in a solution with concentration of approximate 10⁸ bacteriae for 30 minutes. The slides were then washed several times with distilled water to remove unbound or weakly bound bacteria and finally, bound bacteria were treated with DAPI or FITC or rhodamine and imaged microscopically. Glass slides coated with **L-1**, **β-CD** or **M-4** were not found to bind bacteria of *E.coli* strain. However, **M-1** functionalized glass slides revealed a strong cluster of ORN 178, which was not removed even

upon vigorous rinsing with water. On the other hand, all glass slides with ORN-208 did not show binding. These results demonstrate selective and specific carbohydrate-protein interactions in bacterial recognition. Similar experiments were carried out with a *P. aeruginosa* strain. As expected, specific fucose mediated aggregation of bacteria was clearly observed (Fig. 5) which corroborates the selectivity of the binding assay.

2.2.1.6 Sensitivity Study

After assessing the selectivity of the platforms in bacterial recognition, we determined the sensitivity of the detection platform. Glass slides with **M-1/L-1** modified surfaces were immersed and incubated in serially diluted solutions of mannose-binding *E. coli* ORN 178 for various periods of time and surface-bound bacteria were visualized by DAPI staining. We have found that as little as 10^5 bacterial cells bound to the surfaces could be observed by fluorescent staining of the clusters (Fig.6).⁵⁸ It is interesting to note that this is also the minimum number of bacterial cells needed for formation of each bacterial colony.

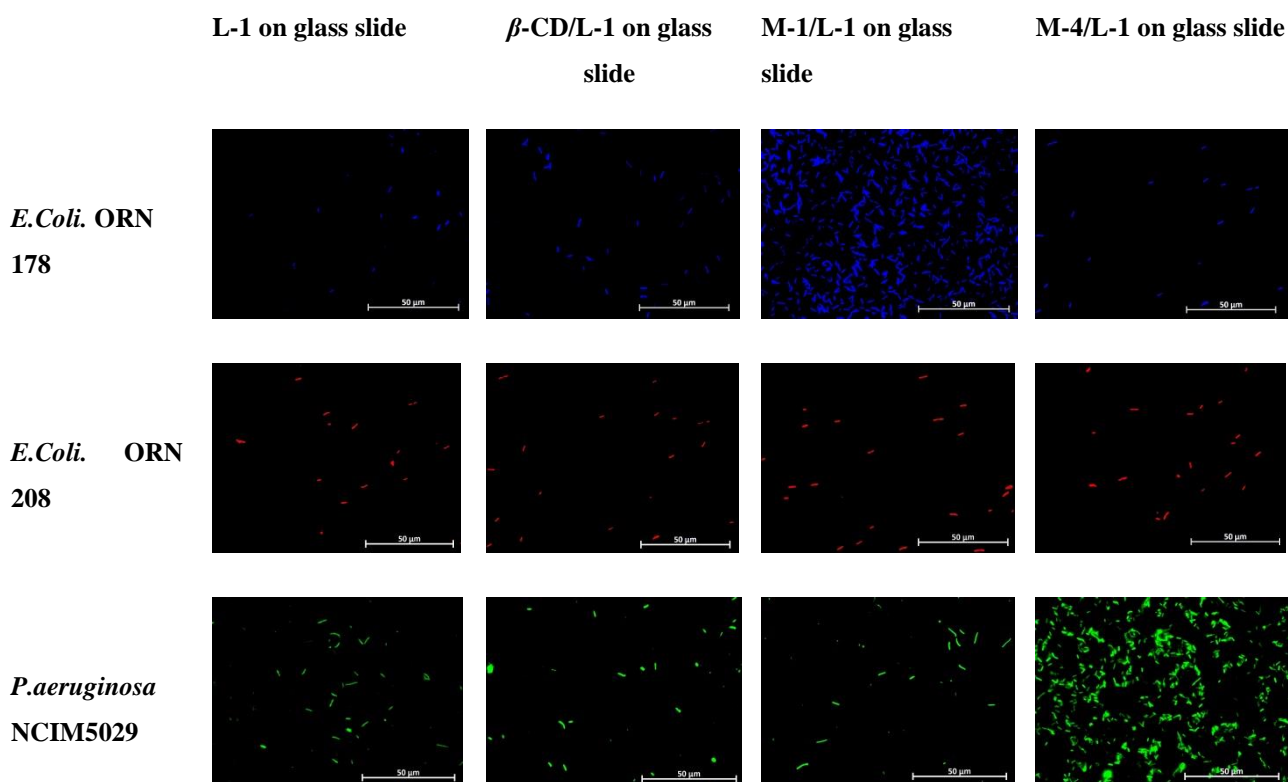


Figure 5 Representative images of bacterial adhesion on different sugar substrates coated onto glass slides

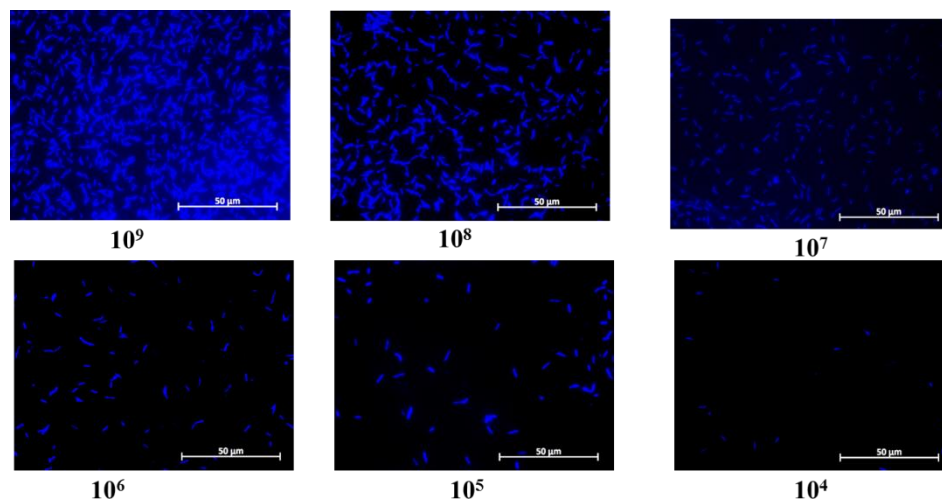


Figure 6 Detection limit for the staining of mannose binding *E.coli* by **M-1/L-1** surface. Number of bacteria used in the incubation mixture is shown above the images

2.2.1.7 Quantification by relative fluorescence unit

Quantification was done by using Relative Fluorescent Unit (Fig.7).

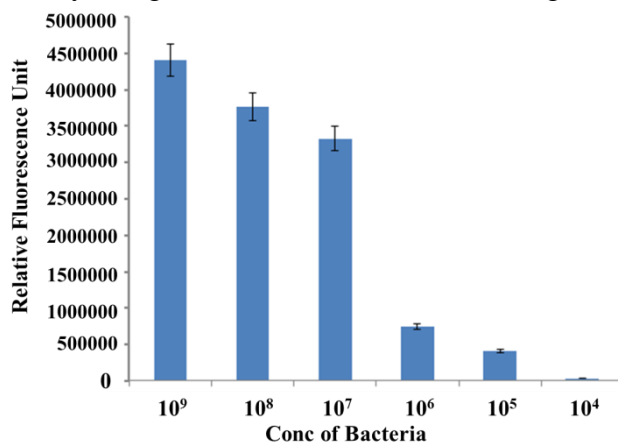
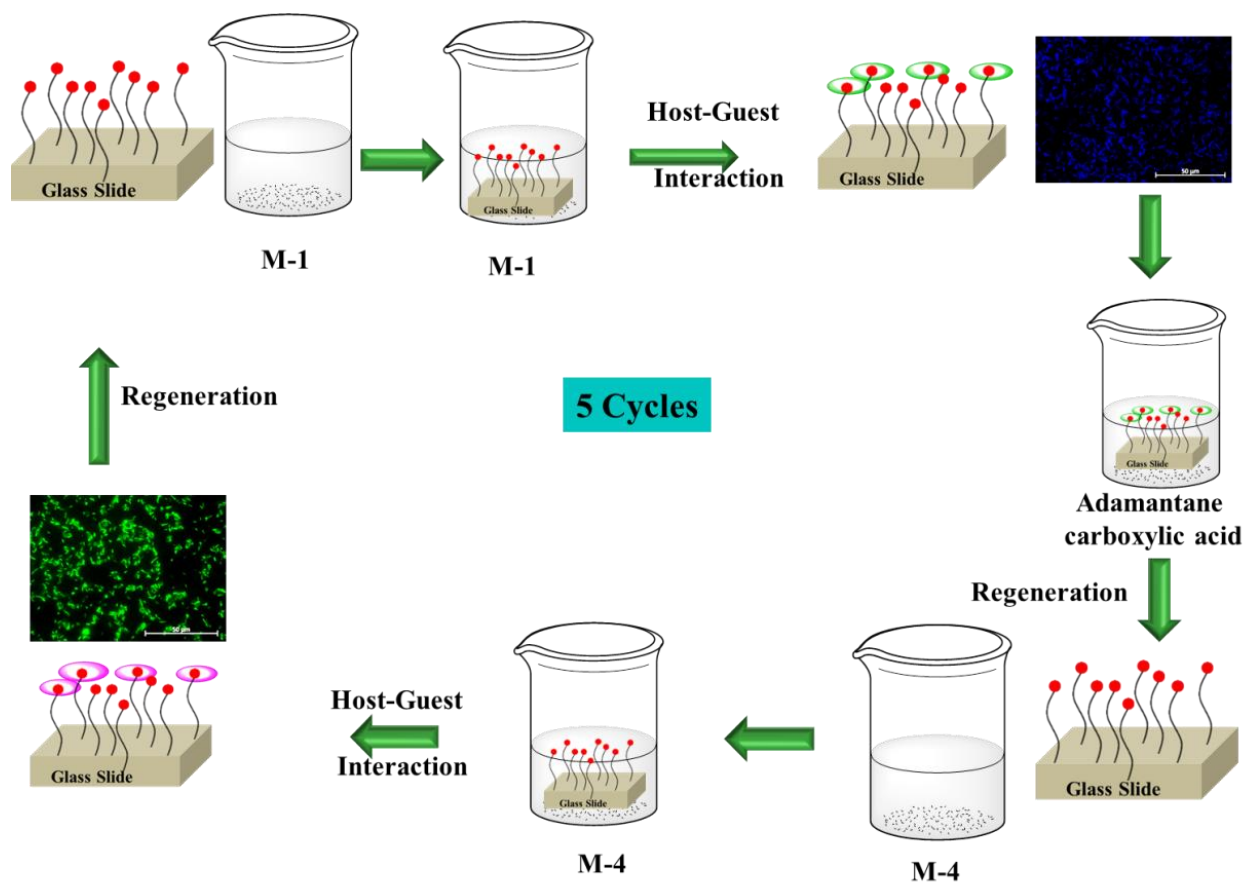


Figure 7 Quantitative analysis of bacterial adhesion at different concentrations on **M-1/L-1** surfaces by relative fluorescence unit

2.2.1.8 Regeneration of Slides

In order to assess the feasibility of the system to serve as a biosensor, it was crucial to demonstrate the reversibility of the system, i.e., to prove that the slides could be used for more

than one binding event and regeneration – generation cycles. This was done by utilizing the high binding constant of β -CD- adamantane complex ($5.7 \times 10^4 \text{ M}^{-1}$) as compared to that of ferrocene ($9.9 \times 10^3 \text{ M}^{-1}$).⁴¹⁻⁴⁵ When glass substrates coated with **M-1** sugar bound to ORN 178 bacteria were incubated in a solution of adamantane carboxylic acid (0.1 mM) for 5 minutes, the sugar was repelled from the slide. The adamantane skeleton replaced ferrocene in the cavity of the β -CD skeleton and detached it from the glass surface. After washing of the glass substrate with PBS, fresh ferrocene modified surfaces were obtained. Visualizing through fluorescence microscopy revealed no bacterial aggregation and corroborated the regeneration process. When the same slide was incubated again in solutions of **M-1** or **M-4** for 30 minutes, sugar respective bacterial aggregations were observed on the glass slides (Scheme 3, Fig 8). Several cycles (5) of degeneration – generation processes were performed and the reproducibility was found to be excellent.



Scheme 3 Schematic describing the regeneration process of sugar coated glass slides and subsequent interaction with *E. coli* (ORN 178) and *P. aeruginosa*- regeneration- generation cycles

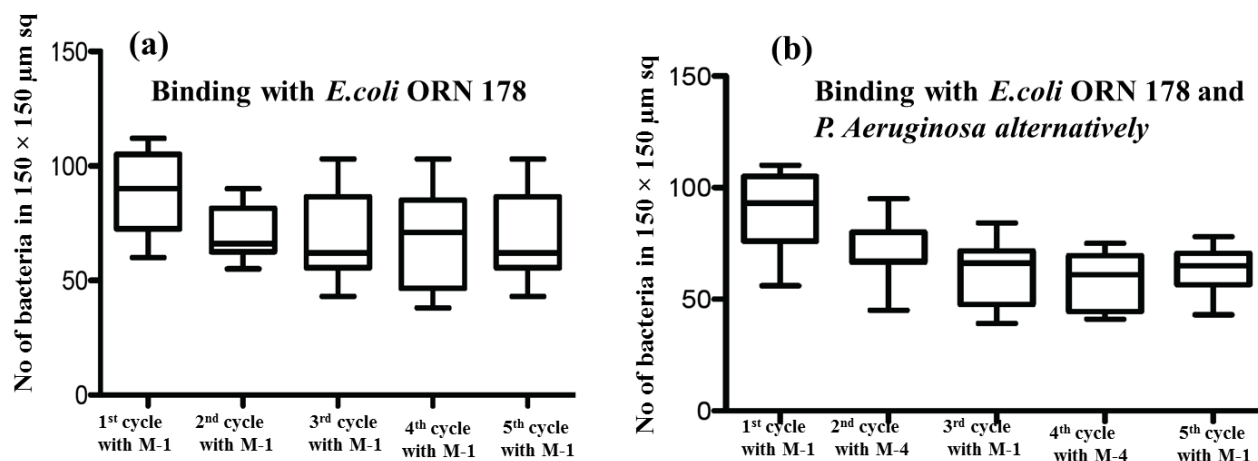


Figure 8 Quantitative analysis of bacterial adhesion on regenerated surfaces: (a) *E. coli* ORN 178 was incubated in **M-1/L-1** glass slides for 30 min (1st cycle). After imaging, the slide was dipped in 0.1 mM of adamantane carboxylic acid solution for 5 min to remove host-guest and bacterial adhesion, later the slide was dipped in **M-1** (10 μM) for 30 min and ORN 178 for another 30 min and imaged again (2nd cycle). The platform was regenerated five times using this reiterative process. The number of adhered bacteria in a 150 X 150 μm sq area was counted manually (n = 9); (b) *E.coli* ORN 178 and *P. aeruginosa* binding on **M-1** and **M-4** modified surface were successively regenerated and bacterial adhesion in 150 X 150 μm sq area was counted manually (n = 9). Note: All experiments were carried out with equal number of bacteria (10^7) and equal concentration of **M-1** or **M-4** respectively (10 μM)

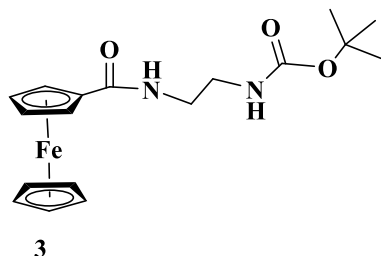
2.2.2 Conclusion

We have demonstrated that CD-based glycodendrimers placed on glass substrates by formation of complexes, controlled by host-guest interactions, produced a platform for detection of specific types of bacteria, such as *E. coli* and *P. aeruginosa* with high sensitivity. The interactions that control the binding are carbohydrate-protein interactions and the sensitivity is determined by the sugar moieties placed on the slide. The assay is reversible; and regeneration of the glass substrate has been demonstrated. The platform described here can be used for continuous bacterial sensing and could potentially be used as a detection method of choice in point of care testing. The possibility of producing microarrays with multitude types of carbohydrate on a single glass substrate for high-throughput detection of several bacteriae on a single platform is currently under study.

2.2.3 Experimental part

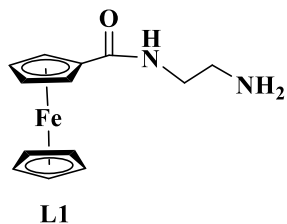
2.2.3.1 Experimental details

Synthesis of ferrocene derivative (3)



Ferrocene carboxylic acid **1** (0.5 g, 2.17 mmol) and mono-boc ethylene diamine **2** (0.34 g, 2.17 mmol) was dissolved in dry DMF (10 mL). Then HOBt (0.35g, 2.60 mmol) and EDC (0.45 g, 2.60 mmol) were added. The reaction mixture was stirred at RT for 12 h. After completion, the reaction mixture was diluted with 50 mL water and extracted with ethyl acetate (3× 50mL). The organic layer was dried over anhydrous Na₂SO₄ and concentrated under reduced pressure to give crude product **3**, which was further purified by flash column using petroleum ether: ethylacetate (Yield = 0.87g 92%), . ¹H NMR (400 MHz, CDCl₃): δ 6.81 (bs, 1H), 5.13 (s, 1H), 4.72 (bs,2H), 4.35(bs, 2H), 4.20 (s, 5H), 3.47 (q, *J* = 8.0 Hz, 2H), 3.36 (q, *J* = 8.0 Hz, 2H), 1.46 (s, 9H);¹³C NMR (100 MHz, CDCl₃): δ. 171.77, 79.99, 70.66, 69.89, 68.29, 41.32, 40.57, 28.50. HRMS *m/z* calc'd for C₁₈H₂₄FeN₂O₃: 373.1215; found: 373.1220.

Synthesis of L-1



To ferrocene derivative **3** added 40% TFA in CH₂Cl₂ was added, which was stirred for 2 h. Then TFA was evaporated under reduced pressure which was further purified by column using CH₂Cl₂: Methanol (Yield = 0.87 g, 83%).¹H NMR (400 MHz, CD₃OD): δ 4.85 (bs, 2H), 4.46 (bs, 2H), 4.24 (s, 5H), 3.63 (t, *J* = 12.0 Hz, 2H), 3.16 (t, *J* = 12.0 Hz, 2H);¹³C NMR (100 MHz, CD₃OD): δ. 137.38, 123.70, 123.03, 49.56, 36.39, 32.01, 19.27, 13.29. HRMS *m/z* calc'd for C₁₃H₁₆ON₂Fe: 273.0690; found: 273.0691.

2.2.3.2 Surface Functionalization:

2.2.3.2.1 Immobilization of ferrocene derivatives: (Approx. 1x1 cm) glass was washed with piranha solution (Caution: Piranha solution reacts violently so use carefully) and immediately dipped in a solution of 3-glycidyloxypropyl trimethoxysilane (GOPTMS) (0.1 M) in 2 mL toluene. The substrates were heated at 85 °C for 52 h in a pressure tube. Samples were then rinsed with toluene to remove excess of GOPTMS. Next, GOPTMS coated glass slides were dipped in a solution of **L-1** (0.02 M) in ethanol for 24 h and rinsed with ethanol to remove excess of ferrocene linker and to neutralize epoxide group.

2.2.3.2.2 Immobilization of cyclodextrin derivatives

Freshly prepared ferrocene glass substrate (modified with **L-1**) was washed twice with ethanol and immersed in solution of either β -CD or **M-1** or **M-4** (10 μ M solution in deionized water) for 30 mins. The samples were rinsed with water, dried under a stream of nitrogen and used bacterial assay.

2.2.3.3 Time-of-Flight Secondary Ion Mass Spectrometer (SIMS-TOF) Characterization

Time-of-Flight Secondary Ion Mass Spectroscopy (ToF SIMS) is a surface sensitive Spectroscopy that uses a pulsed Primary Ion beam to induce the desorption and ionization of atomic and molecular species from a solid sample surface. Approximate (20mmx20mmx20mm) silica wafer was coated with **L-1** followed by and the elementary composition was characterized by TOF-SIMs.

2.2.3.4 Bacterial Strains growth

The mutants *E.coli ORN178* and *ORN208* were provided by Prof. Orndorff (College of Veterinary Medicine, Raleigh, NC United States) and *P. aeruginosa* was obtained from NCL bacterial bank. The bacterial cultures were grown overnight at 37 °C until they reached an approximate OD₆₀₀ of 1.0.

2.2.3.5 Bacterial detection

2 mL aliquot of bacteria of approximate OD₆₀₀ of 1.0 was centrifuge to obtain a bacterial pellet. The resulting pellet was washed twice with PBS buffer and resuspended in 2 mL PBS and adjust the concentration to 10⁸. Different sugar coated glass slides were dipped in this solution for 30 mins and the glass slides was rinsed with PBS, followed by distilled water to remove non-

specific bindings. These slides were mounted on fluorescent microscopic slides to image the bacteria.

2.2.3.6 Concentration dependent studies

The concentration of the bacteria was calculated by using growth promotion curve. 2 mL solutions of different dilution of bacteria were prepared and sugar coated glass slides (**M-1/L-1** with *E. coli* ORN 178 and **M-4/L-1** with *P.aeruginosa*) were immersed for 30 mins. Slides were washed with distilled water and images were collected. Quantification of bacteria was done by measuring relative fluorescence unit.

2.2.3.7 Rewriting the sugar substrate for continuous bacterial sensor

A stock solution of 0.1 mM of adamantyl carboxylic acid in ethanol water was prepared. The glass substrate having bacteria and host-guest complex was immersed in above solution for 5 mins. The sample was then rinsed with PBS, deionized water and then dried under a stream of N₂. This substrate was once again incubated in a solution of **M-1** or **M-4**(10 μM) for 30 min, to obtain the regenerated substrate used for bacterial sensing.

2.2.4 References

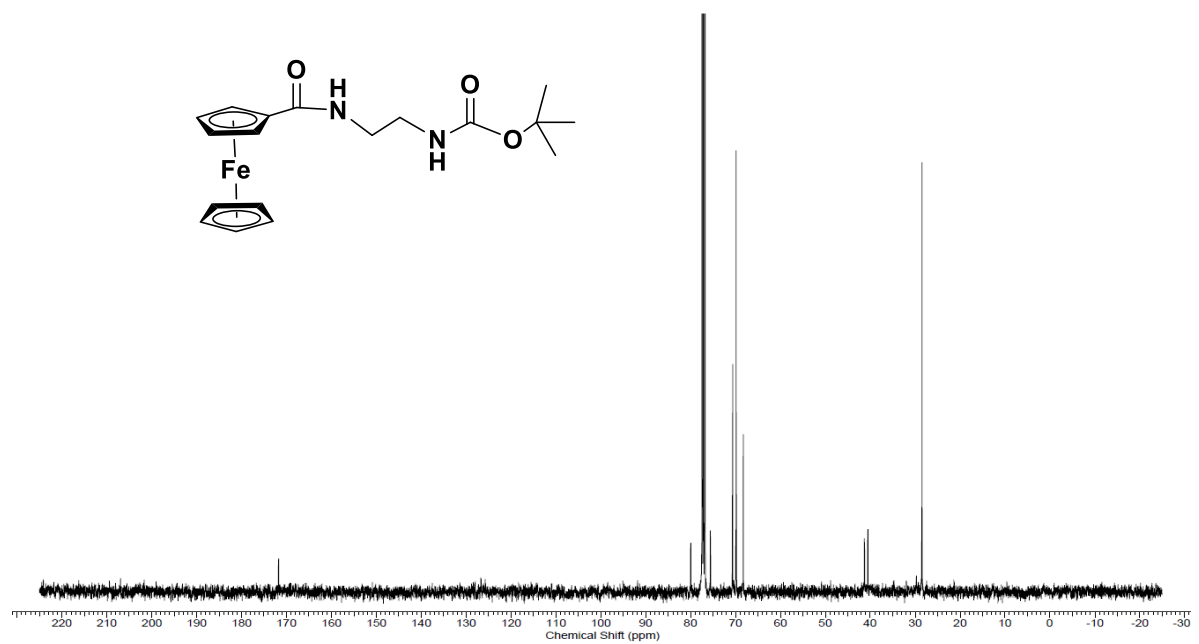
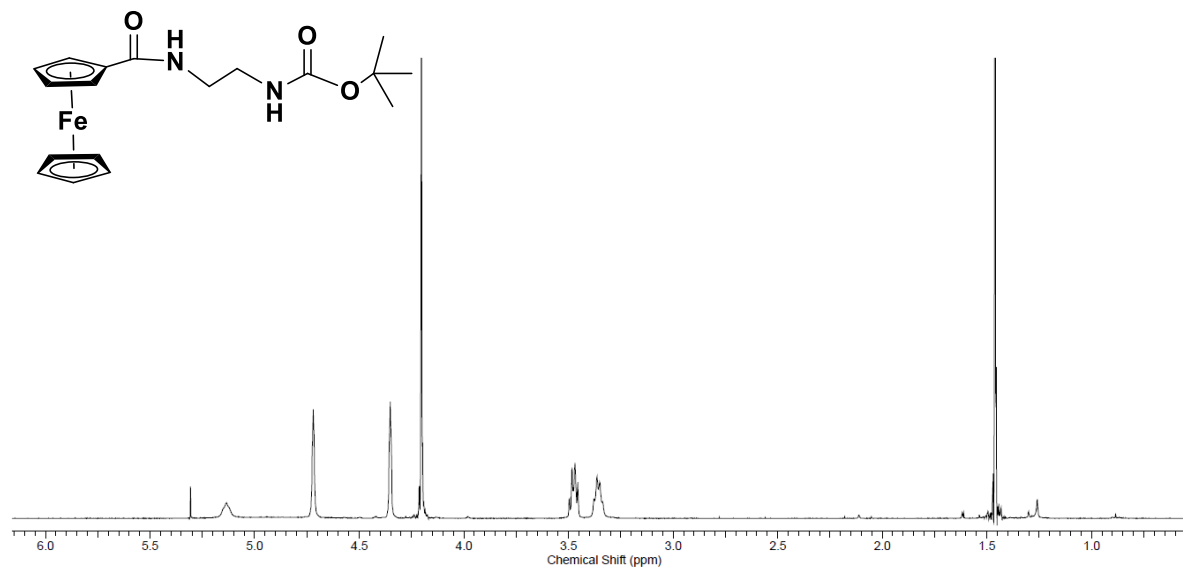
1. <http://www.cdc.gov/foodsafety/facts.html>
2. P. S. Mead, L. Slutsker, V. Dietz, L. F. McCaig, J. S. Bresee, C. Shapiro, P. M. Griffin and R. V. Tauxe, *Emerg. Infect. Dis.*, 1999, **5**, 607-25.
3. D. J. Payne, M. N. Gwynn, D. J. Holmes and D. L. Pompliano, *Nat. Rev. Drug. Discovery.*, 2007,**6**, 29–40.
4. M. F. Lin and C. Y. Lan, *World. J. Clin. Cases.*,2014, **16**, 787-814.
5. V. Makarov, G. Manina, K. Mikusova, U. Mollmann, O. Ryabova, B. Saint-Joanis, N. Dhar, M. R. Pasca, S. Buroni, A. P. Lucarelli, A. Milano, E. De Rossi, M. Belanova, A. Bobovska, P. Dianiskova, J. Kordulakova, C. Sala, E. Fullam, P. Schneider, J. D. McKinney, P. Brodin, T. Christophe, S. Waddell, P. Butcher, J. Albrethsen, I. Rosenkrands, R. Brosch, V. Nandi, S. Bharath, S. Gaonkar, R. K. Shandil, V. Balasubramanian, T. Balganes, S. Tyagi, J. Grosset, G. Riccardi and S. T. Cole, *Science*. 2009, **324**, 801–4.

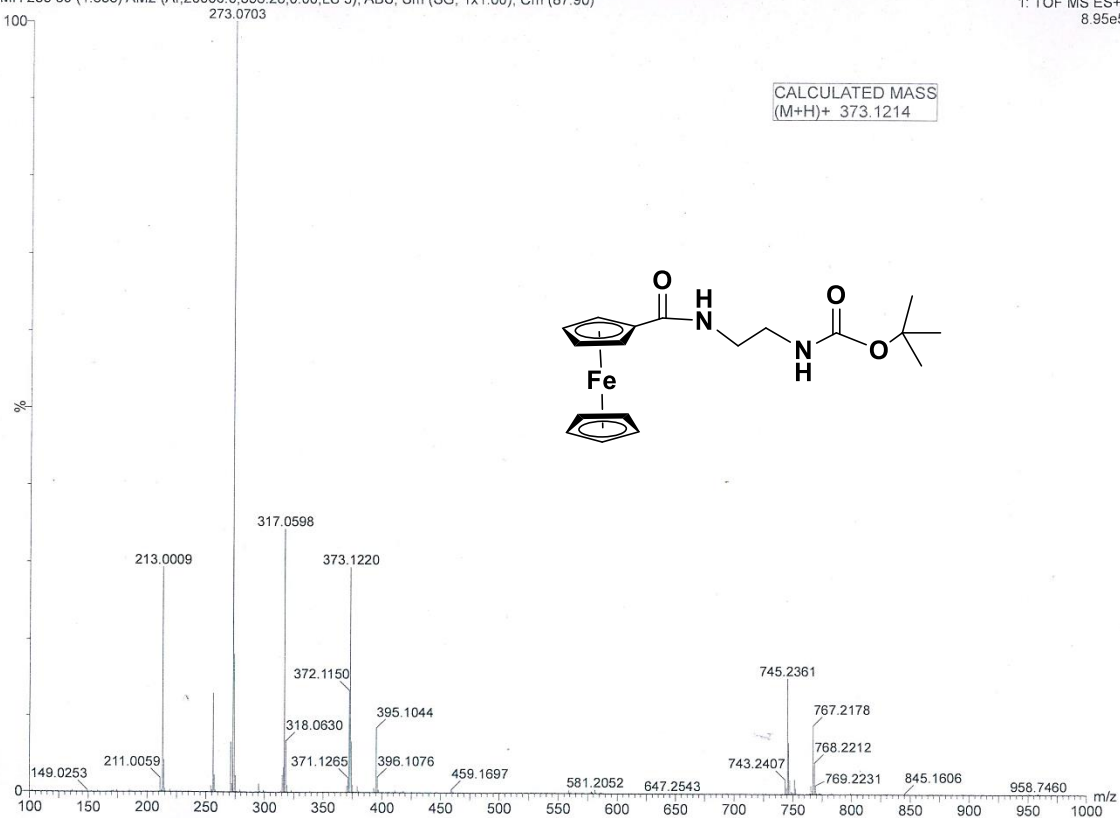
6. B. Swaminathan and P. Feng, *Annu. Rev. microbial.*, 1994, **48**, 401-26.
7. D. Pissuwan, C. H. Cortie, S. M. Valenzuela and M. B. Cortie, *Trends. Biotechnol.*, 2010, **28**, 207–213.
8. J. Joo, C. Yim, D. Kwon, J. Lee, H. H. Shin, H. J. Cha and S. Jeon, *Analyst*, 2012, **137**, 3609–12.
9. E. De Boer and R. R. Beumer, *Int. J. Food, Microbio.*, 1999, **50**, 119-30.
10. R. Singh, M. D. Mukherjee, G. Sumana, R. K. Gupta, S. Sood and B. D. Malhotra, *Sens. Actuators, B : Chemical*. 2014, **197**, 385-404.
11. S. A. Dunbar, C. A. Vander Zee, K. G. Oliver, K. L. Karem and J. W. Jacobson. *J. Microbiol. Methods.*, 2003, **53**, 245-52.
12. D. T. McQuade, A. E. Pullen and T. M. Swager, *Chem. Rev.*, 2000, **100**, 537-574.
13. C. Fan, K. W. Plaxco and A. J. Heeger, *J. Am. Chem. Soc.*, 2002, **124**, 5642-43.
14. M. D. Disney, J. Zheng, T. M. Swager and P. H. Seeberger, *J. Am. Chem. Soc.*, 2004, **126**, 13343–46.
15. C. W. Reid, K. M. Fulton and S. M. Twine, *Future. Microbiol.*, 2010, **5**, 267-88.
16. B. Lepenies and P. H. Seeberger, *Immunopharmacol. Immunotoxicol*, 2010, **32**, 196-207.
17. K. A. Karlsson, *Biochem. Soc. Trans.*, 1999, **27**, 471-4.
18. K. A. Karlsson, *Adv. Exp. Med. Biol.*, 2001, **491**, 431-43.
19. W. Yang, C. Y. Pan, M. D. Luo, H. B. Zhang, *Biomacromolecules*, 2010, **11**, 1840-6.
20. J. E. Gestwicki and L. L. Kiessling, *Nature*, 2002, **415**, 81-4.
21. J. H. Ryu, E. Lee, Y. B. Lim and M. Lee, *J. Am. Chem. Soc.*, 2007, **129**, 4808–14.
22. C. C. Huang, C. T. Chen, Y. C. Shiang, Z. H. Lin and H. T. Chang, *Anal. Chem.*, 2009, **81**, 875-82.
23. C. C. Lin, Y. C. Yeh, C. Y. Yang, C. L. Chen, G. F. Chen, C. C. Chen and Y. C. Wu, *J. Am. Chem. Soc.*, 2002, **124**, 3508-9.
24. M. G. Garcia, J. M. Benito, D. Rodríguez-Lucena, J. X. Yu, K. Chmurski, C.O. Mellet, R. G. Gallego, A. Maestre, J. Defaye and J. M. Garcia Fernandez, *J. Am. Chem. Soc.*, 2005, **127**, 7970-1.
25. J. M. Benito, M. Gomez-Garcia, C. Ortiz Mellet, I. Baussanne, J. Dafaye and J. M. Garcia Fernandez, *J. Am. Chem. Soc.*, 2004, **126**, 10355-63.
26. C. Ortiz Mellet, J. Defaye and J. M. Garcia Fernandez, *Chem. Eur. J.*, 2002, **8**, 1982-90.

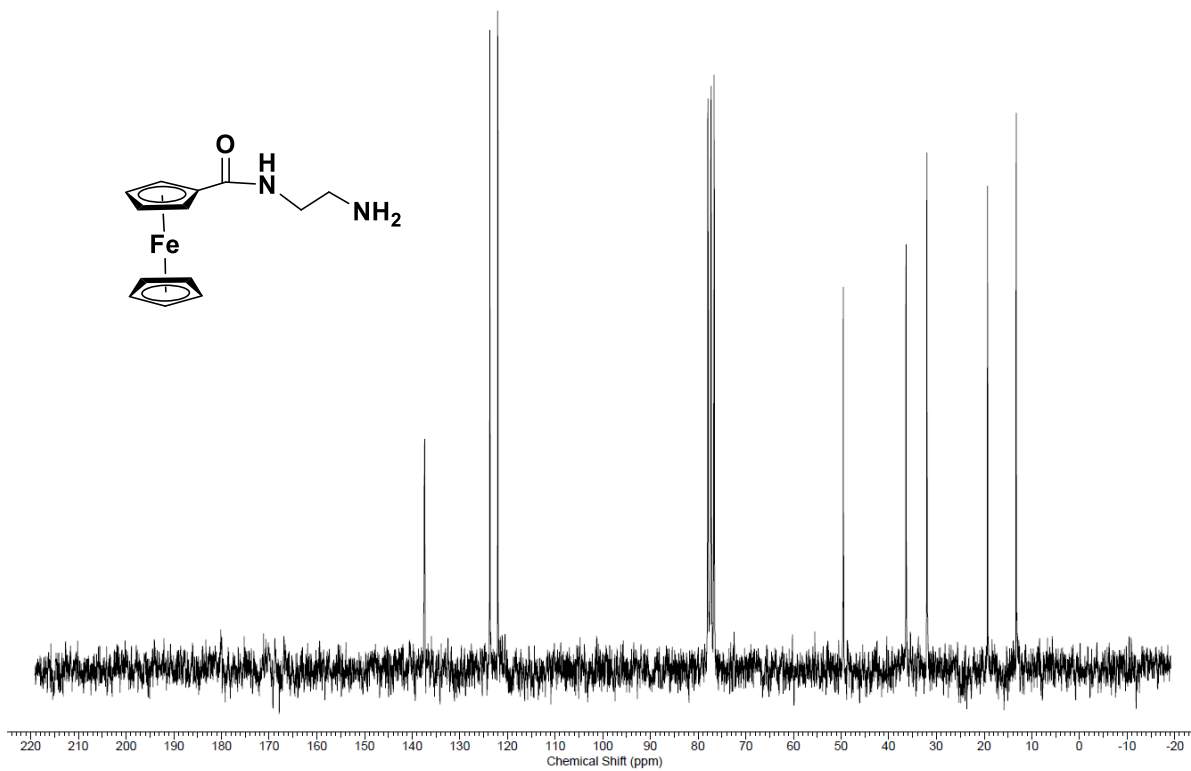
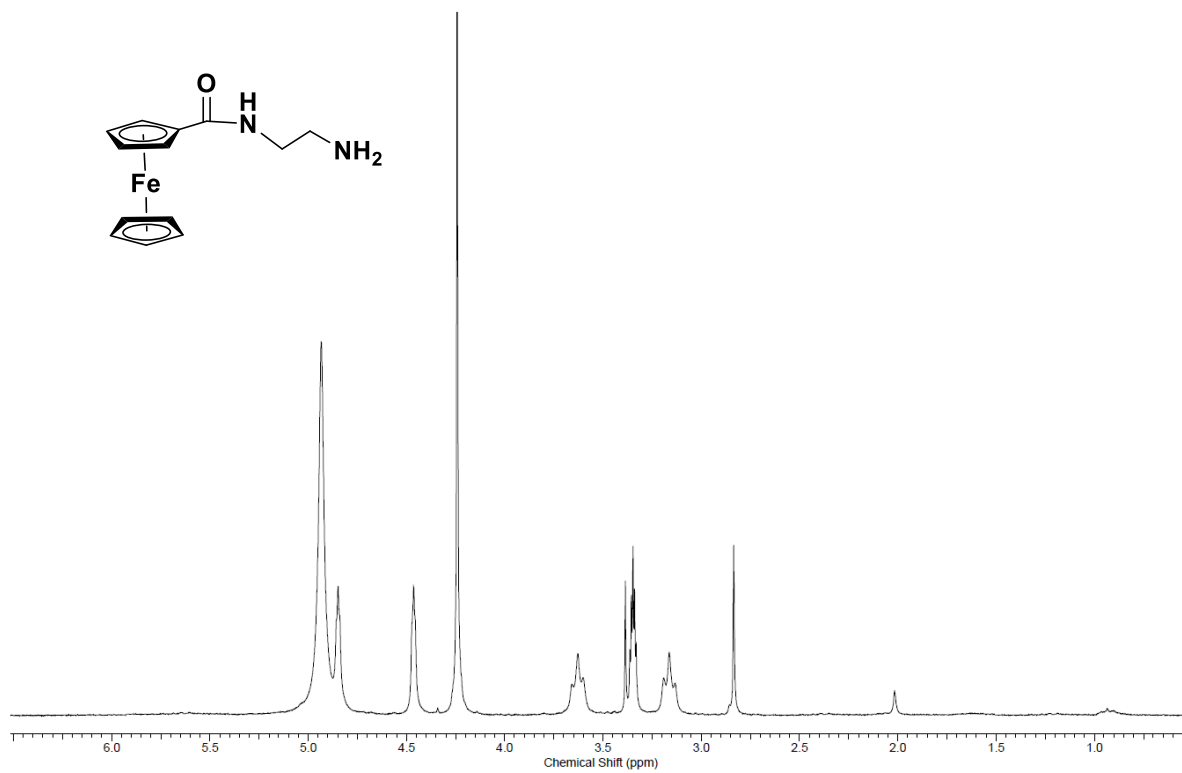
27. R. Yadav and R. Kikkeri, *Chem. Commun.*, 2012, **48**, 1704-6.
28. I. Yazgan, N. M. Noah, O. Toure, S. Zhang and O. A. Sadik, *Biosens. Bioelectro.*, 2014, **61**, 266-73.
29. K. Adak, H. J. Lin and C. C. Lin, *Org. Biomol. Chem.*, 2014, **12**, 5563-73.
30. K. Babiuch and M. H. Stenzel, *Encyclopedia of Polymer Science and Technology*, 2014, 1-58.
31. N. P. Pere and R. J. Pieters, *MedChemComm.*, 2014, **5**, 1027-35.
32. S-J, Richards, E. Fullam, G. S. Besra and M. I. Gibson, *J. Mater. Chem. B.*, 2014, **2**, 1490-98.
33. G. Yu, Y. Ma, C. Han, Y. Yeo, G. Tang, Z. Mao, C. Gao and F. Huang, *J. Am. Chem. Soc.*, 2013, **135**, 10310-13.
34. M. Behra, N. Azzouz, S. Schmidt, D. V. Volodkin, S. Mosca, M. Chanana, P. H. Seeberger and L. Hartmann, *Biomacromolecules*, 2013, **14**, 1927-35.
35. J. Bouckaert, Z. Li, C. Xavier, M. Almant, V. Caveliers, T. Lahoutte, S. D. Weeks, J. Kovensky and S. G. Gouin, *Chem-A Eur. J.*, 2013, **24**, 7847-55.
36. N. Skirtenko, M. Richamann, Y. Nitzan, A. Gedanken and S. Rahimipour, *Chem. Commun.*, 2011, **47**, 12277-79.
37. L. G. Harris, W. C. E. Schofield, K. J. Doores, B. G. Davis and J. P. Badyal, *J. Am. Chem. Soc.*, 2009, **131**, 7755-61.
38. M. K. Muller and L. Brunsveld, *Angew. Chem. Int. Ed.*, 2009, **48**, 2921-24.
39. D. Grunstein, M. Maglinao, R. Kikkeri, M. Collot, K. Barylyuk, B. Lepenies, F. Kamena, R. Zenobi and P. H. Seeberger, *J. Am. Chem. Soc.*, 2011, **133**, 13957-66.
40. P. Laurino, R. Kikkeri, N. Azzouz and P. H. Seeberger, *Nano Lett*, 2011, **11**, 73-78.
41. M. R. de Jong, Cyclodextrin for sensing: solution, surface, and single molecule chemistry, Chapter 6. <http://doc.utwente.nl/36438/1/t0000031.pdf>
42. L. Peng, A. Feng, M. Huo and J. Yuan, *Chem. Commun.*, 2014, **50**, 13005—13014.
43. K. Shang, X. Wang, B. Sun, Z. Cheng and S. Ai *Biosens. Bioelectron.*, 2013, **45**, 40–5.
44. T. Auletta, M. R. Jong, A. Mulder, F. C. J. M. V Veggel, J. Huskens, D. N. Reinhoudt, S. Zou, S. Zapotoczny, H. Schonherr, G. J. Vancso and L. Kuipers; *J. Am. Chem. Soc.*, 2004, **126**, 1577-1584.

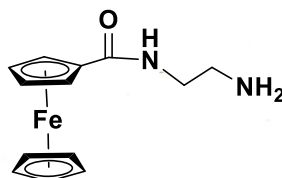
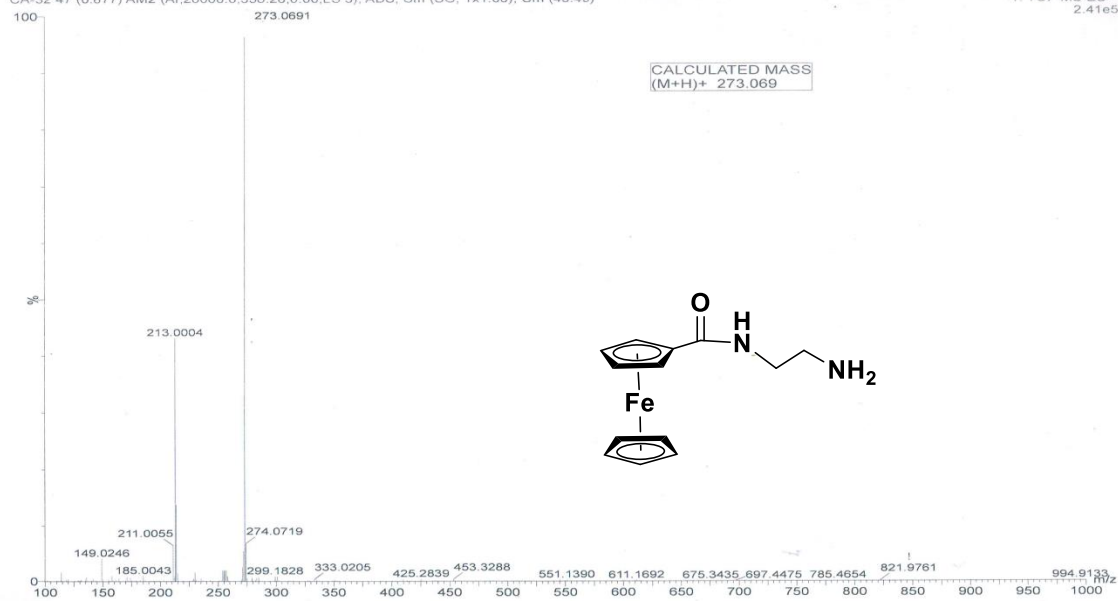
45. A. Harada, Y. Hu, S. Yamamoto and S. Takahashi, *J. Chem. Soc. Dalton Trans.*, 1988, 729-732.
46. M. Khanal, F. Larssonneur, V. Raks, A. Barras, J. S. Baumann, F. A. Martin, R. Boukherroub, J. M. Ghigo, C. Ortiz Mellet, V. Zaitsev and J. M. Garcia Fernandez, C. Beloin,
47. A. Siriwardena and S. Szunerits, *Nanoscale*, 2015, **28**, 2325-35.
48. A. Barras, F. A. Martin, O. Bande, J. S. Baumann, J. M. Ghigo, R. Boukherroub, C. Beloin, A. Siriwardena and S. Szunerits, *Nanoscale*, 2013, **21**, 2307-6.
49. M. L. Gening, D. V. Titov, S. Cecioni, A. Audfray, A. G. Gerbst, Y. E. Tsvetkov, V. B. Krylov, A. Imberty, N. E. Nifantiev and S. Vidal, *Chem. A Eur. J.*, 2013, **19**, 9272-85.
50. M. Stach, T. N. Siriwardena, T. Kohler, C. van Delden, T. Darbre and J. L. Reymond, *Angew. Chem. Int. Ed. Eng.*, 2014, **53**, 12827-31.
51. J. L. Reymond, M. Bergamann and T. Darbre, *Chem. Soc. Rev.*, 2013, **42**, 4814-22.
52. N. Berthet, B. ThoI. Bossu, E. Dufour, E. Gillon, j. Garcia, N. Spinelli, A. Imberty, P. Dumy and O. Renaudet, *Bioconjug. Chem.*, 2013, **24**, 1598-611.
53. B. Garland, A. Goudot, G Pourceau, A. Meyer, S. Vidal, E. Souteyrand, J. J. Vasseur, Y. Chevolot and F. Morvan, *J. Org. Chem.*, 2012, **77**, 7620-6.
54. E. Kolomiets, M. A. Swiderska, R. U. Kadam, E. M. Johansson, K. E. Jaeger, T. Darbre and J. L. Reymond, *ChemMedChem*, 2009, **4**, 562-9.
55. F. J. Rutten, D. Briggs, J. Henderson and M. J. Roe, *Archaeometry.*, 2009, **31**, 966-86.
56. M. R. Das, M. Wang, S. Szunerits, L. Gengembrec and R. Boukherroub, *Chem. Commun.*, **2009**, 2753–2755.
57. U. Bexell, *Surface characterisation using Tof-SIMS, AEsS and XPS of silane films and organic coatings deposited on metal substrates*, 2003, <http://uu.diva-portal.org/smash/get/diva2:162811/FULLTEXT01>
58. M. D. Disney and P. H. Seeberger, *Chemistry & Biology*, 2004, **11**, 1701–1707.

2.2.5. NMR and HRMS of compounds









Chapter 3

Multivalent Homo and Hetero Glycodendrimers Allow Sequence Defined Carbohydrate-Protein Interactions

Abstract

Carbohydrate-protein interactions (CPIs) are involved in a wide range of biological phenomena. Hence, understanding specific factors influencing these interactions is essential to design better targeting probes and inhibitors. Multivalency, Heterogeneity and oligosaccharides have been successfully adopted to increase the avidity of the CPIs. However, there are still a lot of unanswered questions about whether these factors are optional or obligatory to design the glydoclusters. To answer this question, herein we reported the synthesis of homo and heteromultivalent mono and oligomannose glycodendrons and their binding to a series of plant, C-type and galectin lectins. The results showed that each lectin displayed its own set of binding preferences. In case of ConA and PNA lectins, oligosaccharides multivalency is more important than heterogeneity. While GNA lectin displayed heterogeneity of the glycodendrons as critical factor for better CPIs. Overall these results demonstrate that each lectin possess its own set of rules for CPIs and difficult to be rationalized.

3.1. Introduction

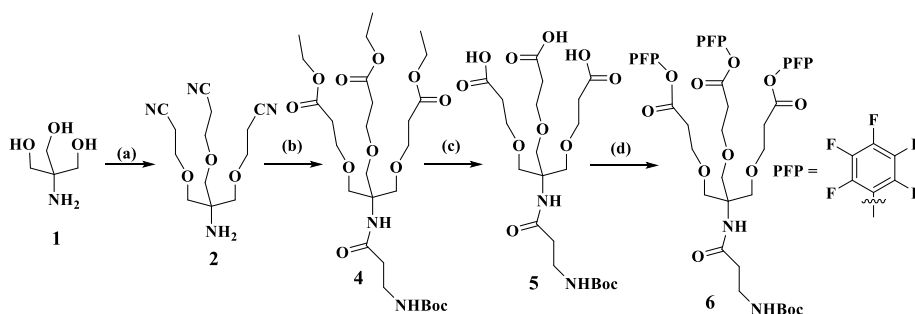
Carbohydrate-protein interactions have become one of the important interactions on cell surfaces.¹⁻⁵ However, the weak binding affinity of monovalent carbohydrate ligands with proteins ascribed to synthesize multivalent system to improve the selectivity and sensitivity of CPIs.^{6,7} Recent several multivalent tools have been developed, which include glycodendrimers,⁸ glycopolymer,⁹ supramolecular glycocomplexes¹⁰⁻¹² and glyconanoparticles.¹³ Although multivalency enhanced the binding avidity, it is still far way to mimic the natural interaction, which is far more selective, sensitive and spontaneous probably due to the heterogeneity, oligosaccharide structure of the biological systems. Hence, glycoprobes were designed with multivalent, heterogeneity, oligomeric composition to optimize the CPIs. For example in 2002, Lindhorst et al. synthesized mixed type oligosaccharide mimics on carbohydrate and peptide backbone to study FimH bacterial adhesion.^{14,15} The anti-adhesion assays showed no significant impact of heterogeneity on the inhibition assay. Lehn et al. synthesized a dynamic library of bis-carbohydrate ligands and screened their binding with ConA lectin.¹⁶ The heterodimers series didn't show binding disparity compared to homodimer series. Similarly, Jimenz Blanco et al. reported the synthesis of trivalent glycodendrons of mannose and glucose or lactose ligands and its binding affinity with ConA lectin.¹⁷⁻¹⁸ ELISA plate assay clearly indicated that the presence of galactose or lactose has the least influence of lectin binding. In contrast, Santoya-Gonzalez et al. synthesized tetravalent heteroglycodendrimers of mannose and glucose ligands.¹⁹ ELISA assay showed that the relative binding affinities of heteroglycodendrons are 1.5-fold higher than homo glyco-dendrons of mannose. Overall, there is a major confusion regarding the lectin preferences of heterogeneity, multivalency and oligomeric nature of the dendrimers influencing the CPIs.

To address this issue, we proposed to synthesize heteroglyco-dendrimers with mannose oligosaccharides and galactose to optimize the binding preferences. We have synthesized mannose oligomers in one-pot strategy and assembled them on a tripod via divergent strategy. The immobilization of these glycoclusters were then carried out on epoxide coated microarray chips to study CPIs. Plant lectins such as ConA, PNA, GNA were used as a control to study basic binding preferences. Finally, mannose specific C-type lectins (DC-SIGN, Dectin-1,) and

galactose specific galectin lectins (H-galectin-1 and 3) were used to rationalize the binding preferences.

3.2. Results and Discussion

Homo- and hetero-glycodendrimers were readily accessible in high yield using active ester coupling between carbohydrate containing an amine linker and tripodal-active ester. Subsequent removal of protecting groups on carbohydrate moieties will provide access to the desired tripodal dendrimers. The formation of desired compounds was confirmed by ^1H and ^{13}C -NMR and HRMS chromatography.

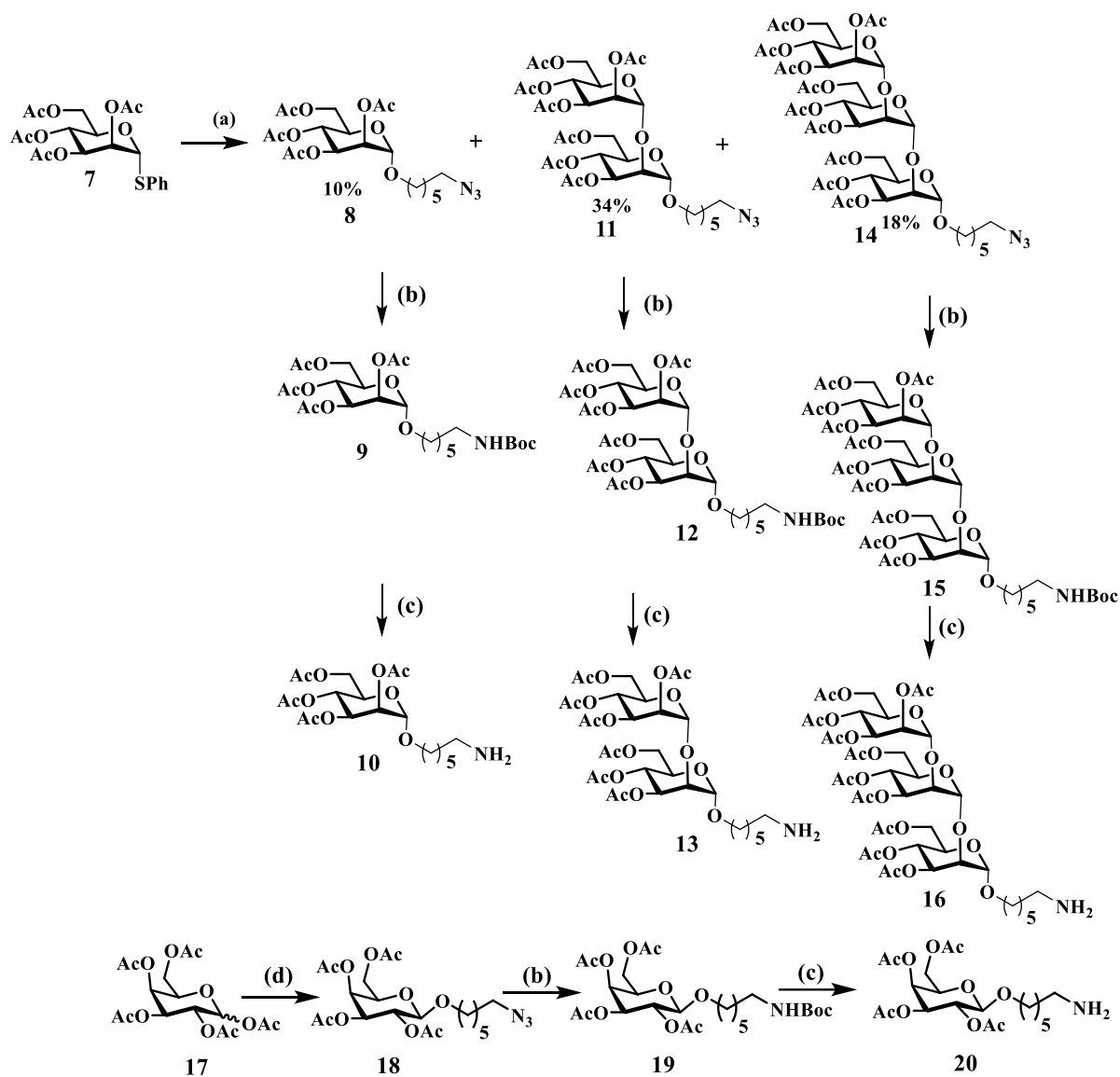


Scheme 1 (a) Acrylonitrile/KOH (40%); (b) Conc. HCl; EtOH; (c) Boc- β -Alanine, DIC, HOBT, Et₃N, CH₂Cl₂; (d) NaOH (2N), MeOH; (e) Pentafluorophenol (PFP), DIC, HOBT, Et₃N, CH₂Cl₂

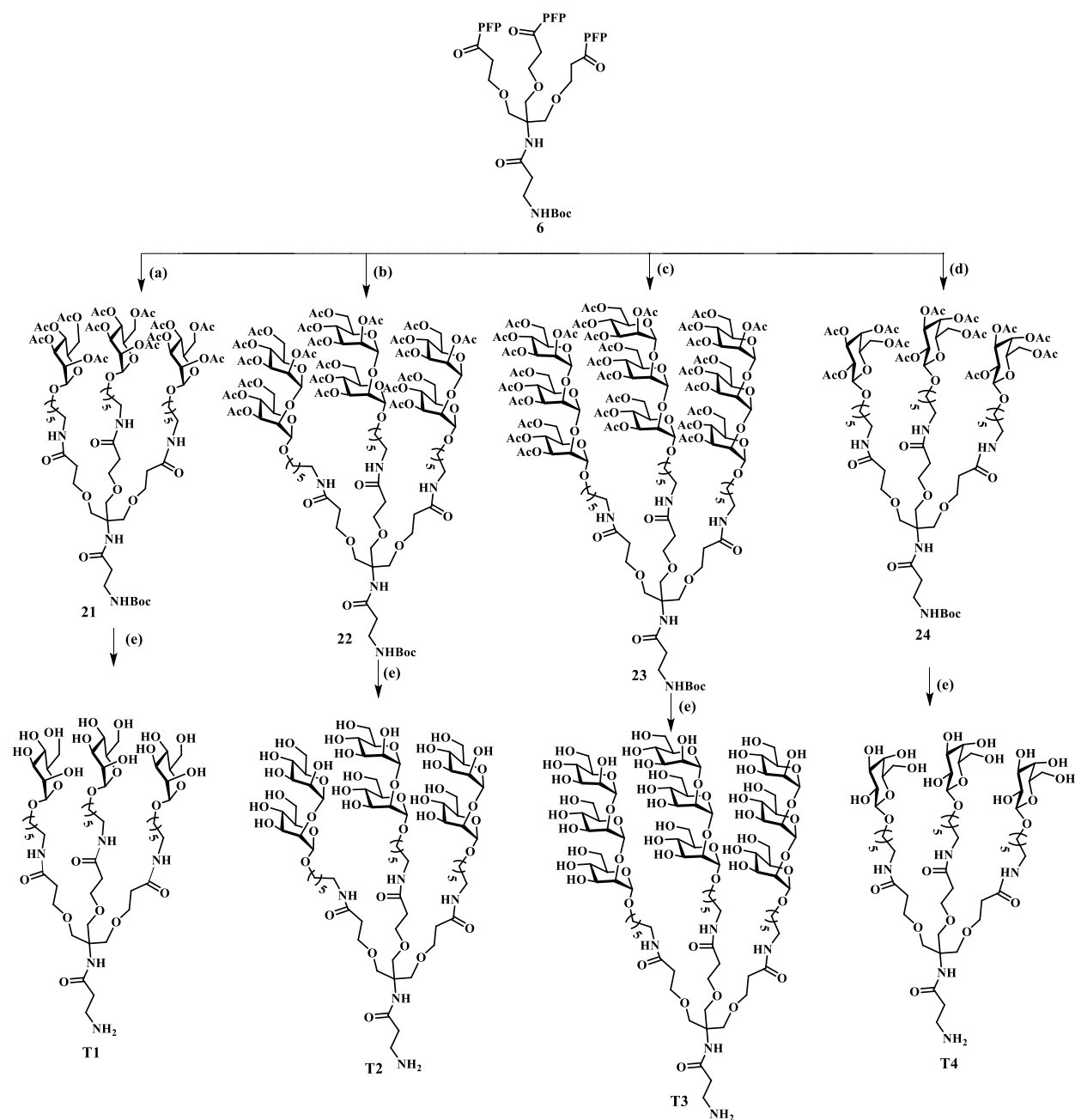
3.2.1. Synthesis of tripod-active ester. Tripod-active ester **6** was readily synthesized from tris-base as described previously (Scheme 1).²⁰ Briefly, Michael addition of acrylonitrile and tris-base **1** in the presence of KOH followed by hydrolysis of nitrile and esterification in the presence of conc. HCl and ethanol and coupling with boc- β -alanine and tripodal-ester yielded compound **4**, which was hydrolyzed in the presence of 2N NaOH, followed by coupling with pentafluorophenol to yield **6** active ester.

3.2.2. One-pot glycosylation for synthesis of Mono, Di and Tri- mannose derivatives with Azide Linker. Acetylated thioglycoside **7** was chosen as mannose donor and in the presence of 0.8 equivalence of linker with NIS/TfOH activator conditions, we got not only the expected monosaccharide **8**, but also di **11** and trisaccharides **14** (Scheme 2).²¹ Monomannose glycosylated with azide linker was confirmed to be of exclusively α - form. The anomeric proton showed $J = 1.6$ Hz. Linker glycosylation was confirmed with the peaks of CH₂ groups at around 3.30 ppm. Dimannose with $\alpha(1 - 2)$ linkage was confirmed by NMR with its anomeric protons

integrating for 2 Hydrogens at δ . 4.93 ppm with $J = 1.8$ Hz thereby confirming the linkage. Similar way, trimannose containing 3 anomeric protons showed peaks at 4.94 ($J = 1.8$ Hz), 4.93 ($J = 2.1$ Hz) and 4.92 ($J = 1.7$ Hz) ppm confirming the formation of desired product.



Scheme 2 Reagents: (a) NIS, TfOH, 6- azidohexan-1-ol, Acetic anhydride (b) PPh_3 , THF, water, Boc_2O ; (c) TFA (20%) in CH_2Cl_2 . (d) 6- azidohexan-1-ol, $\text{BF}_3 \cdot \text{Et}_2\text{O}$



Scheme 3 Synthesis of tripodal structures reagents: (a) **10**, TEA in CH₂Cl₂; (b) **13**, TEA in CH₂Cl₂; (c) **16**, TEA in CH₂Cl₂; (d) **20**, TEA in CH₂Cl₂; (e) (i) NaOMe, MeOH (ii) TFA (20%) in CH₂Cl₂

3.2.3. Synthesis of symmetric tripodal dendrimers of corresponding mannose derivatives

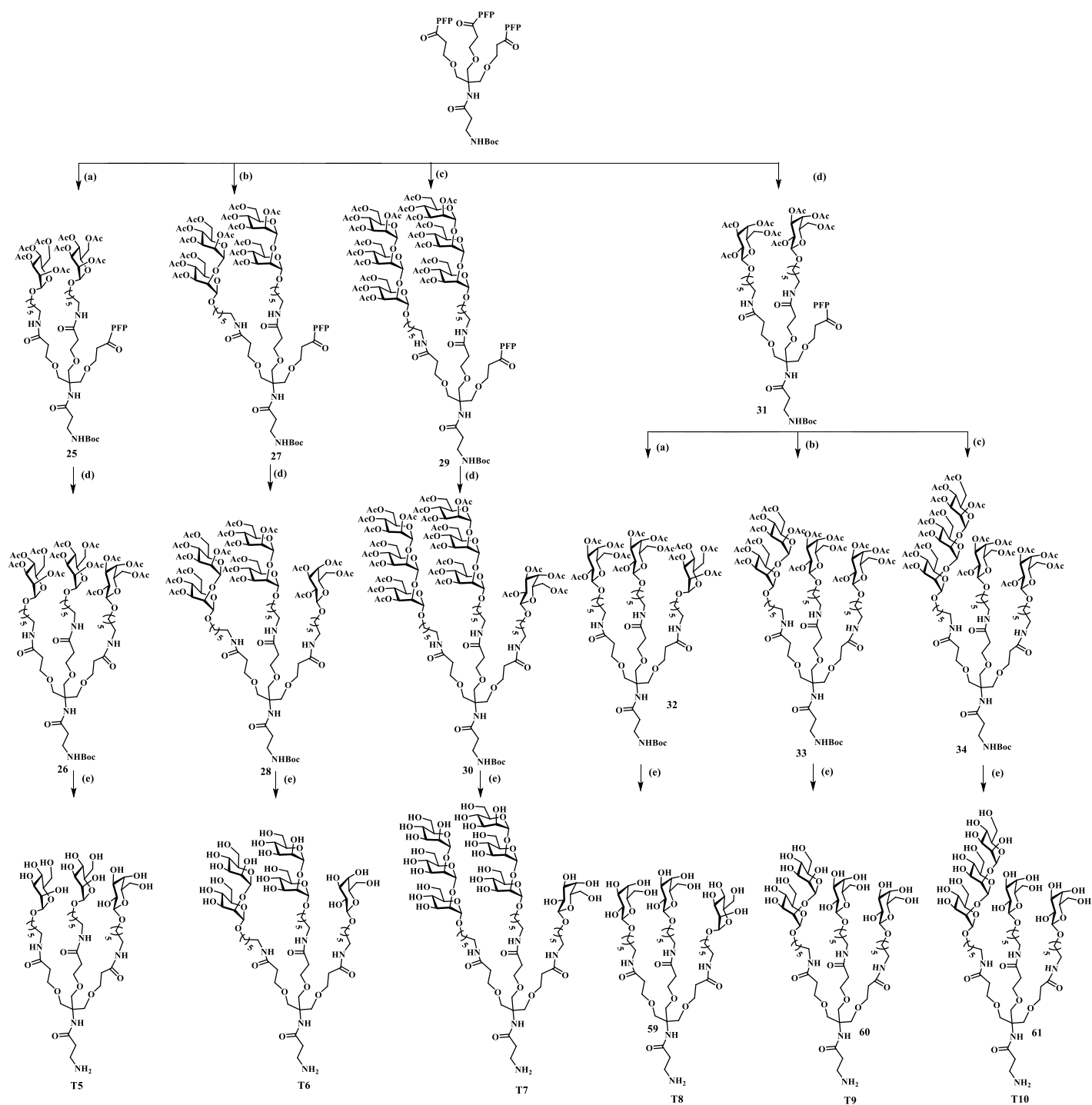
Azide derivatives were converted to amine using triphenylphosphene in THF and water to get boc-protected sugars then boc is deprotected using 20% TFA (Scheme 2) to bearing components for ease of coupling with the PFP active ester **6** to form the desired glycodendrimers under basic

condition (Scheme 3). For one equivalence of the active ester **6**, 3.3 equivalence of sugar derivative was necessary. The deprotection of the compounds were then carried out in NaOMe/MeOH and finally Boc protection was removed to obtain desired final symmetric tripods. In both mono **T1** and di **T2** mannose dendrimer case, anomeric protons were observed as singlet peaks with integrations 3 and 6 respectively. If higher magnetic field is used, we may be able to resolve it better. In tri **T3** mannose case, anomeric protons with peaks at 5.12 (d, $J = 1.7$ Hz, 3H), 4.96 (d, $J = 1.7$ Hz, 3H), 4.94 (d, $J = 1.7$ Hz, 3H), ppm were observed, thus confirming 9 anomeric protons of the desired product. Also the increment in the no. and intensity of peaks in ^{13}C NMR also confirms the formation of homo dendrimers of mannose derivatives. Galactose symmetric tripod **T4** was synthesized by mixing one equivalent of tripod-active ester **6** and galactose glycosylated amine linker **20**. The formation of glycodendrimer was confirmed from the number of anomeric protons in the integration which showed 3 protons at δ . 4.48 ppm.

3.2.4. Synthesis of Hetero Glycodendrimers of Mannose and Galactose. Hetero glycodendrimers of mannose derivatives with galactose (Scheme 4) were synthesized by altering the equivalence. The formation of di substituted compound was confirmed by MALDI as well as by NMR. The hetero dendrimer of each derivative showed two distinct anomeric protons, one with low coupling constant indicating mannose and other with high coupling constant indicating galactose. In deprotection of trimannose heterodendrimer, galactose anomeric proton showed peak at δ . 4.23 ppm and $J = 7.9$ Hz and mannose anomeric protons showed peaks at around δ . 5.13 (d, $J = 0.5$ Hz), 4.92 (d, $J = 0.7$ Hz), 4.88 (d, $J = 0.5$ Hz) with weak coupling constants.

3.3. Mannose glycodendrons microarray fabrication and binding experiments

The tripodal derivatives were printed on epoxide-functionalized microarrays (Fig. 1) at four concentrations (100 μM , 150 μM and 200 μM) in replicates of four as described in the Experimental Section. Plant and animal lectins were incubated on the slide at concentrations of 10 ng/ μL in PBS and binding affinity was evaluated by detection of fluorescence intensity as described in the experimental Section. In order to determine binding preferences of the lectins toward the tripodal derivatives, we used 10 ng/ μL concentration of the lectin and 100 μM concentration of the tripodal derivatives for comparative studies.



Scheme 4 Synthesis of Tripodal structures Reagents: (a) **10**, TEA in CH_2Cl_2 ; (b) **13**, TEA in CH_2Cl_2 ; (c) **16**, TEA in CH_2Cl_2 ; (d) **20**, TEA in CH_2Cl_2 ; (e) (i) NaOMe, MeOH (ii) TFA (20%) in CH_2Cl_2 .

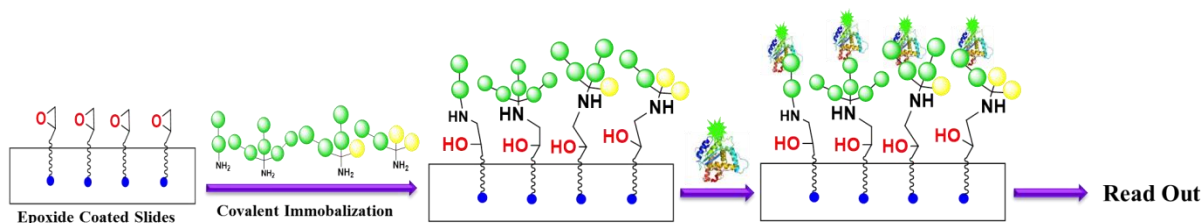


Figure 1 Schematics of microarray fabrication

3.4. Plant lectins binding affinity

As a first step, glycodendrons microarray was analyzed by incubation with plant lectins of known mannose and galactose binding specificities. As would be expected, ConA bound to all homo as well as hetero mannose glycodendrons compared to galactose glycodendrons **T14**. Interestingly, symmetric mannose glycodendrons (**T1**, **T2** and **T3**) showed strong binding preferences compared to asymmetric glycodendrons. It was also observed that as the heterogeneity in the glycodendron decrease the binding preference. Surprisingly, **T6**, which has two dimannose and one galactose epitope, showed similar binding preference compared to symmetric analog **T2**. In contrast, GNA, another mannose specific lectin showed completely a different binding pattern compared to ConA lectin. Interestingly, the asymmetric glycodendron (**T6** and **T7**) showed much strong binding preference to GNA compared to respective symmetric analogs (**T2** and **T3**). Finally, PNA, galactose specific lectins showed binding preference to **T14** compared other glycodendrons. A weak binding of heteroglycodendrons T3 and T4 displayed that as the number of galactose epitope increases the binding preference also increases.

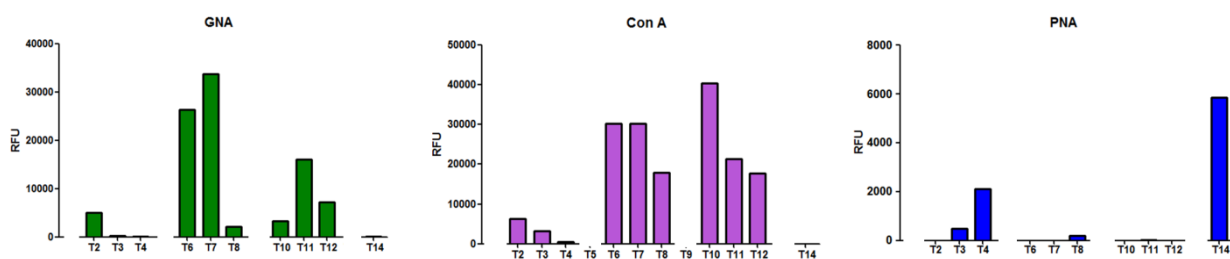


Figure 2 Lectin Binding Assay

According to the plant lectins binding pattern, ConA and GNA possess mannose binding pocket which are specific heterogeneity and oligomeric (di and tri) form of the mannose glycodendrons.

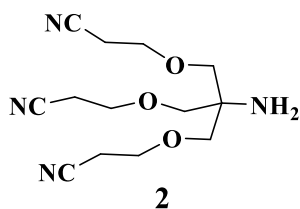
ConA exhibited strong affinity to **T3** indicating that the binding pocket of ConA display sensitivity to trimannose site. While, GNA displayed preferential binding with dimannose glycodendrons. Heterogeneity in the form on mono galactose substitution has significant impact on the GNA lectin binding compared to ConA binding. Whereas, di-galactose substituted glycodendrons showed weak binding toward both mannose specific lectins. These results indicate that ConA and GNA, which has one and three mannose-binding motif in each tetrameric protein displayed selective mannose glycodendron binding pattern.

3.5. Conclusions

Herein we present the synthesis of homo and heteromultivalent mono and oligomannoside glycodendrons and their binding to a series of plant lectins and results showed that each lectins displayed its own set of rules for better CPIs. In case of ConA and PNA lectins, oligosaccharides multivalency is more important than heterogeneity. While, GNA lectin displayed heterogeneity of the glycodendrons as critical factor for better CPIs. Binding with C-type lectins are under progress.

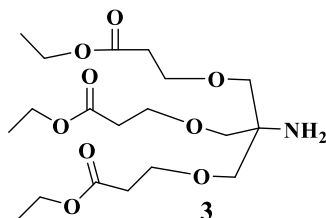
3.6. Experimental Details

3-amino-3-(cyanomethyl)pentanedinitrile (**2**)



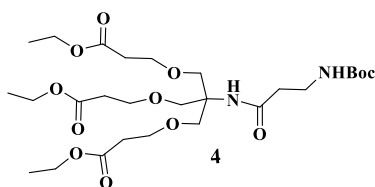
To the mixture of **1** (5g, 41.322 mmole) and acrylonitrile (16.223 ml, 247.934 mmole), 40% KOH (2 ml) was added dropwise at 0 °C. Then, 1, 4-dioxane (5 ml) was added and the mixture was allowed to stir at RT for 16 h to yield 3-amino-3-(cyanomethyl) pentanedinitrile. Pale yellow coloured oil is formed. On completion of reaction, evaporate off dioxane and extract the reaction mixture with EtOAc (100 ml) and minimum amount of water (10 ml) thrice. Give washing to organic layer with brine, dry over Na₂SO₄ and concentrate under reduced pressure. Continue for next reaction without purification.

Diethyl 3, 3'-((2-amino-2-((3-ethoxy-3-oxopropoxy) methyl) propane-1, 3-diyl) bis (oxy)) dipropionate (3)



2 (8.4g, 56.757 mmole) was dissolved in conc. HCl (30 mL) and refluxed for 24 h. To this, ethanol (30 ml) was added and was refluxed for 24 h. After completion, ethanol was evaporated and 10 N NaOH was added to the white precipitate till it reached a pH of 8.6. The mixture was then extracted with EtOAc (25 ml) and water (5 ml) twice. The organic layer was given brine wash once and then dried over Na₂SO₄ and concentrated *in vacuo*. Further purified on silica gel column chromatography using EtOAc/Pet-ether 80: 20) of the crude residue yielded **3** (10.99 g, 46%). ¹H NMR (400 MHz, CDCl₃): δ 4.39 (bs, 2H), 4.14 (q, *J* = 7.13, 7.13 Hz, 6H), 3.73-3.68 (m, 8H), 3.35 (s, 4H), 2.53 (t, *J* = 6.28 Hz, 6H), 1.25 (t, *J* = 7.12 Hz, 9H); ¹³C NMR (100 MHz, CDCl₃): δ 171.68, 72.01, 66.98, 66.39, 60.58, 56.60, 35.15, 14.33. HRMS *m/z* calc'd for C₁₉H₃₆O₉N: 422.2390; found: 422.2395.

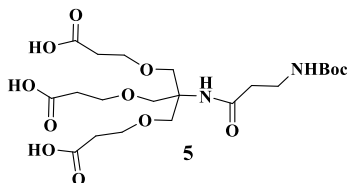
Ethyl 10, 10- bis ((3-ethoxy-3-oxopropoxy) methyl)-2, 2-dimethyl-4, 8-dioxo-3, 12-dioxa-5, 9-diazapentadecan-15-oate (4)



To a mixture of **3** (3 g, 7.126 mmole) and Boc-β-Alanine (2.02g, 10.689 mmole) in CH₂Cl₂ at 0 °C, Diisopropyl carbodiimide (DIC) (1.322 ml, 8.551 mmole) and 1 - hydroxybenzotriazole (HOBt) (0.096 g, 0.712 mmole) were added. Finally to adjust the pH of the reaction mixture to slightly basic condition (pH 8) using triethylamine was also added and the reaction mixture was allowed to stir at RT for 12 h. After completion of reaction, concentrate the reaction mixture under reduced pressure and purify by silica column chromatography using EtOAc/Pet-ether 60: 40) to yield **4** (2.74 g, 66%). ¹H NMR (400 MHz, CDCl₃): δ 6.15 (s, 1H), 5.35 (s, 1H), 4.15 (q,

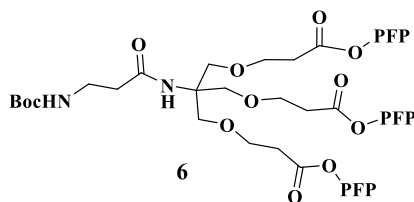
$J = 8.00, 8.00$ Hz, 6H), 3.70-3.67 (m, 12H), 3.37-3.36 (bm, 2H), 2.54 (t, $J = 6.19$ Hz, 6H), 2.35 (t, $J = 5.81$ Hz, 2H), 1.43 (s, 9H), 1.26 (t, $J = 8.00$ Hz, 9H); ^{13}C NMR (100 MHz, CDCl_3): δ . 171.64, 155.95, 68.81, 66.79, 60.18, 59.75, 34.89, 28.76, 23.33, 14.21. HRMS m/z calc'd for $\text{C}_{27}\text{H}_{49}\text{O}_{12}\text{N}_2$: 593.3286; found: 593.3276.

10,10-bis((2-carboxyethoxy)methyl)-2,2-dimethyl-4,8-dioxo-3,12-dioxa-5,9-diazapentadecan-15-oic acid(5)



4 (2.5g, 4.223 mmole) was mixed with 2 N NaOH (2 mL) in MeOH (8 mL) and was allowed to stir for 12 h at RT. After completion, solvent was evaporated under reduced pressure and the crude residue was neutralized with 1N HCl. This was followed by extraction of the mixture with EtOAc (25 ml). The organic layer was then dried over Na_2SO_4 , filtered and concentrated *in vacuo* yielded **5** (1.3 g, 61%). ^1H NMR (400 MHz, CDCl_3): δ 8.60 (bs, 3H), 6.40 (s, 1H), 5.49 (s, 1H), 3.79-3.71 (m, 12H), 3.42-3.36 (m, 2H), 2.59 (t, $J = 5.48$ Hz, 6H), 2.40-2.33 (bm, 2H), 1.45 (s, 9H); ^{13}C NMR (100 MHz, CDCl_3): δ .176.14, 175.99, 171.42, 156.59, 80.05, 69.11, 66.92, 60.22, 42.79, 37.07, 35.04, 28.28, 22.82. HRMS m/z calc'd for $\text{C}_{21}\text{H}_{37}\text{O}_{12}\text{N}_2$: 509.2346; found: 509.2341.

Perfluorophenyl-2, 2-dimethyl-4, 8-dioxo-10, 10-bis ((3-oxo-3-(perfluorophenoxy) propoxy) methyl)-3, 12-dioxa-5, 9-diazapentadecan-15-oate (6)

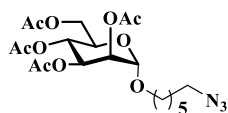


The acid formed **5** (1.8 g, 3.543 mmole) was dissolved in CH_2Cl_2 and 2, 3, 4, 5, 6 - Pentafluorophenol (2.282 g, 12.402 mmole) was added to it. diisopropyl carbodiimide (DIC) (0.665 ml, 4.252 mmole) and hydroxybenzotriazole (HOBt) (0.048 g, 0.354 mmole) were added to the reaction mixture at 0 °C. Later, triethylamine was added to adjust the pH of the system to slightly basic condition (pH 8). The reaction mixture was stirred at RT for 12 h. On completion,

the solvent was evaporated under reduced pressure and the crude residue was purified by silica column chromatography using EtOAc/Pet-ether (50 : 40) to yield UV active product **5** (2.5 g, 52%). ¹H NMR (400 MHz, CDCl₃): δ 5.84 (s, 1H), 5.20 (s, 1H), 3.83 (t, *J* = 5.85 Hz, 6H), 3.79 (s, 6H), 3.37-3.35 (m, 2H), 2.92 (t, *J* = 5.85 Hz, 6H), 2.33 (t, *J* = 5.85 Hz, 2H), 1.43 (s, 9H); ¹³C NMR (100 MHz, CDCl₃): δ.171.95, 167.41, 155.76, 142.33, 139.86, 139.58, 139.03, 138.38, 137.00, 136.61, 79.37, 69.78, 66.88, 61.70, 36.73, 34.44, 28.33. HRMS *m/z* calc'd for C₃₉H₃₄O₁₂F₁₅N₂Na: 1007.1872; found: 1007.1879.

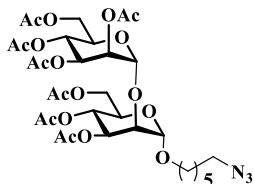
Compound **7** (2.083g, 4.734 mmole) was dissolved in CH₂Cl₂ and 6-azidohexan-1-ol (0.542 g, 3.787 mmole) was added to it. 4 Å molecular sieves were added and the reaction mixture was stirred at RT for 1 h. After 1 h, the reaction mixture was brought to -4 °C using ice and common salt and was allowed to stir for 20 min at the same temperature. To the reaction mixture, *N*-iodosuccinimide (1.272g, 5.681 mmole) was added followed by trifluoromethanesulfonic acid (0.106 ml, 0.947 mmole) and was stirred for 1h at -4 °C. Checked for the consumption of starting material using TLC. If completed, take out RB and allow it to attain RT and then add Ac₂O (1.418 ml, 14.202 mmole) and stir for 30 minutes. Then filter the contents in RB through celite bed using sintered funnel. The filtrate is then extracted twice with CH₂Cl₂ and aqueous Na₂S₂O₅. Give the organic layer one wash with brine and dry over Na₂SO₄. Evaporate and purify the crude residue using silica column chromatography using EtOAc/Pet-ether (60: 40) to yield mono **8** (0.215 g, 10 %), di **11** (1.17 g, 34 %) and tri **14** (0.761 g, 16%) mannose derivatives.

6-azidohexanol sugar derivative of monomannose (**8**)



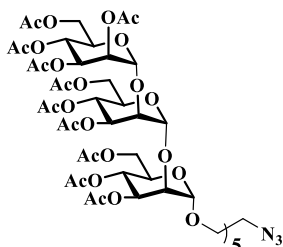
¹H NMR (400 MHz, CDCl₃): δ 5.37, 5.35 (dd, *J* = 3.4, 10.0 Hz, 1H), 5.32-5.29 (m, 1H), 5.27-5.24 (m, 1H), 4.82 (d, *J* = 1.6, Hz, 1H), 4.31, 4.29 (dd, *J* = 12.2, 5.3 Hz, 1H), 4.14, 4.11 (dd, *J* = 12.2, 2.5 Hz, 1H), 4.01-3.97 (m, 1H), 3.974-3.65(m, 1H), 3.50-3.44 (m, 1H), 3.30 (t, *J* = 6.9 Hz, 2H), 2.17 (s, 3H), 2.12 (s, 3H), 2.06 (s, 3H), 2.01 (s, 3H), 1.67-1.61 (m, 4H), 1.43-1.40 (m, 4H); ¹³C NMR (100 MHz, CDCl₃): δ.170.64, 170.11, 169.92, 169.75, 97.57, 69.70, 69.12, 68.44, 68.28, 66.27, 62.54, 51.35 29.12, 28.74, 26.47, 25.72, 20.91, 20.74, 20.70. HRMS *m/z* calc'd for C₂₀H₃₁NaO₁₀N₃: 496.1907; found: 496.1907.

Synthesis of 6azidohexanol sugar derivative of disaccharide of mannose (11)



^1H NMR (400 MHz, CDCl_3): δ 5.42, 5.40 (dd, 10.0, 3.4 Hz, 1H), 5.31-5.26 (m, 4H), 4.93 (d, J = 1.8 Hz, 2H), 4.26, 4.25 (dd, J = 11.7, 4.9 Hz, 2H), 4.19-4.09 (m, 3H), 4.03-4.01 (m, 1H), 3.93-3.89 (m, 1H), 3.74-3.67 (m, 1H), 3.47-3.41 (m, 1H), 3.28 (t, J = 6.8 Hz, 2H), 2.15 (s, 3H), 2.14 (s, 3H), 2.08 (s, 6H), 2.04 (s, 3H), 2.02 (s, 3H), 2.01 (s, 3H), 1.64-1.58 (m, 4H), 1.41-1.39 (m, 4H); ^{13}C NMR (100 MHz, CDCl_3): δ 170.86, 170.44, 170.42, 169.85, 169.73, 169.45, 169.41, 99.19, 98.28, 70.36, 69.79, 69.15, 68.56, 68.42, 68.28, 66.41, 66.28, 62.55, 62.25, 51.33, 29.57, 29.21, 28.73, 26.48, 25.76, 20.84, 20.72, 20.65, 20.65. HRMS m/z calc'd for $\text{C}_{32}\text{H}_{47}\text{O}_{18}\text{NNa}$: 784.2752; found: 784.2750.

6 azidohexanol sugar derivative of trisaccharide of mannose (14)



^1H NMR (400 MHz, CDCl_3): δ 5.38- 5.35 (m, 2H), 5.33-5.30 (m, 4H), 4.94 (d, J = 1.8 Hz, 1H), 4.93 (d, J = 2.1 Hz, 1H), 4.92 (d, J = 1.7 Hz, 1H), 4.44-4.41 (m, 1H), 4.34, 4.32 (dd, J = 12.2, 4.4 Hz, 1H), 4.25-4.19 (m, 3H), 4.16-4.11 (m, 4H), 4.07-4.04 (m, 1H), 3.92-3.88 (m, 1H), 3.81-3.78 (m, 1H), 3.73-3.67 (m, 1H), 3.45-3.43 (m, 1H), 3.28 (t, J = 6.8 Hz, 2H), 2.15 (s, 3H), 2.13 (s, 3H), 2.10 (s, 3H), 2.09 (s, 3H), 2.08 (s, 3H), 2.06 (s, 3H), 2.05 (s, 3H), 2.04 (s, 6H), 2.00 (s, 3H), 1.68-1.90 (m, 4H), 1.42-1.39 (m, 4H); ^{13}C NMR (100 MHz, CDCl_3): δ 170.85, 170.71, 170.57, 170.17, 169.91, 169.83, 169.61, 169.50, 169.44, 98.50, 98.43, 98.40, 74.81, 73.18, 72.59, 70.66, 70.06, 69.88, 69.76, 69.61, 69.41, 68.97, 68.56, 68.51, 68.46, 66.54, 66.47, 66.26, 65.91, 62.70, 62.40, 62.37, 62.30, 51.49, 29.39, 28.90, 26.64, 25.91, 21.05, 20.97, 20.95, 20.92, 20.87, 20.85, 20.82, 20.79, 20.78. HRMS m/z calc'd for $\text{C}_{44}\text{H}_{63}\text{O}_{26}\text{N}_3\text{Na}$: 1072.3597; found: 1072.3623.

General procedure A: Azido sugar derivative (1 equiv.) was dissolved in THF (9 mL) and triphenylphosphine (1.2 equiv.) was added and the reaction mixture was allowed to stir at RT for 4 hr. On consumption of starting, added water (2 mL) and di-*tert*-butyl dicarbonate (Boc₂O) (1.2 equiv.) to the RB and stir for 12 h at RT. On completion, evaporate off THF and extract the reaction mixture with EtOAc (25 mL) thrice. Then, give washing to the organic layer with brine and dry over Na₂SO₄. Concentrate the solvent and purify the crude residue using column chromatography using EtOAc/Pet-ether to yield boc-protected sugar derivatives.

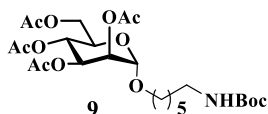
General procedure B:

Boc protected sugar derivative (1 equiv.) was dissolved in TFA (2 mL) and dry CH₂Cl₂ (8 mL) and was stirred for 2 h at RT. On consumption of starting, the reaction mixture was concentrated *in vacuo*. Co-evaporate with toluene and CH₂Cl₂ to yield deprotected compound. Used as such immediately without purification for next reaction.

General procedure C: Boc deprotected sugar (3.2 equiv.) was dissolved in CH₂Cl₂ and the PFP ester **6** (1 equiv.) was added to it. The pH of the reaction mixture was then adjusted to 8 using triethylamine. The mixture was then allowed to stir at RT for 12 h. On completion, the mixture was concentrated *in vacuo* to obtain the crude residue was purified by silica column chromatography using MeOH/CH₂Cl₂ (4:96) to yield tripods.

General procedure D: Acetate de-protection of compounds (1 equiv.) was done using NaOMe (14.4 equiv.) and MeOH (5 mL) for 2h at RT. Then after completion of reaction neutralise with IR 120 H⁺. Then kept for boc de-protection reaction by dissolving it in 20% TFA in CH₂Cl₂. After de-protection, deprotected compounds were obtained after co-evaporation with toluene. The crude residue was purified by sephadex column to yield final dendrimers.

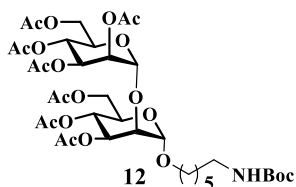
Boc protected sugar derivative of monomannose (9)



Compound **9** was synthesized using general procedure **A** using **8** (0.4 g, 0.846 mmole) in THF (8 mL) and triphenylphosphine (0.266 g, 1.015 mmole, 1.2 eq). Added water (2 mL) and di-*tert*-

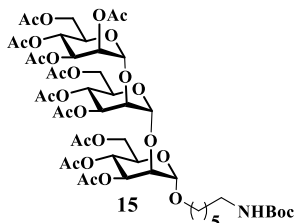
butyl dicarbonate (Boc₂O) (0.233 mL, 1.015 mmole). The crude residue purify by column chromatography using EtOAc/Pet-ether (30: 70) to yield **9** (0.286 g, 62%). ¹H NMR (400 MHz, CDCl₃): δ 5.35, 5.33 (dd, *J* = 3.23, 9.98 Hz, 1H), 5.29-5.26 (m, 1H), 5.24-5.22 (m, 1H), 4.79 (d, *J* = 1.5, Hz, 1H), 4.55 (s, 1H), 4.26, 4.26 (dd, *J* = 12.2, 5.3 Hz, 1H), 4.11-4.08 (m, 1H), 3.98-3.97 (m, 1H), 3.70-3.64 (m, 1H), 3.46-3.42 (m, 1H), 3.11-3.05 (m, 2H), 2.15 (s, 3H), 2.09 (s, 3H), 2.04 (s, 3H), 1.99 (s, 3H), 1.63-1.57 (m, 4H), 1.52-1.47 (s, 2H), 1.43 (s, 9H), 1.35-1.34 (s, 2H); ¹³C NMR (100 MHz, CDCl₃): δ.170.60, 170.21, 169.89, 169.67, 156.00, 97.51, 78.91, 69.72, 69.14, 68.32, 66.17, 62.46, 53.13, 40.43, 29.89, 29.17, 28.74, 26.65, 25.85, 20.02, 20.75, 20.72, 20.70. HRMS *m/z* calc'd for C₂₅H₄₁O₁₂NNa: 570.2526; found: 570.2525.

Boc protected disaccharide mannose (**12**).



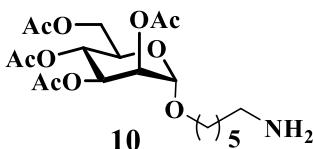
Compound **12** was synthesized using general procedure **A** using **11** (0.842 g, 1.106 mmole) in THF (12 mL) and triphenylphosphine (0.348 g, 1.328 mmole). Added water (2 mL) and di-*tert*-butyl dicarbonate (Boc₂O) (0.305 ml, 1.328 mmole). Purify the crude residue by column chromatography to using EtOAc/Pet-ether (40: 60) yield **12** (0.59 g, 64%). ¹H NMR (400 MHz, CDCl₃): δ 5.40, 5.38 (dd, *J* = 3.36, 10.02, 1H), 5.33-5.24 (m, 4H), 4.90 (bs, 2H), 4.58 (bs, 1H), 4.24-4.18 (m, 2H), 4.16-4.08 (m, 3H), 4.00 3.99 (m, 1H), 3.90-3.87 (m, 1H), 3.69-3.63 (m, 1H), 3.44-3.35 (m, 1H), 3.09-3.08 (m, 2H), 2.13 (s, 3H);, 2.12 (s, 3H), 2.06 (s, 6H), 2.02 (s, 3H), 2.01 (s, 3H), 1.99 (s, 3H), 1.60-1.55 (m, 2H), 1.50-1.45 (m, 2H), 1.41 (s, 9H), 1.34-1.32 (m, 4H); ¹³C NMR (100 MHz, CDCl₃): δ.170.79, 170.37, 170.34, 170.03, 169.77, 169.67, 169.39, 169.37, 155.97, 99.10, 98.19, 78.93, 70.32, 69.73, 69.11, 68.48, 68.39, 68.36, 66.36, 66.24, 62.51, 62.18, 40.44, 29.93, 29.60, 29.56, 29.22, 28.37, 26.50, 25.83, 20.85, 20.77, 20.66, 20.59, 20.56. HRMS *m/z* calc'd for C₃₇H₅₇O₂₀NNa: 858.3372; found: 858.3372.

Boc protected sugar derivative of trisaccharide mannose (**15**)



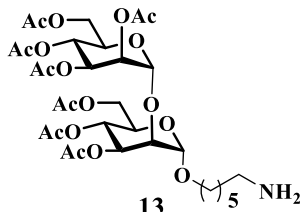
Compound **15** was synthesized using general procedure **A** using **14** (0.341 g, 0.325 mmole) in THF (8 mL) and triphenylphosphine (0.102 g, 0.390 mmole). Added water (2 mL) and di-*tert*-butyl dicarbonate (Boc₂O) (0.089 ml, 0.390 mmole). Purified the crude residue by column chromatography using EtOAc/Pet-ether (50: 50) to yield **15** (0.295 g, 81%). ¹H NMR (400 MHz, CDCl₃): δ 5.43, 5.40 (dd, J = 10.1, 3.3 Hz, 1H), 5.36-5.29 (m, 6H), 5.12 (d, J = 2.00 Hz, 1H), 4.97 (d, J = 1.60 Hz, 1H), 4.95 (d, J = 1.9 Hz, 1H), 4.60 (s, 1H), 4.27, 4.25 (dd, J = 12.3, 4.6, 1H), 4.18-4.11 (m, 7H), 4.03 (t, J = 2.3 Hz, 1H), 3.94-3.92 (m, 1H), 3.77-3.68 (m, 2H), 3.49-3.43 (m, 1H), 3.13-3.12 (m, 2H), 2.17 (s, 3H), 2.15 (s, 3H), 2.14 (s, 3H), 2.10 (s, 3H), 2.08 (s, 3H), 2.18 (s, 3H), 2.06 (s, 9H), 2.02 (s, 3H), 1.64-1.60 (m, 3H), 1.52-1.49 (m, 2H), 1.46 (s, 9H), 1.38-1.35 (m, 3H); ¹³C NMR (100 MHz, CDCl₃): δ.170.86, 170.72, 170.44, 170.44, 170.12, 170.04, 169.77, 169.70, 169.48, 169.37, 155.99, 99.79, 99.37, 98.24, 69.72, 69.60, 69.45, 68.58, 66.40, 66.29, 66.20, 31.91, 40.53, 30.00, 29.68, 29.31, 28.42, 26.57, 25.88, 22.68, 20.83, 20.71 20.63, 20.63, 14.10. HRMS m/z calc'd for C₄₉H₇₃NO₂₈Na: 1146.4217; Found: 1146.4222.

Boc deprotected sugar derivative of monomannose (**10**)



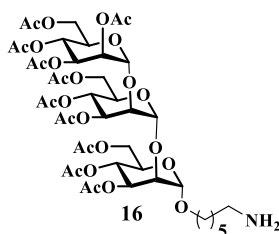
Compound **10** was synthesized using general procedure **B** using **9** (0.224 g, 0.409 mmole) to yield **10** (0.162 g, 89%).

Boc deprotected sugar derivative of disaccharide mannose (**13**)



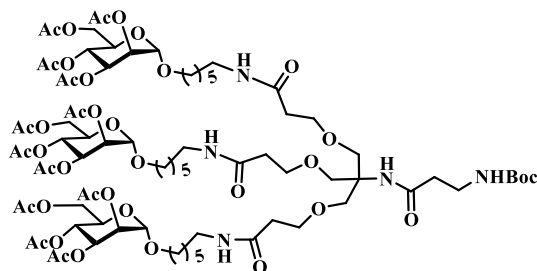
Compound **13** was synthesized using procedure **B** using **12** (0.3g, 0.359 mmole) to yield **13** (0.187g, 71%).

Boc deprotected sugar derivative of trisaccharide mannose (**16**)



Compound **16** was synthesized using procedure **B** using **15** (0.295g, 0.32 mmole) to yield **16** (0.186g, 77%).

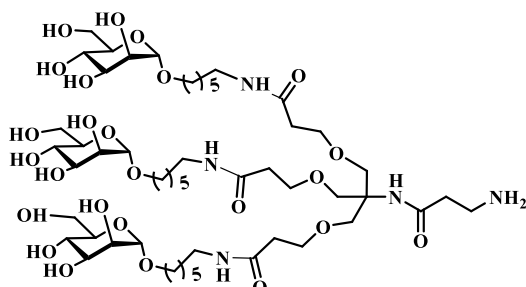
Monomannose substituted tripod (**21**)



21

Compound **21** was synthesized by following the procedure **C** using **10** (0.254 g, 0.567 mmole) in CH_2Cl_2 and PFP ester **6** (0.173 g, 0.172 mmole) and crude residue purified by column chromatography using $\text{MeOH}/\text{CH}_2\text{Cl}_2$ (4:96) was done to get **21** (0.22 g, 49%). ^1H NMR (400 MHz, CDCl_3): δ 6.79 (s, 1H), 6.54 (s, 1H), 6.43 (bs, 3H), 5.34-5.30 (m, 8H), 5.28-5.25 (m, 3H), 4.82 (bs, 3H), 4.32, 4.30 (dd, $J = 12.1, 5.2$ Hz, 4H), 4.15 (d, $J = 12.3$ Hz, 4H), 4.02, 3.98 (m, 3H), 3.74-3.68 (m, 12H), 3.49-3.38 (m, 6H), 3.27, 3.26 (dd, $J = 12.3, 5.7$ Hz, 6H), 2.24 (t, $J = 5.6$ Hz, 6H), 2.18 (s, 9H), 2.13 (s, 9H), 2.07 (s, 9H), 2.02 (s, 9H), 1.57-1.52 (m, 12H), 1.46 (s, 9H), 1.40-1.39 (m, 12H); ^{13}C NMR (100 MHz, CDCl_3): δ 171.57, 170.43, 170.12, 169.91, 169.63, 155.97, 97.50, 69.48, 69.19, 68.52, 67.48, 66.18, 62.49, 59.71, 39.49, 36.58, 29.55, 29.00, 26.48, 25.62, 20.90, 20.74, 20.70. HRMS m/z calc'd for $\text{C}_{81}\text{H}_{130}\text{O}_{39}\text{N}_5$: 1796.8340; found: 1796.8033.

Deprotection of monomannose substituted tripod (**T1**)

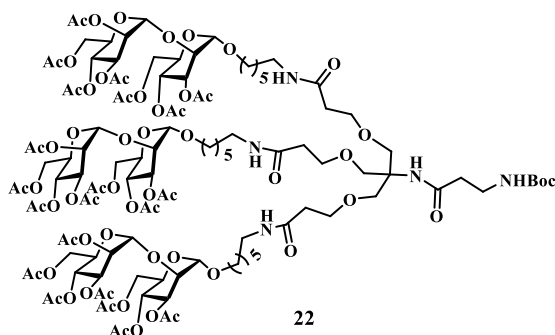


T1

Tripod **T1** was synthesized by following procedure **D** using compound **21** (0.06 g, 0.033 mmole), NaOMe (0.025 g, 0.475 mmole) and 20% TFA. The crude residue was purified by sephadex column to yield **T1** (0.023g, 58% over two step). ^1H NMR (400 MHz, D_2O): δ 4.84 (s,

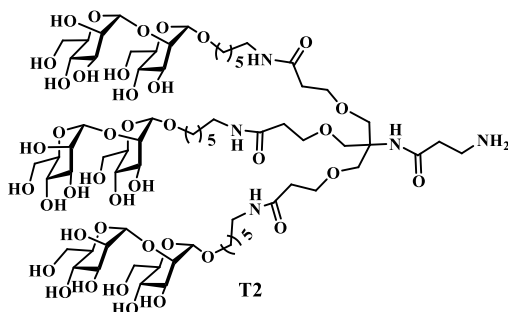
3H), 3.93 (bs, 3H), 3.90 (bs, 2H), 3.87 (bs, 2H), 3.78-3.75 (m, 6H), 3.72-3.71 (m, 12H), 3.66-3.62 (m, 6H), 3.62-3.58 (m, 4H), 3.55-3.49 (m, 3H), 3.22-3.16 (m, 6H), 2.65 (t, $J = 6.7$ Hz, 2H), 2.46 (t, $J = 5.7$ Hz, 6H), 1.60-1.59 (m, 6H), 1.52-1.49 (m, 6H), 1.39-1.34 (bm, 12H); ^{13}C NMR (100 MHz, D_2O): δ .173.69, 171.76, 99.61, 72.65, 70.63, 70.08, 68.43, 67.69, 67.57, 66.69, 60.84, 60.33, 39.38, 36.13, 35.50, 28.43, 28.30, 25.89, 25.07. HRMS m/z calc'd for $\text{C}_{52}\text{H}_{98}\text{O}_{25}\text{N}_5$: 1192.6551; found: 1192.6537.

Synthesis of disaccharide mannose substituted tripod (22)



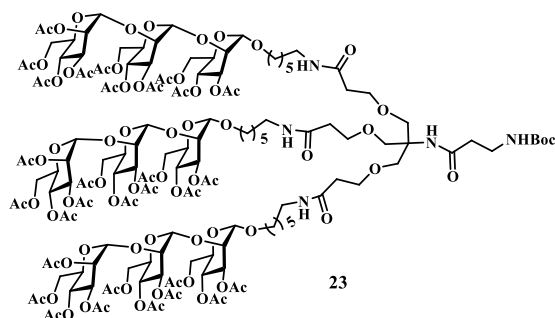
Compound **22** was synthesized by following procedure **C** using **13** (0.465 g, 0.633 mmole, 3.2 equiv.) and PFP ester **6** (0.199g, 0.198 mmole). The crude residue purified by column chromatography using $\text{MeOH}/\text{CH}_2\text{Cl}_2$ (4: 96) to get **22** (0.565g, 46%). ^1H NMR (400 MHz, CDCl_3): δ 6.87 (s, 1H), 6.53 (s, 1H), 6.49 (s, 2H), 6.35 (s, 1H), 5.40, 5.38 (dd, $J = 3.34, 10.00$, 3H), 5.90 (s, 6H), 5.28-5.54 (m, 8H), 4.91 (bs, 6H), 4.23-4.17 (m, 7H), 4.14-4.10 (m, 8H), 4.00 (t, $J = 2$ Hz, 3H), 3.91-3.88 (m, 3H), 3.70-3.65 (m, 12H), 3.44-3.35 (m, 6H), 3.24-3.19 (m, 6H), 2.40 (t, $J = 5.3$ Hz, 8H), 2.14 (s, 9H), 2.13 (s, 9H), 2.07 (s, 18H), 2.03 (s, 9H), 2.02 (s, 9H), 2.00 (s, 9H), 1.60-1.57 (m, 8H), 1.53-1.50 (m, 8H), 1.41 (s, 9H), 1.38-1.34 (m, 8H); ^{13}C NMR (100 MHz, CDCl_3): δ .171.26, 170.87, 170.47, 170.45, 169.84, 169.70, 169.44, 169.39, 156.01, 99.15, 98.23, 70.37, 69.76, 69.14, 68.49, 68.41, 67.49, 66.37, 66.26, 62.52, 62.21, 45.59, 39.49, 36.54, 29.53, 29.30, 28.41, 26.79, 25.93, 20.83, 20.72, 20.68, 20.64, 20.6, 18.14. HRMS m/z calc'd for $\text{C}_{117}\text{H}_{177}\text{O}_{63}\text{N}_5\text{Na}$: 2683.0698; found: 2683.3967.

Deprotection of disaccharide mannose substituted tripod (T2)



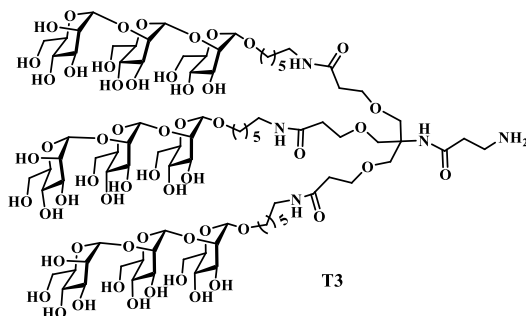
Tripod **T2** was synthesized by following procedure **D** using **22** (0.127 g, 0.049 mmole), NaOMe (0.66 g, 1.24 mmole) and 20% TFA. The crude residue was purified by sephadex column to yield **T2** (0.049g, 62%). ¹H NMR (400 MHz, D₂O): 5.07 (s, 3H), 5.00 (s, 3H), 4.05 (bs, 3H), 3.92 (bs, 3H), 3.88-3.87 (m, 3H), 3.85-3.84 (m, 6H), 3.82-3.81 (m, 2H), 3.77-3.75 (m, 4H), 3.72-3.69 (m, 15H), 3.67-3.65 (m, 9H), 3.62-3.58 (m, 6H), 3.57-3.49 (m, 3H), 3.22-3.16 (m, 9H), 2.65 (t, J = 6.6 Hz, 2H), 2.46 (t, J = 5.7 Hz, 6H), 1.59-1.58 (m, 6H), 1.52-1.49 (m, 6H), 1.35 (bm, 12H); ¹³C NMR (100 MHz, D₂O): δ. 173.63, 171.63, 102.48, 97.95, 78.86, 73.15, 72.58, 70.06, 69.82, 68.40, 67.85, 67.43, 66.81, 66.64, 60.94, 60.75, 60.05, 39.08, 36.16, 35.22, 28.34, 28.19, 25.65, 25.08. HRMS m/z calc'd for C₇₀H₁₂₈O₄₀N₅: 1678.8136; found [M+2H]²⁺: 839.9104.

Trisaccharide mannose substituted tripod (**23**)



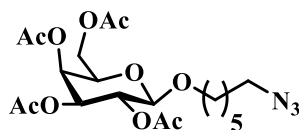
Compound **23** was synthesized by following procedure **C** using **16** (0.177 g, 0.173 mmole) and PFP ester **6** (0.054 g, 0.054 mmole). The crude residue was purified by column chromatography using MeOH/CH₂Cl₂ (4: 96) was done to get **23** (0.279 g, 45%). ¹H NMR (400 MHz, CDCl₃): δ 6.57 (s, 2H), 6.50 (s, 2H), 6.34 (s, 1H), 5.41, 5.40 (dd, J = 10.0, 3.3 Hz, 4H), 5.36-5.34 (m, 6H), 5.31 (s, 6H), 5.12 (d, J = 1.7 Hz, 3H), 4.96 (d, J = 1.7 Hz, 3H), 4.94 (d, J = 1.7 Hz, 3H), 4.33-4.23 (m, 7H), 4.21-4.14 (m, 23 H), 4.02 (s, 3H), 3.96-3.91 (m, 3H), 3.74-3.70 (m, 16H), , 3.49-3.41 (m, 6H), 3.27-3.22 (m, 6H), 2.59-2.53 (m, 2H), 2.44-2.38 (m, 6H), 2.17 (s, 9H), 2.14 (s,9H), 2.14 (s, 9H), 2.10 (s, 9H), 2.08 (s, 9H), 2.07 (s, 9H), 2.05 (s, 27H), 2.02 (s, 9H), 1.63-1.59 (m, 6H), 1.55-1.50 (m, 6H), 1.44 (s, 9H), 1.37-1.33 (m, 12H); ¹³C NMR (100 MHz, CDCl₃): δ. 170.29, 170.01, 169.78, 169.41, 169.38, 155.99, 99.76, 99.34, 98.29, 70.53, 69.75, 69.53, 69.41, 69.25, 68.50, 68.38, 66.72, 66.31, 66.23, 66.16, 62.46, 62.24, 62.09, 38.97, 34.60, 29.61, 29.37, 29.22, 28.31, 26.82, 26.64, 25.84, 20.80, 20.60, HRMS m/z calc'd for C₁₅₃H₂₂₅N₅O₈₇Na: 3547.3233; found [M+2H]²⁺: 1785.6632.

Trisaccharide mannose substituted tripod (**T3**)



Tripod **T3** was synthesized by following procedure **D** using **23** (0.11 g, 0.033 mmole), NaOMe (0.064 g, 1.20 mmole) and 20% TFA. Further the crude residue was purified by sephadex column to yield **T3** (0.021g, 55%). ^1H NMR (400 MHz, D_2O): δ 5.20 (bs, 3H), 4.99 (bs, 3H), 4.95 (s, 3H), 4.02 (bs, 3H), 3.98 (bs, 3H), 3.88-3.74 (m, 20H), 3.73-3.51 (m, 42H), 3.15-3.08 (m, 8H), 2.57 (t, $J = 6.2$ Hz, 6H), 2.39 (t, $J = 5.5$ Hz, 6H), 1.55-1.48 (m, 6H), 1.45-1.41 (m, 6H), 1.31-1.23 (m, 12H); ^{13}C NMR (100 MHz, D_2O): δ . 171.79, 168.94, 102.20, 100.66, 98.02, 78.91, 78.54, 73.21, 72.73, 70.30, 69.93, 67.88, 67.05, 66.93, 66.81, 61.07, 60.86, 60.19, 39.39, 36.22, 35.52, 34.29, 32.40, 28.43, 28.31, 25.89, 25.06. HRMS m/z calc'd for $\text{C}_{88}\text{H}_{157}\text{O}_{55}\text{N}_5\text{Na}$: 2186.9540; found $[\text{M}+2\text{Na}]^{2+}$:1104.9755.

6 azidohexanol sugar derivative of monogalactose (**18**)

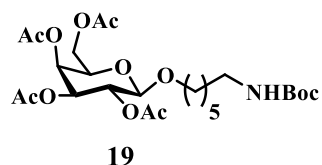


18

Compound **17** (0.612g, 1.348 mmole) was dissolved in CH_2Cl_2 and 6- azidohexan-1-ol (0.193g, 1.348 mmole) was added. Then slow addition of $\text{BF}_3 \cdot \text{Et}_2\text{O}$ (0.556g, 3.92 mmole) over 30 min. stir reaction overnight. Check TLC for ensuring the consumption of starting material. Extract the filtrate with NaHCO_3 and CH_2Cl_2 twice. Then give one wash with brine for the organic layer. Dry over Na_2SO_4 and then concentrate under reduced pressure. Purify the crude residue using silica column chromatography using EtOAc/Pet-ether (50: 50) to yield **18** (0.55 g, 75%). ^1H NMR (400 MHz, CDCl_3) 5.39-5.38 (m, 1H), 5.21-5.18 (m, 1H), 5.03, 5.01 (dd, $J = 10.5, 3.4$ Hz, 1H), 4.46 (d, $J = 7.9$ Hz, 1H), 4.21-4.10 (m, 2H), 3.92-3.86 (m, 2H), 3.51-3.85 (m, 1H), 3.27 (t, J

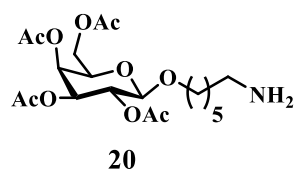
= 6.9 Hz, 2H), 2.15 (s, 3H), 2.05 (s, 3H), 2.05 (s, 3H), 1.99 (s, 3H), 1.69-1.56 (m, 4H), 1.42-1.37 (m, 4H); ^{13}C NMR (100 MHz, CDCl_3): δ 170.40, 170.28, 170.18, 169.34, 101.34, 70.94, 70.59, 69.96, 68.92, 67.27, 51.24, 29.27, 28.76, 28.58, 26.40, 25.41, 20.75, 20.68, 20.60. HRMS m/z calc'd for $\text{C}_{20}\text{H}_{31}\text{O}_{10}\text{N}_3\text{Na}$: 496.1907; found: 496.1913.

Boc protected sugar derivative of monogalactose (**19**)



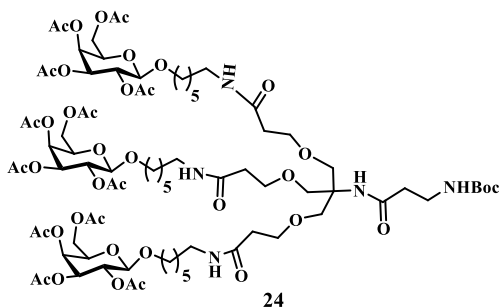
Compound **19** was synthesized using general procedure **A** using **18** (0.3 g, 0.634 mmole) in THF (12 mL) and triphenylphosphine (0.119 g, 0.760 mmole). Added water (2 mL) and di-*tert*-butyl dicarbonate (Boc_2O) (0.174 mL, 0.760 mmole) purified the crude residue by column chromatography using EtOAc/Pet-ether (60: 40) to yield **19** (0.295 g, 81%). ^1H NMR (400 MHz, CDCl_3) 5.40, 5.39 (dd, $J = 3.4, 1.0$ Hz, 1H), 5.21, 5.18 (dd, $J = 10.5, 7.9$ Hz, 1H), 5.03, 5.00 (dd, 10.5, 3.4 Hz, 1H), 4.53 (s, 1H), 4.46 (d, $J = 7.9$ Hz, 1H), 4.22-4.11 (m, 2H), 3.92-3.86 (m, 1H), 3.64 (t, $J = 6.2$ Hz, 1H), 3.50-3.44 (m, 1H), 3.15-3.08 (m, 2H), 2.16 (s, 3H), 2.06 (s, 6H), 1.99 (s, 3H), 1.59-1.56 (m, 2H), 1.53-1.45 (m, 2H), 1.45 (s, 9H), 1.34-1.30 (m, 4H); ^{13}C NMR (100 MHz, CDCl_3): δ 170.59, 170.46, 170.36, 169.55, 156.40, 101.49, 71.11, 70.73, 70.25, 69.05, 67.22, 62.87, 61.40, 32.74, 30.23, 30.17, 29.51, 28.57, 26.62, 25.63, 20.92, 20.83, 20.76. HRMS m/z calc'd for $\text{C}_{25}\text{H}_{41}\text{O}_{12}\text{NNa}$: 570.2526; found: 570.2525.

Synthesis of Boc deprotected sugar derivative of monogalactose (**20**)



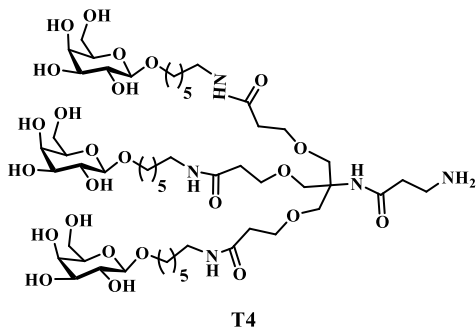
Compound **20** was synthesized using general procedure **B** using **19** (0.295g, 0.659 mmole) to yield **20** (0.174g, 76%).

monogalactose substituted tripod (24)



Compound **24** was synthesized by following procedure **C** using **20** (0.175 g, 0.393 mmole) and PFP ester **6** (0.120 g, 0.119 mmole). The crude residue was purified by column chromatography using MeOH/CH₂Cl₂ (4: 96) to get **24** (0.11 g, 52%). ¹H NMR (400 MHz, CDCl₃): δ 6.79 (bs, 1H), 6.48 (bs, 1H), 6.37 (bs, 1H), 6.29 (bs, 1H), 5.41-5.40 (m, 3H), 5.22-5.18 (m, 2H), 5.04, 5.03 (dd, 10.5, 3.4 Hz, 3H), 4.48 (d, J = 7.9 Hz, 3H), 4.23-4.12 (m, 8H), 3.94-3.87 (m, 9H), 3.73-3.68 (m, 8H), 3.52-3.46 (m, 4H), 3.41-3.35 (m, 2H), 3.27-3.22 (m, 3H), 2.92-2.87 (m, 4H), 2.58 (t, J = 6.0 Hz, 2H), 2.42 (t, J = 5.6 Hz, 4H), 2.17 (s, 12H), 2.07 (s, 12H), 2.00 (s, 12H), 1.78-1.72 (m, 6H), 1.63-1.59 (m, 12H), 1.53-1.50 (m, 6H), 1.45 (s, 9H) ; ¹³C NMR (100 MHz, CDCl₃): δ 170.41, 170.25, 170.14, 169.48, 156.98, 101.35, 70.82, 70.59, 70.14, 69.90, 69.04, 67.03, 61.22, 56.38, 40.06, 39.36, 36.21, 29.67, 29.36, 29.12, 29.08, 28.41, 26.82, 26.52, 25.60, 25.40, 24.18, 20.84, 20.81, 20.70, 20.69, 20.60. HRMS m/z calc'd for C₈₁H₁₂₉O₃₉N₅Na: 1818.8162; found: 1818.8165.

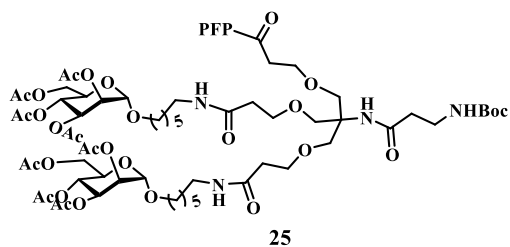
Deprotection of monogalactose substituted tripod (T4)



Tripod **T4** was synthesized by following procedure **D** using **24** (0.09 g, 0.053 mmole), NaOMe (0.041 g, 0.764 mmole) and 20% TFA. The crude residue was purified by sephadex column to yield **T4** (0.035 g, 60%). ¹H NMR (400 MHz, D₂O): δ 4.31 (d, J = 7.9 Hz, 3H), 3.85-3.83 (m, 6H), 3.69-3.64 (m, 12H), 3.58-3.53 (m, 17H), 3.43-3.38 (m, 4H), 3.15-3.08 (m, 6H), 3.02-2.95

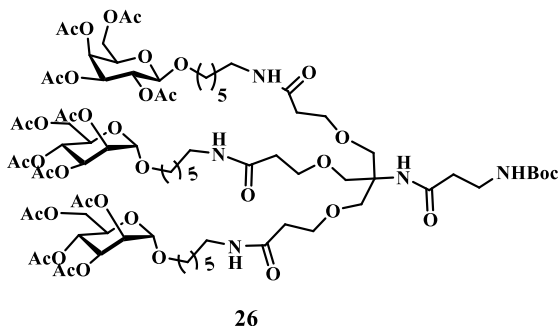
(m, 1H), 2.63-2.56 (m, 3H), 2.39 (t, $J = 5.7$ Hz, 3H), 1.68-1.62 (m, 3H), 1.57-1.53 (m, 6H), 1.47-1.40 (m, 3H), 1.32-1.28 (m, 12H). ^{13}C NMR (100 MHz, D_2O): δ .173.78, 172.23, 102.73, 75.08, 72.98, 70.66, 70.42, 70.23, 68.75, 60.92, 39.59, 39.38, 36.14, 28.75, 28.30, 25.80, 25.26, 24.80, 24.54, 23.40. HRMS m/z calc'd for $\text{C}_{52}\text{H}_{98}\text{O}_{25}\text{N}_5$: 1192.6551; found: 1192.6541.

Di substituted monomannose to tripod derivative (25)



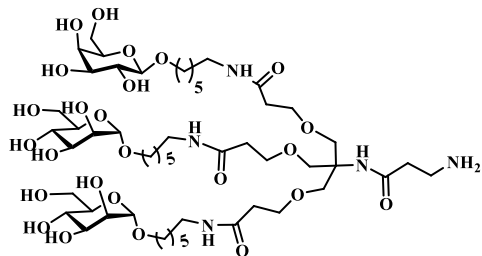
Compound **25** was synthesized using procedure **C** using **10** (0.159 g, 0.357 mmole, 2 equiv.) and the PFP ester **6** (0.180 g, 0.178 mmole, 1 equiv.). The crude residue was purified by column chromatography using acetone/ethyl acetate (30 : 70) to get **25** (0.092 g, 35%). ^1H NMR (400 MHz, CDCl_3): 6.44 (bs, 1H), 6.39 (s, 1H), 6.35 (bs, 1H), 6.26 (s, 1H), 5.37-5.31 (m, 2H), 5.29-5.26 (m, 1H), 5.23-5.22 (m, 2H), 4.81 (d, $J = 1.2$ Hz, 2H), 4.35 (t, $J = 6.6$ Hz, 1H), 4.31-4.27 (m, 2H), 4.13, 4.10 (dd, $J = 12.2, 2.3$ Hz, 2H), 4.00-3.96 (m, 1H), 3.84-3.80 (m, 6H), 3.77-3.68 (m, 8H), 3.47-3.43 (m, 1H), 3.40-3.36 (m, 2H), 3.27-3.22 (m, 6H), 2.92 (t, $J = 5.9$ Hz, 2H), 2.43 (t, $J = 4.8$ Hz, 6H), 2.17 (s, 6H), 2.11 (s, 6H), 2.06 (s, 6H), 2.00 (s, 6H), 1.63-1.59 (m, 4H), 1.55-1.52 (m, 4H), 1.44 (s, 9H), 1.38-1.37 (m, 8H); ^{13}C NMR (100 MHz, CDCl_3): δ .171.18, 170.01, 169.78, 169.65, 169.49, 169.39, 141.03, 140.53, 140.18, 99.76, 99.34, 70.53, 69.66, 69.53, 69.41, 69.14, 68.50, 68.38, 66.31, 66.23, 66.11, 62.52, 62.24, 29.65, 29.31, 28.31, 26.74, 25.86, 20.80, 20.69, 20.60. HRMS m/z calc'd for $\text{C}_{67}\text{H}_{98}\text{O}_{30}\text{N}_4\text{F}_5$: 1533.6186; found: 1533.6208.

Monomannose and monogalactose substituted tripod derivative (26)



25 (0.09 g, 0.058 mmole) was taken in an RB and **20** (0.031 g, 0.07 mmole) dissolved in CH₂Cl₂ was added to it. The pH of the reaction mixture was adjusted to 8 using triethylamine. It was allowed to stir for 12 h at RT. On completion, the solvent was evaporated under reduced pressure and the crude residue was purified by column chromatography using MeOH/CH₂Cl₂ (4 : 96) to yield **25** (0.066g, 63%). ¹H NMR (400 MHz, CDCl₃): 6.88 (s, 1H), 6.52 (s, 2H), 6.42 (s, 2H), 5.37 (bm, 1H), 5.34-5.28 (m, 2H), 5.21-5.14 (m, 3H), 5.01, 4.99 (dd, J = 10.5, 3.4 Hz, 2H), 4.78 (d, J = 1.6 Hz, 2H), 4.44 (d, J = 7.9 Hz, 1H), 4.27, 4.26 (dd, J = 12.2, 5.2 Hz, 2H), 4.20-4.07 (m, 6H), 3.97-3.93 (m, 1H), 3.90-3.83 (m, 4H), 3.74-3.64 (m, 13H), 3.47-3.40 (m, 4H), 3.26-3.18 (m, 6H), 2.39 (t, J = 5.2 Hz, 8H), 2.14 (s, 3H), 2.13 (s, 6H), 2.09 (s, 3H), 2.03 (s, 18H), 1.98 (s, 3H), 1.97 (s, 3H), 1.58-1.48 (m, 12H), 1.41 (s, 9H), 1.35-1.31 (m, 12H) ; ¹³C NMR (100 MHz, CDCl₃): δ.170.67, 170.42, 170.26, 170.16, 169.72, 155.94, 101.35, 97.64, 70.87, 70.59, 70.21, 69.74, 69.23, 68.98, 68.43, 67.50, 67.06, 66.24, 62.74, 61.67, 39.45, 39.21, 36.84, 32.35, 29.62, 29.49, 29.35, 29.13, 28.58, 26.79, 26.71, 26.46, 26.01, 25.59, 25.40, 20.83, 20.80, 20.76, 20.71, 20.69, 20.67, 20.60. HRMS m/z calc'd for C₈₁H₁₂₉O₃₉N₅Na: 1818.8162; found: 1818.8160.

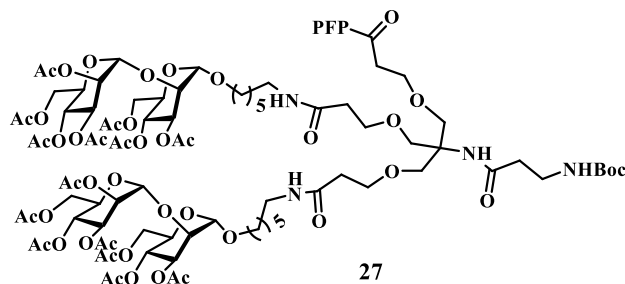
Deprotected monomannose and monogalactose tripod derivative (**T5**)



T5

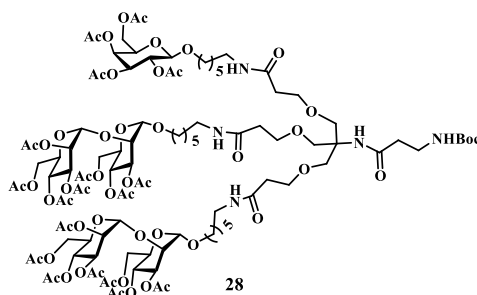
Tripod **T5** was synthesized by following procedure **D** using **26** (0.05 g, 0.027 mmole) and NaOMe (0.016 g, 0.401 mmole) and 20% TFA. The crude residue was purified by sephadex column to yield **T5** (0.025g, 76%). ¹H NMR (400 MHz, D₂O) 4.76 (bs, 2H), 4.30 (d, J = 7.9 Hz, 1H), 3.87-3.77 (m, 6H), 3.67 - 3.61 (m, 15H), 3.61 - 3.50 (m, 13H), 3.46 - 3.38 (m, 4H), 3.15 - 3.09 (m, 6H), 2.57 (t, J = 10.7 Hz, 4H), 2.39 (t, J = 5.4 Hz, 4H), 1.54-1.49 (m, 6H), 1.45 - 1.42 (m, 6H), 1.34-1.20 (m, 12H); ¹³C NMR (100 MHz, D₂O): δ. 170.54, 169.37, 102.72, 99.62, 75.06, 72.83, 72.72, 70.71, 70.64, 70.38, 70.16, 68.55, 67.72, 67.61, 66.71, 39.31, 36.20, 35.51, 28.70, 28.40, 28.32, 25.82. HRMS m/z calc'd for C₅₂H₉₈O₂₅N₅: 1192.6551; found: 1192.6530.

Di substituted disaccharide mannose to tripod derivative (27)



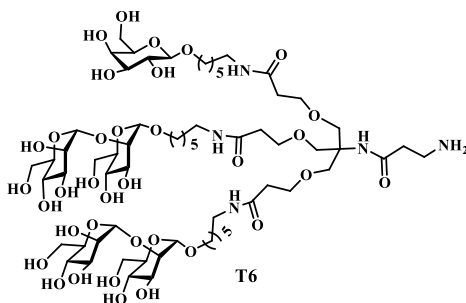
13 (0.233 g, 0.318 mmole) was dissolved in CH_2Cl_2 and the PFP ester **6** (0.16 g, 0.159 mmole) was added to it. The pH of the reaction mixture was then adjusted to 8 using triethylamine. The mixture was then allowed to stir at RT for 12h. On completion, the mixture was concentrated *in vacuo* to obtain the crude residue was purified by column chromatography using acetone/ethyl acetate (30 : 70) to get **27** (0.124 g, 37%). R_f = (CH_2Cl_2 /acetone, 70:30). ^1H NMR (400 MHz, CDCl_3): 6.73 (s, 1H), 6.36 (s, 1H), 6.26 (s, 2H), 5.40, 5.38 (dd, J = 10.0, 3.3 Hz, 2H), 5.31-5.29 (m, 2H), 5.27-5.26 (m, 2H), 5.25-5.24 (m, 3H), 4.90 (m, 4H), 4.22-4.16 (m, 3H), 4.15-4.08 (m, 6H), 3.99-3.98 (m, 2H), 3.90-3.86 (m, 2H), 3.80-3.76 (m, 4H), 3.68-3.61 (m, 12H), 3.42-3.32 (m, 4H), 3.23-3.18 (m, 4H), 2.89 (t, J = 5.9 Hz, 2H), 2.39 (t, J = 5.7 Hz, 6H), 2.16 (s, 3H), 2.13 (s, 3H), 2.12 (s, 6H), 2.06 (s, 12H), 2.02 (s, 6H), 2.01 (s, 6H), 1.99 (s, 6H), 1.58-1.56 (m, 4H), 1.49-1.48 (m, 4H), 1.40 (s, 9H), 1.34-1.32 (m, 8H) ; ^{13}C NMR (100 MHz, CDCl_3): δ . 171.31, 170.84, 170.38, 169.88, 169.75, 169.47, 169.23, 155.98, 142.32, 141.58, 139.27, 99.18, 98.25, 70.36, 69.79, 69.54, 69.45, 69.37, 69.01, 68.50, 68.36, 67.48, 67.45, 66.45, 66.25, 66.15, 62.52, 62.20, 53.78, 39.50, 37.09, 36.61, 34.26, 33.73, 31.96, 29.69, 29.66, 29.60, 29.36, 29.31, 29.26, 28.41, 26.81, 25.96, 22.66, 20.87, 20.76, 20.71, 20.67, 20.65. HRMS m/z calc'd for $\text{C}_{91}\text{H}_{129}\text{O}_{46}\text{N}_5\text{F}_5\text{Na}$: 2131.7696; found $[\text{M}+2\text{Na}]^{2+}$: 1077.5936.

Synthesis of disaccharide mannose and monogalactose substituted tripod derivative (28)



27 (0.1 g, 0.047 mmole) was taken in an RB and **20** (0.056 g, 0.025 mmole) dissolved in CH₂Cl₂ was added to it. The pH of the reaction mixture was adjusted to 8 using triethylamine. It was allowed to stir for 12h at RT. On completion, the solvent was evaporated under reduced pressure and the crude residue was purified by column chromatography using CH₂Cl₂/MeOH (4: 96) to yield **28** (0.066 g, 59%). ¹H NMR (400 MHz, CDCl₃): δ 6.83 (s, 1H), 6.71 (s, 1H), 6.49 (s, 1H), 6.41 (s, 2H), 5.43-5.40 (m, 4H), 5.36-5.34 (m, 2H), 5.31-5.30 (m, 2H), 5.29-5.27 (m, 6H), 5.21-5.15 (m, 1H), 5.03, 5.01 (dd, *J* = 10.5, 3.4 Hz, 2H), 4.93 (bs, 3H), 4.45 (d, *J* = 7.9 Hz, 1H), 4.25-4.10 (m, 12H), 4.02 (bs, 2H), 3.93-3.86 (m, 4H), 3.72-3.67 (m, 12H), 3.50-3.37 (m, 6H), 3.26-3.23 (m, 6H), 2.41 (t, *J* = 5.5 Hz, 6H), 2.16 (s, 9H), 2.15 (s, 6H), 2.09 (s, 12H), 2.06-2.04 (m, 18 H), 2.02 (s, 6H), 1.99 (s, 3H), 1.61-1.58 (m, 6H), 1.53-1.52 (m, 6H), 1.44 (s, 9H), 1.40-1.31 (m, 12H); ¹³C NMR (100 MHz, CDCl₃): δ 171.21, 170.77, 170.41, 170.26, 169.90, 169.65, 169.45, 169.40, 155.99, 101.33, 99.16, 98.24, 70.84, 70.65, 70.54, 70.52, 70.36, 70.17, 69.85, 69.77, 69.22, 68.84, 68.41, 67.58, 67.10, 66.42, 66.21, 62.52, 62.19, 39.49, 39.45, 36.60, 29.56, 29.31, 28.49, 28.37, 26.80, 26.67, 25.94, 25.54, 20.85, 20.77, 20.74, 20.69, 20.66, 20.63, 20.57. HRMS *m/z* calc'd for C₁₀₅H₁₆₁O₅₅N₅Na: 2394.9853; found: 2394.9558.

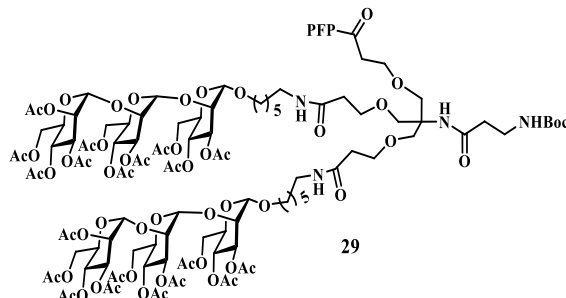
Deprotection of disaccharide mannose and monogalactose to tripod derivative (T6)



Tripod **T6** was synthesized by following procedure **D** using **28** (0.06g, 0.025 mmole) and NaOMe (0.025 g, 0.47 mmole) and 20% TFA. The crude residue was purified by sephadex column to yield **T6** (0.027g, 72%). ¹H NMR (400 MHz, D₂O): 4.99 (bs, 2H), 4.92 (bs, 2H), 4.27 (d, *J* = 7.9 Hz, 1H), 3.97 (bm, 2H), 3.84-3.80 (m, 14H), 3.77-3.61 (m, 15H), 3.59-3.50 (m, 15H), 3.46-3.38 (m, 4H), 3.14-3.08 (m, 6H), 2.57 (t, *J* = 6.6 Hz, 2H), 2.38 (t, *J* = 5.7 Hz, 6H), 1.53-1.52 (m, 6H), 1.44-1.41 (m, 6H), 1.27 (bm, 12H); ¹³C NMR (100 MHz, D₂O): δ. 173.74, 171.78, 102.76, 102.30, 98.04, 78.72, 75.04, 73.23, 72.82, 72.71, 70.74, 70.38, 70.27, 69.90, 68.60, 68.40, 67.82, 67.59, 66.92, 66.84, 61.08, 60.87, 60.36, 39.38, 36.17, 35.41, 28.68, 28.42, 28.31,

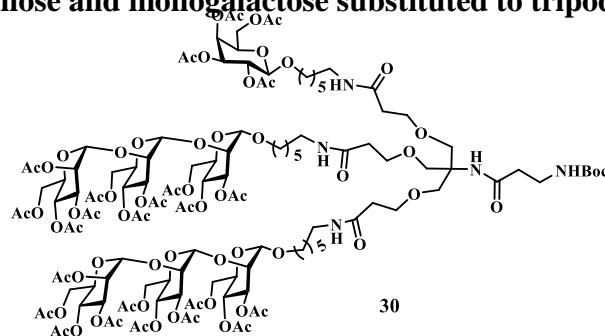
25.89, 25.07, 24.73. HRMS m/z calc'd for $C_{64}H_{118}O_{35}N_5$: 1516.7607; found $[M+2H]^{2+}$: 758.8847.

Synthesis of 2 substituted trisaccharide mannose to tripod derivative (29)



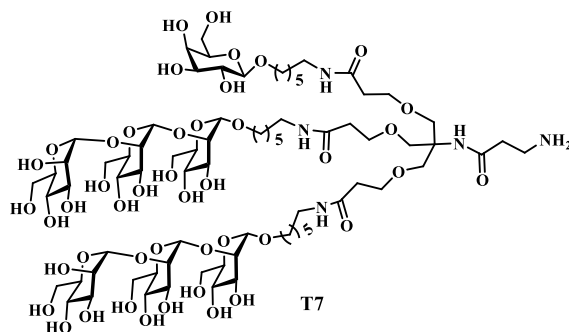
16 (0.291 g, 0.298 mmole) was dissolved in CH_2Cl_2 and the PFP ester **6** (0.15 g, 0.149 mmole) was added to it. The pH of the reaction mixture was then adjusted to 8 using triethylamine. The mixture was then allowed to stir at RT for 12 h. On completion, the mixture was concentrated *in vacuo* to obtain the crude residue was purified by column chromatography using acetone/ethyl acetate (30 : 70) to get **29** (0.14 g, 36%). $R_f = (CH_2Cl_2 /acetone, 70:30)$. 1H NMR (400 MHz, $CDCl_3$): 6.39 (s, 1H), 6.27 (s, 3H), 5.42, 5.40 (dd, $J = 10.0, 3.4$ Hz, 2H), 5.37-5.35 (m, 3H), 5.32-5.30 (m, 3H), 5.12 (d, $J = 1.8$ Hz, 2H), 4.97 (d, $J = 1.7$ Hz, 2H), 4.95 (d, $J = 1.9$ Hz, 2H), 4.27, 4.25 (dd, $J = 12.3, 4.5$ Hz, 3H), 4.18-4.15 (m, 12H), 4.03 (bm, 2H), 3.94-3.91 (m, 2H), 3.84-3.80 (m, 5H), 3.73-3.65 (m, 12H), 3.46-3.44 (m, 2H), 3.41-3.38 (m, 2H), 3.28-3.23 (m, 6H), 2.93 (t, $J = 5.9$ Hz, 6H), 2.43 (t, $J = 5.6$ Hz, 6H), 2.21 (s, 6H), 2.20 (s, 6H), 2.18 (s, 6H), 2.15 (s, 6H), 2.15 (s, 6H), 2.11 (s, 6H), 2.09 (s, 6H), 2.06 (s, 6H), 2.05 (s, 6H), 2.03 (s, 6H), 1.70-1.60 (m, 4H), 1.54-1.52 (m, 4H), 1.45 (s, 9H), 1.38-1.36 (m, 8H); ^{13}C NMR (100 MHz, $CDCl_3$): δ 171.27, 170.94, 170.81, 170.52, 170.12, 169.87, 169.76, 169.60, 169.56, 169.47, 156.023, 140.59, 139.87, 139.40, 99.88, 99.44, 98.33, 70.60, 69.78, 69.63, 69.52, 69.32, 68.64, 68.50, 66.38, 66.32, 66.22, 62.60, 62.30, 62.21, 39.47, 36.56, 32.00, 31.78, 29.77, 29.43, 29.33, 28.44, 26.88, 26.00, 20.82, 22.76, 20.88, 20.77, 20.69. HRMS m/z calc'd for $C_{115}H_{161}O_{62}N_5F_5Na$: 2707.9386; found: 2707.9155.

Trisaccharide mannose and monogalactose substituted to tripod derivative (30)



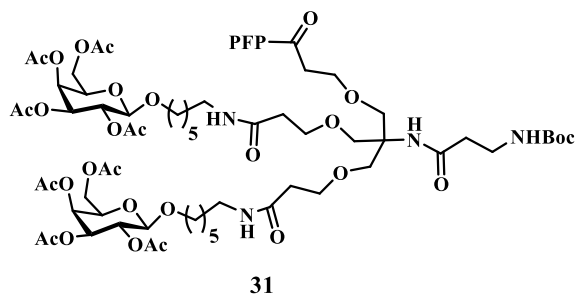
29 (0.1 g, 0.037 mmole) was taken in an RB and **20** (0.019 g, 0.044 mmole) dissolved in CH_2Cl_2 was added to it. The pH of the reaction mixture was adjusted to 8 using triethylamine. It was allowed to stir for 12 h at RT. On completion, the solvent was evaporated under reduced pressure and the crude residue was purified by column chromatography using $\text{MeOH}/\text{CH}_2\text{Cl}_2$ (4 : 96) to yield **30** (0.062 g, 57%). ^1H NMR (400 MHz, CDCl_3): δ 6.41 (bs, 3H), 6.32 (bs, 1H), 6.24 (bs, 1H), 5.41-5.37 (m, 6H), 5.32-5.28 (m, 14H), 4.95 (d, $J = 1.3$ Hz, 3H), 4.93 (d, $J = 1.4$ Hz, 3H), 4.45 (d, $J = 6.1$ Hz, 1H), 4.18-4.12 (m, 18H), 3.92-3.89 (m, 6H), 3.71-3.66 (m, 12H), 3.47-3.42 (m, 4H), 3.39-3.36 (m, 2H), 3.26-3.21 (m, 6H), 2.56 (t, $J = 5.7$ Hz, 2H), 2.42-2.39 (m, 6H), 2.15 (s, 9H), 2.13 (s, 6H), 2.12 (s, 6H), 2.08 (s, 9H), 2.06 (s, 3H), 2.06 (s, 3H), 2.05 (s, 9H), 2.03 (s, 15H), 2.00 (s, 9H), 1.98 (s, 3H), 1.69-1.66 (m, 6H), 1.61-1.56 (m, 12H), 1.53-1.50 (m, 6H), 1.43 (s, 9H).); ^{13}C NMR (100 MHz, CDCl_3): δ 171.46, 170.41, 170.36, 169.86, 169.64, 169.23, 156.22, 101.49, 99.52, 98.40, 69.83, 69.73, 69.56, 69.36, 69.23, 69.07, 68.69, 68.58, 68.52, 68.30, 67.19, 66.41, 66.31, 62.67, 62.37, 62.28, 61.35, 32.07, 29.84, 29.50, 26.96, 26.07, 23.13, 22.83, 20.99, 20.88, 20.82, 20.76, 20.41. HRMS m/z calc'd for $\text{C}_{129}\text{H}_{193}\text{O}_{71}\text{N}_5\text{Na}$: 2971.1543; found $[\text{M}+2\text{H}]^{2+}$: 1497.5760.

Deprotection of trisaccharide mannose and monogalactose substituted tripod derivative (T7)



Tripod **T7** was synthesized by following procedure **D** using compound **30** (0.05g, 0.021 mmole), NaOMe (0.09 g, 0.387 mmole) and 20% TFA. The crude residue was purified by sephadex column to yield **T7** (0.025g, 35%). ¹H NMR (400 MHz, D₂O): δ; 5.13(d, J = 0.5 Hz, 2H), 4.92 (d, J = 0.7 Hz, 2H), 4.88 (d, J = 0.5 Hz, 2H), 4.23 (d, J = 8.0 Hz, 1H), 3.95-3.94 (m, 2H), 3.90-3.89 (m, 2H), 3.80-3.75 (m, 8H), 3.72-3.67 (m, 9H), 3.61-3.55 (m, 27H), 3.52-3.48 (m, 12H), 3.03 (t, J = 7.1 Hz, 6H), 2.50 (t, J = 6.4 Hz, 4H), 2.31 (t, J = 5.7 Hz, 6H), 1.48-1.43 (m, 6H), 1.37-1.34 (m, 6H), 1.27-1.20 (m, 12H). ¹³C NMR (100 MHz, D₂O): δ. 173.38, 172.88, 102.23, 99.74, 98.64, 73.22, 72.37, 70.27, 70.20, 69.88, 69.80, 68.28, 68.25, 67.97, 67.90, 67.69, 67.04, 66.90, 66.81, 61.09, 60.74, 39.39, 36.20, 36.03, 28.50, 28.44, 28.41, 28.31, 28.18, 28.09, 27.15, 27.04, 25.69, 25.55, 25.05, 24.76. HRMS m/z calc'd for C₇₆H₁₃₈O₄₅N₅: 1840.8664; found [M+H]²⁺: 920.9336.

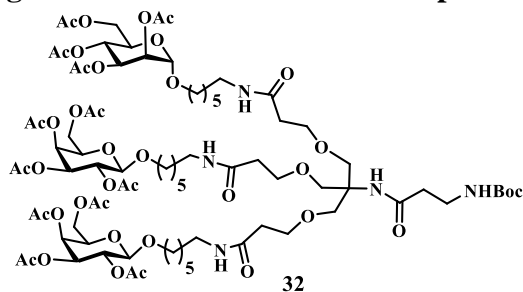
2 substituted monogalactose to tripod derivative (31)



6 (0.2 g, 0.198 mmole) was dissolved in CH₂Cl₂ and the **20** (0.177 g, 0.397 mmole) was added to it. The pH of the reaction mixture was then adjusted to 8 using triethylamine. The mixture was then allowed to stir at RT for 12h. On completion, the mixture was concentrated *in vacuo* to obtain the crude residue was purified by silica column chromatography using acetone/ethyl acetate (30: 70) **31** (0.09 g, 29%). ¹H NMR (400 MHz, CDCl₃): 6.39 (s, 1H), 6.30 (s, 2H), 5.37 (d, J = 2.9 Hz, 2H), 5.27 (s, 1H), 5.19-5.14 (m, 2H), 5.01, 4.98 (dd, J = 10.4, 3.4 Hz, 2H), 4.44 (d, J = 7.9 Hz, 2H), 4.17-4.08 (m, 4H), 3.90-3.87 (m, 4H), 3.80-3.75 (m, 4H), 3.71-3.61 (m, 8H), 3.47-3.41 (m, 2H), 3.37-3.32 (m, 2H), 3.23-3.18 (m, 4H), 2.89 (t, J = 5.8 Hz, 2H), 2.40 (t, J = 5.7 Hz, 4H), 2.32 (t, J = 12 Hz, 2H), 2.11 (s, 6H), 2.03 (s, 12H), 1.97 (s, 6H), 1.59-1.53 (m, 4H), 1.49-1.46 (m, 4H), 1.41 (s, 9H), 1.31-1.28 (m, 8H); ¹³C NMR (100 MHz, CDCl₃): δ. 171.54, 170.55, 170.39, 169.60, 156.12, 139.36, 139.20, 139.10, 101.42, 70.98, 70.64, 70.22, 69.51, 69.02, 67.51, 67.12, 61.39, 39.58, 36.58, 34.18, 33.71, 31.99, 29.76, 29.59, 29.53, 29.41, 29.02,

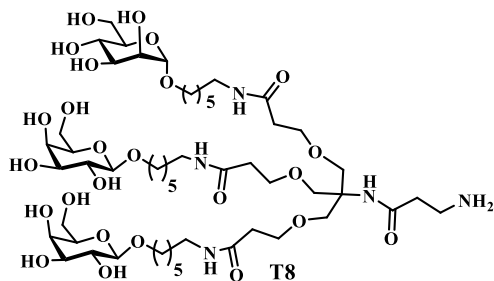
28.47, 26.75, 25.65, 22.76, 20.85, 20.75, 20.67. HRMS m/z calc'd for $C_{67}H_{98}O_{30}N_4F_5$: 1533.6186; found: 1533.6199.

Di substituted monogalactose and monomannose tripod derivative (32)



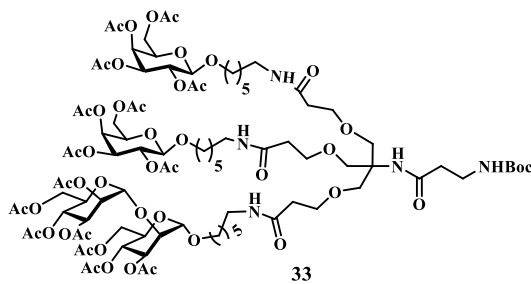
31 (0.07g, 0.045 mmole) was dissolved in CH_2Cl_2 and the **10** (0.024 g, 0.054 mmole) was added to it. The pH of the reaction mixture was then adjusted to 8 using triethylamine. The mixture was then allowed to stir at RT for 12 h. On completion, the mixture was concentrated *in vacuo* to obtain the crude residue purified by column chromatography using acetone/ethyl acetate (30 : 70) to get **32** (0.033 g, 41%). 1H NMR (400 MHz, $CDCl_3$): 6.81 (s, 1H), 6.48 (s, 1H), 6.39 (s, 2H), 5.37 (d, $J = 2.8$ Hz, 2H), 5.32 (s, 1H), 5.29-5.23 (m, 2H), 5.20-5.14 (m, 2H), 5.00, 4.99 (dd, $J = 10.5, 3.4$ Hz, 2H), 4.78 (d, $J = 1.4$ Hz, 1H), 4.44 (d, $J = 7.9$ Hz, 2H), 4.22-4.07 (m, 6H), 3.90-3.83 (m, 4H), 3.69-3.61 (m, 14H), 3.47-3.40 (m, 3H), 3.38-3.33 (m, 3H), 3.26-3.18 (m, 6H), 2.38 (t, $J = 5.3$ Hz, 8H), 2.13 (s, 9H), 2.08 (s, 3H), 2.03 (s, 15H), 1.96 (s, 9H), 1.58-1.46 (m, 12H), 1.41 (s, 9H), 1.35-1.31 (m, 12H); ^{13}C NMR (100 MHz, $CDCl_3$): δ .171.25, 170.68, 170.44, 170.27, 170.18, 169.73, 169.49, 156.01, 101.43, 97.55, 70.92, 70.59, 70.14, 69.66, 69.18, 68.97, 68.49, 68.42, 67.49, 67.06, 66.25, 62.51, 61.23, 39.48, 36.63, 29.56, 29.36, 28.44, 26.71, 25.59, 20.92, 20.80, 20.77, 20.72, 20.69, 20.60. HRMS m/z calc'd for $C_{81}H_{130}O_{39}N_5$: 1796.8343; found: 1796.8157.

Deprotection of 2 substituted monogalactose and monomannose to tripod derivative (T8)



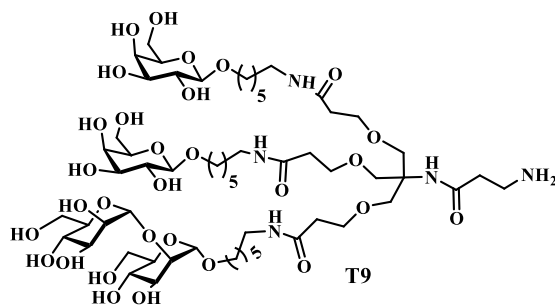
Tripod **T8** was synthesized by following procedure **D** using compound **32** (0.05g, 0.021 mmole) and NaOMe (0.09 g, 0.387 mmole) and 20% TFA. The crude residue was purified by sephadex column to yield **T8** (0.025g, 35%). ¹H NMR (400 MHz, D₂O): 4.77 (d, J = 1.3 Hz, 1H), 4.31 (d, J = 7.9 Hz, 2H), 3.85-3.83 (m, 4H), 3.69-3.50 (m, 31H), 3.16-3.09 (m, 9H), 2.58 (t, J = 6.7 Hz, 2H), 2.39 (t, J = 5.8 Hz, 6H), 1.58-1.51 (m, 6H), 1.48-1.42 (m, 6H), 1.29-1.27 (m, 12 H); ¹³C NMR (100 MHz, D₂O): δ.174.10, 171.67, 102.77, 99.30, 75.07, 72.84, 72.67, 70.70, 70.65, 70.40, 70.09, 68.63, 68.43, 67.74, 67.62, 66.73, 61.69, 60.82, 60.39, 39.21, 36.06, 35.45, 32.44, 31.22, 28.61, 28.32, 25.88, 25.06, 24.75. HRMS m/z calc'd for C₅₂H₉₈O₂₅N₅: 1192.6551; found: 1192.6541.

Synthesis of 2 substituted monogalactose and disaccharide mannose tripod derivative (**43**)



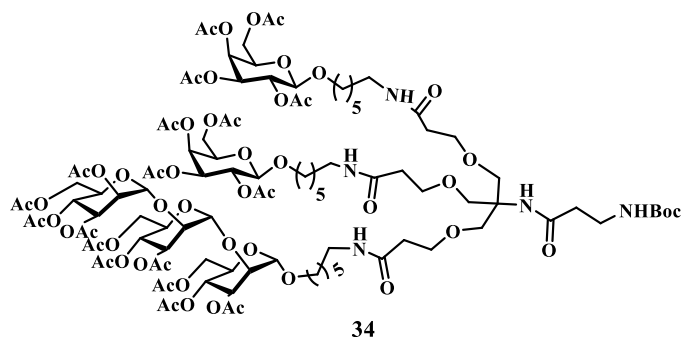
31 (0.06g, 0.039 mmole) was dissolved in CH₂Cl₂ and the **13** (0.034 g, 0.046 mmole) was added to it. The pH of the reaction mixture was then adjusted to 8 using triethylamine. The mixture was then allowed to stir at RT for 12 h. On completion, the mixture was concentrated *in vacuo* to obtain the crude residue was purified by column chromatography using acetone/ethyl acetate (30 : 70) **33** (0.026 g, 44%). ¹H NMR (400 MHz, CDCl₃): 6.80 (s, 1H), 6.71 (s, 1H), 6.49 (s, 1H), 6.39 (s, 2H), 5.45-5.40 (m, 4H), 5.33-5.29 (m, 3H), 5.22-5.18 (m, 2H), 5.06, 5.03 (dd, J = 10.5, 3.4 Hz, 2H), 4.95 (d, J = 1.7 Hz, 2H), 4.48 (d, J = 7.9 Hz, 2H), 4.27-4.12 (m, 10H), 3.94-3.89 (m, 5H), 3.73-3.69 (m, 12H), 3.51-3.38 (6H), 3.28-3.22 (m, 6H), 2.42 (t, J = 5.5 Hz, 8H), 2.17 (s, 12H), 2.10 (s, 6H), 2.07 (s, 18H), 2.03 (s, 3H), 2.00 (s, 6H), 1.64-1.59 (m, 6H), 1.55-1.50 (m, 6H), 1.45 (s, 9H), 1.38-1.35 (m, 12H); ¹³C NMR (100 MHz, CDCl₃): δ.170.33, 170.64, 170.53, 170.38, 170.29, 169.54, 101.41, 99.25, 98.32, 70.93, 70.63, 70.24, 69.01, 68.54, 68.47, 67.54, 67.11, 62.58, 61.29, 39.55, 36.68, 29.65, 29.42, 28.52 26.72, 20.98, 20.90, 20.78, 20.70 HRMS m/z calc'd for C₉₃H₁₄₅O₄₇N₅Na: 2106.9008; found [M+2Na]²⁺: 1064.9480.

Deprotection of 2 substituted monogalactose and monomannose to tripod derivative (44)



Tripod **T9** was synthesized by following procedure **D** using compound **33** (0.05g, 0.021 mmole) and NaOMe (0.09 g, 0.387 mmole) and 20% TFA. The crude residue purified by sephadex column to yield **T9** (0.025g, 35%). ¹H NMR (400 MHz, D₂O): 5.01 (s, 1H), 4.93 (d, J = 1.4 Hz, 1H), 4.31 (d, J = 7.9 Hz, 2H), 3.86-3.75 (m, 10H), 3.68-3.62 (m, 16H), 3.60-3.53 (m, 16H), 3.14-3.09 (m, 8H), 2.58 (t, J = 6.7 Hz, 2H), 2.39 (t, J = 5.8 Hz, 6H), 1.56-1.51 (m, 6H), 1.46-1.39 (m, 6H), 1.29-1.23 (m, 12H); ¹³C NMR (100 MHz, D₂O): δ.173.72, 171.76, 102.71, 102.30, 98, 78.74, 75.07, 73.26, 72.81, 72.73, 70.76, 70.40, 70.29, 69.92, 68.62, 68.41, 67.85, 67.62, 66.94, 66.87, 61.11, 60.90, 60.38, 39.39, 36.20, 35.52, 32.39, 28.70, 28.44, 28.32, 25.88, 25.08, 24.75. HRMS m/z calc'd for C₅₈H₁₀₈O₃₀N₅: 1354.7079; found: 1354.7068.

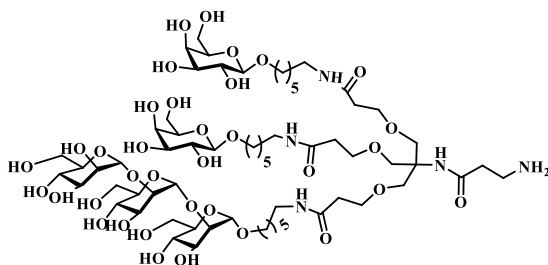
Synthesis of di substituted monogalactose and trisaccharide mannose to tripod derivative (34)



31 (0.04g, 0.026 mmole) was dissolved in CH₂Cl₂ and the **16** (0.032 g, 0.031 mmole) was added to it. The pH of the reaction mixture was then adjusted to 8 using triethylamine. The mixture was then allowed to stir at RT for 12h. On completion, the mixture was concentrated *in vacuo* to obtain the crude residue which was purified by silica column chromatography using Acetone/Ethyl acetate (30: 70) to get **34** (0.024 g, 39%). ¹H NMR (400 MHz, CDCl₃): 6.79 (s, 1H), 6.50 (1H), 6.42 (s, 3H), 5.40-5.39 (m, 3H), 5.33-5.27 (m, 6H), 5.19-5.16 (m, 2H), 5.10 (d, J

= 1.4 Hz, 1H), 5.02, 5.00 (dd J = 10.5, 3.4 Hz, 1H), 4.94 (s, 1H), 4.92 (d, J = 1.2 Hz, 1H), 4.45 (d, J = 7.9 Hz, 2H), 4.21-4.09 (m, 13H), 3.91-3.85 (m, 6H), 3.70-3.65 (m, 12H), 3.48-3.41 (m, 4H), 3.36-3.35 (m, 3H), 3.22-3.19 (m, 6H), 2.39 (t, J = 5.5 Hz, 8H), 2.14 (s, 9H), 2.11 (s, 6H), 2.08 (s, 3H), 2.06 (s, 3H), 2.04 (s, 15H), 2.02 (s, 9H), 1.99 (s, 3H), 1.97 (s, 6H), 1.59-1.56 (m, 6H), 1.52-1.47 (m, 6H), 1.42 (s, 9H), 1.34-1.32 (m, 12H); ¹³C NMR (100 MHz, CDCl₃): δ. 171.36, 171.04, 170.91, 170.55, 170.40, 170.30, 170.20, 169.92, 169.62, 169.52, 101.47, 99.93, 99.49, 98.36, 71.04, 70.71, 70.26, 69.83, 69.71, 69.55, 69.34, 69.09, 68.52, 67.60, 67.18, 66.39, 61.35, 39.60, 36.76, 29.70, 29.48, 28.57, 26.83, 26.05, 25.72, 20.97, 20.93, 20.88, 20.85, 20.82, 20.80, 20.73. HRMS m/z calc'd for C₁₀₅H₁₆₁O₅₅N₅Na: 2394.9853; found: 2394.8267.

Deprotection of 2 substituted monogalactose and disaccharide mannose to tripod derivative (T10)

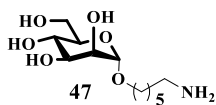


Tripod **T10** was synthesized by following procedure **D** using **34** (0.05g, 0.021 mmole) and NaOMe (0.09 g, 0.387 mmole) and 20% TFA. The crude residue was purified by sephadex column to yield **T10** (0.025g, 35%). ¹H NMR (400 MHz, D₂O): 5.29 (s, 1H), 5.08 (s, 1H), 5.04 (s, 1H), 4.39 (d, J = 7.9 Hz, 2H), 4.10-4.06 (m, 3H), 3.96-3.91 (m, 7H), 3.89-3.84 (m, 3H), 3.77-3.72 (m, 16H), 3.68-3.64 (m, 14H), 3.54-3.47 (m, 4H), 3.24-3.17 (m, 9H), 2.66 (t, J = 6.7 Hz, 2H), 2.47 (t, J = 5.8 Hz, 6H), 1.66-1.61 (m, 6H), 1.55-1.50 (m, 6H), 1.36-1.35 (m, 12H); ¹³C NMR (100 MHz, D₂O): δ. 173.76, 171.80, 102.83, 102.20, 100.60, 97.90, 78.83, 78.45, 74.99, 73.21, 72.90, 72.66, 70.68, 70.39, 70.28, 69.92, 68.61, 68.40, 67.60, 67.60, 67.05, 66.92, 66.81, 61.08, 60.82, 60.40, 39.38, 36.19, 35.51, 32.41, 28.69, 28.39, 28.31, 25.87, 25.07, 24.74. HRMS m/z calc'd for C₆₄H₁₁₈O₃₅N₅: 1516.7607; found: 1516.7546.

General Procedure for deprotection Sugars

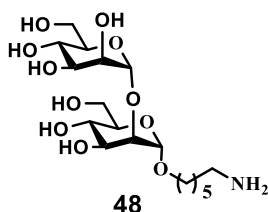
Acetate de-protection of compound was done in NaOMe and MeOH (10 ml) for 2 hr at RT. Then after completion of reaction neutralise with IR 120 H⁺. The crude residue on evaporation of MeOH was purified by sephadex column to yield deprotected form of sugars.

Deprotected monomannose sugar (47)



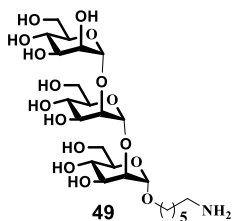
^1H NMR (400 MHz, D_2O): δ 4.77 (s, 1H), 3.84 (bs, 1H), 3.78 (bs, 1H), 3.73-3.62 (m, 4H), 3.59-3.51 (m, 2H), 3.50-3.43 (m, 1H), 2.74 (t, $J = 7.3$ Hz, 1H), 1.59-1.43 (m, 4H), 1.30 (bs, 4H); ^{13}C NMR (100 MHz, D_2O): δ . 99.61, 72.70, 70.61, 70.04, 67.69, 66.73, 60.90, 39.68, 28.26, 27.93, 25.46, 24.96. HRMS m/z calc'd for $\text{C}_{12}\text{H}_{26}\text{O}_6\text{N}$: 280.1760; found: 280.1765.

Deprotected disaccharide mannose sugar (48)



^1H NMR (400 MHz, D_2O): δ 5.01 (d, $J = 1.4$ Hz, 1H), 4.93 (d, $J = 1.6$ Hz, 1H), 3.99-3.97 (m, 1H), 3.86-3.85 (m, 1H), 3.81-3.80 (m, 1H), 3.79-3.78 (m, 2H), 3.74-3.73 (m, 1H), 3.70-3.67 (m, 1H), 3.66-3.62 (m, 3H), 3.60-3.57 (m, 1H), 3.54-3.50 (m, 2H), 3.48-3.42 (m, 1H), 2.90 (t, $J = 7.6$ Hz, 2H), 1.58-1.54 (m, 4H), 1.33-1.30 (m, 4H); ^{13}C NMR (100 MHz, D_2O): δ . 102.25, 97.98, 78.67, 73.18, 72.66, 70.24, 69.87, 67.68, 66.91, 66.83, 61.04, 60.86, 39.37, 29.36, 28.11, 26.53, 25.25, 24.78. HRMS m/z calc'd for $\text{C}_{18}\text{H}_{36}\text{O}_{11}\text{N}$: 442.2288; found: 442.2289.

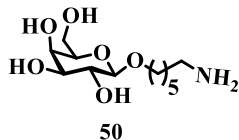
Deprotected trisaccharide mannose sugar (49)



^1H NMR (400 MHz, D_2O): δ 5.34-5.19 (m, 1H), 5.09-4.96 (m, 2H), 4.77-4.67 (m, 1H), 4.57-4.42 (m, 1H), 4.06 (d, $J = 1.6$ Hz, 1H), 4.00 (d, $J = 2$ Hz, 2H), 3.94-3.79 (m, 6H), 3.76-3.67 (m, 6H), 3.65-3.55 (m, 3H), 2.64 (t, $J = 7.5$ Hz, 2H), 1.70-1.58 (m, 4H), 1.45-1.41 (m, 4H); ^{13}C NMR (100 MHz, D_2O): δ . 102.83, 100.94, 98.42, 79.52, 79.13, 73.61, 73.25, 70.75, 70.48, 67.83, 67.70,

67.40, 66.97, 61.92, 61.81, 61.65, 39.24, 29.21, 27.34, 25.55, 25.33. HRMS m/z calc'd for $C_{24}H_{46}O_{16}N$: 604.2817; found: 604.2818.

Deprotected monogalactose sugar (50)



1H NMR (400 MHz, D_2O) 4.31 (d, $J = 7.9$ Hz, 1H), 3.88-3.82 (m, 2H), 3.70-3.65 (m, 2H), 3.61-3.54 (m, 3H), 3.44-3.39 (m, 1H), 3.24 (t, $J = 5.9$ Hz, 2H), 1.58-1.52 (m, 4H), 1.33-1.30 (m, 4H); ^{13}C NMR (100 MHz, D_2O): 102.75, 75.07, 72.83, 70.76, 70.39, 68.63, 60.90, 51.12, 28.59, 27.87, 25.67, 24.60. HRMS m/z calc'd for $C_{12}H_{26}O_6N$: 280.1760; found: 280.1773.

3.6.1. Glycan microarray details

3.6.1.1. Microarray fabrication

Arrays were printed on epoxide-derivatized corning slides as described for Array²³ with some modifications. Arrays were fabricated with NanoPrint LM 60 Microarray Printer (Arrayit, CA) on epoxide-derivatized slides (Corning) with 16 sub-array blocks on each slide. Glycoconjugates were distributed into one 384-well source plates using 4 replicate wells per sample and 8 μ l per well. Each glycoconjugates were prepared at 100 μ M in an optimized print buffer (300 mM phosphate buffer, pH 8.4). The arrays were printed with four 946MP3 pins (5 μ m tip, 0.25 μ l sample channel, \sim 100 μ m spot diameter; Arrayit, CA) with spot to spot spacing of 225 μ m. The humidity level in the arraying chamber was maintained at about 66% during printing. Printed slides were left on arrayer deck over-night, allowing humidity to drop to ambient levels (40-45%). Next, slides were packed, vacuum-sealed and stored in a desiccant chamber at room temperature (RT) until used.

3.6.1.2. Microarray binding assay

Slides were developed {23520510} and analyzed²³ as previously described. Slides were rehydrated with dH_2O and incubated for 30 min in a staining dish with 50 $^\circ$ C pre-warmed 0.05 M ethanolamine in 0.1 M Tris, pH 9.0 to block the remaining reactive epoxy groups on the slide surface, then washed with 50 $^\circ$ C pre-warmed dH_2O . Slides were centrifuged at 200 \times g for 3 min

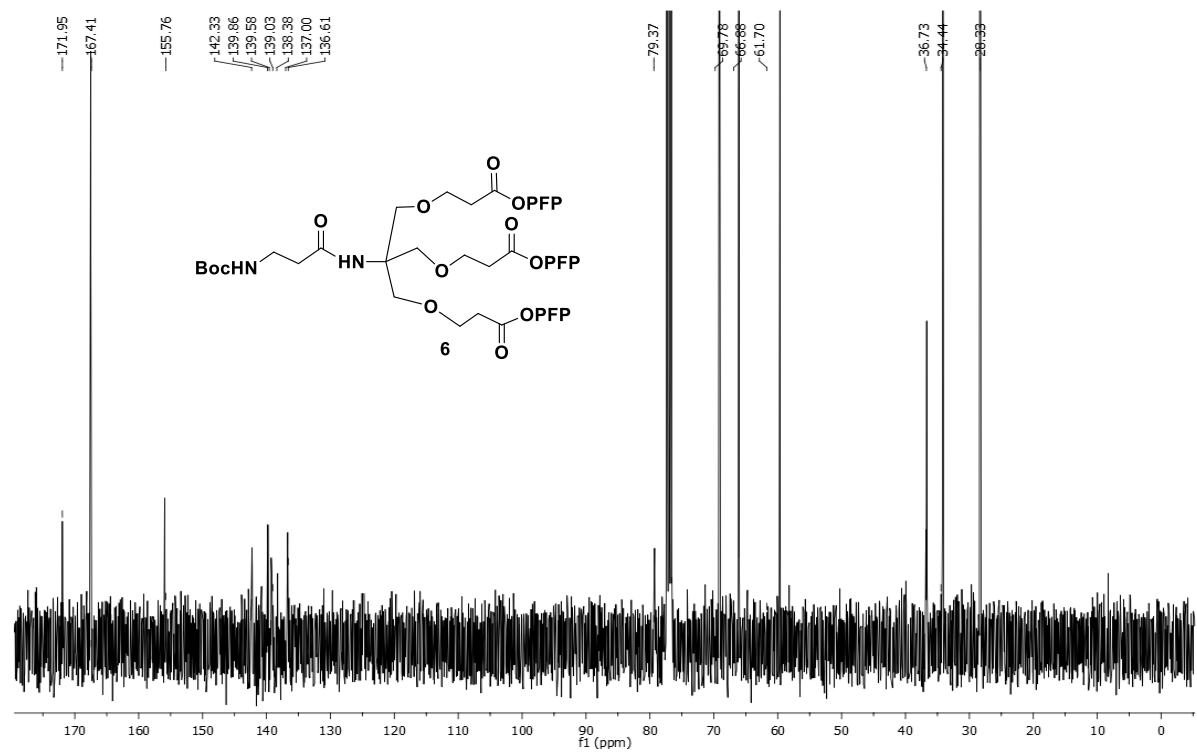
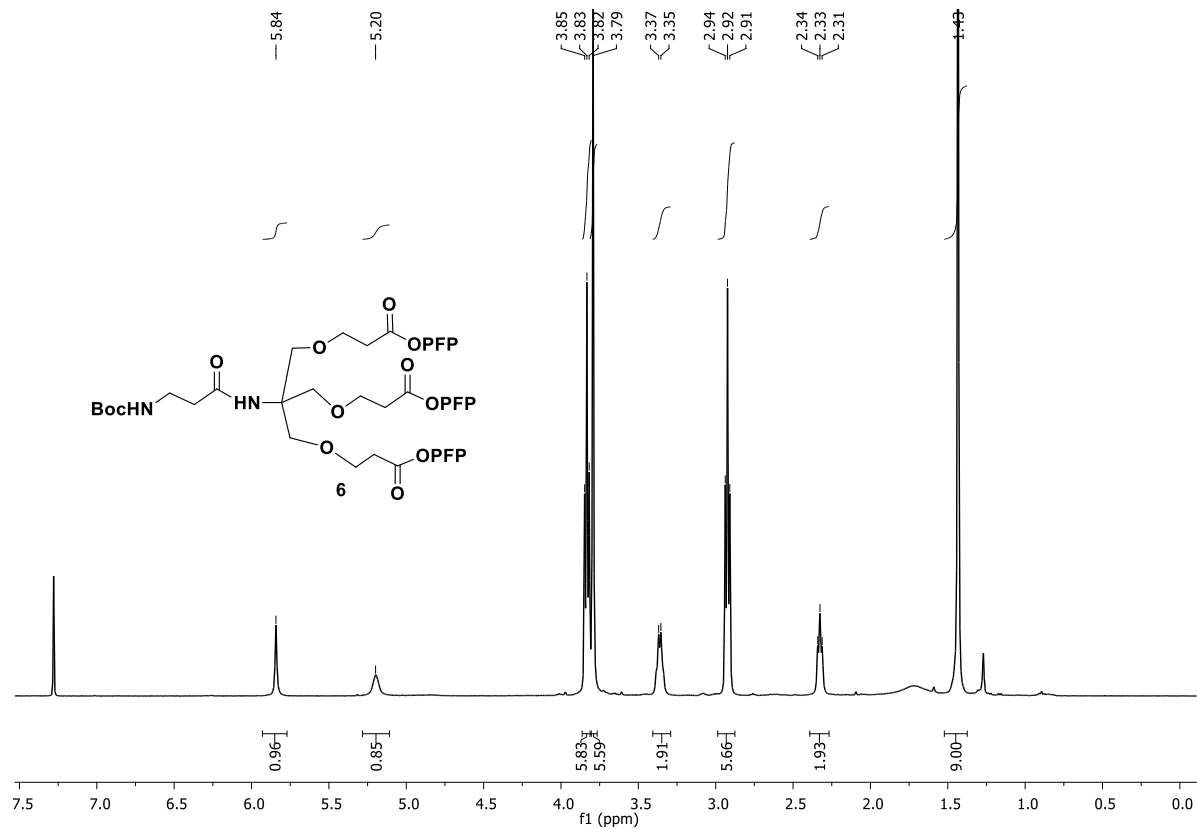
then fitted with ProPlate™ Multi-Array 16-well slide module (Invitrogen) to divide into the sub-arrays (blocks). Slides were washed with PBST (PBS pH 7.4, 0.1% Tween-20), aspirated and blocked with 200 µl/sub-array of blocking buffer (PBS pH 7.4, 1% ovalbumin; PBS/OVA) for 1 h at RT with gentle shaking. Next, ConA/PNA/GNA-FITC conjugates were aspirated and 200 µl/block of primary detection was added. Primary detections were incubated with gentle shaking for 2h at RT. Slides were washed three times with PBST then with PBS for 5 min/wash with shaking. MultiArray slide module and immediately dipping slide in a staining dish with dH₂O for 10 min with shaking, then centrifuged at 200×g for 5 min. Dry slides were vacuum-sealed and stored in dark until scanning. 24 Array slide processed and processed slides were scanned and analyzed as described²³ at 10 µm resolution with a Genepix 4000B microarray scanner (Molecular Devices) using 350 gain. Image analysis was carried out with Genepix Pro 6.0 analysis software (Molecular Devices). Spots were defined as circular features with a variable radius as determined by the Genepix scanning software. Local background subtraction was performed. Data was analyzed by Excel using pivot tables.

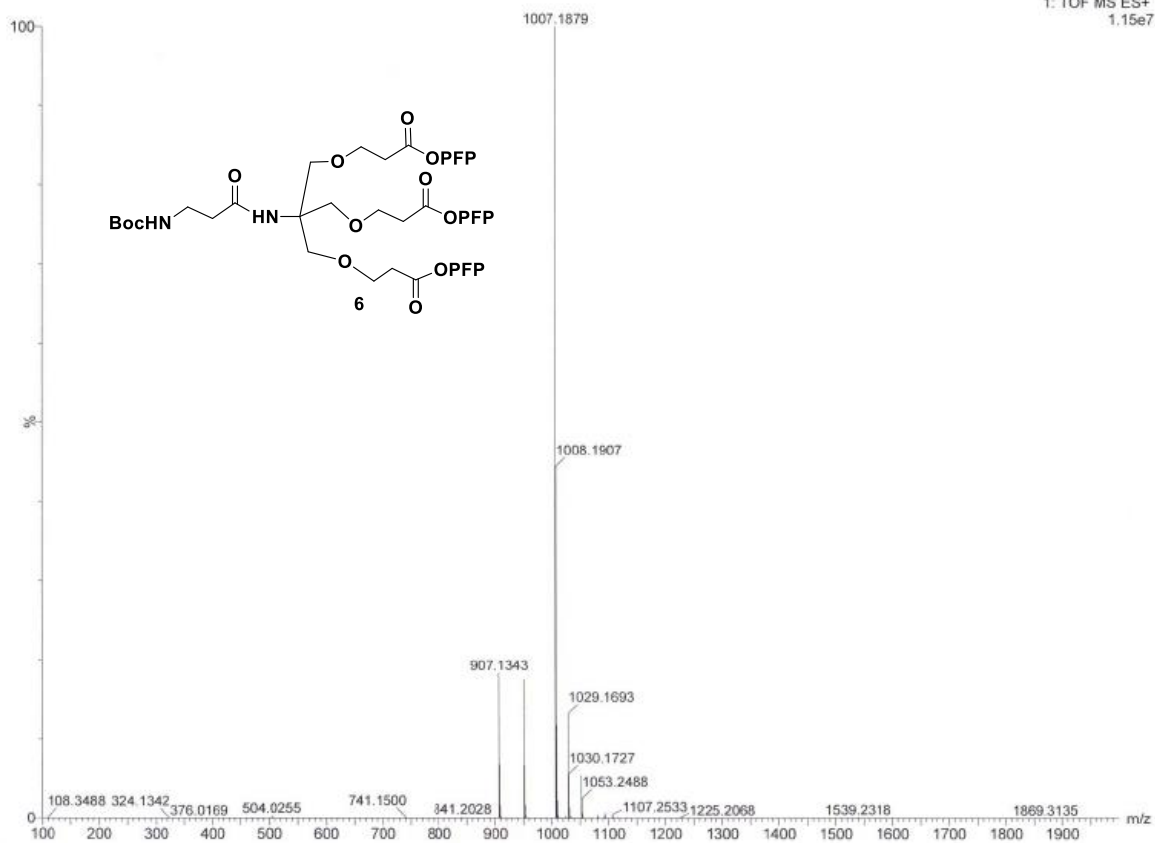
3.7. Reference

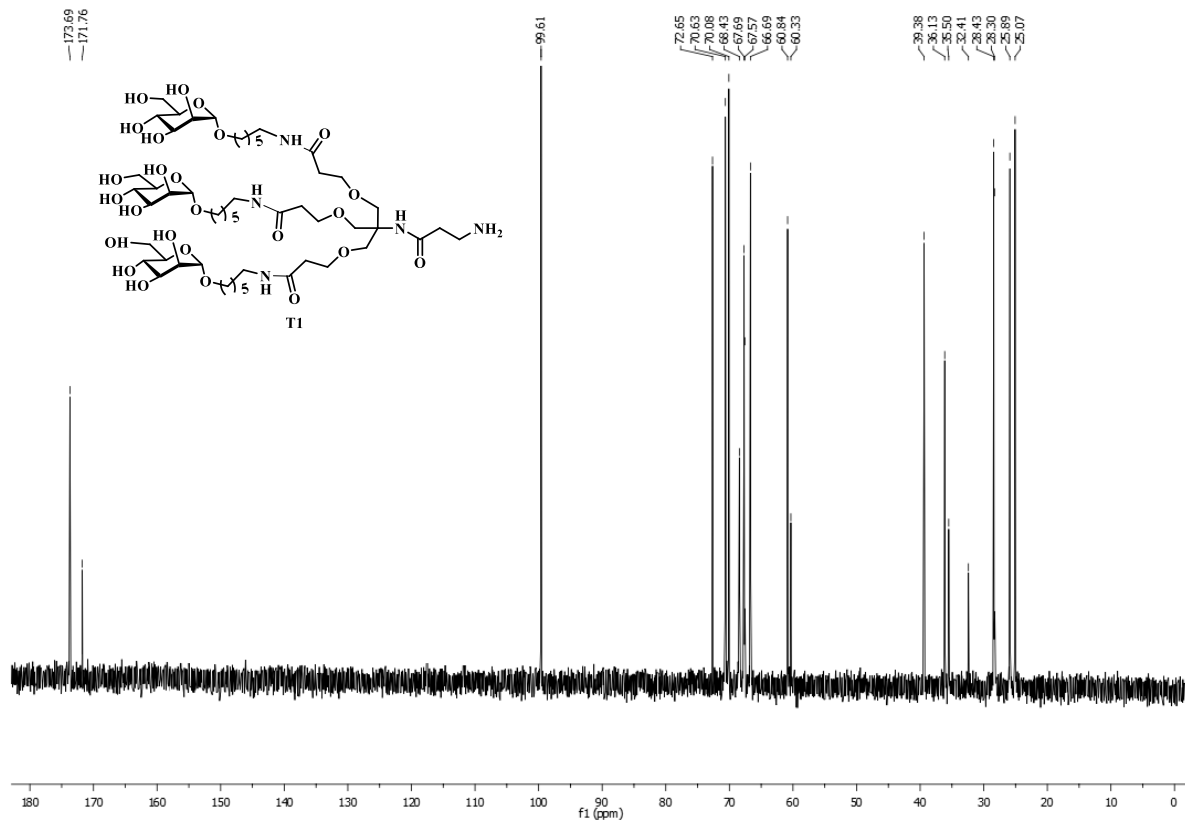
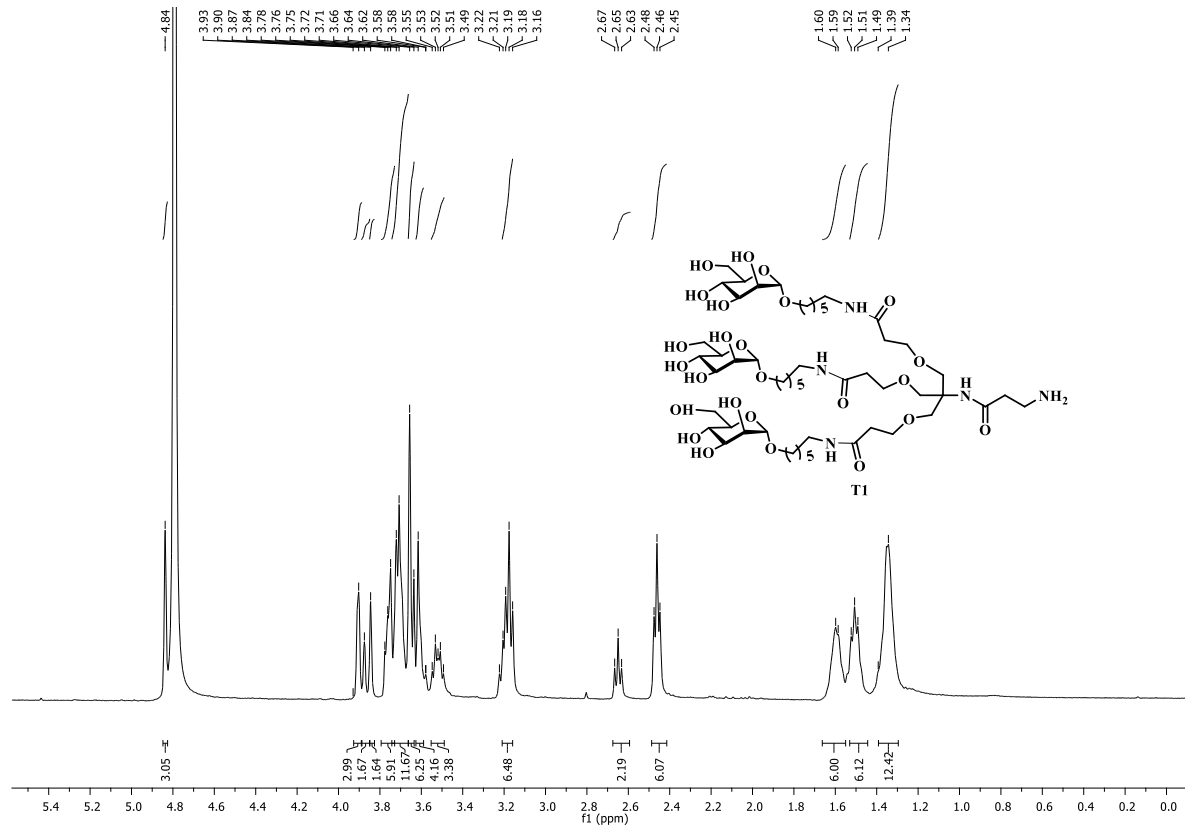
1. N. Sharon, *Acta. Anat. (Basel)*, 1998, **161**, 7-17.
2. B. Alberts, Johnson, A., Lewis, J., Raff, M., Roberts, K. and Walter, P. *Molecular biology of the cell*. Garland Science, Tylor & Francis Group, New York, 4th edition, 2002.
3. D. Wang, S. Liu, B. J. Trummer, C. Deng and A. Wang, *Nat. Biotechnol.*, 2002, **20**, 275-281.
4. E. O. G. A. Varki et al., 2nd Edition, 2009.
5. C. R. Bertozzi and L. L. Kiessling, *Science*, 2001, **291**, 2357-2364.
6. W. B. Turnbull and J. F. Stoddart, *J. Biotechnol.*, 2002, **90**, 231-255.
7. C. Fasting, C. A. Schalley, M. Weber, O. Seitz, S. Hecht, B. Kokschi, J. Dervede, C. Graf, E. W. Knapp and R. Haag, *Angew. Chem. Int. Ed. Engl.*, 2012, **51**, 10472-10498.
8. R. Roy and T. C. Shiao, *Chem Soc Rev*, 2015, **44**, 3924-394.
9. L. L. Kiessling and J. C. Grim, *Chem Soc Rev*, 2013, **42**, 4476-4491.
10. Martinez, C. Ortiz Mellet and J. M. Garcia Fernandez, *Chem. Soc. Rev.*, 2013, **42**, 4746.

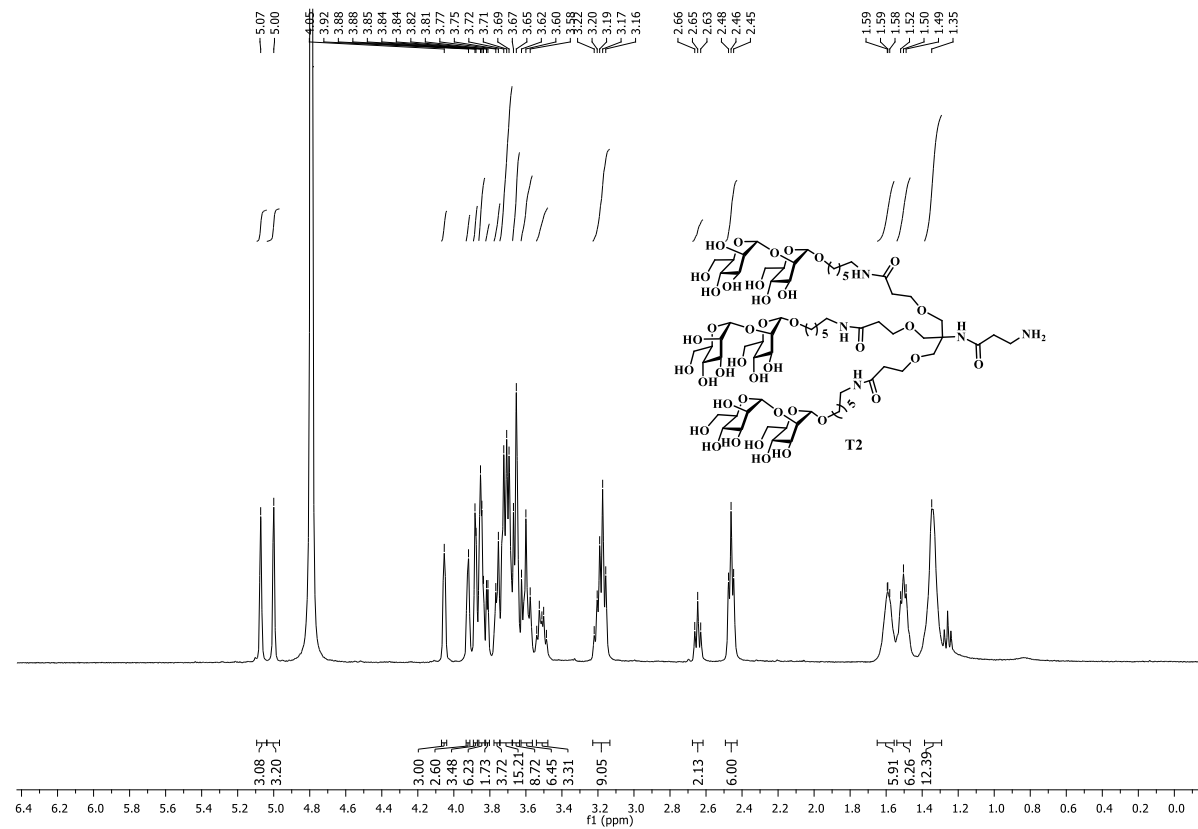
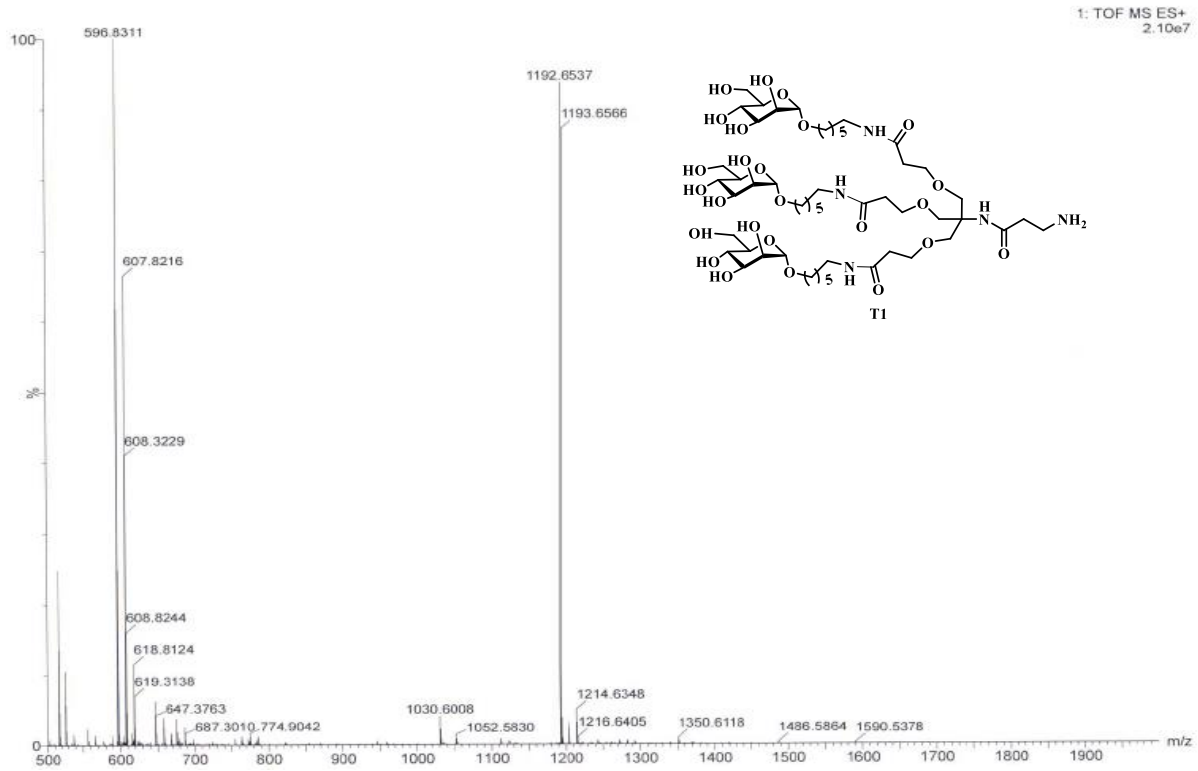
11. M. Delbianco, P. Bharate, S. Varela-Aramburu and P. H. Seeberger, *Chem. Rev.*, 2016, **116**, 1693.
12. Z. Qi, P. Bharate, C. H. Lai, B. Ziem, C. Böttcher, A. Schulz, F. Beckert, B. Hatting, R. Mülhaupt, P. H. Seeberger, R. Haag, *Nano Lett.*, 2015, **15**, 6051-6157.
13. S. Sangabathuni, R. Vasudeva Murthy, P. M. Chaudhary, M. Surve, A. Banerjee and R. Kikkeri, *Nanoscale*, 2016, **8**, 12729-12735.
14. A. Patel and T. K. Lindhorst, *Eur. J. Org. Chem.*, 2002, **2002**, 79-86.
15. T. K. Lindhorst, K. Bruegge, A. Fuchs and O. Sperling, *Beilstein J. Org. Chem.*, 2010, **6**, 801-809.
16. O. Ramstrom and J.M. Lehn, *ChemBioChem*, 2000, **1**, 41-48.
17. M. Gomez-Garcia, J. M. Benito, R. Gutierrez-Gallego, A. Maestre, C. O. Mellet, J. M. G. Fernandez and J. L. J. Blanco, *Org. Biomol. Chem.*, 2010, **8**, 1849-1860.
18. M. Gomez-Garcia, J. M. Benito, A. P. Butera, C. Ortiz Mellet, J. M. Garcia Fernandez and J. L. Jimenez Blanco, *J. Org. Chem.*, 2012, **77**, 1273-1288.
19. O. M. Munoz, F. Perez-Balderas, J. Morales-Sanfrutos, F. Hernandez-Mateo, J. Isac-Garcia and F. Santoyo-Gonzalez, *Eur. J. Org. Chem.* 2009, 2454-2473.
20. R. Kikkeri, Laila H. Hossain and P. H. Seeberger, *Chem. Commun.* 2008, 2127-2129.
21. H. J. Schuster, B. Vijayakrishnan, B. G. Davis, *Carbohydr. Res.*, 2015, **403**, 135-141.
22. V. Padler-Karavani, X. Song, H. Yu, N. Hurtado-Ziola, S. Huang, S. Muthana, H. A. Chokhawala, J. Cheng, A. Verhagen, M. A. Langereis, R. Kleene, M. Schachner, R. J. De Groot, Y. Lasanajak, H. Matsuda, R. Schwab, X. Chen, D. F. Smith, R. D. Cummings and A. Varki, *J. Biol. Chem.*, 2012, **287**, 22593-22608.
23. V. P. Karavani, N. H. Ziola N, M. Pu, H. Yu, S. Huang, S. Muthana, H. A. Chokhawala, H. Cao, P. Secrest, D. F. Morvinski, O. Singer, D. Ghaderi, I. M. Verma, Y. T. Liu, K. Messer, X. Chen, A. Varki and Schwab R. *Cancer Res.* 2011, **71**, 3352-63.

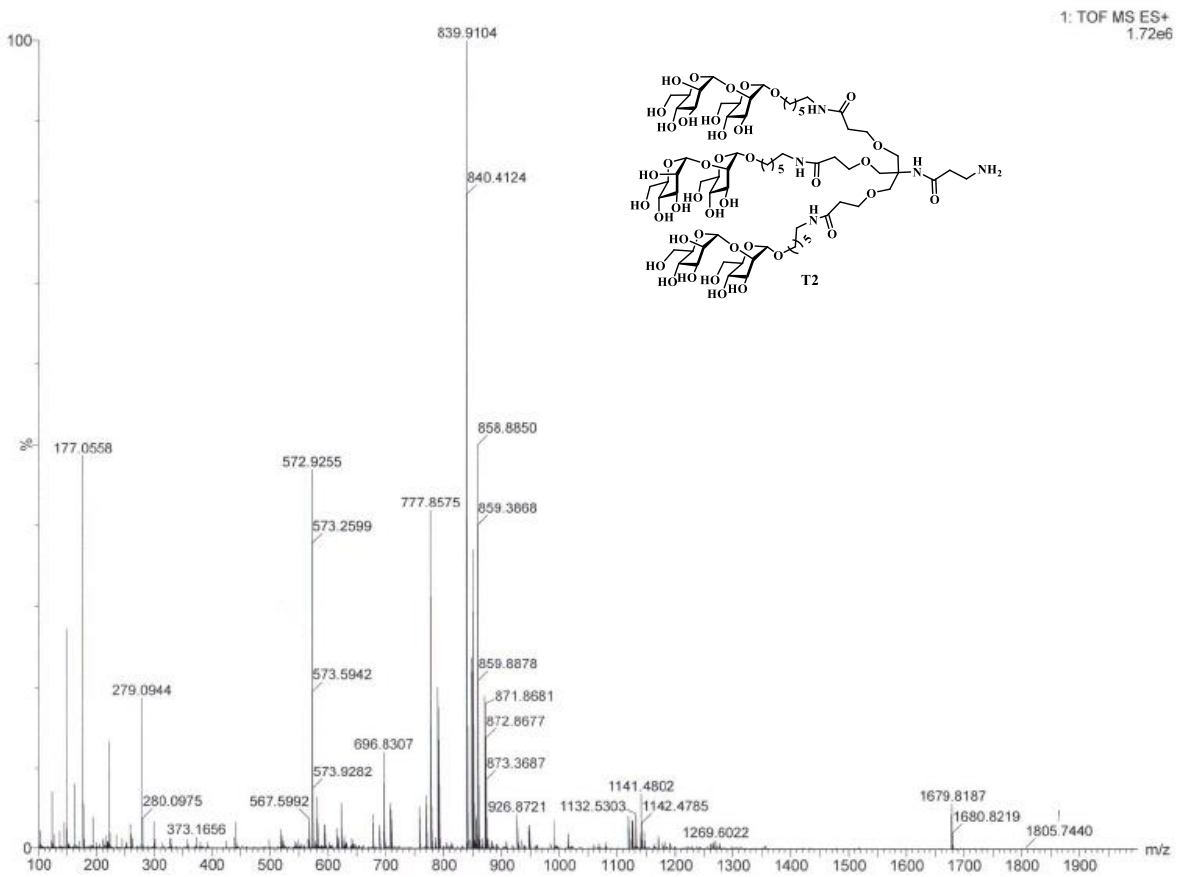
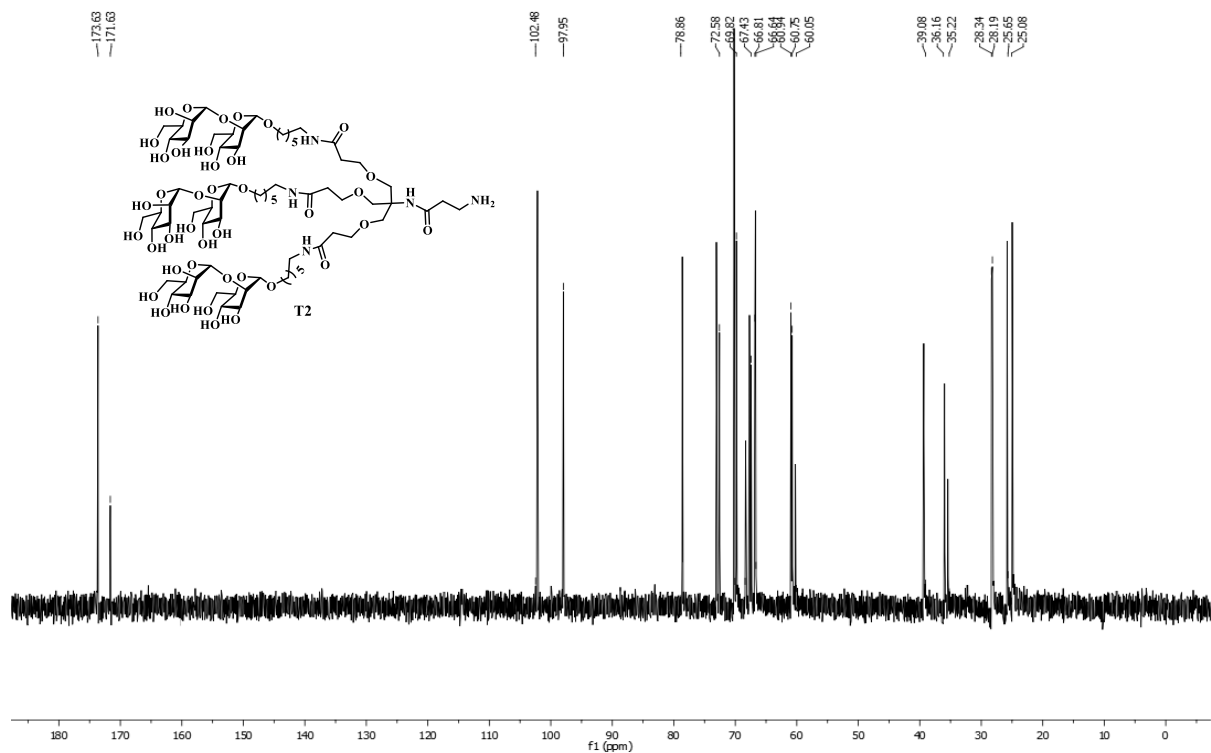
3.8. NMR and HRMS of compounds

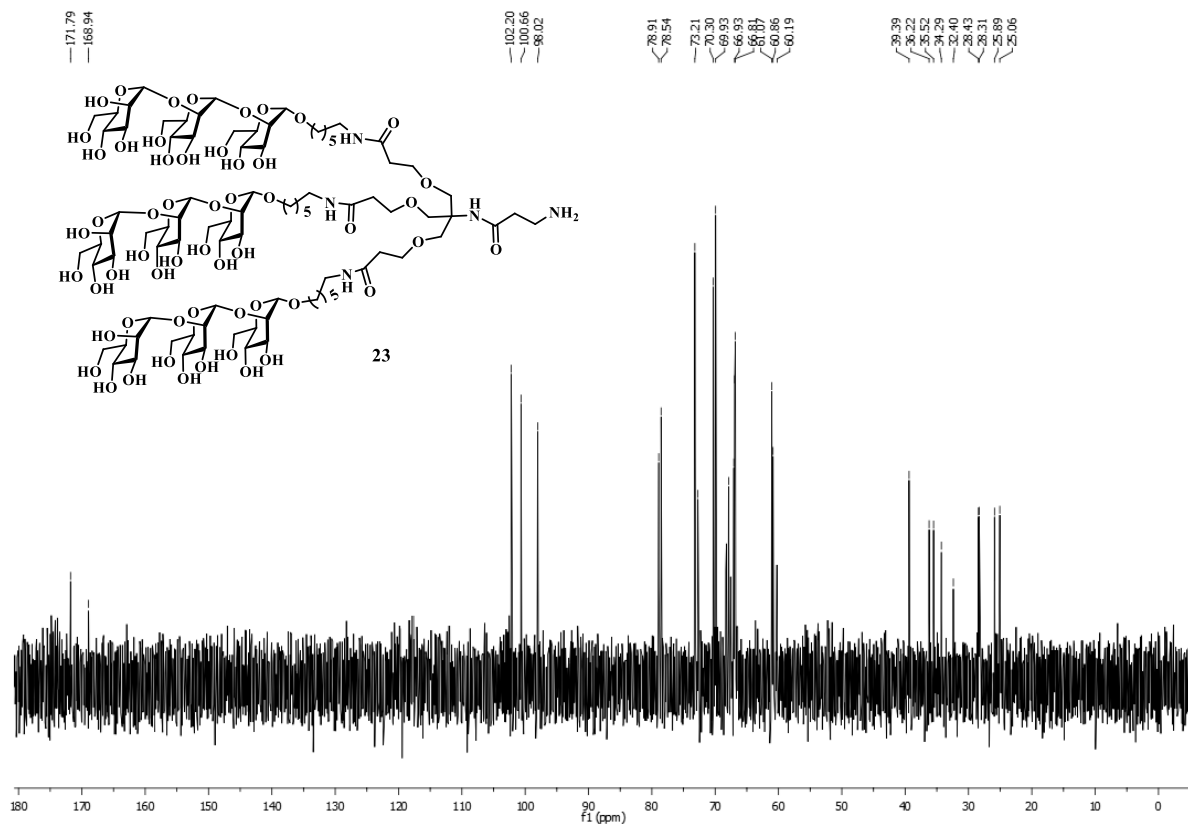
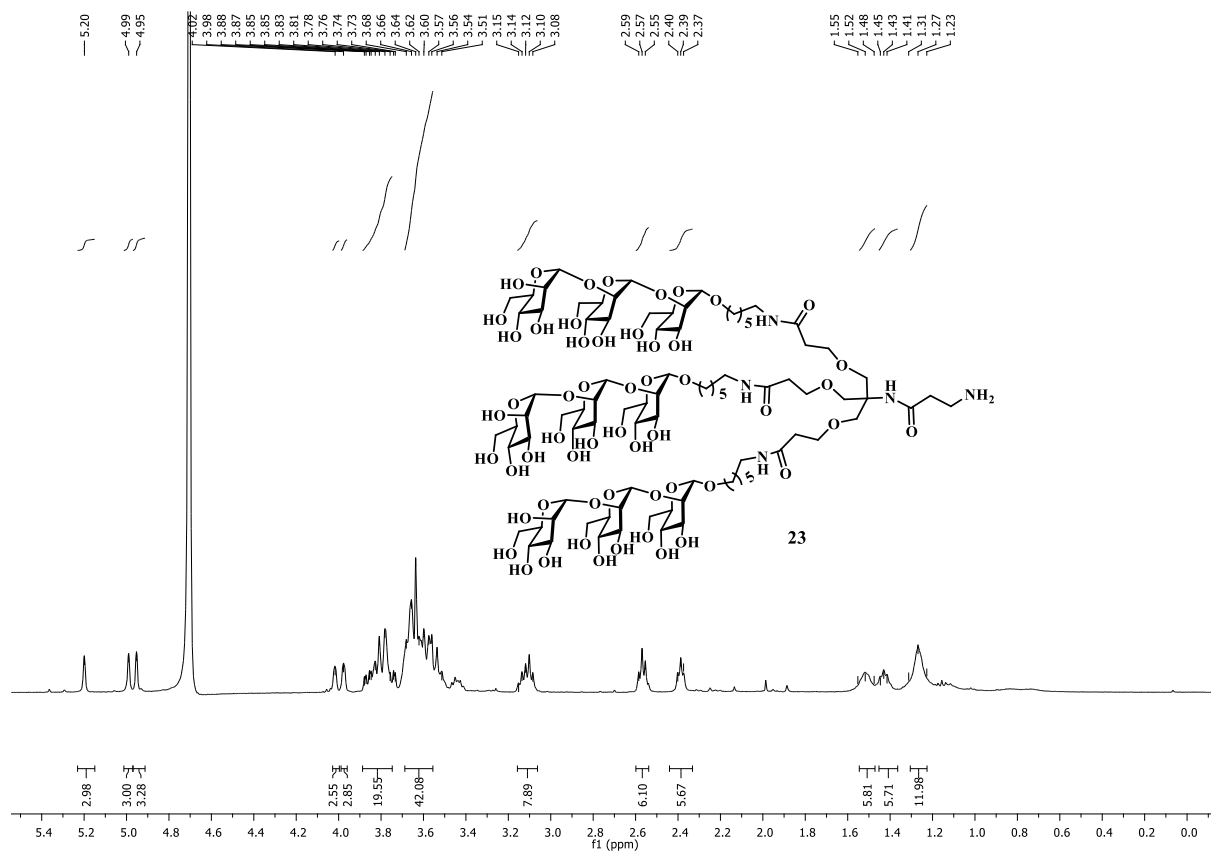


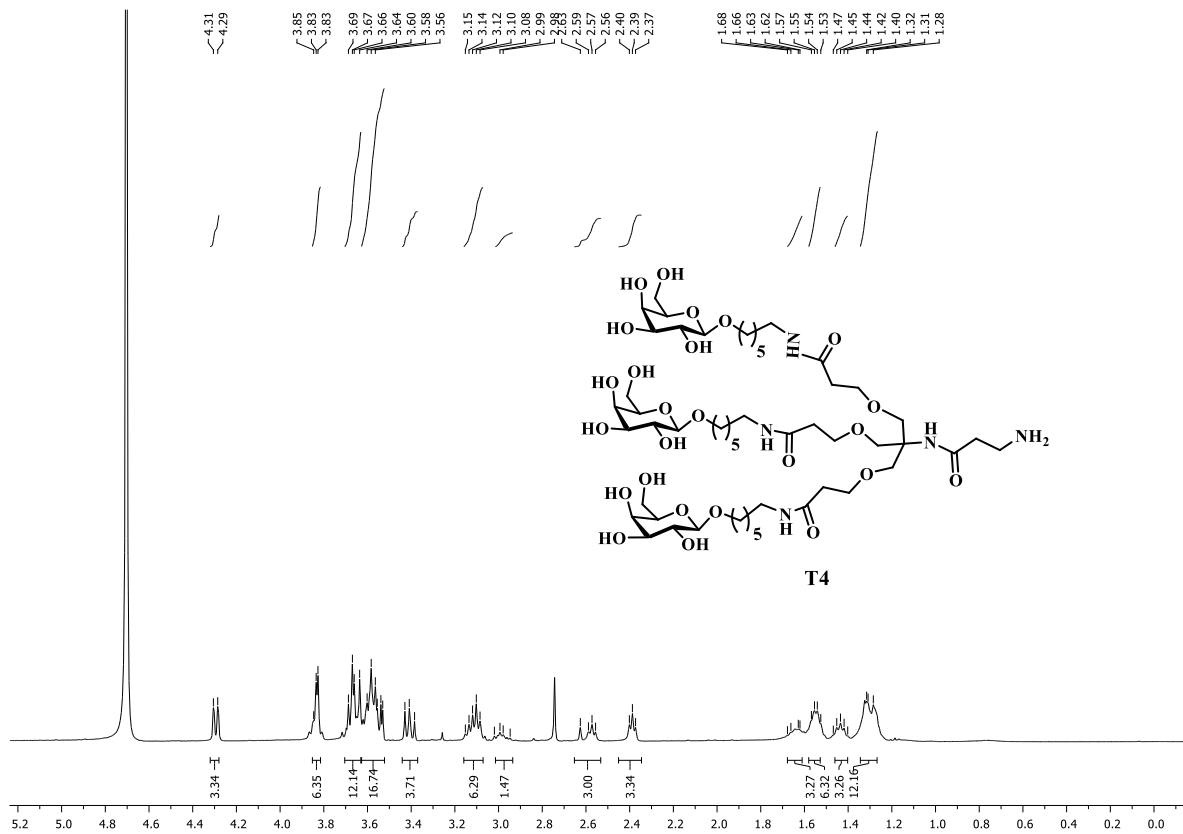
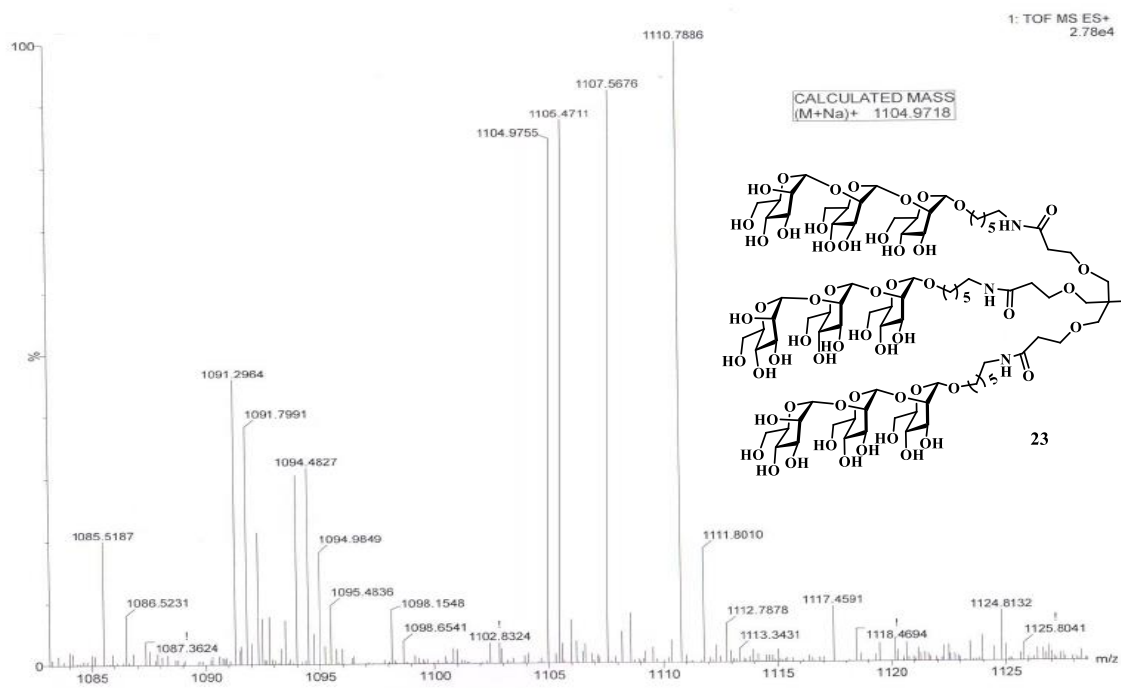


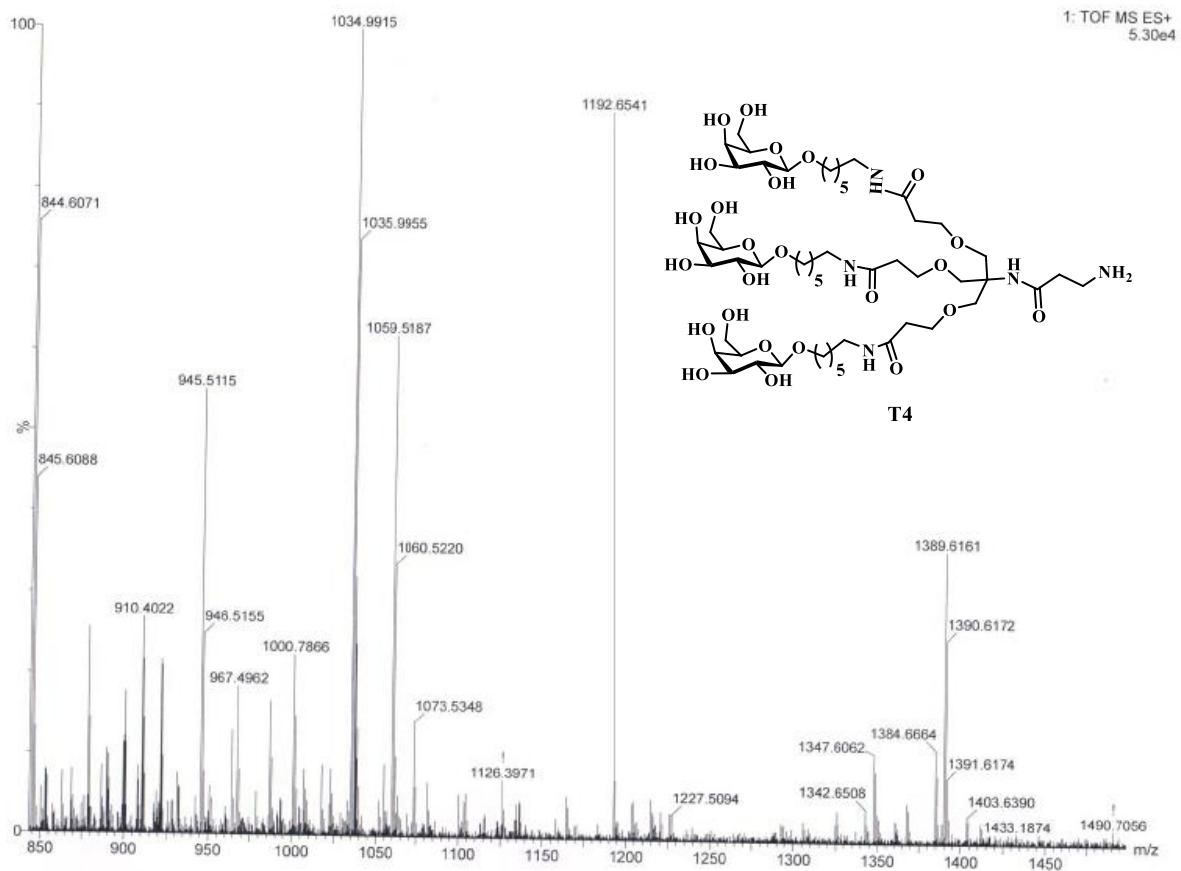
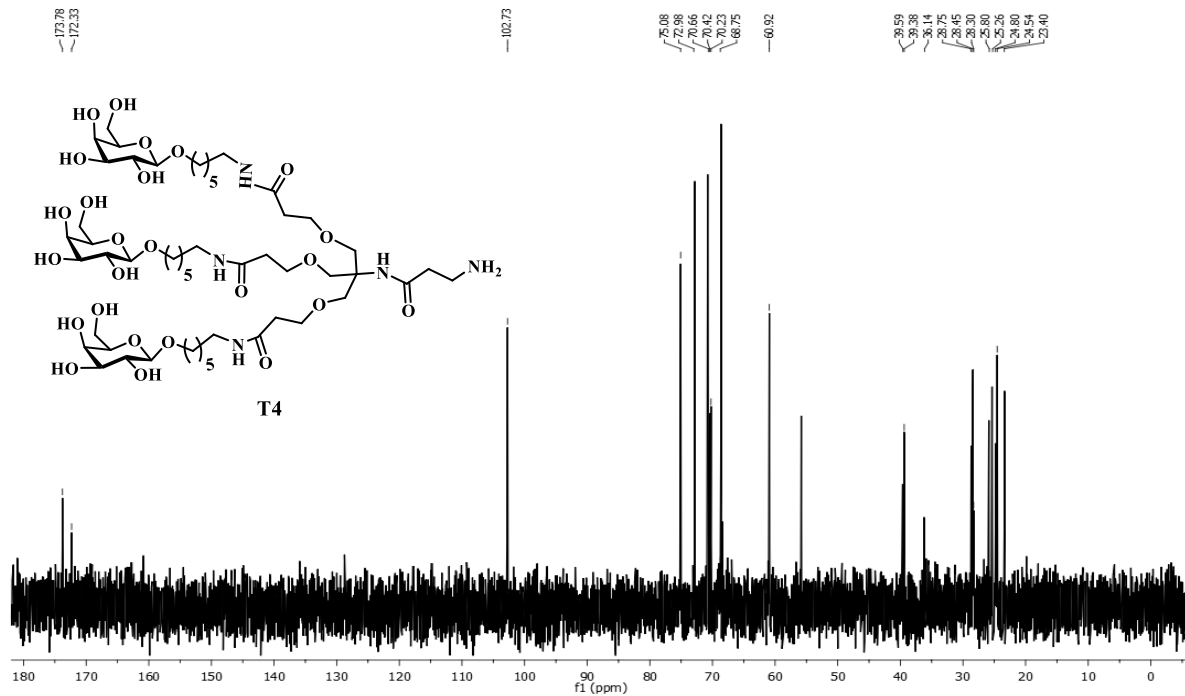


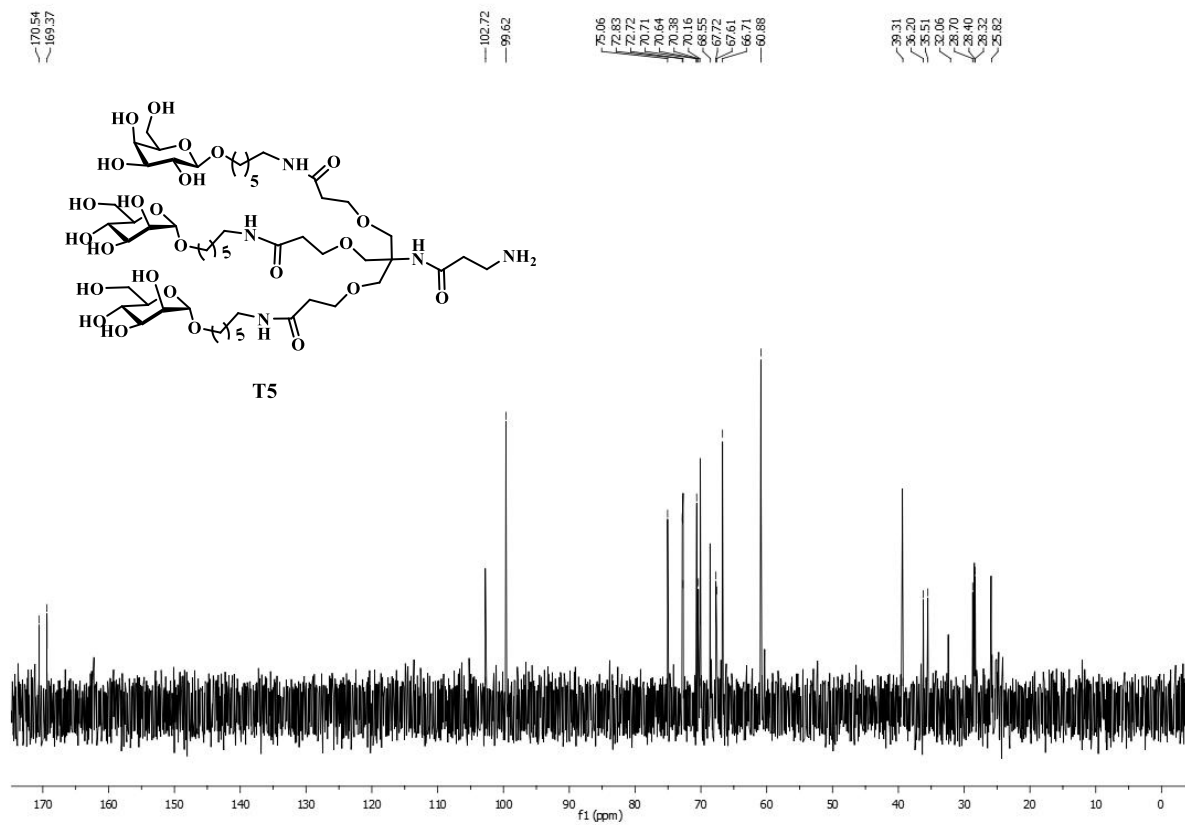
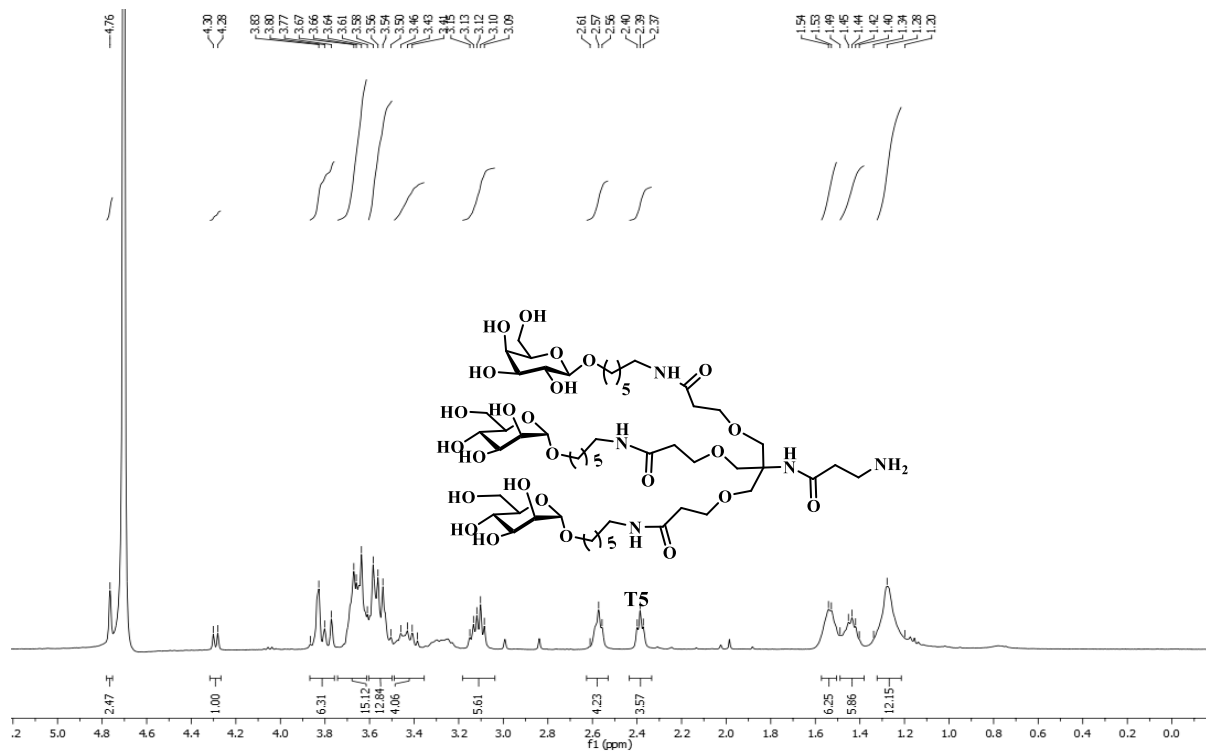


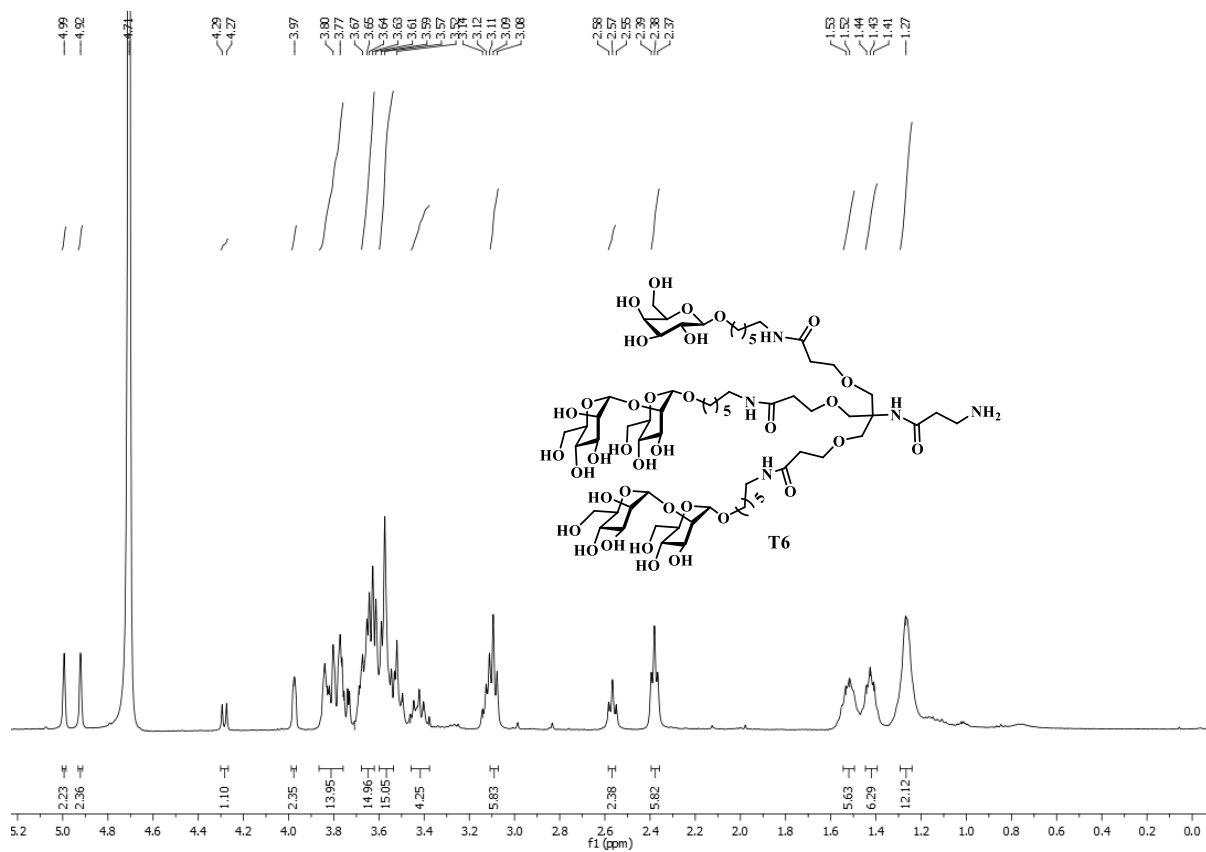
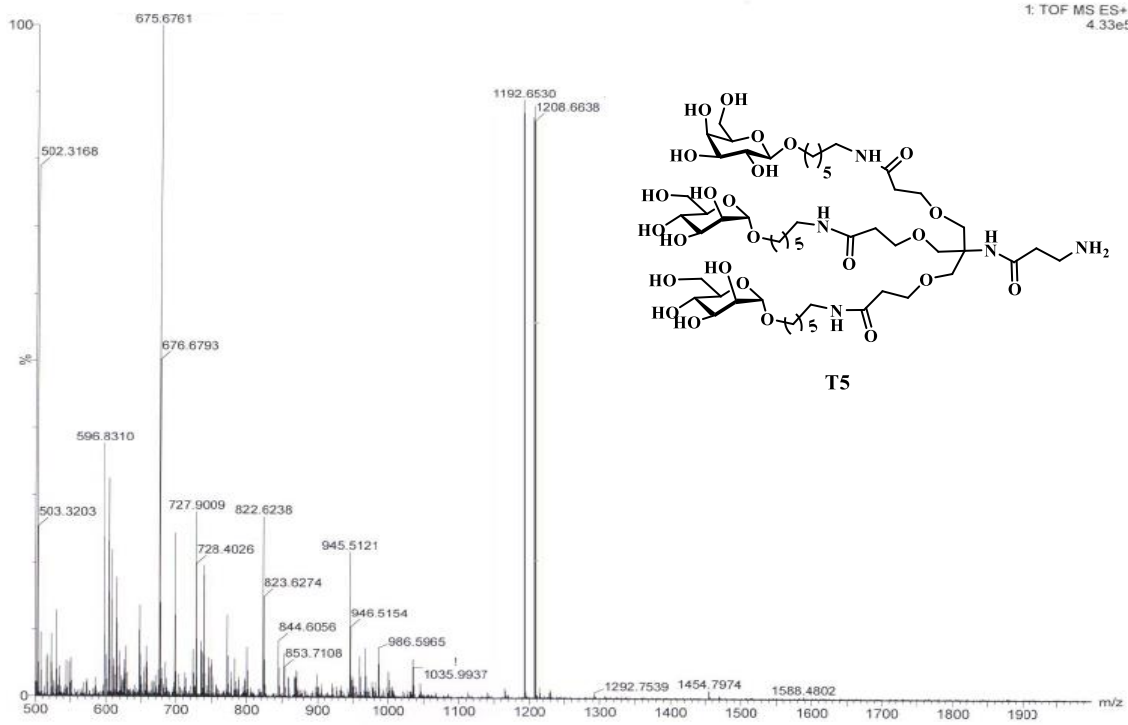


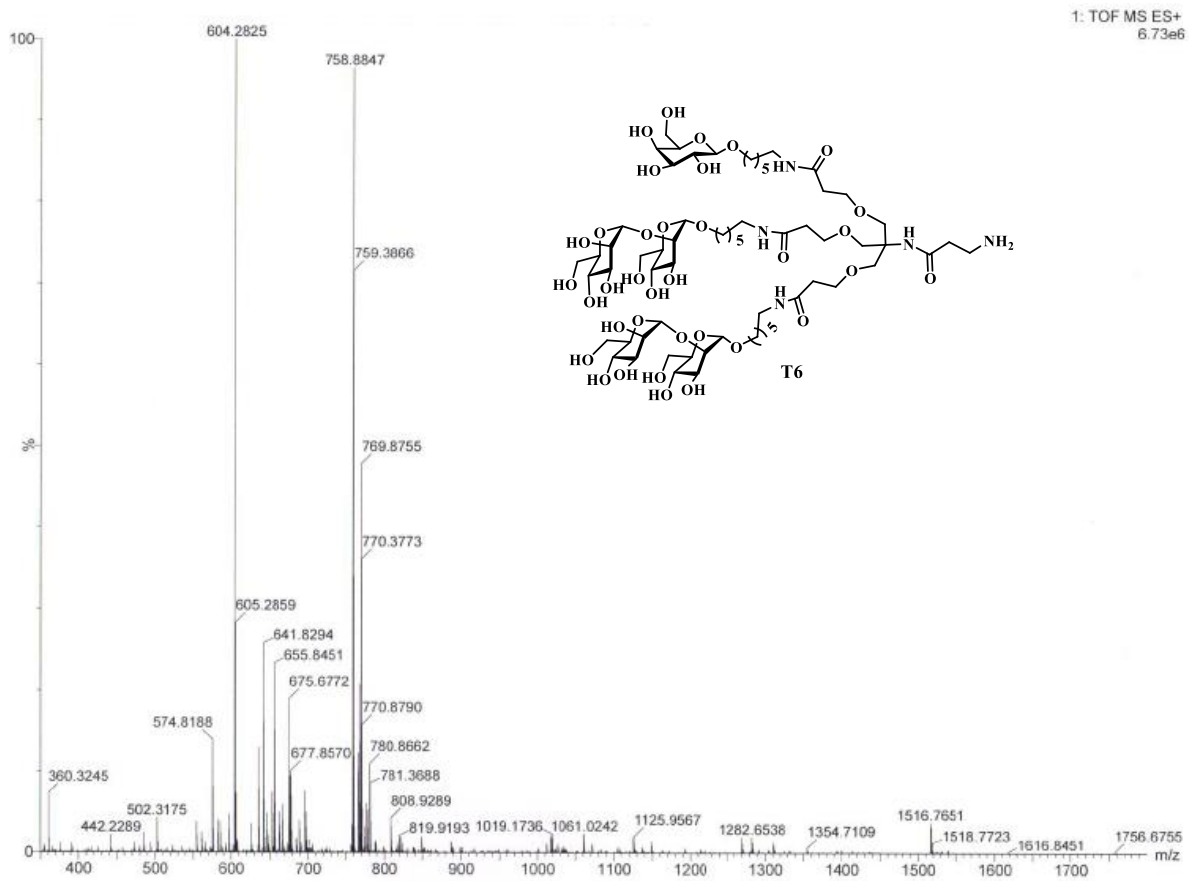
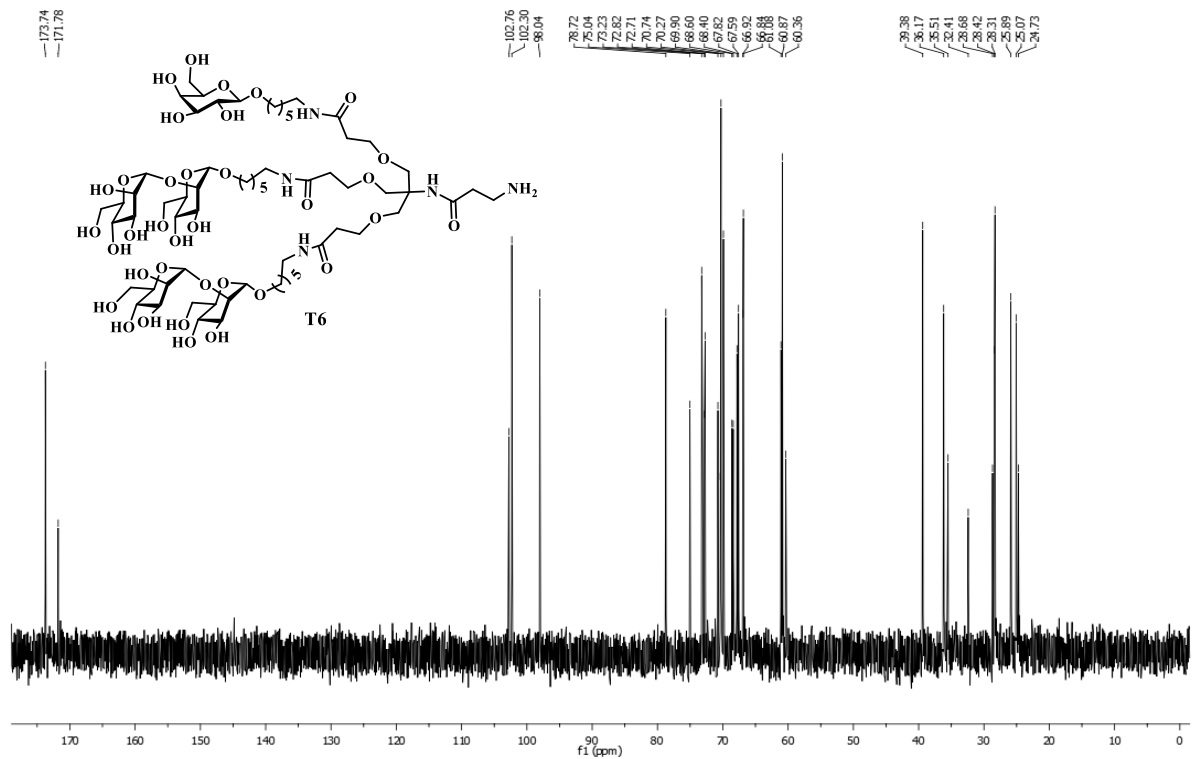


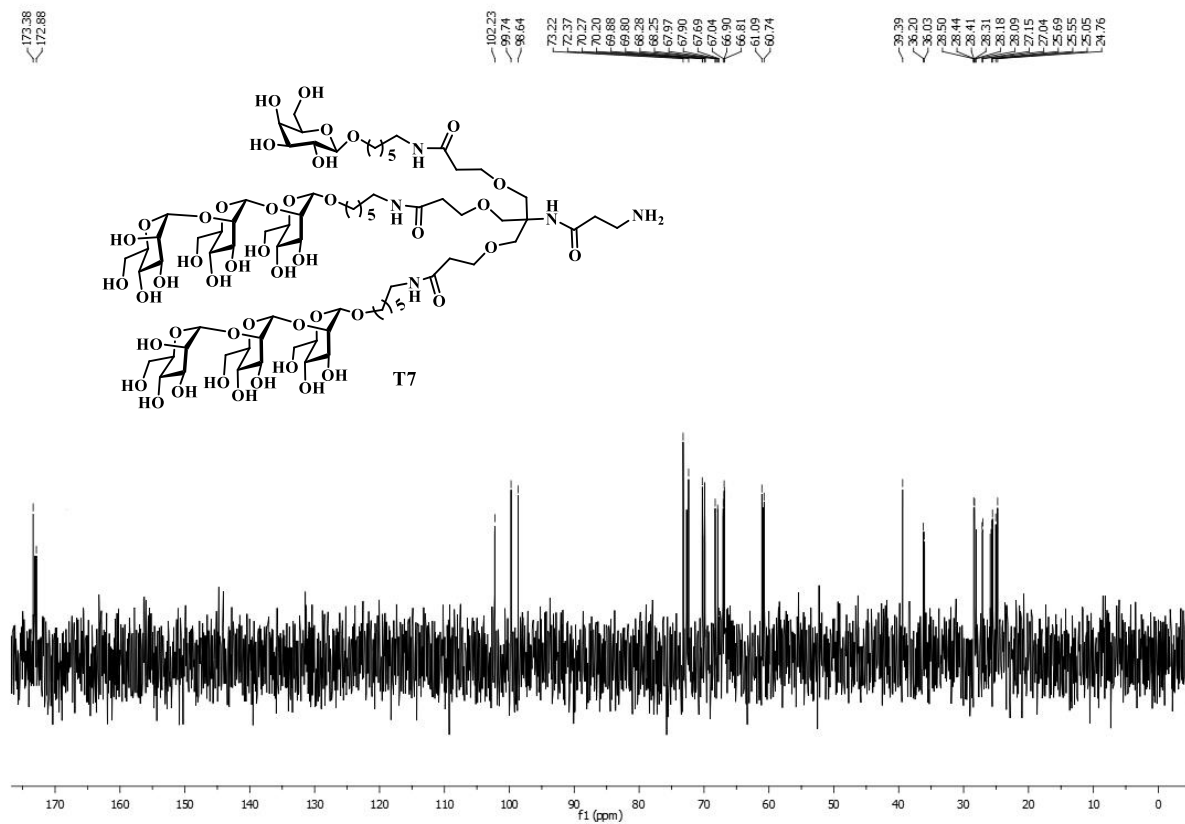
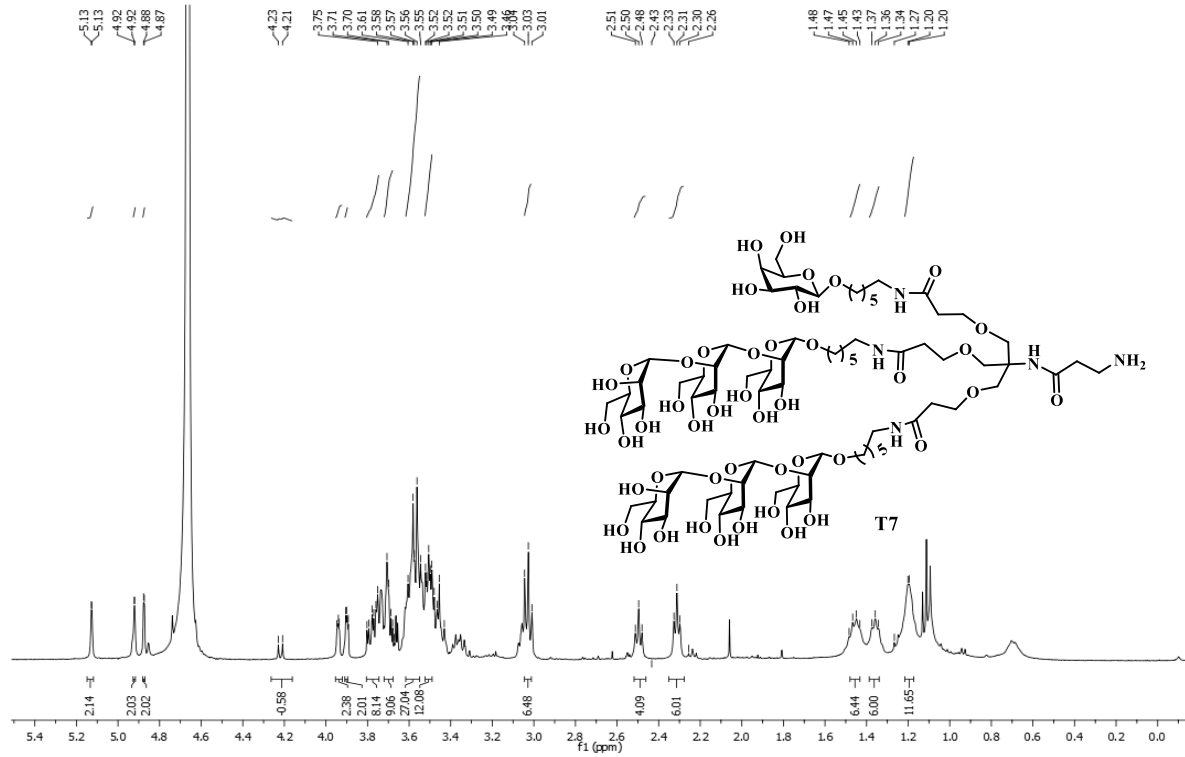


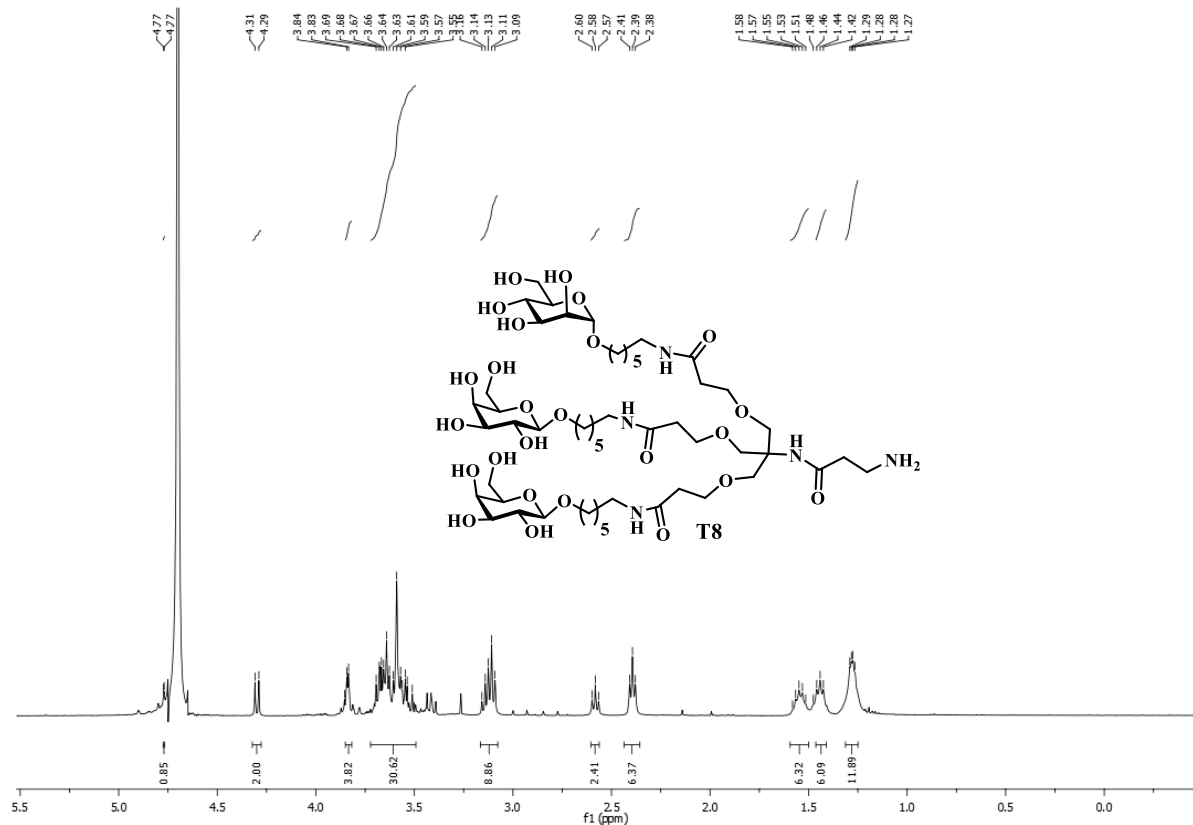
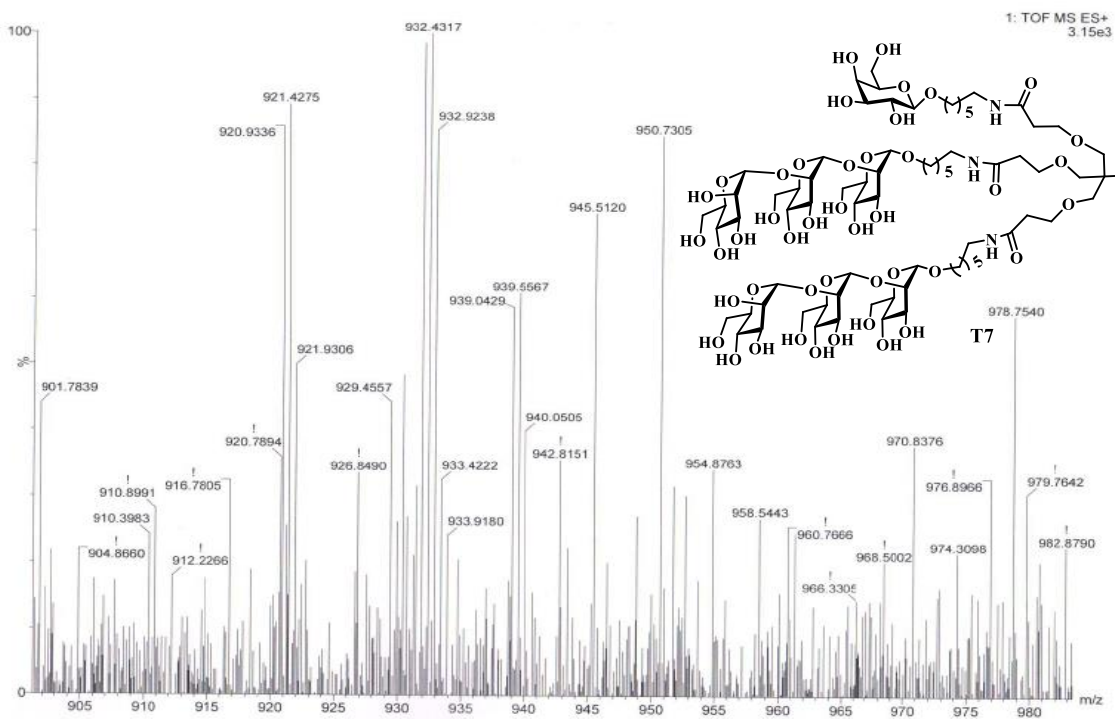


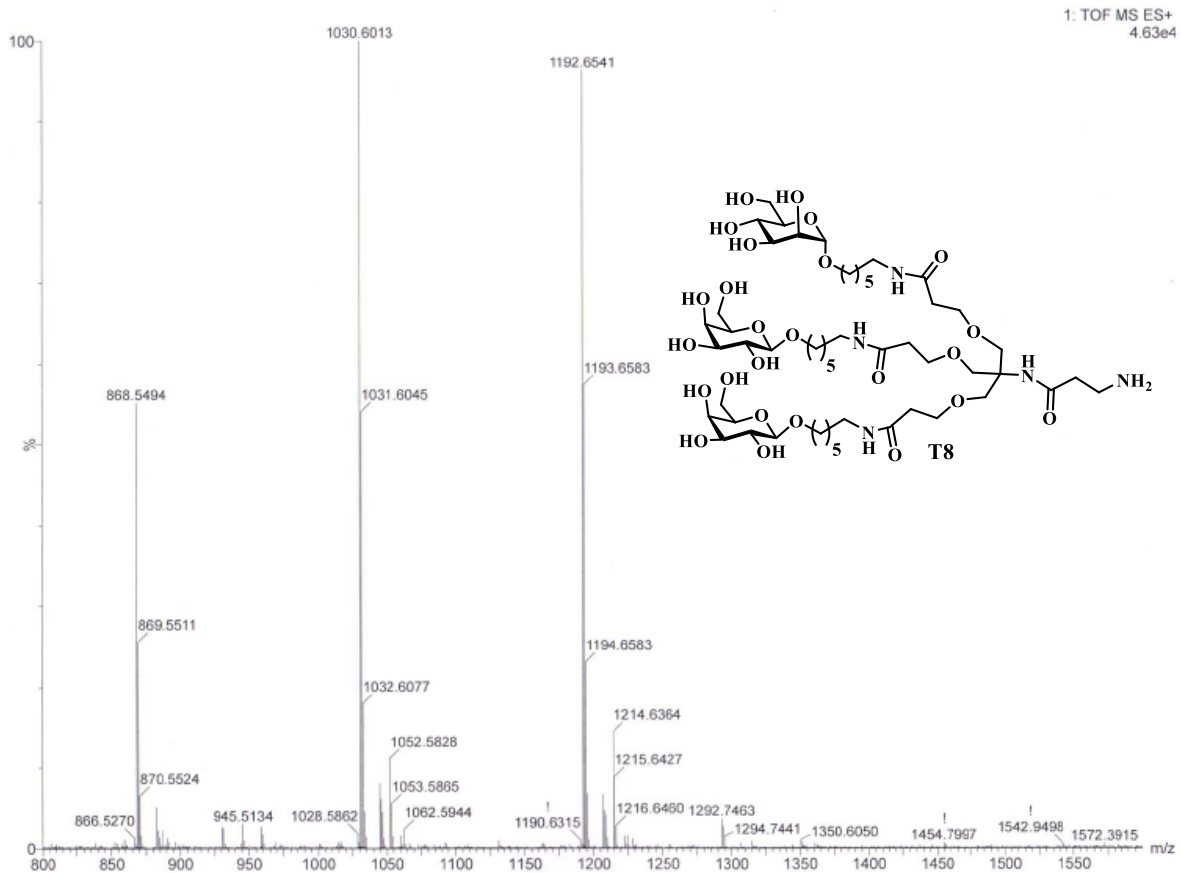
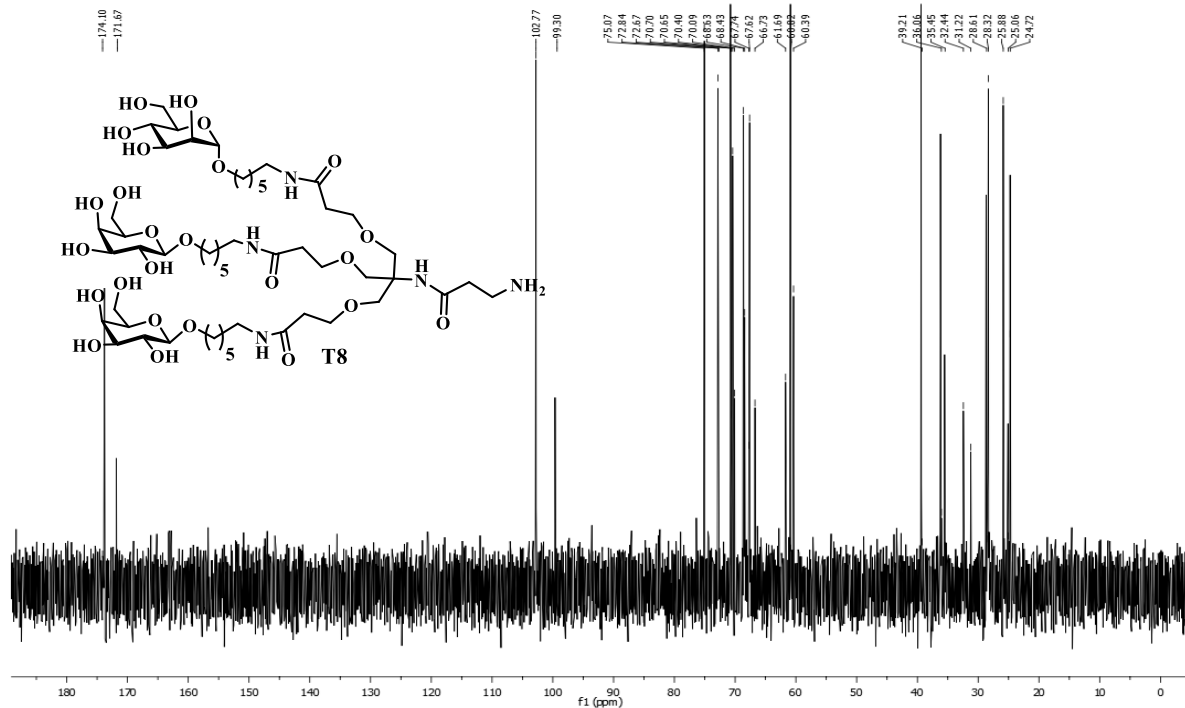


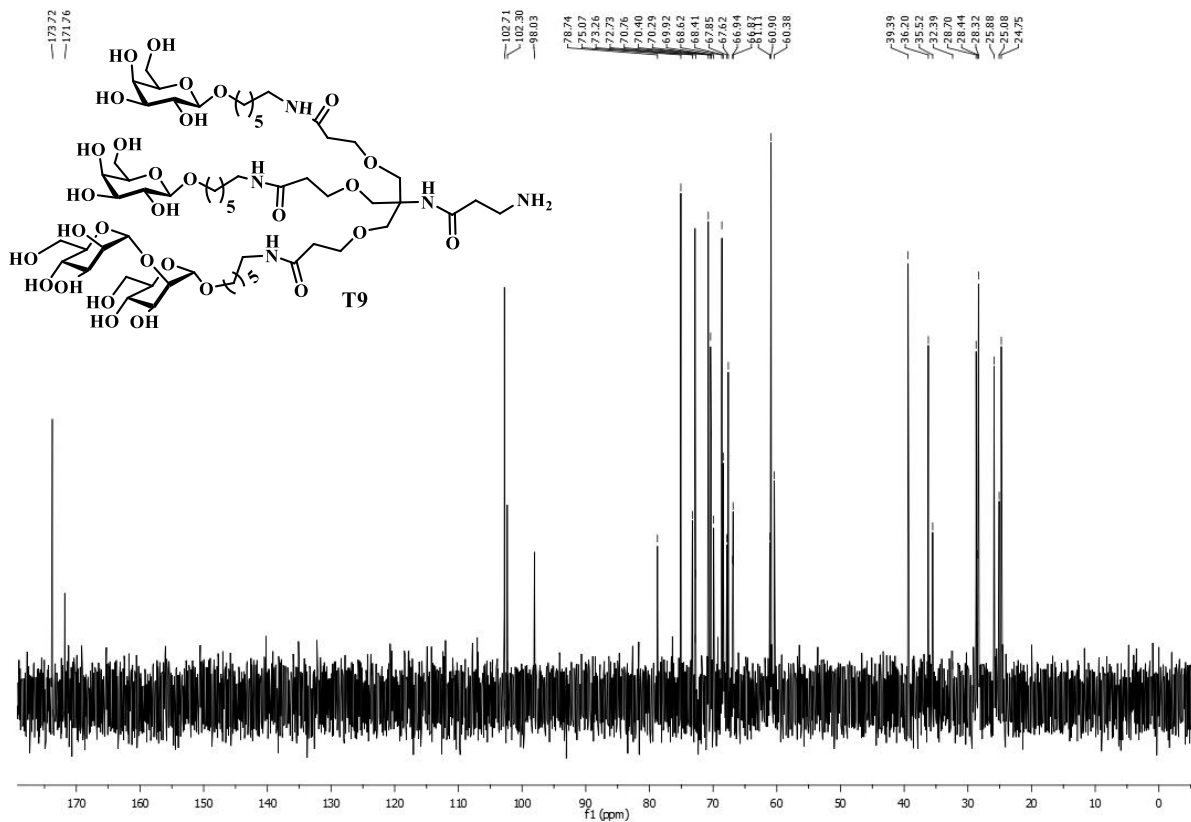
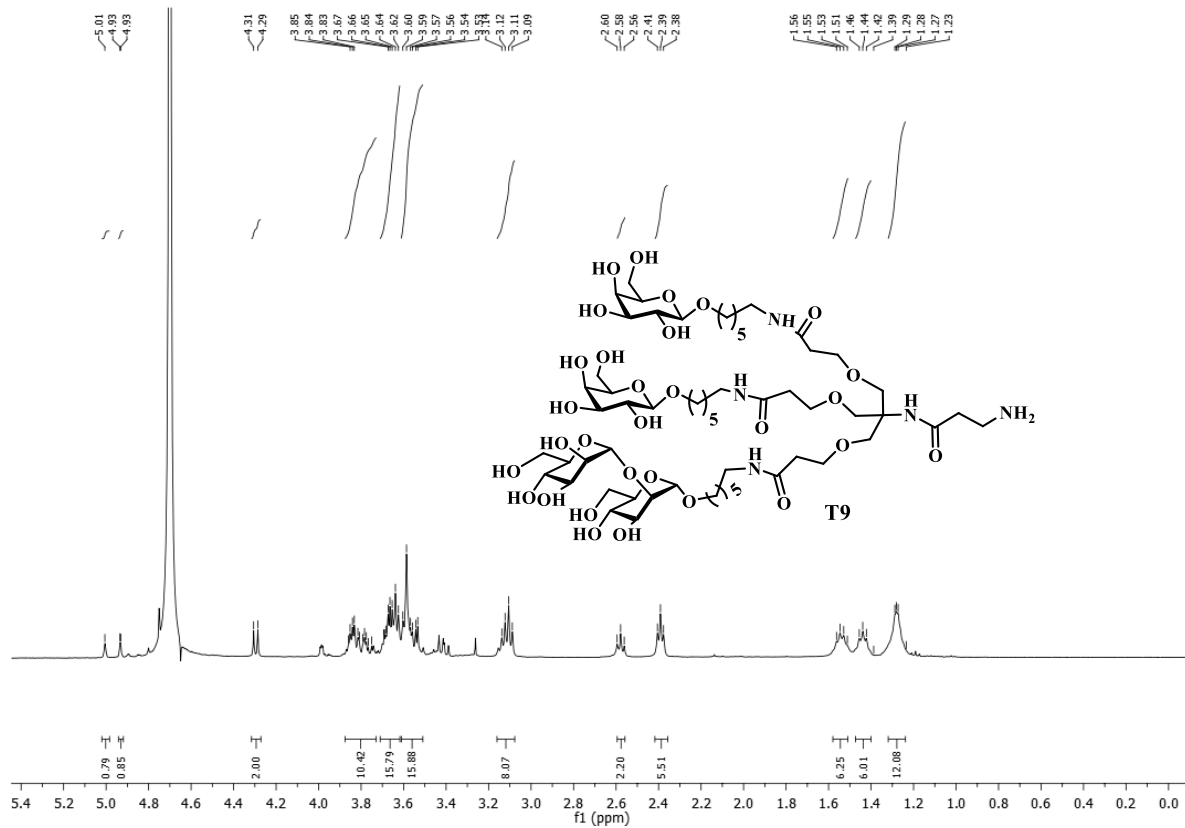


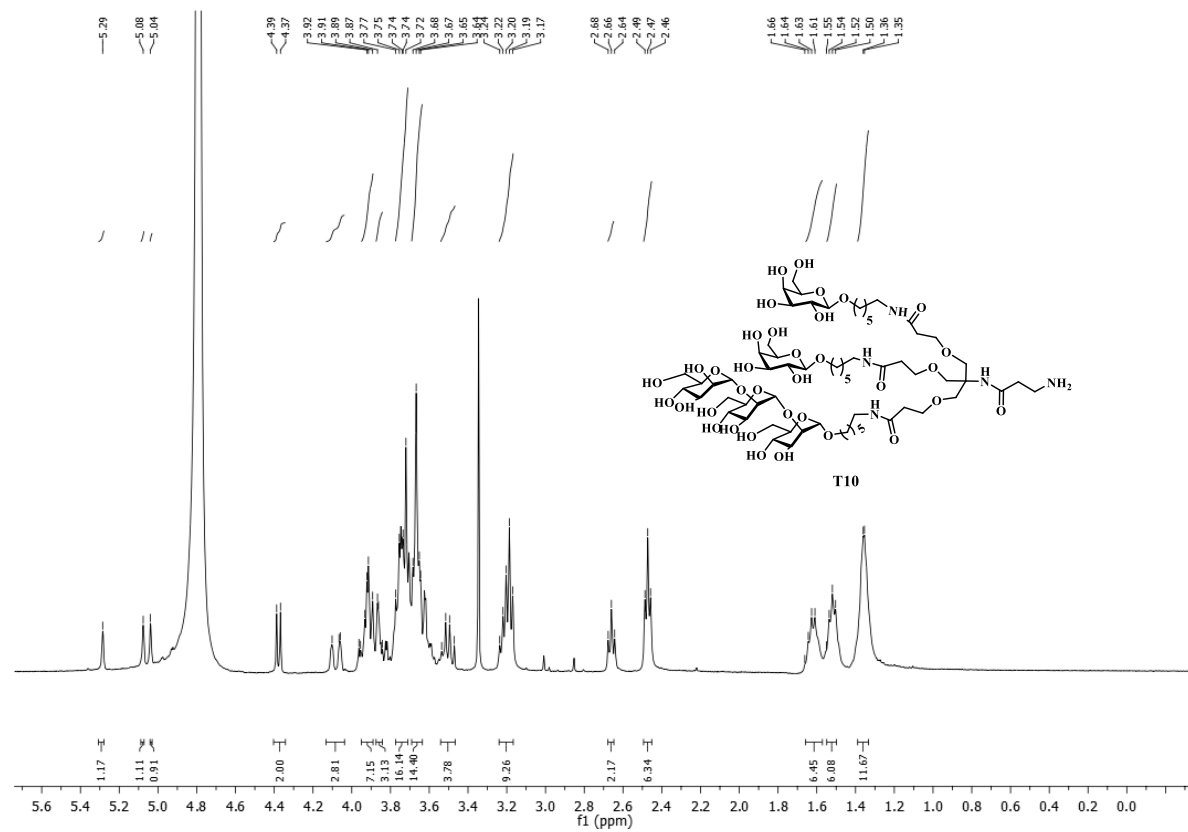
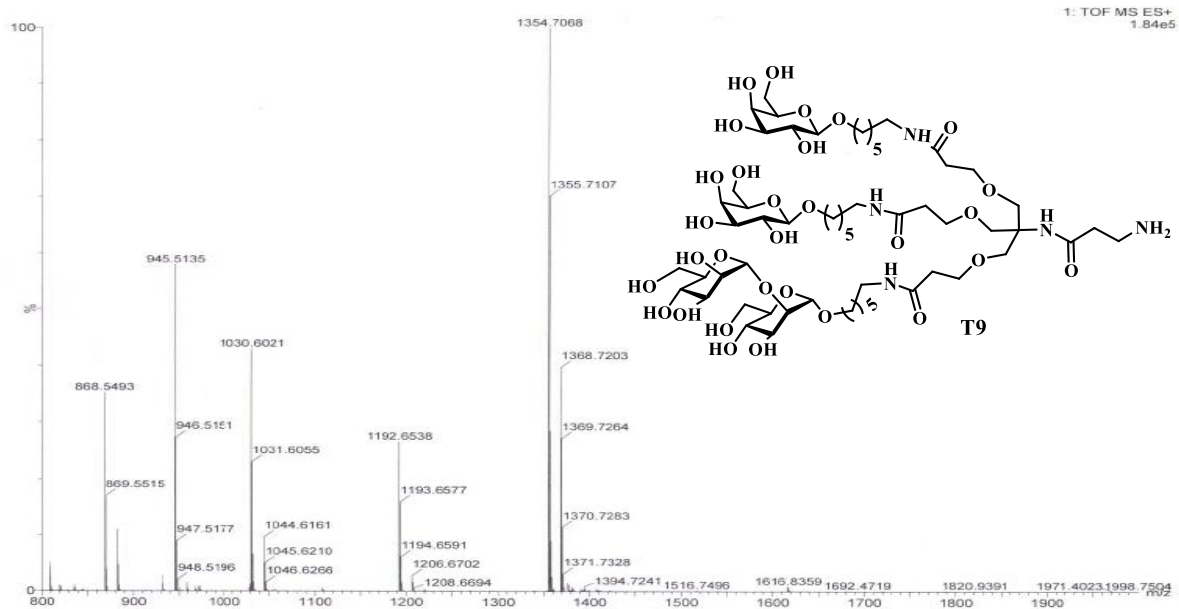


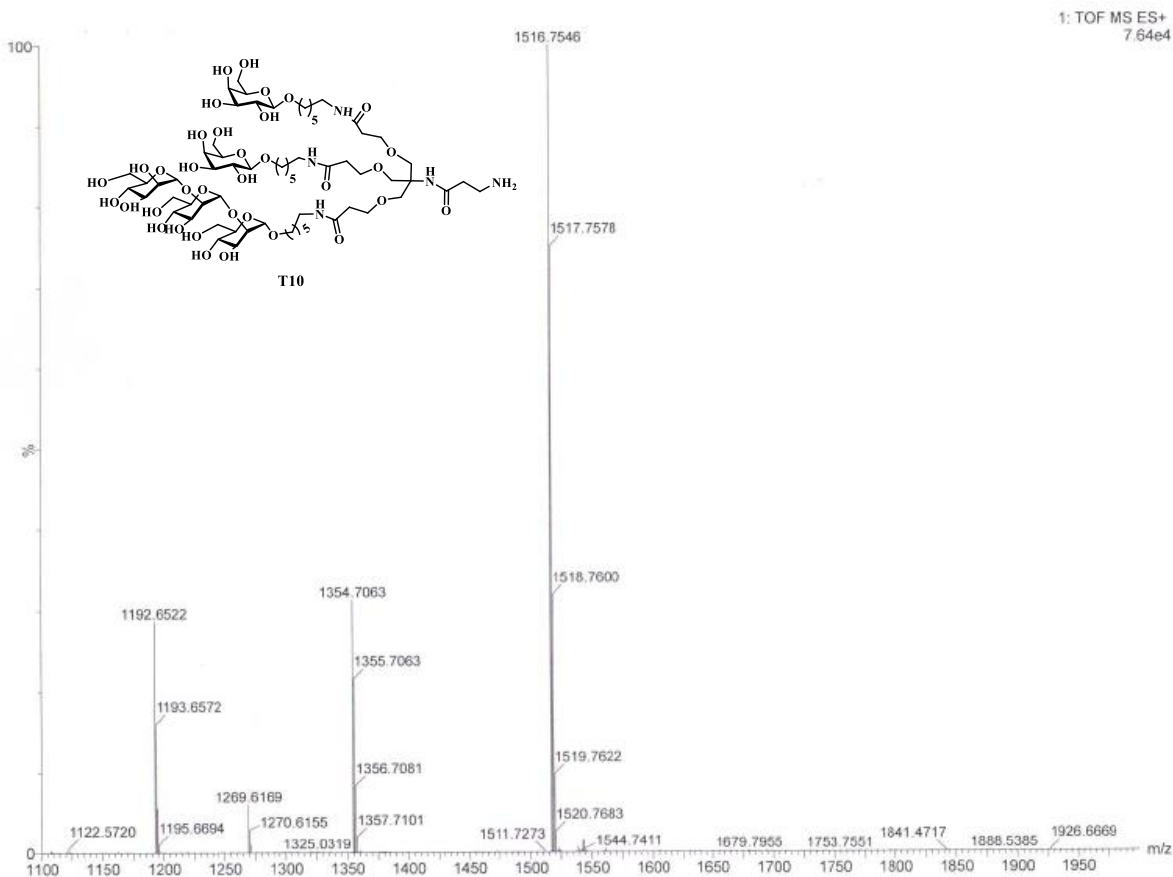
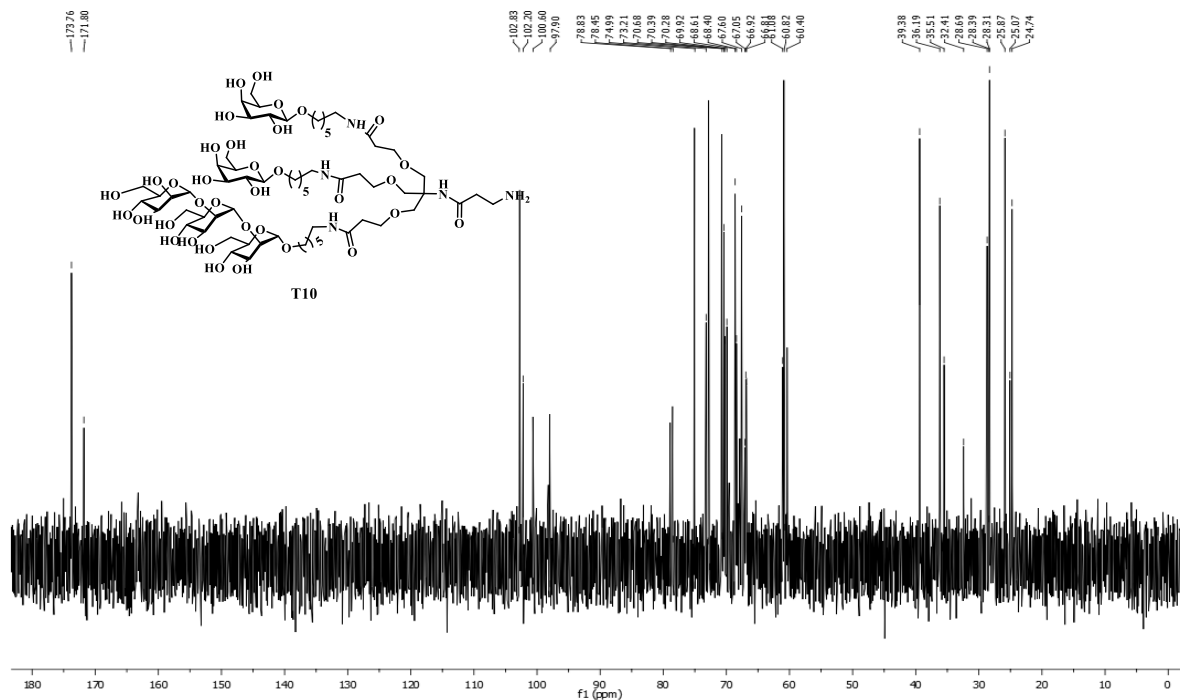












CHAPTER 4

Enantiomeric Effect of Sugar on Cellular and Bacterial Binding and Infections

Abstract

Carbohydrate-protein interactions are the most common cause of bacterial adhesion, biofilm formation and infections. Hence, studying the interaction between the enantiomers of sugars and bacteria is fundamental for the design of novel biomarkers and origin of chiral preference in Biosystems. Thus, herein we developed a model system to establish the role of D- and L-mannose on *E. coli* pathological and physiological interactions. Finally, we have shown that bioorthogonal conjugation of mannose enantiomers on HeLa cell surfaces displayed selective prevention of bacterial infection and shed new insight into the development of next-generation chiral drug molecules and biomaterials.

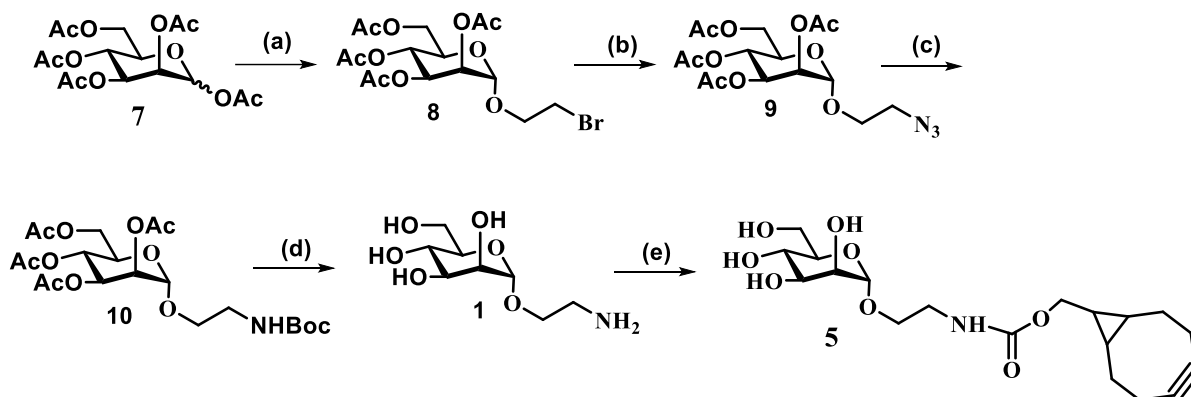
4 Introduction

The ability of biomolecules to distinguish between D and L configurations is crucial in all biological events, including cell-cell, cell-proteins and cell-bacterial interactions.¹⁻⁷ Nearly all mammalian lectins prefer the D-form over the L-form of carbohydrates, the exceptions to this are L-fucose and L-iduronic acids. L-fucose is found in mammalian cell surfaces in the form of Lewis x/a- and sialyl Lewis x/a-carbohydrates and are pivotal ligands for C-type and selectin lectins.⁸⁻¹⁰ L-iduronic acid is found in glycosaminoglycans (GAGs) in a sulfated state and is crucial for the extracellular signaling proteins, including growth factors, cytokines and chemokines.¹¹⁻¹⁵ In addition to sugar chirality, a huge body of results demonstrates that the both, glycosidic linkages and anomeric-configurations^{16,17} are extremely important parameters in fine-tuning carbohydrate-protein interactions. As an example, α -D-mannose derivatives interact effectively with the FimH receptor on uropathogenic *E. Coli* bacteria¹⁸ thus inhibiting infection. Similarly treatment of *H. pylori* with Neu5Ac α (2-3)Lac prevents damages in human gastric tissues.¹⁹⁻²² Due to the crucial role of chirality in biological processes in general and of carbohydrates in particular, many efforts were put in research using glycoclusters and hydrogels modified with enantiomers of amino acids and carbohydrates in effort to probe lectin binding affinity and cellular recognition.²³⁻²⁵ Systematic studies exploring the impact of carbohydrate D/L-configurations on different orders of unicellular organism and potential applications of these interactions, have not yet been published. In this chapter we describe our studies with D/L-monosaccharides-functionalized surfaces aiming to understand the specific interactions with bacteria, pathogens, cells and for harnessing these interactions for future potential applications. As prototypes we have synthesized glass slides functionalized with D- and L- α -mannose and D- and L- β -galactose and studied cell-adhesion and proliferation phenomena of cells from human and mice origin and have demonstrated specific binding of the bacterial strains *E. coli* and *Toxoplasmosis Gondi* pathogens. Moreover, we have utilized the preference of cellular interactions to different types of bacteria to modify the glycans on cell surfaces and by doing so succeeded to inhibit bacterial infection.

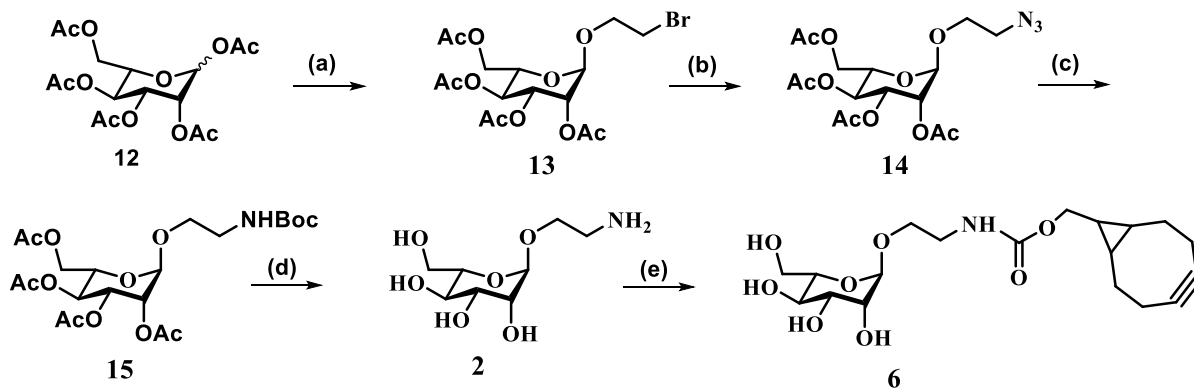
4.1 Result and Discussion

4.1.1 Synthesis of sugars

D- and L-monosaccharides (**1-4**) having amino-terminated linkers were synthesized and characterized following our previously reported methods (scheme 1 and 2).²⁶ ¹H and ¹³C-NMR spectra of the two enantiomers are identical, whereas the specific rotations (CD spectrum) of the molecules were (+) 52° and (-) 64°, respectively, as expected from two enantiomers.



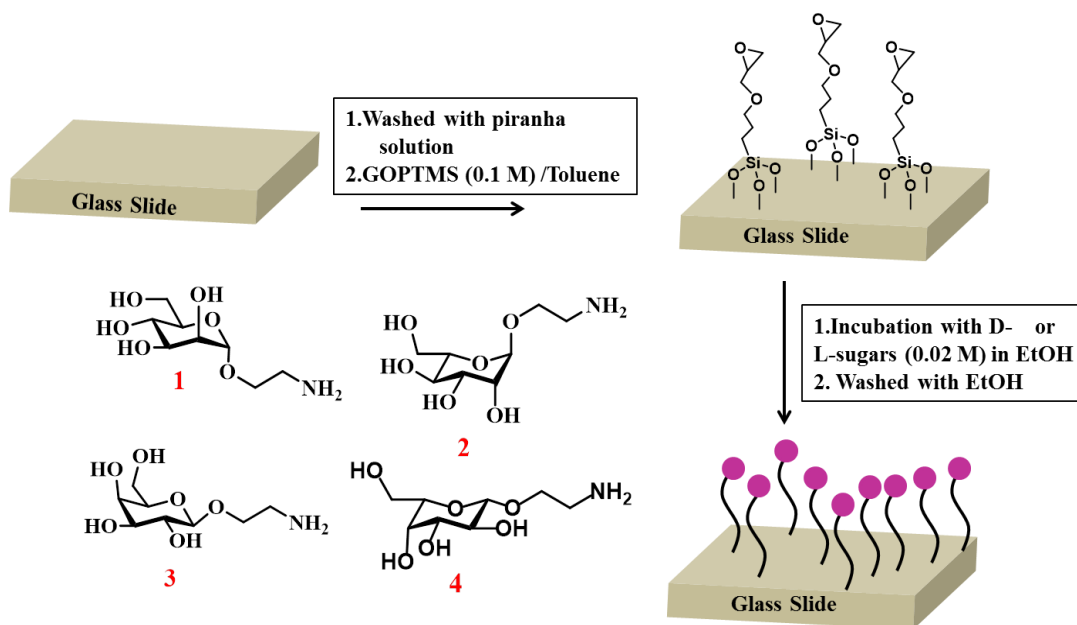
Scheme 1 (a) 2-bromoethanol/ $\text{BF}_3 \cdot \text{Et}_2\text{O}$, CH_2Cl_2 , 0 °C To RT, 12 h, 85% ; (b) NaN_3/DMF , 80 °C, 12 h, 90% ; (c) PPh_3/THF , RT, 4h then H_2O , Boc_2O 12h, 67% ; (d) i) NaOMe/MeOH ii) 20% $\text{TFA}/\text{CH}_2\text{Cl}_2$, 2h, 57%. (e) (1R, 8S, 9S)-Bicyclo[6.1.0]non-4-yn-9-ylmethyl N-succinimidyl carbonate/ DMF , RT, 2h, 78%



Scheme 2 (a) 2-bromoethanol/ $\text{BF}_3 \cdot \text{Et}_2\text{O}$, CH_2Cl_2 , 0 °C To RT, 12 h, 87% ; (b) NaN_3/DMF , 80 °C, 12h, 88% ; (c) PPh_3/THF , RT, 4h then H_2O , Boc_2O 12 h, 65% ; (d) i) NaOMe/MeOH ii) 20% $\text{TFA}/\text{CH}_2\text{Cl}_2$, 2 h, 61%. (e) (1R, 8S, 9S)-Bicyclo[6.1.0]non-4-yn-9-ylmethyl N-succinimidyl carbonate/ DMF , RT, 2h, 72%

4.1.2 Immobilization of sugars on slides

Robust monolayers of the monosaccharides were prepared by attaching compounds **1-4** to epoxide groups present on GOPTMS-coated glass slides.²⁷ This was done by washing glass slides (approx. 1x1 cm in size) with piranha solution (this is explosive solution use it carefully) followed by dipping them into a solution of 3-glycidyloxypropyltrimethoxysilane (GOPTMS) in toluene. The substrates were heated at 85 °C for 52h in a pressure tube, rinsed with toluene to remove excess GOPTMS²⁷ and were dipped in a solution of sugar-linker (0.02 mM) in ethanol for 24 h. Finally the substrates were rinsed with ethanol to remove excess sugar derivative and to remove residual epoxide groups (scheme 3). The process yielded glass slides covered with monolayers of the mannose with two different enantiomeric forms, which were analysed by XPS. Presence of sugar scaffold on the glass slides was confirmed by the relative abundance of carbon, oxygen and nitrogen atoms on the chips (Fig. 1 & Fig. 2).



Scheme 3 Molecular structures of monosaccharides with linker (**1-4**) and schematic representation of different steps to immobilize saccharides onto glass slides

4.1.3 XPS Analysis

XPS technique plays a vital role in analyzing the chemical composition of molecules on surfaces. We used this method to confirm the conjugation of **1, 2** to the glass slides. Carbon 1s spectrums for **1**, peaks are situated at 284.1 eV (C-C, C-H), 285.48 eV (C-O), and 287.01 eV (C-N). High resolution nitrogen 1s spectrum for **1** is centred at 401.5 eV and oxygen 1s spectrum is located at

532.7 eV (Fig. 1). Similarly for **2** C 1s spectrum at 284.43 eV (C-C, C-H), 285.1 eV (C-O), 287.2 eV (C-N), N 1S at 400 eV, whereas oxygen 1s spectrum is located at 532.9 eV (Fig. 2). This clearly indicates the presence of **1**, **2** on glass slides.

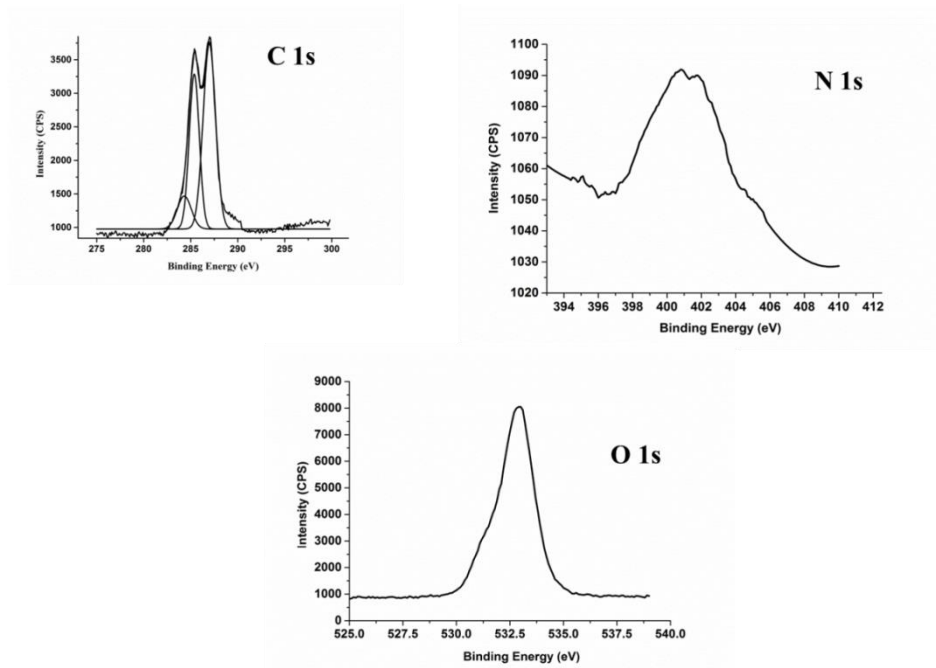


Figure 1 XPS spectra for D mannose **1** coated glass slide

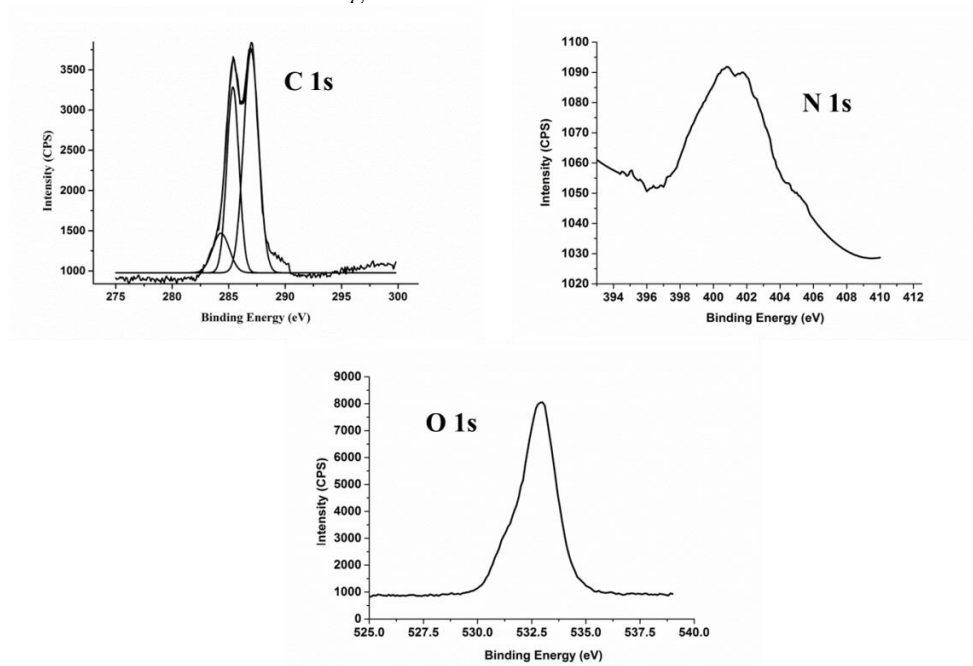


Figure 2 XPS spectra for L mannose **2** coated glass slide

4.1.4 Cell adhesion experiment

The effect of the D/L-configuration of mannose and galactose on cell adhesion and cell proliferation were explored using mouse (NIH-3T3) and human cell lines from brain (LN229), breast (T47D, MDA-MB-231) and cervix (HeLa). The rationale for choosing these cell lines was based on the fact that fibroblast cells are directly involved in tissue remodeling. Cancer cell lines HeLa, T47D and MDA-MB-231 that express specific sugar receptors were used.²⁸⁻³¹ Glass slides coated with compounds **1-4** were placed in an eight-well chamber, incubated with known numbers of the cells for 2 hours, washed and viewed by Brightfield microscopy (Fig. 3). To our surprise, we didn't see significant differences between cell-adhesion and cell-proliferation patterns between the D- and L- sugar coated slides. Similar observation was found after 24h, indicating a small effect of the D/L-configuration of carbohydrates on the cellular physiology and morphology.

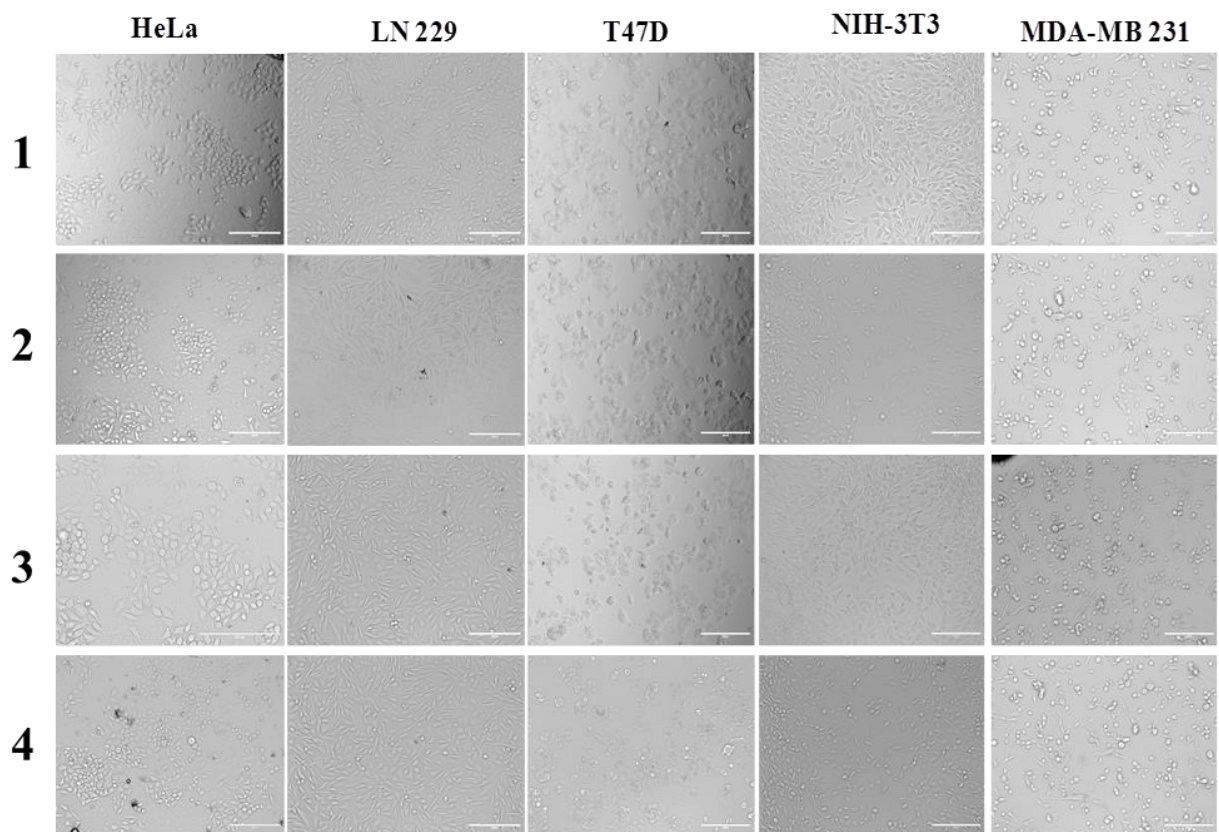


Figure 3 Profiling cellular adhesion on glass slides coated with D and L-enantiomers of mannose and galactose (**1-4**)

4.1.5 Bacterial adhesion experiment

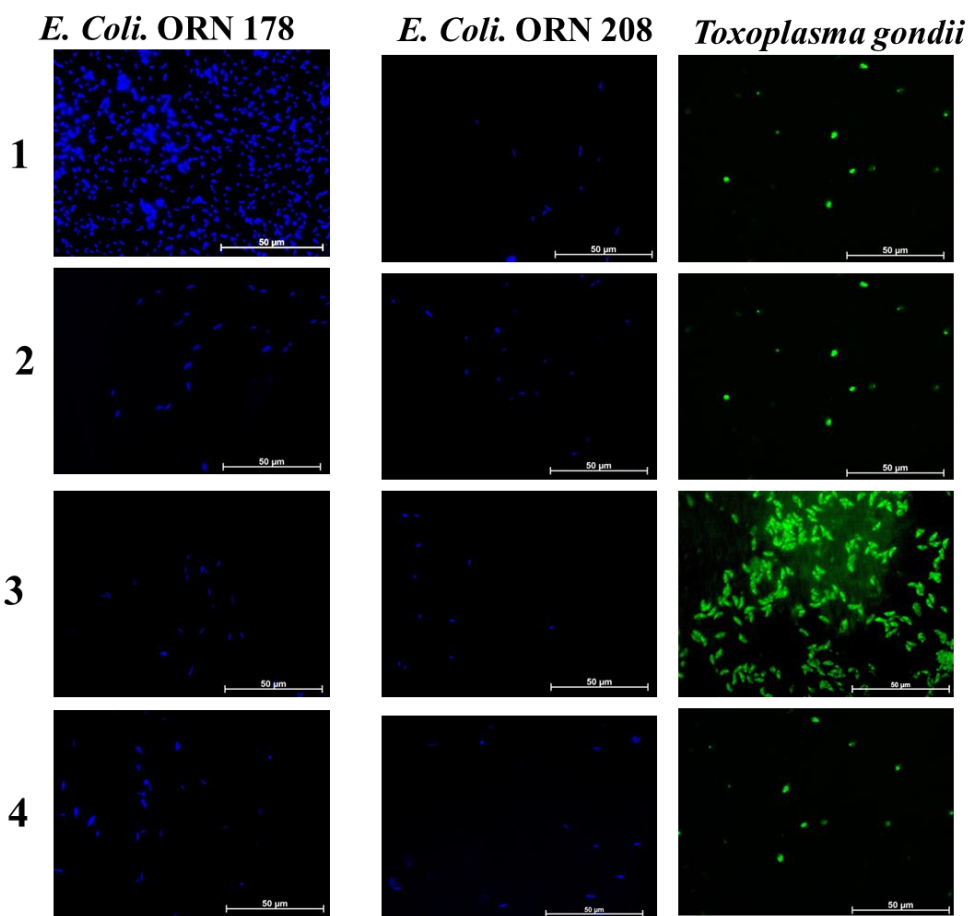


Figure 4 Profiling bacterial and pathogens adhesion on glass slides coated with D and L-enantiomers of mannose and galactose (**1-4**)

After establishing the cellular behaviour in the presence of both carbohydrate enantiomers, we investigated the effect of sugar chirality on the recognition of bacteria and pathogens. Prototype *E. coli* ORN 178 and its mutant ORN 208 were treated for 30 minutes with glass slides coated with compounds **1-4** and washed several times with distilled water to remove unbound or weakly bound bacteria. The bound bacteria were treated with hoechst 33258 and imaged by a microscope. (Fig. 4) No bacteria of the *E. coli* strain were bound to glass slides coated with compounds **2-4**, whilst a huge cluster of ORN 178, which was not removed even upon vigorous rinsing with water, was found on slides functionalized with compound **1**. However, when the glass slides were “decorated” with the mutant ORN 208, no binding was observed, indicating

selective and specific chiral recognition of the bacteria. Selectivity of D/L sugar molecules was also observed in the study of toxoplasmosis gondii, which has T. gondii micronemal protein (TgMIC4) receptor. It was found that the TgMIC4 complex binds selectively to galactose based ligand.^{32,33} We have found that T. Gondii binds preferentially to compound **3** as compared to **1** **2**- and **4** coated slides (Fig. 4) indicating that microorganisms of lower order, such as bacteria and pathogens, display chiral selectivity to carbohydrate scaffolds as opposed to higher-order organisms, i.e., cell lines. Moreover, we have found that even though the differences in conformation of the D/L monosaccharides are too weak to display distinct binding or alter biological properties of complex cellular interactions, bacteria and pathogens recognize the chirality differences.

4.1.6 Bio-orthogonal reaction

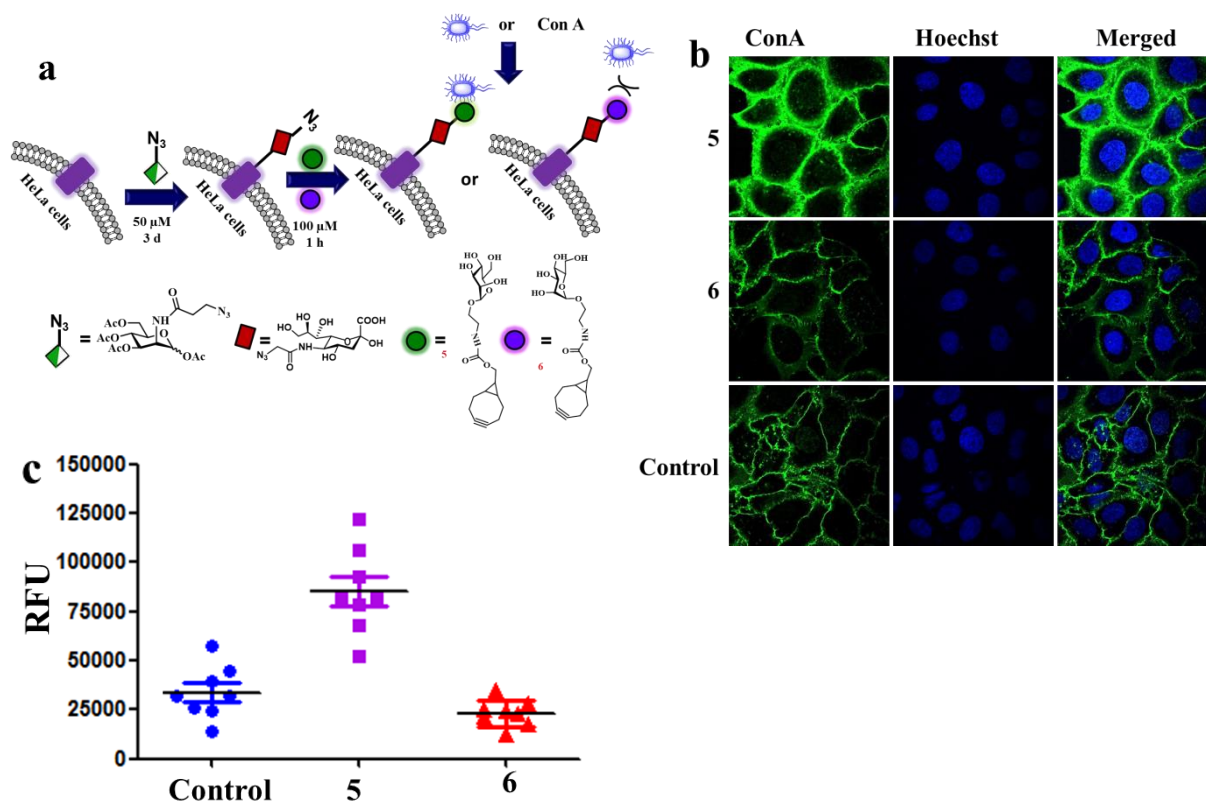


Figure 5 (A) Schematic representation of D and L-mannose sugar express on HeLa cell surfaces. a) Ac₄ManNAz was feed to HeLa cells; azide will get expressed on cell surface by metabolic oligosaccharide engineering (MOE). b) Copper free click reaction between **5** or **6** with azide expressed on cell surface. c) Binding with *E.coli*. 178; (B) Fluorescence confocal microscopy images of HeLa cells incubated with FITC conjugated ConA for 1 h; (C) Statistical analysis of ConA binding in presence of **5** and **6** on the cell surfaces (n = 8)

Finally, in order to suggest a potential application of the enantiomeric effect, we have functionalized cell surfaces by attaching D/L enantiomers of mannose to human cervix cells (HeLa) and *E. coli* ORN 178 using biorthogonal reactions.³⁴ At the first step, the copper-free click reagent bicyclo[6.1.0]non-4-yn-9-ylmethyl was attached to compounds **1** and **2** by coupling the *N*-succinimidyl carbonate derivative of the reagent to the mannose enantiomers, thus functionalizing the mannose bound to cell surfaces, yielding compounds **5** and **6**. Incorporation of the enantiomers on the cell surfaces was done by incubation of HeLa cells with tetra acetylated *N*-azidoacetyl-D-mannosamine (Ac4ManNAz, 50 μ M). The metabolic Ac4ManNAz engineering of HeLa cells after 3 days result in the occurrence of azido-terminal sialic acid moieties on the surface to be used for biorthogonal reactions (Fig 5 A).³⁵ Azido groups on the cell surface were reacted with 100 μ M solutions of molecules **5** and **6** and mannose molecules were bound on the surface. The amount of the sugar on the surface was qualitatively and quantitatively established and characterized by confocal imaging using FITC-conjugated ConA lectin (Fig 5 B). Functionalized HeLa cells modified with compound **5** revealed a substantial amount of ConA binding compared to that of the control and to that of its enantiomer (Fig. 5c).

4.1.7 Inhibition of bacterial infection

After confirming the biorthogonality of the reaction and the functioning of the sugar molecules, we investigated *E. coli* ORN 178 - mediated infection of HeLa cells (Fig. 5). Expressed HeLa cells (1×10^6 per well) decorated with azido-mannose groups were incubated in solutions (0-200 μ M) of compounds **5** or **6** for 1h using untreated cells as control. The functionalized HeLa cells were treated with *E.coli* ORN 178 (1×10^8 per well) for 1h followed by removal of the unbound bacteria. The amount of bound bacteria was quantified using microplate reader (OD₆₀₀). When the D/L-mannose derivatives **5** and **6** were used, the results indicated that the bacterial infection was significantly higher in the presence of the D-mannose derivative (**5**) as compared to the L-mannose derivative (**6**), confirming the assumption that chirality has a significant effect on the adhesion of bacteria to surfaces and a major role in infection. Quantification was done with respect to the OD₆₀₀ and percentage of inhibition was calculated from the average of three independent experiments. In case of control it is *N*-azidoacetyl-D-mannosamine concentration (50 μ M).

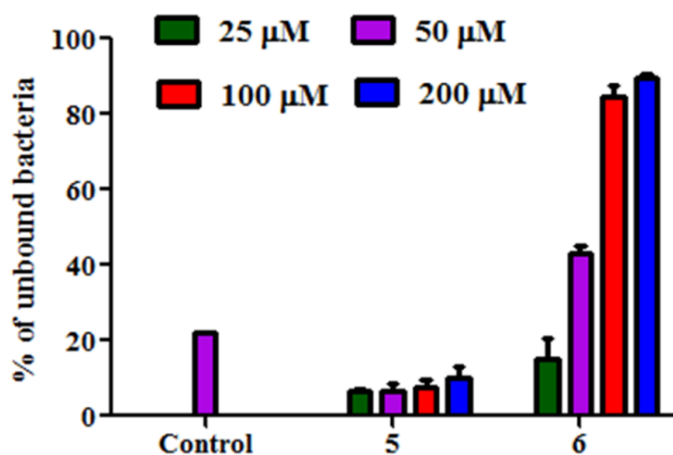


Figure 6 Percentage of unbound bacteria

4.2 Conclusion

We have prepared glass slides modified with D/L-monosaccharides and used these substrates for studying binding patterns of different orders of unicellular organisms. Higher-order unicellular organism, such as cells lines, that are complex systems to target, have shown no such significant differences towards the enantiomers of monosaccharides, while lower-order organisms have clearly shown significant differences in bacterial and pathogen adhesion. We have found a clear relation between chirality, cell adhesion, and infection. We believe that wise use of monosaccharides chirality, can lead to significant blocking of carbohydrate reactivity and to development of potential inhibitors of bacterial adhesion and infections.

4.3 Experimental Section

General Procedure for synthesis of bromoethanol sugar derivatives (**8**, **13**)

Peracetylated mannose **7** or **12** (1 g, 2.56 mmole) and bromoethanol (0.36 mL, 5.12 mmol) were dissolved in CH₂Cl₂ (10 mL). Maintain 0 °C, followed by slow addition of BF₃.Et₂O (0.44 mL, 5.12 mmole) for 30 minutes. The reaction mixture was allowed to stir at RT for 12 h. Completion of reaction was monitored by TLC. After completion, the reaction mixture was neutralized with triethyl amine, and added CH₂Cl₂ (50 mL) to the reaction mixture, gave washing with sodium bicarbonate (2 × 10 mL) and with water (2 × 10 mL). Organic layer was dried over anhydrous Na₂SO₄ and concentrated under reduced pressure to give crude product, which was further purified on silica gel column chromatography using EtOAc/Pet-ether (50 : 50) to get pure bromoethanol sugar derivatives **8** or **13** (Yield = 0.99 g, 85%).

General Procedure for synthesis of Azido-sugar derivatives (9, 14)

Dissolve bromoethanol sugar derivative **8** or **13** (0.5 g, 1.10mmol) in DMF then added NaN₃ (0.36 g, 5.5 mmole) to it, stirred reaction at 80 °C for 12 h. After completion of reaction mixture was extracted with ethyl acetate several times. Then organic layer washed with brine (2 × 10 mL). Organic layer was dried over anhydrous Na₂SO₄ and concentrated under reduced pressure to give crude product, which was further purified on silica gel column chromatography using EtOAc/Pet-ether (50 : 50) to get pure azido sugar derivatives **9** or **14** (Yield = 0.41 g, 90%).

General Procedure for synthesis of Boc protected-sugar derivatives (10, 15)

Azido sugar derivative **9** or **14** (0.4 g, 0.96 mmole) was dissolve in THF then PPh₃ (0.3 g, 1.15 mmole) added. Stirred reaction for 4h then water (5mL) and Boc anhydride (0.26 mL, 1.15 mmol) added. Reaction was stir for overnight. After completion of reaction THF was evaporated then reaction mixture was extracted with ethyl acetate (3 × 20 mL). Organic layer was dried over anhydrous Na₂SO₄ and concentrated under reduced pressure to give crude product, which was further purified on silica gel column chromatography using EtOAc/Pet-ether (50: 50) to get pure Boc protected-sugar derivatives **10** or **15** (Yield = 0.31 g, 67%).

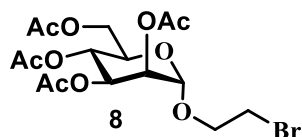
General Procedure for synthesis of deprotection of sugar derivative (1, 2)

Compound **10** or **15** (0.2 g, 0.40 mmole) was kept for Boc de-protection reaction by dissolving it in 20% TFA in CH₂Cl₂ (2mL TFA, 8 ml CH₂Cl₂). Boc deprotected compound (0.093g, 59%) was obtained after co-evaporation with toluene and CH₂Cl₂ several times. Further acetate de-protection (0.093 g, 0.237 mmole) was done in NaOMe (0.063 g, 1.14 mmole) and MeOH (10 mL) for 2h at RT. The crude residue on evaporation of MeOH was purified by sephadex column to yield **1** or **2** (0.030 g, 57%).

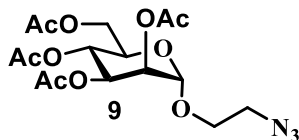
General Procedure for synthesis of sugar derivative (5, 6)

(1R, 8S, 9S)-Bicyclo[6.1.0]non-4-yn-9-ylmethyl N-succinimidyl carbonate (0.010g, 0.034 mmole) and deprotected sugars(0.008 g, 0.037 mmole) was dissolved in DMF and stirred for 2 h. On completion of reaction DMF was evaporated under pressure to get crude product, purified by sephadex column to yield **5** or **6** (0.01g, 78%).

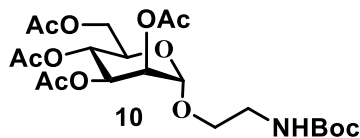
4.3.1 Immobilization of sugar derivatives (1-4): (Approx. 1x1 cm) glass was washed with piranha solution (Caution: Piranha solution reacts violently so use carefully) and immediately dipped in a solution of 3-glycidyloxypropyl trimethoxysilane (GOPTMS) (0.5 M) in 2 ml toluene. The substrates were heated at 85 °C for 52h in a pressure tube. Samples were then rinsed with toluene to remove excess of GOPTMS. Next, GOPTMS coated glass slides were dipped in a solution of **1-4** (0.02 M) in ethanol for 12 h and rinsed with ethanol to remove excess of sugars and to neutralize epoxide group.



^1H NMR (400 MHz, CDCl_3): δ 5.35-5.32 (m, 1H), 5.27-5.24 (m, 2H), 4.86 (d, $J = 1.7$ Hz, 1H), 4.26, 4.23 (dd, $J = 12.7, 5.9$ Hz, 1H), 4.14-4.09 (m, 2H), 3.99-3.93 (m, 1H), 3.90-3.84 (m, 1H), 3.50 (t, $J = 6.0$ Hz, 2H), 2.14 (s, 3H), 2.09 (s, 3H), 2.04 (s, 3H), 1.98 (s, 3H); ^{13}C NMR (100 MHz, CDCl_3): δ 170.89, 170.30, 170.13, 170.03, 98.02, 69.70, 69.30, 69.21, 68.76, 66.28, 62.69, 29.88, 21.14, 21.02, 20.98, 20.95. HRMS m/z calc'd for $\text{C}_{16}\text{H}_{23}\text{O}_{10}\text{BrNa}$: 477.0372; found: 477.0372.

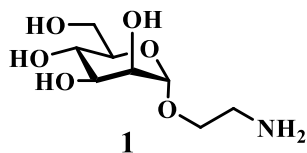


^1H NMR (400 MHz, CDCl_3): δ 5.38-5.34 (m, 1H), 5.32-5.27 (m, 2H), 4.87 (d, $J = 1.7$ Hz, 1H), 4.30, 4.28 (dd, $J = 12.3, 5.3$ Hz, 1H), 4.14, 4.11 (dd, $J = 12.3, 2.3$ Hz, 1H), 4.07-4.02 (m, 1H), 3.90-3.84 (m, 1H), 3.69-3.64 (m, 1H), 3.53-3.41 (m, 2H), 2.16 (s, 3H), 2.10 (s, 3H), 2.05 (s, 3H), 1.99 (s, 3H); ^{13}C NMR (100 MHz, CDCl_3): δ 169.92, 169.32, 169.32, 169.06, 97.04, 68.69, 68.15, 66.35, 65.30, 61.76, 49.66, 20.17, 20.04, 20.01, 19.96 HRMS m/z calc'd for $\text{C}_{16}\text{H}_{23}\text{O}_{10}\text{N}_3\text{Na}$: 440.1281; found: 440.1286.

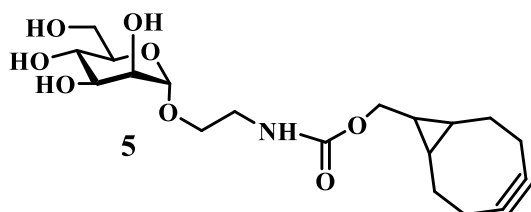


^1H NMR (400 MHz, CDCl_3): δ 5.33-5.29 (m, 1H), 5.26-5.24 (m, 2H), 4.91 (bs, 1H), 4.81 (d, $J = 1.5$ Hz, 1H), 4.29, 4.26 (dd, $J = 12.2, 5.5$ Hz, 1H), 4.10-4.07 (m, 1H), 3.99-3.94 (m, 1H), 3.77-

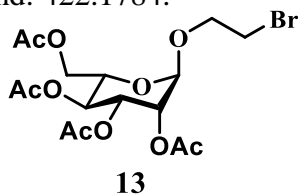
3.73 (m, 1H), 3.55-3.50 (m, 1H), 3.44-3.38 (m, 1H), 3.33-3.25 (m, 1H), 2.15 (s, 3H), 2.09 (s, 3H), 2.04 (s, 3H), 1.99 (s, 3H), 1.44 (s, 9H) ; ^{13}C NMR (100 MHz, CDCl_3): δ 170.71, 170.13, 170.05, 169.67, 155.89, 97.78, 79.68, 69.46, 69.09, 68.71, 67.85, 66.15, 62.51, 40.30, 28.45, 20.95, 20.79, 20.76. HRMS m/z calc'd for $\text{C}_{21}\text{H}_{33}\text{O}_{12}\text{BrNa}$: 514.1900; found: 514.1899.



^1H NMR (400 MHz, D_2O): δ 4.85 (s, 1H), 3.99-3.94 (m, 2H), 3.89-3.86 (m, 1H), 3.78-3.75 (m, 2H), 3.70-3.65 (m, 2H), 3.57-3.56 (m, 1H), 3.21 (bm, 2H); ^{13}C NMR (100 MHz, D_2O): δ 100.56, 73.57, 70.91, 70.29, 67.01, 63.48, 61.22, 39.14. HRMS m/z calc'd for $\text{C}_8\text{H}_{18}\text{NO}_6$: 224.1134; found: 224.1139. $[\alpha]_{25}^{\text{D}} + 56$ (c 0.1%, MeOH)

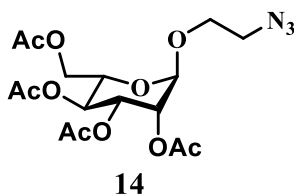


^1H NMR (400 MHz, CD_3OD): δ 4.78 (d, $J = 1.6$ Hz, 1H), 4.53 (d, $J = 8.4$ Hz, 1H), 4.18 (d, $J = 8.1$ Hz, 2H), 3.86-3.82 (m, 2H), 3.77-3.70 (m, 2H), 3.63 (t, $J = 9.4$ Hz, 1H), 3.57-3.50 (m, 2H), 2.85-2.84 (m, 2H), 2.34-2.18 (m, 6H), 1.67-1.58 (m, 2H), 1.10-1.06 (m, 1H), 1.00-0.91 (m, 2H); ^{13}C NMR (100 MHz, CD_3OD): δ 157.60, 99.67, 98.03, 97.96, 73.30, 71.03, 70.68, 69.88, 67.37, 61.30, 61.41, 40.09, 28.76, 28.56, 20.53, 20.00, 20.53, 17.53, 16.94. HRMS m/z calc'd for $\text{C}_{19}\text{H}_{29}\text{O}_8\text{NNa}$: 422.1791; found: 422.1784.

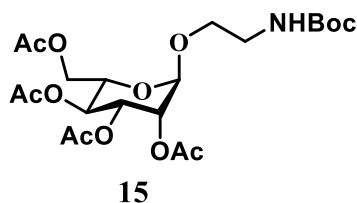


^1H NMR (400 MHz, CDCl_3): δ 5.38-5.35 (m, 1H), 5.32-5.28 (m, 2H), 4.89 (d, $J = 1.5$ Hz, 1H), 4.29, 4.28 (dd, $J = 12.7, 5.9$ Hz, 1H), 4.17-4.14 (m, 2H), 4.02-3.96 (m, 1H), 3.93-3.87 (m, 1H), 3.53 (t, $J = 6.0$ Hz, 2H), 2.17 (s, 3H), 2.12 (s, 3H), 2.07 (s, 3H), 2.01 (s, 3H); ^{13}C NMR (100 MHz, CDCl_3): δ 171.07, 170.48, 170.31, 170.22, 98.22, 69.90, 69.50, 69.41, 68.95, 66.48, 62.89,

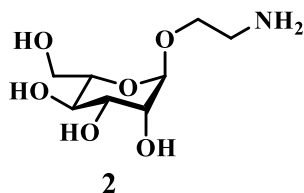
30.06, 21.33, 21.21, 21.17, 21.13. HRMS m/z calc'd for $C_{16}H_{23}O_{10}BrNa$: 477.0372; found: 477.0362.



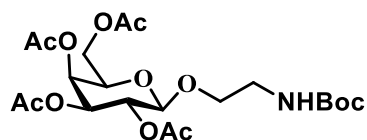
1H NMR (400 MHz, $CDCl_3$): δ 5.37-5.33 (m, 1H), 5.28-5.26 (m, 2H), 4.86 (d, $J = 1.5$ Hz, 1H), 4.29, 4.27 (dd, $J = 12.3, 5.3$ Hz, 1H), 4.13, 4.10 (dd, $J = 12.3, 2.4$ Hz, 1H), 4.06-4.02 (m, 1H), 3.89-3.83 (m, 1H), 3.71-3.60 (m, 1H), 3.52-3.49 (m, 2H), 2.15 (s, 3H), 2.10 (s, 3H), 2.04 (s, 3H), 1.98 (s, 3H); ^{13}C NMR (100 MHz, $CDCl_3$): δ 170.62, 170.01, 169.81, 169.76, 162.54, 97.74, 69.39, 68.85, 67.05, 66.00, 50.35, 36.48, 31.43, 20.87, 20.74, 20.71, 20.66. HRMS m/z calc'd for $C_{16}H_{23}O_{10}N_3Na$: 440.1281; found: 440.1281.



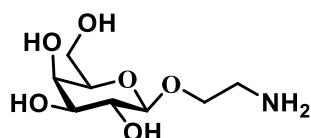
1H NMR (400 MHz, $CDCl_3$): δ 5.30-5.27 (m, 1H), 5.23-5.21 (m, 2H), 4.91 (bs, 1H), 4.79 (d, $J = 1.5$ Hz, 1H), 4.26, 4.22 (dd, $J = 12.3, 5.5$ Hz, 1H), 4.08, 4.05 (dd, $J = 12.2, 2.4$ Hz, 1H), 3.96-3.92 (m, 1H), 3.75-3.70 (m, 1H), 3.53-3.48 (m, 1H), 3.40-3.35 (m, 1H), 3.30-3.23 (m, 1H), 2.12 (s, 3H), 2.07 (s, 3H), 2.01 (s, 3H), 1.96 (s, 3H), 1.42 (s, 9H); ^{13}C NMR (100 MHz, $CDCl_3$): δ 170.70, 170.11, 170.0, 169.74, 155.89, 97.75, 69.45, 69.09, 68.69, 67.81, 66.14, 62.50, 40.18, 28.43, 20.92, 20.76, 20.74. HRMS m/z calc'd for $C_{21}H_{33}O_{12}BrNa$: 514.1900; found: 514.1906.



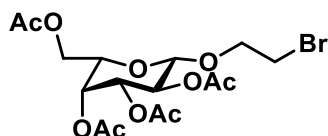
1H NMR (400 MHz, D_2O): δ 4.84 (s, 1H), 4.00-3.95 (m, 1H), 3.90-3.87 (m, 2H), 3.76-3.72 (m, 3H), 3.71-3.66 (m, 1H), 3.56-3.52 (m, 1H), 3.24-3.15 (m, 2H); ^{13}C NMR (100 MHz, D_2O): δ 100.66, 73.75, 71.01, 70.34, 67.15, 63.53, 61.48, 39.18. HRMS m/z calc'd for $C_8H_{18}NO_6$: 224.1134; found: 224.1138. $[\alpha]^{D_{25}} - 60$ (c 0.1%, MeOH).



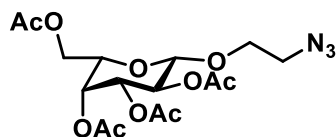
^1H NMR (400 MHz, CDCl_3): δ 5.39-5.28(m, 1H), 5.22-5.17 (m, 1H), 5.03, 5.00(dd, $J = 10.5, 3.4$ Hz, 1H), 4.91 (bs, 1H), 4.47 (d, $J = 7.9$ Hz, 1H), 4.16-4.12 (m, 2H), 3.93-3.85 (m, 2H), 3.67-3.61 (m, 1H), 3.38-3.33 (m, 2H), 2.15 (s, 3H), 2.07 (s, 3H), 2.05 (s, 3H), 1.98 (s, 3H), 1.44 (s, 9H); ^{13}C NMR (100 MHz, CDCl_3): δ . 170.37, 170.21, 170.12, 169.59, 155.81, 101.60, 70.76, 69.81, 68.86, 67.00, 61.22, 40.31, 28.40, 20.74, 20.66, 20.85. HRMS m/z calc'd for $\text{C}_{21}\text{H}_{33}\text{O}_{12}\text{BrNa}$: 514.1900; found: 514.1909.



^1H NMR (400 MHz, D_2O): δ 4.46 (d, $J = 7.8$ Hz, 1H), 4.16-4.10 (m, 1H), 4.00-3.93(m, 2H), 3.80-3.78 (m, 2H), 3.75-3.71 (m, 1H), 3.69-3.65 (m, 1H), 3.59-3.54 (m, 1H), 3.28 (t, $J = 5.1$ Hz, 2H); ^{13}C NMR (100 MHz, CD_3OD): δ 102.66, 75.21, 72.57, 70.73, 68.57, 65.74, 61.02, 39.50. HRMS m/z calc'd for $\text{C}_8\text{H}_{18}\text{NO}_6$: 224.1134; found: 224.1115.

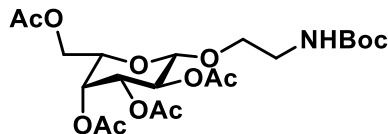


^1H NMR (400 MHz, CDCl_3): δ 5.40-5.39 (m, 1H), 5.25-5.23 (m, 1H), 5.04, 5.01(dd, $J = 10.5, 3.4$ Hz, 1H), 4.54 (d, $J = 7.9$ Hz, 1H), 4.21-4.14 (m, 3H), 3.93-3.90 (m, 1H), 3.87-3.80 (m, 1H), 3.52-3.42 (m, 2H), 2.15 (s, 3H), 2.08 (s, 3H), 2.05 (s, 3H), 21.98 (s, 3H); ^{13}C NMR (100 MHz, CDCl_3): δ 170.51, 170.34, 170.26, 169.66, 101.64, 70.92, 70.85, 69.87, 68.64, 67.06, 61.36, 30.07, 20.98, 20.80, 20.70. HRMS m/z calc'd for $\text{C}_{16}\text{H}_{23}\text{O}_{10}\text{BrNa}$: 477.0372; found: 477.0365.

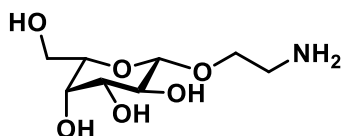


^1H NMR (400 MHz, CDCl_3): δ 5.40-5.39 (m, 1H), 5.26-5.22 (m, 1H), 5.04, 5.01 (dd, $J = 10.5, 3.4$ Hz, 1H), 4.57 (d, $J = 8.0$ Hz, 1H), 4.21-4.15 (m, 2H), 4.07-4.02 (m, 1H), 3.94-3.90 (m, 1H), 3.72-3.66 (m, 1H), 3.54-3.47 (m, 1H), 3.33-3.27 (m, 1H), 2.15 (s, 3H), 2.06 (s, 3H), 2.05 (s, 3H),

1.98 (s, 3H); ^{13}C NMR (100 MHz, CDCl_3): δ 170.49, 170.33, 170.26, 169.59, 101.22, 70.98, 70.89, 68.60, 68.49, 67.07, 61.33, 50.64, 20.87, 20.76, 20.67. HRMS m/z calc'd for $\text{C}_{16}\text{H}_{23}\text{O}_{10}\text{N}_3\text{Na}$: 440.1281; found: 440.1284.



^1H NMR (400 MHz, CDCl_3): δ 5.41-5.32 (m, 1H), 5.21-5.14 (m, 1H), 5.02-5.01 (M, 1H), 4.91 (bs, 1H), 4.46 (d, $J = 7.9$ Hz, 1H), 4.15-4.10 (m, 2H), 3.92-3.84 (m, 2H), 3.66-3.61 (m, 1H), 3.38-3.25 (m, 2H), 2.14 (s, 3H), 2.06 (s, 3H), 2.03 (s, 3H), 1.98 (s, 3H), 1.43 (s, 9H); ^{13}C NMR (100 MHz, CDCl_3): δ 170.36, 170.20, 170.10, 169.57, 155.79, 101.60, 70.76, 69.79, 68.85, 66.96, 61.26, 40.31, 28.40, 20.74, 20.65, 20.57. HRMS m/z calc'd for $\text{C}_{21}\text{H}_{33}\text{O}_{12}\text{BrNa}$: 514.1900; found: 514.1897.



^1H NMR (400 MHz, D_2O): δ 4.47 (d, $J = 7.8$ Hz, 1H), 4.16-4.10 (m, 1H), 3.99-3.93 (m, 2H), 3.80-3.78 (m, 2H), 3.75-3.73 (m, 1H), 3.69-3.66 (m, 1H), 3.59-3.54 (m, 1H), 3.28 (t, $J = 5.1$ Hz, 2H); ^{13}C NMR (100 MHz, CD_3OD): δ 102.66, 75.21, 72.53, 70.72, 68.56, 65.74, 61.02, 39.50. HRMS m/z calc'd for $\text{C}_8\text{H}_{18}\text{NO}_6$: 224.1134; found: 224.1116.

4.3.2. Cell-adhesion assay. HeLa, NIH-3T3, MDA-MB-231, LN229, T47D cells were grown at 37°C in 5% CO_2 atmosphere in DMEM medium containing 10% fetal bovine serum and 0.1% streptomycin. Freshly prepared glass slides coated with comp (1-4) were placed in eight well chambered plates and 1×10^6 cells/well were seeded and incubated overnight in 5% CO_2 incubator at 37°C for attachment. Cells were then washed and fixed with paraformaldehyde solution. Glass slides were then fixed on microscopic slides and imaged in a bright field microscope.

4.3.3 Bacterial Strains growth The *E.coli* ORN178 and its mutant ORN 208 was provided by Prof. Orndorff (College of Veterinary Medicine, Raleigh, NC United States). The bacterial cultures were grown overnight at 37°C until they reached an approximate OD_{600} of 1.0.

4.3.4 Bacterial detection 1 ml aliquot of bacteria of approximate OD_{600} of 1 was centrifuged to obtain a bacterial pellet. The resulting pellet was washed twice with PBS buffer, resuspended in

1 ml PBS. Different sugar coated glass slides were dipped in this solution for 30 mins and the glass slides was rinsed with PBS, followed by distilled water to remove non-specific bindings. Then bound bacteria were stain with DAPI for 20 minutes. Slides were mounted on fluorescent microscope to image the bacteria.

4.3.5 Parasite culture and purification of parasites

Toxoplasma gondii RH-wt strain was maintained in continuous propagation using HFF as the host cell. The growth conditions were same as that for HFF cell growth, except that the culture media contained only 1% heat-inactivated FBS. Typically T25 flask containing confluent monolayer of HFF cells is infected with 10^5 freshly isolated tachyzoite stage *T. gondii*. After two day of growth, the parasites are harvested by scraping monolayer and passed through a 25-gauge needle to release the parasites, which are then purified by filtration through 3 μ m Nucleopore membrane (Whatman). The number of parasites in the filtrate is counted using a Countess Cell counter (Invitrogen). The parasites are then collected as a pellet by centrifugation and used in further studies.

4.3.6 Generation of transgenic *T. gondii* expressing the reporter protein-

Parasites were harvested from infected HFF monolayers and counted. 2×10^7 parasites and 50 μ g of linearized plasmid were resuspended into 300 μ l and 100 μ l of DMEM respectively and mixed. This parasite suspension was electroporated using 0.2 cm electroporation cuvette with capacitance of 10 Farad and voltage of 1.5 kV using Biorad Gene Pulser Xcell . After 12h, transfected parasites were exposed to drug pressure followed by two to three rounds of drug selection and clonal lines were obtained by limiting dilution method. Clonal lines that were positive for cytosolic YFP expression were used in further studies. For microscopic imaging, MICL-YFP expressing parasites were allowed to infect and grow in HFF monolayers grown on glass coverslips for 24h, before fixing with 4% Formaldehyde and mounting on glass slides using Fluoro shield mounting medium (Sigma). Images were taken with Ziess Axio Observer using a 63X oil immersion objective with excitation at 488 nm and emission at 530 nm.

4.3.7 Testing the binding of *T. gondii*

Freshly lysed prpB-YFP parasites were inoculated in a T-25 flask containing confluent monolayer of HFF cells and incubated at 37 °C 5% CO₂ incubator for 48h. Intracellular parasites were harvested and counted. Carbohydrate coated cover slips were kept in each well of 6 well plates and 1×10^5 parasites/2 ml were diluted and inoculated on these coated cover slips. These

plates were incubated for 4 h in optimal growth condition, following which the cell culture medium from each well was removed and the glass cover slips were washed with 2 ml DMEM followed by addition of 1x fixative in each well. After 10 mins, all cover slips were washed with MQ and mounted on glass slide using fluoro shield mounting medium.

4.3.8 Biorthogonal reaction on HeLa cell surfaces

HeLa cells were grown at 37 °C in 5% CO₂ atmosphere in DMEM medium containing 10% fetal bovine serum and 0.1% streptomycin. HeLa cells (1 × 10⁶ cells/well) were seeded on an eight well chambered cover glass and incubated overnight in a 5% CO₂ incubator at 37 °C for attachment. Cells were then first washed with PBS and then treated with azidoacetyl-D-mannosamine (at a concentration 50 μM) for 3 days. Cells were then washed with PBS and fresh medium was added and treated with Comp **5** or **6** (100 μM) for 1 h. Then cells were washed with PBS and treated with FITC-ConA (10 μg/mL) and incubated in dark for 1 h. The cells were treated with Hoechst 33342 (10 μL of 2 μg/mL solution) to stain nuclei for 30 mins, washed 3 times with PBS buffer.

4.3.9 Inhibition assay

HeLa cell line (1 × 10⁶ cells/well) were seeded per well into a 24-well plate and incubated for 24 h at 37°C in CO₂ atmosphere. Cells were washed three times with PBS before performing biorthogonal reaction using azidoacetyl-D-mannosamine (at a concentration 50 μM) and Comp **5** or **6** were added at different concentration (25-200 μM). After biorthogonal conjugation of D and L-mannose on HeLa cell surfaces, *E. Coli* ORN 178 bacteria (1 × 10⁸ cells/ml) were added. After 1 h, unbound bacteria were removed and quantified.

4.4 References

1. W. Wei, C. Xu, N. Gao, J. Ren and X. Qu, *Chem. Sci.*, 2014, **5**, 4367-4374.
2. T. Sun, D. Han, K. Rhemann, L. Chi and H. Fuchs, *J. Am. Chem. Soc.*, 2007, **69**, 1496-1497.
3. N. S. Kehr, *Biomacromolecules*, 2016, **17**, 1117–1122.
4. X. Yao, Y. Hu, B. Cao, R. Peng and J. Ding, *Biomaterials*, 2013, **34**, 9001-9009.
5. X. Wang, H. Gan and T. Sun, *Adv. Funct. Mater.*, 2011, **21**, 3276–3281.
6. N. S. Kehr, H. J. Galla, K. Riehemanna and H. Fuchsa, *RSC Adv.*, 2015, **5**, 5704-5710.
7. K. Baranes, H. Moshe, N. Alon, S. Schwartz and O. Shefi, *ACS Chem. Neurosci.*, 2014, **5**, 370–376.

8. D. O'Connell, A. Koenig, s. Jennings, B. Hicke, H. L. Han, T. Fitzwater, Y. F. Chang, N. Varki, D. Parma and A. Varki, *Proc. Natl. Acad. Sci. USA.*, 1996, **93**, 5883-5887.
9. M. Eriksson, S. Serna, M. Maglinao, M. K. Schlegel, P. H. Seeberger, N. C. Reichardt and B. Lepenies. *ChemBioChem*. 2014, **15**, 844-851.
10. K. Brzezicka, b. Echeverria, S. Serna, A. van Diepen, C. H. Hokke and N. C. Reichardt, *ACS Chem. Biol.*, 2015, **10**, 1290-1302.
11. M. Nonaka, X. Bao, F. Matsumura, S. Götze, J. Kandasamy, A. Kononov, D. H. Broide, J. Nakayama, P. H. Seeberger and M. Fukuda, *Proc. Natl. Acad. Sci. USA.*, 2014, **111**, 8173-8178.
12. R. M. Witt, M. L. Hecht, M. F. Pzyra-Murphy, S. M. Cohen, C. Noti, T. H. van Kuppevelt, M. Fuller, J. A. Chan, J. J. Hopwood, P. H. Seeberger and R. A. Segal, *J. Biol. Chem.*, 2013, **288**, 26275-26288.
13. J. R. Brown, Y. Nishimura and J. D. Esko. *Bioorg. Med. Chem. Lett.*, 2006, **16**, 532-536.
14. Y. C. Li, I. H. Ho, C. C. Ku, Y. Q. Zhong, Y. P. Hu, Z. G. Chen, C. Y. Chen, W. C. Lin, M. M. Zulueta, S. C. Hung, M. G. Lin, C. C. Wang and C. D. Hsiao, *ACS Chem. Biol.*, 2014, **9**, 1712-1717.
15. J. C. Lee, S. W. Chang, C. C. Lioa, F. C. Chi, C. S. Chen, Y. S. Wen, C. C. Wang, S. S. Kulkarni, R. Puranik, Y. H. Liu and S. C. Hung, *Chem. Eur. J.*, 2004, **10**, 399-415.
16. *The Anomeric effect and Essociated Stereoelectronic Effect*; G. R. Thatcher, Ed.; American Chemical Society: Washington, DC, 1993.
17. E. Juaristi, G. Cuevas, *The Anomeric Effect*; CRC Press: Boca Raton, FL, 1995.
18. M. Hartmann and T. K. Lindhorst, *Eur. J. Org. Chem.*, 2011, 3583-3609.
19. N. Sharon, *Biochim. Biophys. Acta.*, 2006, **1760**, 527-537.
20. C. Fessele and T. K. Lindhorst, *Biology*, 2013, **2**, 1135-1149.
21. A. Bernardi, J. Jiménez-Barbero, A. Casnati, C. de Castro, T. Darbre, F. Fieschi, J. Finne, H. Funken, K. E. Jaeger, M. Lahmann T. K. Lindhorst, M. Marradi, P. Messner, A. Molinaro, P. V. Murphy, C. Nativi, S. Oscarson, S. Penadés, F. Peri, R. J. Pieters, O. Renaudet, J. -L. Reymond, B. Richichi, J. Rojo, F. Sansone, C. Schäffer, W. B. Turnbull, T. Velasco-Torrijos, S. Vidal, S. Vincent, T. Wennekes, H. Zuilhof and A. Imberly, *Chem. Soc. Rev.*, 2013, **42**, 4709-4727.

22. M. Hartmann, A. K. Horst, P. Klemm and T. K. Lindhorst, *Chem. Commun.*, 2010, **46**, 330-332.
23. K. Benson, H. J. Galla and N. S. Kehr, *Macromol Biosci.*, 2014, **14**, 793–798.
24. J. E. Gindi, K. Benson, L. De Cola, H. J. Galla and N. S. Kehr, *Angew. Chem. Int. Ed.*, 2012, **51**, 3716–3720.
25. N. S. Kehr, J. E. Gindi, H. J. Galla and L. D. Cola, *Microporous Mesoporous Mater.*, 2011, **144**, 9-14.
26. R. Gentsch, F. Pippig, K. Nilles, P. Theato, R. Kikkeri, M. Maglinao, B. Lepenies, P. H. Seeberger and H. G. Börner, *Macromolecules*, 2010, **43**, 9239-47.
27. M. Gade, A. Paul, C. Alex, D. Choudhury, H. V. Thulasiram and R. Kikkeri *Chem. Commun.*, 2015, **51**, 6346-6349.
28. D. Benito-Alifonso, S. Tremel, B. Hou, H. Lockyear, J. Mantell, D. J. Fermin, P. Verkade, M. Berry, M. C. Galan. *Angew. Chem. Int. Ed.*, 2014, **53**, 810-814.
29. G. Quan, X. Pan, Z. Wang, Q. Wu, G. Li, L. Dian, B. Chen, C. Wu. *J. Nanobiotechnology.*, 2015, **13**, 7-11.
30. Y. Ma, H. Chen, S. Su, T. wang, C. Zhang, G. Fida, S. Cui, J. Zhao and Y. Gu. *J. Cancer.*, 2015, **6**, 658-70.
31. Y. Yang, M. Yu, T. T. Yan, Z. H. Zhao, Y. L. Sha and Z. J. Li. *Bioorg. Med. Chem.*, 2010, **18**, 5234-5240.
32. J. Marchant, B. Cowder, Y. Liu, L. Lai, C. Pinzan, J. B. Marq, N. Friedrich, K. Sawmynaden, L. Liew, W. chai, R. A. Childs, S. Saouros, P. Simpson, M. C. R. Barreira, T. Feizi, D. Soldati-Favre and S. Matthews, *J. Bio. Chem.*, 2012, **287**, 16720-16733.
33. A. Santos, F. C. Carvalho, M-C. Roque-Barreira, A. L. Zorzetto-Fernades, D. Gimenez-Romero, I. Monzo and P. R. Bueno. *Langumir*, 2015, **31**, 1211-1219.
34. K. Mahal, K. J. Yarema and C. R. Bertozzi, *Science*, 1997, **276**, 1125-11288.
35. H. I. Yoon, J. Y. Yhee, J. H. Na, S. Lee, H. Lee, S. W. Kang, H. Chang, J. H. Ryu, S. Lee, I. C. Kwon, Y. W. Cho, and K. Kim, *Bioconjugate Chem.*, 2016, **27**, 927–936.